INFORMATION TO USERS

This manuscript has been reproduced from the microfilm master. UMI films the text directly from the original or copy submitted. Thus, some thesis and dissertation copies are in typewriter face, while others may be from any type of computer printer.

The quality of this reproduction is dependent upon the quality of the copy submitted. Broken or indistinct print, colored or poor quality illustrations and photographs, print bleedthrough, substandard margins, and improper alignment can adversely affect reproduction.

In the unlikely event that the author did not send UMI a complete manuscript and there are missing pages, these will be noted. Also, if unauthorized copyright material had to be removed, a note will indicate the deletion.

Oversize materials (e.g., maps, drawings, charts) are reproduced by sectioning the original, beginning at the upper left-hand corner and continuing from left to right in equal sections with small overlaps.

Photographs included in the original manuscript have been reproduced xerographically in this copy. Higher quality 6" x 9" black and white photographic prints are available for any photographs or illustrations appearing in this copy for an additional charge. Contact UMI directly to order.

ProQuest Information and Learning
300 North Zeeb Road, Ann Arbor, MI 48106-1346 USA
800-521-0600



Downloaded from SHAREOK. Persistent Handle URL: https://hdl.handle.net/11244/404

UNIVERSITY OF OKLAHOMA

GRADUATE COLLEGE

DIMENSIONAL MEASUREMENT OF CONICAL FEATURES USING COORDINATE METROLOGY

A Dissertation

SUBMITTED TO THE GRADUATE FACULTY

in partial fulfillment of the requirements for the

degree of

Doctor of Philosophy

By

CHAKGUY PRAKASVUDHISARN
Norman, Oklahoma
2002

UMI Number: 3034887

UMI®

UMI Microform 3034887

Copyright 2002 by ProQuest Information and Learning Company.

All rights reserved. This microform edition is protected against unauthorized copying under Title 17, United States Code.

ProQuest Information and Learning Company
300 North Zeeb Road
P.O. Box 1346
Ann Arbor, MI 48106-1346

© Copyright by Chakguy Prakasvudhisarn 2002
All Rights Reserved

DIMENSIONAL MEASUREMENT OF CONICAL FEATURES USING COORDINATE METROLOGY

A Dissertation APPROVED FOR THE
SCHOOL OF INDUSTRIAL ENGINEERING

BY

Dr. Shivakumar Raman, Chair

Dr. Thomas L. Landers

Dr. John Y. Cheung

Dr. Pakize S. Pulat

Dr. Theodore B. Trafalis

ACKNOWLEDGEMENTS

I would like to express my sincere gratitude to many individuals for their support and encouragement throughout my tenure as a Ph.D. student. First, my parents are responsible for everything I have accomplished in my life. Their love, understanding, patience, and sacrifice have inspired me to overcome all obstacles. I would also like to thank my sister for her encouragement and for taking care of our parents while I am away.

Special thanks are due to my advisor, Dr. Shivakumar Raman, for his guidance and support during these past years. I would also like to express my appreciation to my committee members, Dr. Thomas L. Landers, Dr. John Y. Cheung, Dr. Pakize S. Pulat, and Dr. Theodore B. Trafalis, for their valuable suggestions leading to the completion of this work despite their busy schedules. Further gratitude is extended to the entire faculty and staff of the School of Industrial Engineering, especially Dr. Randa L. Shehab for her statistical advice and Ms. Allison G. Richardson for her academic support.

I would also like to thank several friends for their companionship, jokes, and food.

Thank you.

TABLE OF CONTENTS

Page

LIST OF TABLES viii

LIST OF FIGURES ix

ABSTRACT xi

CHAPTER 1
INTRODUCTION 1

CHAPTER 2
LITERATURE REVIEW 9

2.1 TOLERANCE TERMINOLOGY 9
2.1.1 Tolerances of Location 11
2.1.2 Tolerances of Form 11
2.1.3 Tolerances of Profile 14
2.1.4 Tolerances of Orientation 14
2.1.5 Tolerances of Runout 16
2.2 COORDINATE MEASURING MACHINES (CMMS) 18
2.3 SAMPLING STRATEGIES FOR DIMENSIONAL SURFACE MEASUREMENT 22
2.4 CMM PROBE PATH PLANNING FOR DIMENSIONAL INSPECTION 29
2.5 MINIMUM TOLERANCE ZONE ALGORITHMS 32
2.5.1 Computational Geometry Based Algorithms 34
2.5.2 Numerical Based Algorithms 45

CHAPTER 3
OVERVIEW OF RESEARCH 65

CHAPTER 4
SAMPLING STRATEGIES FOR CONICAL OBJECT 68

4.1 THE HAMMERSLEY SAMPLING STRATEGY 71
4.2 THE HALTON-ZAREMBA SAMPLING STRATEGY 81
4.3 THE ALIGNED SYSTEMATIC SAMPLING STRATEGY 84
4.4 THE RANDOM NUMBERS GENERATION 86
4.4.1 Frequency Test 90
4.4.2 Runs Tests 91
4.4.2.1 Runs Up and Runs Down 91
4.4.2.2 Runs Above and Below The Mean 92
4.4.2.3 Length of Runs 93
4.4.3 Tests for Autocorrelation 95

CHAPTER 5
CMM PATH PLANNING FOR EXTERNAL CONICAL SURFACE INSPECTION **97**

5.1 THE PATH PLANNING PROCEDURE FOR CONICAL FEATURE 98
5.1.1 Equations for Conical Horizontal Positioning 107
5.1.2 Equations for Conical Hypotenuse Positioning 108
5.1.3 Mapping Equations between Actual Surface and Imaginary Surface 110
5.2 THE INSTALLATION OF THE OFF-LINE PATH PLANNING PROCEDURE 113
5.3 LIMITATIONS OF THE CONICAL FEATURE PATH PLANNING PROCEDURE 114

CHAPTER 6
EXPERIMENTAL DESIGN **117**

6.1 EXPERIMENTAL SAMPLES 117
6.2 EQUIPMENT AND TOOLS 120
6.3 DESIGNING OF THE EXPERIMENT 120

CHAPTER 7
MINIMUM CONICAL TOLERANCE ZONE EVALUATION **134**

7.1 LINEAR FORMULATION 137
7.1.1 Straightness 137
7.1.2 Flatness 138
7.1.3 The Limacon Approximation 138
7.1.4 Circularity (Roundness) 140
7.1.5 Cylindricity 141
7.1.6 Conicity 142
7.2 NONLINEAR FORMULATION 144
7.2.1 Straightness 144
7.2.2 Flatness 146
7.2.3 Circularity (Roundness) 147
7.2.4 Cylindricity 148
7.2.5 Conicity 150
7.3 THE LEAST SQUARES BASED ZONE EVALUATION 152
7.3.1 Straightness Tolerance Zone 155
7.3.2 Flatness Tolerance Zone 156
7.3.3 Circularity Tolerance Zone 156
7.3.4 Cylindricity Tolerance Zone 157
7.3.5 Conicity Tolerance Zone 157
7.4 THE OPTIMIZATION BASED MINIMUM ZONE EVALUATION 159
7.4.1 The Additional Constraints for Straightness 162
7.4.2 The Additional Constraints for Flatness 163
7.4.3 The Additional Constraints for Circularity 163
7.4.4 The Additional Constraints for Cylindricity 163
7.4.5 The Additional Constraints for Conicity 164

CHAPTER 8
RESULTS AND ANALYSES **165**

8.1 CYLINDRICITY COMPARISONS 165
8.2 RESULTS FROM EXPERIMENTAL ANALYSES 177
8.2.1 Model Adequacy Checking 177
8.2.2 Analysis of Variance for the Conicity Testing Experiment 181

CHAPTER 9
CONTRIBUTIONS, CONCLUSIONS AND RECOMMENDATIONS **192**

9.1 CONTRIBUTIONS 193
9.2 CONCLUSIONS 194
9.3 RECOMMENDATIONS FOR FUTURE RESEARCH 197

REFERENCES **199**

APPENDIX A. PERFORMING GUIDES FOR THE EXPERIMENT 208

APPENDIX B. MODEL ADEQUACY CHECKING PLOTS FOR THE EXPERIMENTAL DESIGN USED BEFORE REMOVING THE INVALID DATA 211

APPENDIX C. INVALID PARAMETERS OBTAINED BY USING ALIGNED SYSTEMATIC SAMPLING 217

APPENDIX D. EXAMPLES OF VALID PARAMETERS OBTAINED BY USING ALIGNED SYSTEMATIC SAMPLING 224

APPENDIX E. STATISTICAL RESULTS AFTER INVALID DATA REMOVAL 228

LIST OF TABLES

Page

TABLE 1. COORDINATES OF 10 HAMMERSLEY SAMPLING POINTS. 73
TABLE 2. POLAR COORDINATES OF 10 HAMMERSLEY SAMPLING POINTS. 76
TABLE 3. COORDINATES OF 16 HALTON-ZAREMBA SAMPLING POINTS. 83
TABLE 4. OVERVIEW OF DATA SHEET TABLE. 125
TABLE 5. DEGREE OF FREEDOM. 128
TABLE 6. EXPECTED MEAN SQUARE DERIVATION 129
TABLE 7. THE COORDINATES DATA SET OF CYLINDER (SHUNMUGAM, 1987B). 167
TABLE 8. COMPARISON OF RESULTS FOR CYLINDRICITY USING TRANSFORMED Z_i. 168
TABLE 9. COMPARISON OF RESULTS FOR CYLINDRICITY USING ACTUAL Z_i. 168
TABLE 10. THE COORDINATES DATA SET 1 OF CYLINDER (CARR AND FERRIERA, 1995B). 169
TABLE 11. COMPARISON OF RESULTS FOR CYLINDRICITY USING DATA IN TABLE 10. 170
TABLE 12. THE COORDINATES DATA SET 2 OF CYLINDER (CARR AND FERRIERA, 1995B). 172
TABLE 13. COMPARISON OF RESULTS FOR CYLINDRICITY USING DATA IN TABLE 12. 172
TABLE 14. THE COORDINATES DATA SET 3 OF CYLINDER (CARR AND FERRIERA, 1995B). 173
TABLE 15. COMPARISON OF RESULTS FOR CYLINDRICITY USING DATA IN TABLE 14. 174
TABLE 16. THE COORDINATES DATA SET OF CYLINDER (ROY AND XU, 1995). 174
TABLE 17. COMPARISON OF RESULTS FOR CYLINDRICITY USING DATA IN TABLE 16. 177

LIST OF FIGURES

Page

FIGURE 1. SPECIFYING STRAIGHTNESS OF SURFACE ELEMENTS (SOURCE: ANSI Y14.5M-1994). 12
FIGURE 2. SPECIFYING FLATNESS (SOURCE: ANSI Y14.5M-1994) 13
FIGURE 3. SPECIFYING CIRCULARITY FOR A SPHERE (SOURCE: ANSI Y14.5M-1994). 15
FIGURE 4. SPECIFYING CYLINDRICITY (SOURCE: ANSI Y14.5M-1994) 15
FIGURE 5. SPECIFYING CONICITY (SOURCE: ANSI Y14.5M-1994). 16
FIGURE 6. SPECIFYING PROFILE OF A PLANE SURFACE (SOURCE: ANSI Y14.5M-1994). 17
FIGURE 7. SPECIFYING PARALLELISM FOR AN AXIS (SOURCE: ANSI Y14.5M-1994). 18
FIGURE 8. INTEGRATIVE INVESTIGATION OF CONE TOLERANCES USING COORDINATE METROLOGY. 67
FIGURE 9. DISTRIBUTION OF 10 HAMMERSLEY SAMPLING POINTS. 74
FIGURE 10. DISTRIBUTION OF 10 RANDOMIZED HAMMERSLEY SAMPLING POINTS. 74
FIGURE 11. DISTRIBUTION OF 10 HAMMERSLEY POINTS ON A CIRCULAR SURFACE. ... 76
FIGURE 12. THE PROJECTION BETWEEN A CONE AND ITS BASE CIRCLE. 78
FIGURE 13. TOP VIEW OF A CONICAL FRUSTUM. 78
FIGURE 14. SIDE VIEW SECTION OF A CONICAL FRUSTUM. 79
FIGURE 15. TOP VIEW OF A FRUSTUM USED TO FIND THE PARAMETRIC EQUATIONS.. 80
FIGURE 16. AUXILIARY VIEW NORMAL TO THE PLANE PASSING THE ORIGIN AND POINT *P*. 80
FIGURE 17. DISTRIBUTION OF 16 HALTON-ZAREMBA SAMPLING POINTS. 84
FIGURE 68. AN EXAMPLE OF 9 ALIGNED SYSTEMATIC SAMPLING POINTS. 85
FIGURE 19. A TOP VIEW OF 16 RANDOMIZED HAMMERSLEY POINTS ON A CONE. 87
FIGURE 20. A 3-D VIEW OF 16 RANDOMIZED HAMMERSLEY POINTS ON A CONE. 87
FIGURE 21. A TOP VIEW OF 16 RANDOMIZED HALTON-ZAREMBA POINTS ON A CONE. 88
FIGURE 22. A 3-D VIEW OF 16 RANDOMIZED HALTON-ZAREMBA POINTS ON A CONE. 88
FIGURE 23. A TOP VIEW OF 16 ALIGNED SYSTEMATIC SAMPLING POINTS ON A CONE. 89
FIGURE 24. A 3-D VIEW OF 16 ALIGNED SYSTEMATIC SAMPLING POINTS ON A CONE. 89
FIGURE 25. AN EXAMPLE RESULT OF AUTOCORRELATION TESTS. 96
FIGURE 26. VERTICAL POSITIONING MOVEMENTS. 100
FIGURE 27. HORIZONTAL POSITIONING MOVEMENTS. 103
FIGURE 28. HYPOTENUSE POSITIONING MOVEMENTS. 104
FIGURE 29. FLOW CHART OF PATH PLANNING PROCEDURE. 105
FIGURE 30. FLOW CHART OF HORIZONTAL PATH POSITIONING. 106
FIGURE 31. SIDE VIEW SNAP SHOT OF THE INSPECTED CONICAL FRUSTUM. 108
FIGURE 32. TOP VIEW FOR THE PROJECTED HYPOTENUSE MOVEMENT. 108

FIGURE 33. TOP VIEW OF THE MAPPED POINTS. 110
FIGURE 34. AN EXAMPLE OF PATH PLANNING FOR HAMMERSLEY SEQUENCE. 111
FIGURE 35. AN EXAMPLE OF PATH PLANNING FOR HALTON-ZAREMBA SEQUENCE.. 112
FIGURE 36. AN EXAMPLE OF PATH PLANNING FOR ALIGNED SYSTEMATIC SAMPLING. 112
FIGURE 37. A DIMENSIONAL DRAWING OF THE CONICAL FRUSTUM SPECIMEN. 118
FIGURE 38. A DIMENSIONAL DRAWING OF THE BIG SQUARE PLATE. 118
FIGURE 39. A DIMENSIONAL DRAWING OF THE CONICAL SPECIMEN. 119
FIGURE 40. A DIMENSIONAL DRAWING OF THE SMALL SQUARE PLATE. 119
FIGURE 41. ASSESSMENT OF LINEAR STRAIGHTNESS ERROR. 137
FIGURE 42. ASSESSMENT OF LINEAR FLATNESS ERROR. 138
FIGURE 43. DEFINITION OF CIRCLE. 139
FIGURE 44. ASSESSMENT OF LINEAR CIRCULARITY ERROR. 141
FIGURE 45. ASSESSMENT OF LINEAR CYLINDRICITY ERROR 141
FIGURE 46. THE RELATIONSHIP OF CONE'S RADIUS AND CONE'S HEIGHT. 143
FIGURE 47. ASSESSMENT OF LINEAR CONICITY ERROR. 144
FIGURE 48. ASSESSMENT OF NONLINEAR STRAIGHTNESS ERROR. 145
FIGURE 49. ASSESSMENT OF NONLINEAR FLATNESS ERROR 146
FIGURE 50. ASSESSMENT OF NONLINEAR CIRCULARITY ERROR. 147
FIGURE 51. ASSESSMENT OF NONLINEAR CYLINDRICITY ERROR 148
FIGURE 52. ASSESSMENT OF NONLINEAR CONICITY ERROR. 150
FIGURE 53. A SLIGHTLY TILTED CONE 151
FIGURE 54. SAMPLED POINTS OF AN IDEAL FORM AND ITS TOLERANCE ZONE 162
FIGURE 55. THE CORRESPONDING RESIDUALS OF EACH SET ARE IDENTICAL. 168
FIGURE 56. MAIN EFFECTS AND A 2-WAY INTERACTION PLOTS 183
FIGURE 57. 2-WAY INTERACTION PLOTS 184
FIGURE 58. 3-WAY INTERACTION PLOTS 185
FIGURE 59. 3-WAY INTERACTION PLOTS BETWEEN FITTING ALGORITHM, SAMPLE SIZE, AND SURFACE AREA. 186
FIGURE 60. 3-WAY INTERACTION PLOTS BETWEEN FITTING ALGORITHM, SAMPLE SIZE, AND SAMPLING STRATEGY. 187

ABSTRACT

Coordinate metrology employs a discrete sampling of data points to verify the size, form, orientation, and location of features contained in parts. Usually data points are collected intuitively with simple schemes that attempt to cover the surface of the features as best as possible. Data fitting methods are used to determine the zones of deviations about the ideal feature. A multitude of linear and nonlinear optimization procedures and the least squares method have been used to estimate the tolerance zone for straightness, flatness, circularity, and cylindricity. More complex forms such as conicity have been largely ignored in the literature, in spite of the sufficient need to inspect them in parts such as nozzles and tapered rollers in bearings.

This dissertation attempts to develop suitable guidelines for inspection of cones and conical frustums using probe-type coordinate measuring machines. The sampling problem, the path determination, and fitting of form zones are each addressed in great detail. Moreover, an integrative approach is taken for form verification and detailed experimental analysis is conducted as a pilot study for demonstrating the need for the same. Three separate sampling methods are derived: Hammersley, Halton-Zaremba, and Aligned Systematic; at various sample sizes using sampling theory and prior work in two dimensional sampling. A path plan is developed to illustrate the complexity of employing these sampling strategies for data sampling in cones. Linear and nonlinear deviations are formulated using optimization and least-squared methods and solved to yield competitive solutions. Comprehensive experimental analysis investigated issues of model adequacy, nesting, interactions, and individual effects, while studying conicity as a response variable in the light of sampling strategies, sizes, cone surface areas, and fitting methods.

In summary, an orderly procedure for sampling and fitting cones is developed which can lead to the development of comprehensive standards and solutions for industry.

DIMENSIONAL MEASUREMENT OF CONICAL FEATURES USING COORDINATE METROLOGY

CHAPTER 1

INTRODUCTION

In any discrete mechanical manufacturing process, manufactured features always vary from their nominal values in some random and/or systematic manner that manifests as errors. In order to maintain part quality, interchangeability, and functionality, geometric tolerances or constraints are usually assigned to those features. Measurement of products is considered as a basic function to assure that the products meet the design standards and to achieve customer satisfaction.

Inspection using Coordinate Measuring Machines (CMMs) is predominantly employed in mechanical manufacturing industries (Groover, 2001). In coordinate metrology, inspection of discrete manufactured parts is affected by a variety of data collection and data fitting methods. Usually data or sample points are collected intuitively with simple schemes for measurement locations. The commonly practiced methods are the uniform sampling and the random sampling methods (Liang et al., 1998b). Since probe-type CMMs are coordinate sampling machines, the sample deviations are only part of the deviation space that ought to be examined. Theoretically, if all points on a workpiece can be measured, then their real deviations

from ideal shape could be identified. This is difficult in practice. Hence, a good sampling strategy consisting of a selected sample size and locations is needed for efficiently collecting data.

Once the sample points have been obtained, data fitting methods are applied to describe the part feature. The errors introduced by the fitting procedure must conform to the specified design tolerance, given that the manufacturing operations are able to make the products according to the design standards. The least squares method (LSQ) is widely used in industry to fit the measured points in spite of the fact that it might overestimate form tolerances. LSQ often leads to the unnecessary reworks and higher production costs. As a result, inspection procedures of manufactured parts with three-dimensional (3D) complex features such as cone or torus have been inconsistent, somewhat unreliable, and/or unavailable. Data collection and data fitting procedures for such features should be studied more extensively to improve inspection procedures and assure better quality of parts.

To help circumvent the adequacy of the data collection problems, Menq et al. (1990) suggested a statistical sampling plan to determine a suitable sample size which can represent the entire population of the part surface with sufficient confidence and accuracy. A trade-off between the measurement time, data processing time, cost and the number of measurement points was taken into consideration along with manufacturing process capability, tolerance specification, and an assumption that the deviation is normally distributed around the nominal value. However, the sample locations were not taken into account. This might lead to some confusion in

measuring data. Moreover, the normality assumption is not true when systematic errors exist or when local geometric attributes or process deflections have a direct effect on the formation of the deviations.

Historically, dimensional surface measurements have involved the use of deterministic sequences of numbers for determination of sample coordinates (Woo and Liang, 1993; Woo et al., 1995). According to their studies, two sampling methods called the Hammersley sequence and Halton-Zaremba sequence outperformed the uniform sampling method, both theoretically and experimentally. The lower bounds of discrepancy (from accuracy) were determined for these methods and compared to that of uniform sampling. The clear advantage of the mathematical sequences is that their Root-Mean-Square (RMS) error is lower than that of the uniform sampling while preserving the repeatability of sampled points. The mathematical foundations of those suggested sequences are based on the theorems proposed by Roth (1954), Hammersley (1960), and Halton and Zaremba (1969).

In addition, a sampling strategy which could be used to specify a set of measuring points that led to adequately accurate sampling while minimizing the sampling time and cost was proposed by Lee et al. (1997). The characteristics such as geometric features, manufacturing processes, and surface finish were taken into consideration in determining such sampling strategy. A comparison between promising sampling strategies was shown while maintaining the same level of accuracy. The results obtained exhibited that the sampling strategy based on the Hammersley sequence outperformed those of the uniform sampling method and the

random sampling method. This implies that the commonly practiced procedures, the uniform sampling and the random sampling, for measurement locations are far from optimal. Liang et al. (1998b) also presented similar results with the Zaremba sequence method for surface roughness measurement. Similarly, Kim and Raman (2000) investigated different sampling strategies and different sample sizes for flatness measurement. Their results suggested similar findings to others' studies mentioned before.

In spite of the need for having a sampling strategy to resolve data collection problems, the advantages of such plans have not yet been fully recognized and applied for complex features. Hence, the sampling strategies should be developed and analyzed for complex feature surfaces.

In data fitting, geometrical tolerances are used as defined by the ANSI Standard Y14.5M-1994 (ASME, 1995), to ensure the high quality and reliability of precision manufacturing products. The Standard "establishes uniform practices for stating and interpreting principles and methods of dimensioning, tolerancing, and related requirements for use on engineering drawings and related documents". Geometrical tolerances state the maximum allowable variations of individual and related features from the perfect geometry specified on the design drawing. The so-called minimum tolerance zone is also covered in the ANSI Standard (ASME, 1995). However, it gives very little direction concerning the evaluation of these zones. The most commonly used method for zone estimation in practice is the least squares method (LSQ) due to its uniqueness, efficiency, robustness, and simplicity for linear

systems. Also, it could be applied to every form tolerance. Nevertheless, a theoretical problem of LSQ is that it does not guarantee a minimum zone as defined by the ANSI Standard. In other words, it might overestimate the tolerance zone since it attempts to minimize the sum of the squares of the errors and does not attempt to minimize the zone of the errors directly. This results in rejecting some good parts. In addition, if the LSQ is applied perpendicularly to the imaginary mean features, the resulting normal equations are very complex. In case of three-dimensional features, the solutions of the normal equations become even more complicated (Murthy and Abdin, 1980; Traband et al., 1989). Hence, many researchers have suggested improved techniques that are simpler and better than the LSQ method to determine such zone solutions. These techniques can be roughly categorized into two groups: computational geometry based approaches and numerical based approaches.

The former approaches utilize the properties of convex hull, EigenPolyGon (EPG), Voronoi diagrams, and control line/plane rotation scheme (CLRS/CPRS) in developing minimum zones. Such approaches (Traband et al., 1989; Hong et al., 1991; Roy and Zhang, 1992; Roy, 1995; Huang et al., 1993a and 1993b) are computationally efficient because they exploit the problem structure but are limited to particular features. The computational efficiency becomes minor in the modern day due to the aggressive advancement of computer technologies. This approach is very difficult to be extended to cover other features if at all possible. The extensions may not deal with the complex shapes properly. For example, Roy (1995) modified the Voronoi diagram technique for circularity to estimate cylindricity tolerance using

profile tolerance definition. A profile as defined by the ANSI Standard is "the outline of an object in a given plane (two-dimensional figure) by projecting a three-dimensional figure onto it". The elements of a profile are straight lines, arcs, and other curved lines. Hence, only the tolerance estimations of those elements are verified individually. Such a procedure may be impractical in cases where accuracy of the whole profile is a requirement. Therefore, the use of profile tolerancing should be limited to only the necessary cases where the equations of the inspected features are unable to be determined.

The numerical or optimization based approaches use linear or nonlinear models for errors and perform an optimization to determine the minimum zone. They are flexible since they can be extended to cover many form tolerances but are often not computationally efficient, especially for nonlinear equations. Nevertheless, the advancement of computer technologies, both hardware and software, helps ease this cause.

There are quite a number of articles dealing with basic features such as straightness, circularity, flatness, and cylindricity. The corresponding equations for those features have been investigated and optimization models have been suggested to fine-tune the minimum zone solutions. Prior to the recent computational advancements, if the equations of the surface features obtained were too complicated, a limacon approximation (Chetwynd, 1979; Chetwynd, 1985) and the well-alignment of the objects (Shunmugam, 1986; Shunmugam, 1987a and 1987b) were used to find the easier forms. Many optimization algorithms such as simplex search, Monte Carlo

search, sequential quadratic programming, neural network interval regression method, and genetic algorithm have been employed to verify the minimum zone solutions.

Interestingly, the form tolerances for cones, spheres and other such complex shapes are left to be dealt-with by the use of profile tolerance definition, except in few cases. The corresponding equations for cones are very complex that has partially led to a relative absence of research works dealing with the conicity tolerance in the literature.

Sufficient number of industrial parts such as nozzles, tapered cylinders, frustum holes and tapered rollers in bearings possess conical features that must be efficiently inspected for form. Considering these many applications of conical shape objects, cone tolerances and its sampling strategies should be studied more exclusively and extensively. The need to develop effective guidelines for conicity measurement is the subject of this dissertation. The objective of this dissertation is to address sampling, path determination, and zone estimation for conicity, within an integrated framework.

Chapter 2 presents a summary of the literature regarding data collection and data fitting methods, machined part inspection, sampling strategies, minimum tolerance zone verification, and techniques for sampling and minimum zone estimations for conical features. Chapter 3 defines the specific problems addressed by this dissertation. Chapter 4 describes the development of sampling strategies for cone inspection. The steps in the development of the corresponding equations are discussed with particular attention given to their validity. Chapter 5 addresses a

simple method for generalized CMM probe path planning in cone verification. The limitation of CMM motion planning is discussed. The experimental methodology is presented in Chapter 6. This explains the experimental model and its procedure. Chapter 7 presents the derivation of the related equations for minimum zone cone verification in detail. This includes discussions of the limacon approximation, the least square based method, and the linear and nonlinear optimization models. Chapter 8 discusses the results of data analysis. The final chapter, Chapter 9, presents the contributions and conclusions of this dissertation along with recommendations for future research.

CHAPTER 2

LITERATURE REVIEW

This chapter presents a review of the pertinent literature in dimensional inspection and discrete measurement. The first section provides a tutorial on tolerancing as depicted in the ANSI Standard. A brief introduction of CMMs is presented in the second section and is followed by a review of literature addressing the sampling methods used in data collection for measurement inspection. A review of literature addressing the CMM inspection path planning algorithms used for automatic inspection process is discussed in a fourth section. Last but not the least, potential minimum zone procedures for conical feature inspection are presented. This final section is separated into two sub-categories, computational geometry-based procedures and numerical based approaches.

2.1 Tolerance Terminology

This section introduces terminology and a brief overview of tolerances as defined in ANSI Y14.5M-1994 (ASME, 1995). The definition of conicity is presented in Subsection 2.1.2. The terminology used in engineering drawings and inspection are reproduced here from ANSI standards:

Nominal Dimension is the designation used for the purpose of general identification of the dimension on the engineering drawing.

Basic Dimension is the dimension that a part can vary from the specified dimension within tolerances.

Limit Dimension is the maximum and minimum sizes assigned by the designer for a tolerance dimension; and are also called limits.

Maximum Material Condition (MMC) is a feature of a finished part containing the most material permitted by tolerance dimension. That is, the internal features like holes, slots, etc. are at their minimum size or the external features such as shafts, keys, etc. are at their maximum size.

Least Material Condition (LMC) is a feature of a finished part containing the least material permitted by tolerance dimension. That is, the internal features are at their maximum size or the external features are at their minimum size.

Allowance is the minimum clearance space intended between the MMC of mating parts. Therefore, allowance represents the tightest permissible fit and is simply the smallest hole minus the largest shaft.

A nominal dimension is the theoretical or true size. This can be obtained only if the perfect manufactured parts are achieved. However, such perfection is very likely impossible due to variations in machining such as operators' skills, tools characteristics, machines characteristics, and cost. Tolerances are the total amount by which a specified dimension is permitted to vary. For example, a dimension given on the engineering drawing as 12" ± 0.4" means that it may be 11.6" or 12.4" or somewhere in between. In addition to size, there are five types of geometric tolerances identified as follows:

(1) tolerances of location,

(2) tolerances of form,

(3) tolerances of profile,

(4) tolerances of orientation,

(5) tolerances of runout.

2.1.1 Tolerances of Location

According to the ANSI Y14.5M-1994 (ASME, 1995), location includes position, concentricity, and symmetry used to control the following relationships:

(1) center distance between such features as holes, slots, bosses, and tabs,

(2) location of features as a group, from datum features, such as plane and cylindrical surfaces,

(3) coaxiality of features,

(4) concentricity or symmetry of features.

Therefore, the tolerances of location define a zone within which the above relationships are permitted to vary from a true or ideal location. Datum reference is usually required.

2.1.2 Tolerances of Form

"Form tolerances are applicable to single (individual) features or elements of single features" (ASME, 1995). Some common types of form tolerances such as straightness, flatness, circularity or roundness, and cylindricity are illustrated according to the ANSI Y14.5M-1994 (ASME, 1995) as follows:

Straightness is a condition where an element of a surface, or an axis, is a straight line as shown in Figure 1.

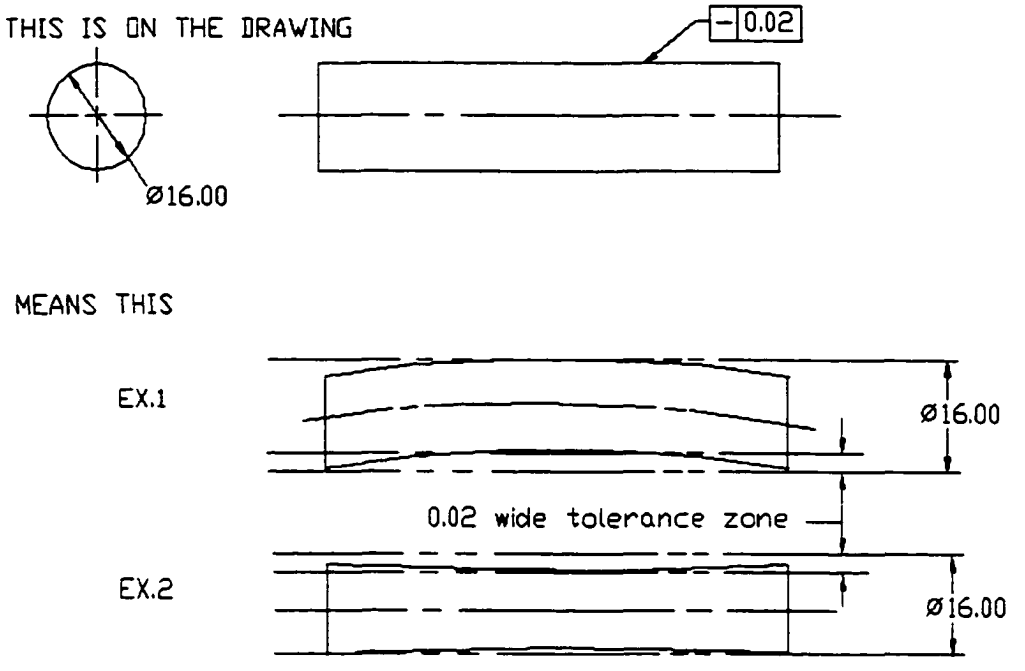


Figure 1. Specifying Straightness of Surface Elements

(Source: ANSI Y14.5M-1994).

Flatness is the condition of a surface having all elements in one plane as depicted in Figure 2.

Circularity (Roundness) is a condition of a surface where:

(a) for a feature other than a sphere, all points of the surface intersected by any plane perpendicular to an axis are equidistant from that axis,

(b) for a sphere, all points of the surface intersected by any plane passing through a common center are equidistant from that center.

The circularity is illustrated in Figure 3.

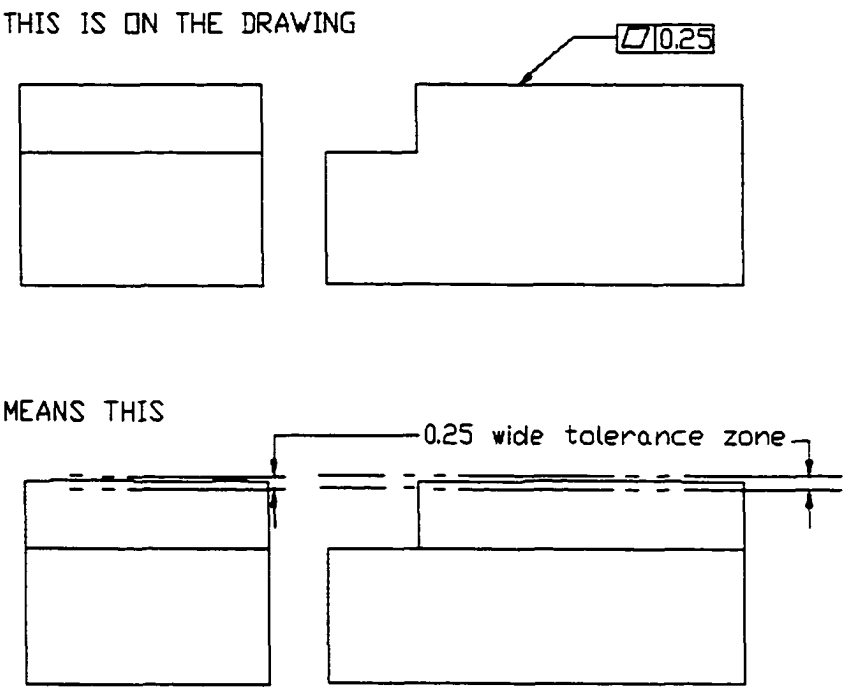


Figure 2. Specifying Flatness (Source: ANSI Y14.5M-1994).

Cylindricity is a condition of a surface of revolution in which all points of the surface are equidistant from a common axis as shown in Figure 4.

Conicity is a condition of a surface generated by rotating the hypotenuse of a right triangle about one of its leg (axis) with its vertex above the center of its base. A conicity is depicted in Figure 5. The conical frustum created by slicing the top off a cone with the cut made parallel to the base is considered a type of a circular cone. Hence, the definition of conicity is extended to cover the conical frustum as well. It may be stated that many practical applications featuring cone features are frustums rather than true cones. Therefore, a form tolerance specifies a zone within which the

considered feature must be contained. Further, it must be noted that the conicity has not yet been clearly defined by the ANSI Y14.5M-1994 (ASME, 1995). "A profile tolerance may be specified to control the conicity of a surface in either of two ways: as an independent control of form, or as a combined control of form and orientation" (ASME, 1995).

2.1.3 Tolerances of Profile

"A profile is the outline of an object in a given plane (two-dimensional figure). Profiles are formed by projecting a three-dimensional figure onto a plane or by taking cross sections through the figure. The elements of a profile are straight lines, arcs, and other curved lines" (ASME, 1995). For example, Figure 6 shows a profile of a plane surface.

2.1.4 Tolerances of Orientation

"Angularity, parallelism, perpendicularity, and in some instances, profile are orientation tolerances applicable to related features" (ASME, 1995). The following terminologies are reproduced from the ANSI Y14.5M-1994 (ASME, 1995):

Angularity is the condition of a surface, center plane, or axis at a specified angle (other than 90°) from a datum plane or axis. Figure 6 also shows an angularity.

Parallelism is the condition of a surface or center plane, equidistant at all points from a datum plane; or an axis, equidistant along its length from one or more datum planes or a datum axis. Figure 7 depicts such condition.

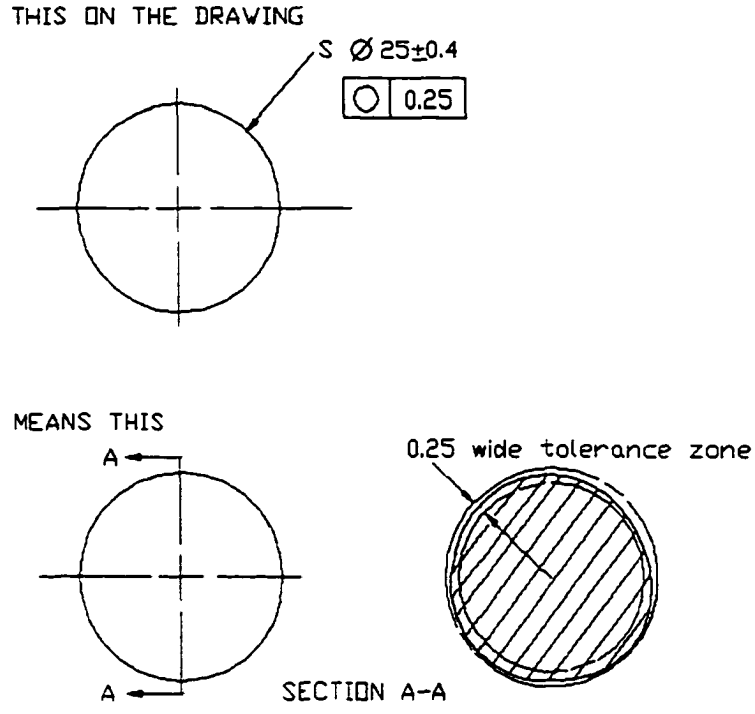


Figure 3. Specifying Circularity for a Sphere (Source: ANSI Y14.5M-1994).

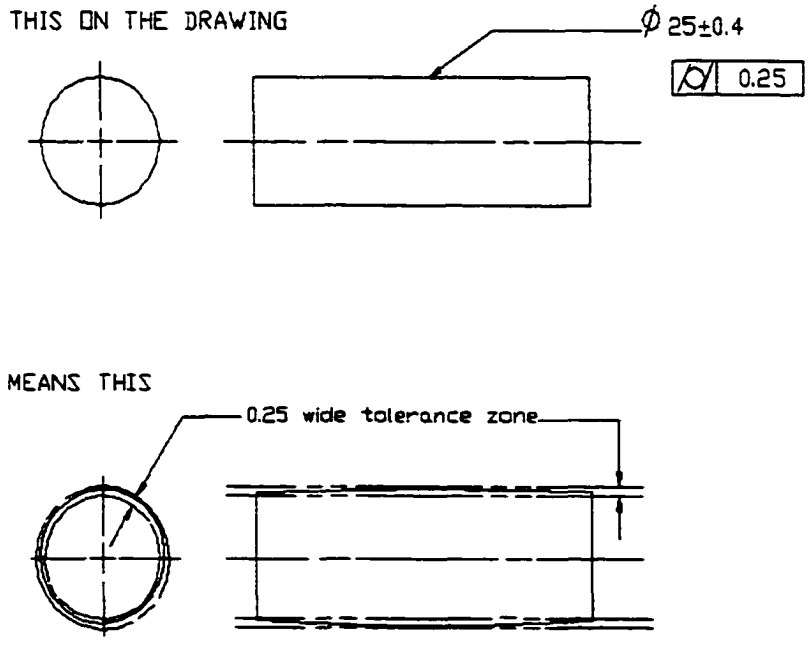


Figure 4. Specifying Cylindricity (Source: ANSI Y14.5M-1994).

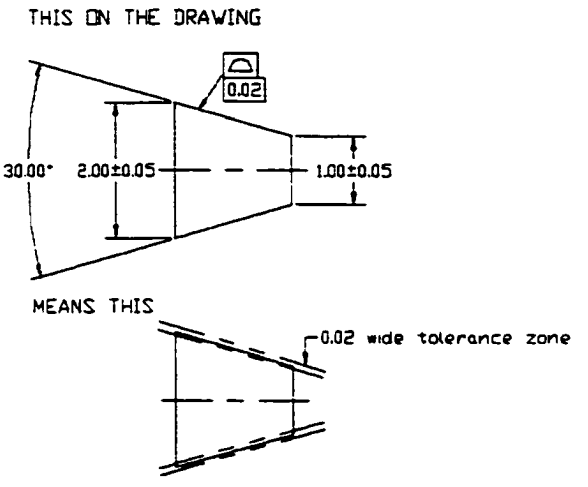


Figure 5. Specifying Conicity (Source: ANSI Y14.5M-1994).

Perpendicularity is the condition of a surface, center plane, or axis at a right angle to a datum plane or axis. Figure 6 also shows a perpendicularity of a shoulder feature to datum axis A.

Therefore, the orientation tolerance specifies a zone defined by two parallel planes at the specified basic angle from one or more datum planes or a datum axis within which the surface or center plane or the axis or the line element of the considered feature must lie.

2.1.5 Tolerances of Runout

"Runout is a composite tolerance used to control the functional relationship of one or more features of a part to a datum axis" (ASME, 1995). There are two types

of runout control, circular runout and total runout. The type selected is dependent upon design requirements and manufacturing considerations.

The ANSI Y14.5M-1994 (ASME, 1995) defines dimensioning and tolerancing to standardize and harmonize the United States practices and methodology with the universal standards. This should improve coordinating and integrating these techniques into electronic data systems. However, it gives very little direction regarding the evaluation of these zones and the definition of the conicity.

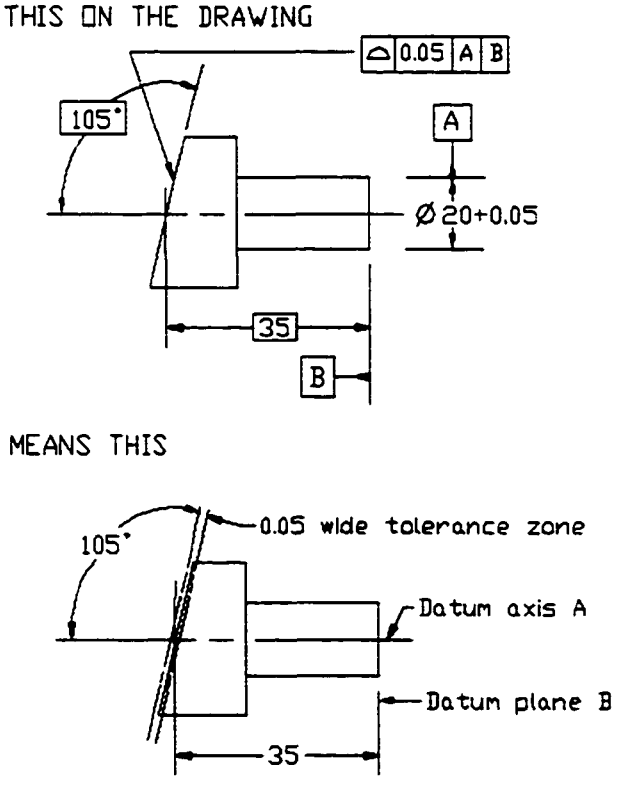


Figure 6. Specifying Profile of a Plane Surface (Source: ANSI Y14.5M-1994).

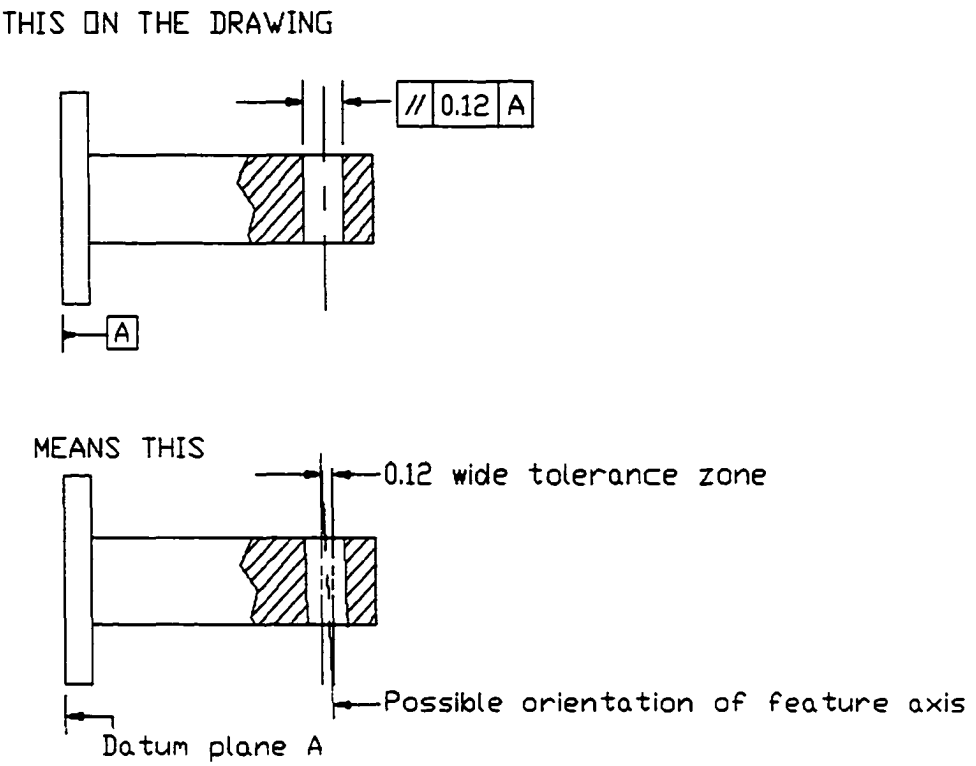


Figure 7. Specifying Parallelism for an Axis (Source: ANSI Y14.5M-1994).

The International Organization for Standardization (ISO), a worldwide federation of national standards, discusses conicity tolerances in ISO 7388-1:1983/Add 1:1984. Tolerancing of cones is also presented in Henzold (1995).

2.2 Coordinate Measuring Machines (CMMs)

Inspection is the means to determine the quality of product/process. It is traditionally done using labor-intensive methods that are time consuming and costly (Groover, 2001). Automated inspection is an alternative to the manual inspection and

almost always reduces inspection time implying better cost effectiveness. A coordinate measuring machine is an electromechanical system designed to measure/verify the actual shape and dimensions of an object and compare these with the desired shape and dimensions as specified on an engineering drawing for inspection of the manufactured parts. In general, a basic CMM is composed of the following components: (1) probe head and probe to contact the measured part surface, (2) mechanical structure that provides motion of the probe in the Cartesian coordinates and displacement transducers to measure the coordinate values of each axis, (3) drive system and control unit to move each of the three axes, and (4) digital computer system with application software (Groover, 2001).

When a part is to be measured, it is placed on a worktable that provides a stable and precision surface to locate and clamp the workpiece (Brown & Sharpe Mfg. Co., 1996). The contact probe, a key component of a CMM, is used to detect the workpiece features by indicating when contact has been made with the part surface during measurement. Its tip is normally a ruby ball (aluminum oxide) providing high hardness for wear resistance and low density for minimum inertia. Immediately after the contact has been made between the tip and the object surface, the coordinates of the probe are measured by displacement transducer associated with each of the three axes (X, Y, Z) and recorded by the CMM controller (a computer system with application software). Probe compensation is automatically corrected for the probe tip radius by measurement software (in the present case, the TUTOR™ software). All probes must be qualified before accurate measurements can be made.

The main purposes are to (1) calculate the probe tip diameter and (2) learn the location of the center of the probe tip in the measuring volume (Brown & Sharpe Mfg. Co., 1996). The most widely used probes are touch-trigger probes that are designed to give the optimum results when the probe hits are taken perpendicular to the probe body. If hits are not taken perpendicular to the object surface, skidding may occur causing inconsistent and non-repeatable results. Probe hits taken parallel to the probe body are not as repeatable as those taken perpendicular to the body. The hits neither perpendicular nor parallel to the body give results that are less repeatable than those taken parallel. Probe hits taken at an angle to the probe body are not repeatable and should be avoided if possible. If probe points are taken within 80 degrees of perpendicular, skidding is much less than one micron or 0.000040 inch (Brown & Sharpe Mfg. Co., 1996). Also, the slow measurement velocity of the probe should be used to avoid damages that might occur to the probing system and overtravel due to momentum. This can be accomplished by using the machine parameters settings module in the CMMs (TUTOR™ software in this case) to configure the suitable speed.

Positioning the probe and measuring the object can be accomplished by using manual operation and/or direct computer control (DCC). In direct computer control mode, a CMM operates like a computer numerical control (CNC) machine. It is motorized and the movements are controlled by a digital computer system running the measurement software (TUTOR™). Similar to a CNC machine, the DCC CMM requires part programming that can be prepared by using manual leadthrough or off-

line programming. In the manual leadthrough method, the operator leads the probe through the various motions (positioning and measuring) required in the inspection sequences. These motions are recorded into the control memory of the CMM controller. Then the controller plays back the program to execute the inspection sequences. Off-line programming as its name suggests is prepared off-line based on the drawing of the inspected object and then downloaded to the CMM controller for execution.

The advantages of using CMMs over manual inspection methods are (Groover, 2001) (1) reduced inspection cycle time, (2) flexibility, (3) reduced operator errors, (4) greater inherent accuracy and precision, and (5) avoidance of multiple setups.

A flexible inspection system (FIS) takes the capability of the CMMs one step further. A FIS is a highly automated inspection workcell consisting of one or more CMMs and other types of inspection equipment plus the parts handling systems. With all the mentioned advantages, CMMs are one of the most widely used technologies in contact inspection. In addition, another category of inspection techniques is noncontact inspection. Noncontact inspection technologies utilize sensors set up at a certain distance from the object to measure the desired features. They can be classified into two groups: (1) optical and (2) nonoptical. Optical inspection techniques use light to accomplish the measurement. Examples are machine vision systems, scanning laser systems, linear array devices, and optical triangulation techniques. The main difference between machine vision, the most

popular technique, and other optical techniques is that machine vision tends to imitate the capabilities of human optical sensory system, both the eyes and the interpretation powers of the brain. The others are operative in much simpler modes. Nonoptical inspection technologies utilize energy forms other than light to perform the inspection. Examples of these energies are electrical field, radiation, and ultrasonics (Groover, 2001).

2.3 Sampling Strategies for Dimensional Surface Measurement

Inspection of discrete manufactured parts using CMM is affected by a variety of data collection methods. Usually data or sampled points are collected intuitively with a simple scheme for measurement locations. The commonly practiced methods are the uniform sampling and the random sampling methods. Once the sample points have been obtained, the data fitting method is applied to describe the part feature. Problems may arise when all the sampled points or deviations fall within tolerances while some non-sampled points are in fact out of bound. This implies that the sampling strategy used must be very reliable so that the sample points are regarded as a good representative of the entire surface. Different sample size with the same sampling method may give different results. Clearly, sampling accuracy depends on both sample size and sample locations. Theoretically, if all points on a workpiece can be measured, its real deviations should also be identified and analyzed. However, it is practically impossible. Hence, a good sampling strategy consisting of sample size and locations is definitely needed for efficiently collecting data at the minimum cost.

To help circumvent the adequacy of the data collecting problems, Menq et al. (1990) suggested a statistical sampling plan to determine a suitable sample size which can represent the entire population of the part surface with sufficient confidence and accuracy. A trade-off between the measurement time, data processing time, and cost and the number of measurement points were taken into consideration along with manufacturing process capability, tolerance specification, and an assumption that the deviation is normally distributed around the nominal value. However, the sample locations were not taken into account. This might lead to some confusion in measuring data. Moreover, the normality assumption is not true when systematic errors exist or when local geometric attributes have direct effect to the formation of the deviations.

Caskey et al. (1992) examined the interaction between the various procedures involved in mechanical parts measurement using CMMs. The experimentation was done on computer models of features and on actual measurement process on a CMM including measuring machine and process characterization, random measurement errors, probing performance, and measurement methodology. The fitting algorithms used were the least squares method and the mini-max technique. The efficiency of a sampling strategy, stratified sampling, was tested on a basic geometric feature, plane, using those fitting algorithms. In addition, a set of sample sizes was taken into consideration to find the better fitting results. The results obtained showed that there were rooms for improvement for the fitting algorithms and the sampling strategies with higher but acceptable sample sizes.

Woo and Liang (1993) and Woo et al. (1993) investigated the number and location of the discrete samples for the dimensional measurement of 2D machined surfaces. Accuracy and time were considered as the criteria for assessing sampling errors. Accuracy was expressed by a mathematical notion called the discrepancy of a finite set of N points for which a lower bound exists. Time could be quantified in terms of N. The deterministic sequences of numbers were used as sample coordinates. The Hammersley sequence was compared against the uniform sampling. The surface measurements results of the Hammersley points showed a remarkable improvement over those of the uniform points in reducing the number of samples and units of time, while maintaining the same level of accuracy.

Hocken et al. (1993) discussed sampling issues in coordinate metrology. There were various factors that may affect mechanical parts measurement such as systematic and pseudo-random machine errors, surface and forms errors, fitting algorithms, and sampling strategies. There were also several issues discussed in each factor. Systematic and pseudo-random machine errors consisted of parametric and machine errors, probe errors, thermal errors, and so on. Surface and form errors dealt with surface roughness, waviness, and form errors due to different manufacturing processes. Fitting algorithms employed two types of algorithms, the least squares method and the mini-max method. Sampling strategies dealt with metrology sampling strategies and production sampling strategies. Both strategies should be considered with the minimum number of points possible. Computer experiments were conducted with line, plane, circle, sphere, and cylinder. The results obtained

showed that "current inspection techniques, used daily in manufacturing, drastically under-sample geometric features in the presence of unknown part form and measuring machine errors." This led to two following corollaries. First, much higher sampling densities than those in current use must be incorporated. If inspection times were not to be increased, a new type of measuring machine capable of high-speed surface scanning would be needed. Second, the intelligent decision systems were required to control the inspection and analysis process regarding how to measure a part and the choice of algorithms.

Woo et al. (1995) attempted to answer two basic questions regarding the relationship between the sample size and the error in measurement. The first question raised the issue of increasing the accuracy of sampling for the same sample size. The second question dealt with the reduction of the sample size while maintaining the same level of accuracy. The answers to both questions were relevant to the sample point distribution. A couple of mathematical sequences, the Hammersley sequence and the Halton-Zaremba sequence, were selected since their discrepancy lower bounds were nearly optimal comparing to a lower bound prescribed by Roth (1954). Compared against the uniform sampling, both sequences outperformed the uniform sampling theoretically and experimentally. The clear advantages of the mathematical sequences are that their discrepancy (or deficiency) is lower than that of the uniform sampling and their sample coordinates are equivalently repeatable. Also, there was no discernable difference in the performance between the Hammersley and the

Halton-Zaremba in 2D space. The choice is just a matter of convenience whether the sample size is a power of two or not (a requisite for the Halton-Zaremba).

A feature-based sampling strategy integrating the Hammersley sequence and the stratified sample method was proposed by Lee et al. (1997). The characteristics such as geometric features, manufacturing processes, and surface finish were taken into consideration in determining such sampling strategy. The geometric features included flat, circular, conical, and hemispherical features. There were two ways to select the specified measuring points by starting from the central point or the edge point. The central point approach could be applied for a workpiece with a non-uniform surface finish, especially with the rough edges. Otherwise, the edge point approach should be used. A comparison between the Hammersley sequence based sampling, the uniform based sampling, and the random based sampling was shown while maintaining the same level of accuracy. The results obtained exhibited that the sampling strategy based on the Hammersley sequence outperformed those of the uniform sampling and the random sampling. Clearly, the commonly practiced procedures, the uniform sampling and the random sampling, for measurement locations are far from optimal.

Liang et al. (1998a and 1998b) theoretically and experimentally presented the results of surface roughness measurement with a 2D optimal sampling strategy, the Zaremba sequence based sampling. Liang et al. (1998a) discussed the theoretical advantage of such an optimal sampling strategy which can be obtained by utilizing the point sequence developed in Number Theory. A machined surface was modeled

as a Weiner process and its root-mean-square (RMS) error was equivalent to the L_2 discrepancy of the complement of the sampling points. The relationship was also shown to hold for more general surfaces. Liang et al. (1998b) addressed an application of the Zaremba sequence as an optimal sampling sequence for the surface roughness measurement. The experiment was done on a computer simulation to demonstrate the effectiveness of the Zaremba sequence based sampling method over the uniform and the random sequence based sampling methods. The Zaremba sequence required almost quadratically fewer points than did the uniform or the random sequence while maintaining the same order of accuracy in measurement.

Namboothiri and Shunmugam (1999) introduced a determination of sample size in form error evaluation. A new parameter based on the asymptotic distribution of the form errors was proposed with the assumption that the errors followed a normal distribution. The new parameter, which was a function of sample size and the corresponding values of errors, calculated the probability that the form error was less than a predicted value. Simulation studies and their results were also discussed to verify its capability. Moreover, sampling patterns played important roles in measurements. If the maximum error point could be identified at the initial stages following a sampling pattern, then further prolonging of measurement process was not necessary. As a result, the measurement time (cost) could be saved.

Kim and Raman (2000) investigated accuracy and path length (time) of four different sampling strategies and five different sample sizes for flatness measurement in actual experiments with a CMM. The sampling methods used were the

Hammersley sequence sampling, the Halton-Zaremba sequence sampling, the aligned systematic sampling, and the systematic random sampling. Sample sizes of 4, 8, 16, 32, and 64 were studied. A two-factor factorial design with 30 replicates was used for experiment and analysis. The main effects of sample size and sampling method were significant to the accuracy of the flatness measurement. A significant interaction between sample size and sampling method was also evident. The length of the probe path was taken into consideration with respect to the two factors using a computer simulation. The shortest length of the CMM probe path was computed based on the traveling salesman problem (TSP) algorithm. A trade-off priority coefficient between the accuracy of flatness and the shortest CMM probe path was then developed to determine the effects of accuracy and path length while selecting sampling strategies and sample size. The most efficient sampling method was varied according to the priority coefficient and the sample size.

An adaptive search-based selection of sample points for form error estimation was proposed by Badar et al. (2000 and 2001). This method used the search-based optimization methods for reducing the sample size while maintaining the same level of accuracy. Examples shown were straightness and flatness. For straightness estimation, region-elimination search was introduced. For flatness verification, Tabu search and a hybrid search were used. The hybrid search consisted of Coordinate search, Hooke-Jeeves search, and Tabu search. A number of initial points were chosen randomly to verify an inspected feature first. Points were then added based on the mentioned search methods, finding improvements in the zone fit in both

maximum and minimum directions. After the maximum and minimum deviations were reached, their corresponding points were added to the set of initial points. The form error was then computed. The analysis presented identifies some potential for sample reduction in coordinate methodology.

2.4 CMM Probe Path Planning for Dimensional Inspection

The CMM probe path planning allows the determination of the inspection path joining the CMM measurement points based on the geometry of the inspected part model and the inspection specification. Few works have been done in the development of the CMM probe path planning. The majority of the studies has concentrated on generating the collision-free inspection path for parts having multiple surfaces.

Lu et al. (1994) developed an algorithm for generating an optimum CMM inspection path. A modified 3D ray tracing technique was used in conjunction with an octree database of a CMM configuration space to detect obstacles between any two target points. This ray tracing technique utilized the special geometry of the cubic octant to simplify the search for obstacles in the octree data structure. The algorithm also used the global information on obstacle vertices to reduce the zigzag nature of the path by imitating a line of one's vision in avoiding the obstacles and finding all new vertices that were on the tangent contour of the object. These silhouette vertices were again checked for a free path. The iterative steps between the collision detection process and the silhouette vertex selection process were continued

until a vertex was found to be on the potential collision-free path. The silhouette vertices were then advanced to the target again using the ray tracing and the above iterative steps. The total distance from a start node to the target node was used to select the minimum cost path after all collision-free paths had been compared. Since the optimum collision-free path in a 3D space lied on the edge of a polyhedron, the vertex path must be processed to an edge path. A selection strategy was employed to ensure a correct edge path sequence by solving an optimization problem from edges and points. A simulation test and an experimental test were conducted. In addition, a comparison was made between a graphic interactive path planning method and the proposed algorithm. The total time taken by the algorithm was much less than that of the interactive graphic method.

Lim and Menq (1994) studied the accessibility of CMMs and its path generation in dimensional inspection. Probe orientation had not been paid much attention in inspection planning research because it does not affect the tip trajectory significantly. However, for a complex surface, probe orientation might be needed to be addressed to avoid a collision with an inspected part. Feature accessibility analysis and optimal angle search were used to automatically determine the probe orientation. The analysis of half-space and ray-tracing techniques were applied to find a collision-free probe orientation while inspecting a part. All the feasible probe orientations were determined first and the best angle was then selected. A minimum set of required angles for the entire path was chosen by the simple search algorithm through all possible combinations. This search algorithm was fast but not a complete search.

Hence, better heuristic search should be used for a more thorough search. The path generation included the probe orientation information by grouping the inspection points with the same probe angle. Also, the probe approached the inspection point at a direction similar to the angle. These improved the path by reducing the number of necessary rotations and the chances of collision. Computer simulations in a computer aided design (CAD) system were used to demonstrate the proposed techniques.

Yau and Menq (1995) presented a hierarchical planning system using heuristics for path planning in dimensional inspection using CMMs. Instead of solving general cases, the objective was to automate the planning of a collision-free inspection path for dies and molds. Also, the issue of minimizing the path distance was not taken into account. The hierarchical structure consisted of three different levels of trajectory planning for the probe tip, the stylus, and the CMM column, respectively. First, an initial inspection plan was constructed by (1) selecting an available probe, (2) determining probe orientations based on the local accessibility analysis of the surfaces, (3) obtaining measurement points, and (4) connecting all the points together without considering collision. Second, a hierarchical procedure was initiated to find collisions for each path segment. If any, the path would be modified heuristically. This modification referred to the changes of the trajectory of the probe tip at the first level, the changes of the probe orientations at the second level, and the changes of the probe styluses at the third level. The resulting inspection was then replayed in a CAD environment before it was carried out by a real CMM. The computational time was proportional to the number of measurement points and

number of surfaces for collision detection and was quite efficient. Two experimental examples were tested to show the effectiveness of the path planning. The probe successfully traveled through the entire inspection path for each example without interference.

Kim and Raman (2000) studied the length of probe path with reference to the sampling strategy and sample size for flatness measurement on plates in addition to the issue of accuracy of measurement. The collision between the probe while positioning and an inspected object (plate) was highly unlikely due to the nature of the inspected part (flatness measurement). Instead, the focus of this work was to find the most suitable sampling strategies and sizes considering the accuracy and time (path length) factors. Therefore, the CMM probe path problem was formulated as a traveling salesman problem. TSP solution methods were then employed to minimize the total distance of the probe path while visiting every point generated, for a given sampling strategy and size.

2.5 Minimum Tolerance Zone Algorithms

Tolerance verification usually undertaken during measurement and inspection affects tolerance specification as well as process selection to achieve it. Form tolerance (for individual features) verification using CMMs has been studied extensively in the last fifteen years. The method of least squares (LSQ) is the most commonly used in CMM inspection for data fitting and many commercial machines use this method for tolerance zone estimation due to its uniqueness, efficiency,

robustness, and simplicity. Also, it can be applied to most geometries, quite easily. However, its major drawback in determining the tolerance zone is that it does not guarantee a minimum zone. In other words, it might overestimate the tolerance zone resulting in the rejection of some good parts. Hence, the minimum zone estimation methods have been pursued. The majority of the works in literature have dealt with straightness, flatness, roundness, and cylindricity.

The minimum zone evaluation methods can be largely divided into two categories, computational geometry approach and numerical approach. The computational geometry approach deals with algorithms and data structures. The information of the problem is organized in such a way that would permit the algorithms to run in the most effective manner. Some computational geometry methods such as convex hull, eigenpolygon, and Voronoi diagram are used in obtaining the minimum tolerance zones of basic features. This approach is computationally efficient since it exploits the problem structure but is limited to particular form tolerances. The numerical approach consists of using linear and nonlinear optimization methods with various numerical search techniques including intelligent ones such as genetic algorithms and neural networks. Its main advantage is flexible extension to cover various form tolerances; but it is not computationally efficient. Before the optimization model can be formulated, the relationship function of relevant parameters must be determined. There are generally two types of inspection error models: linear and nonlinear models. The linear error model can be obtained by using an approximation technique such as the limacon approximation.

The nonlinear deviations model can be extracted directly from the problem. Both models are then formulated into mathematical programming forms (decision variables, constraints, and objective function). Since the mathematical programming techniques may trap in local optima, different starting points coupled with the experimental verifications should assist them in getting a global optimal solution. The results from the LSQ method may not be optimal, yet are close enough. Thus, they are often used as the initial solutions.

2.5.1 Computational Geometry Based Algorithms

Traband et al. (1989) presented a computational geometry based method, a convex hull concept, in evaluating the straightness and flatness tolerances. According to Traband et al. (1989), the following two observations can be made about the minimum zone for straightness without violating the property of convex hull: (1) the minimum zone of a set of points is the minimum zone of the convex hull of set S, and (2) the minimum zone is parallel to one of the edges of the convex hull and one of the parallel supporting lines coincides with this edge. The computational complexity of the first algorithm suggested was $O(n^2)$. The improved algorithm was then developed using the observation that only a few pairs of points, antipodal pairs, on the convex hull admitted parallel lines satisfying the definition of a minimum zone. The antipodal pairs could be enumerated in $O(n)$ time (Preparata and Shamos, 1985). Using the antipodal pairs in determining the minimum zone reduced the complexity of the final algorithm to $O(n \log n)$. The authors proved these observations.

A similar procedure was employed for evaluating the flatness tolerance. However, determining the antipodal pairs for the 3D convex hull was more difficult than that for the 2D case. The generation of the antipodal pairs would take $O(n^2)$ time (Preparata and Shamos, 1985). Hence, the authors suggested that it would be easier to brute force the minimum zone from the convex hull by determining all possible combinations of zones. As a result, the computational complexity for this algorithm was $O(n^2)$.

The above procedures for straightness and flatness were suitable for on-line inspection process. Upon the addition of a new point to the hull, the minimum zone could be easily found by checking its location in the zone and computing the previously discussed algorithms if needed. Thus, this dynamic convex hull algorithm would take only $O(\log n)$ time between the successive inputs to update the hull. In addition, the obtained results were shown to be superior to those of the least squares method.

Le and Lee (1991) introduced another standard, called the minimum area difference center for evaluating the roundness. Even though this center was different from the most common standard, the minimum radial separation center, recommended by the American National Standards Institute (ANSI) in characteristics, the approach to finding both centers shared many commonalities. The authors presented an algorithm to compute the minimum radial separation center of a simple polygon G from the medial axis of the polygon and the farthest neighbor Voronoi diagram of the vertex set of the polygon. The computational complexity of this

algorithm was $O(n \log n + k)$ where n was the number of vertices of G and k was the number of intersection points of the medial axis and the farthest neighbor Voronoi diagram. Next, the relationship between both centers was disclosed and the minimum area difference center was derived. The center of a simple polygon G could be established from the nearest neighbor Voronoi diagram of the skeleton region elements, the farthest neighbor Voronoi diagram of the vertex set of the polygon, and the boundary edges of G that are not on the convex hull. Its computational complexity was also $O(n \log n + k)$ time, where n was the number of vertices G and k was the maximum of the number of intersection of the nearest neighbor Voronoi diagram of G with the farthest neighbor Voronoi diagram of the vertex set S of G, and the number of intersection of the farthest neighbor Voronoi diagram of the vertex set S of G with the internal boundary of G. Even though the minimum radial separation could be used to find the circularity, the application of the minimum area difference center remains to be explored.

Another computational geometry approach to minimum zone straightness was proposed by Hong et al. (1991). The relationship between a geometrical eigenpolygon and straightness was described. Then, the straightness algorithm was developed. The main idea of this work is very similar to the straightness convex hull based approach proposed by Traband et al. (1989). In addition, an analysis comparison between this method, the least squares method, and the minimax algorithm was tabularized. This method was superior to the method of least squares

and as good as the minimax method without difficulties caused by optimization approximations such as convergent and local optimum problems.

Roy and Zhang (1992) proposed a computational geometry based method in determining roundness error. The properties of convex hull and Voronoi diagrams were used to develop an algorithm for establishing the concentric circles which would contain all the measured points while minimizing the radial separation between the circles. It was evident from plane geometry that at least four points were required to determine a pair of concentric circles. Such circles created by these four points were not unique. Three possible cases of concentric circles might arise: (1) both outer and inner circles passed through two points, 2-2 model, (2) the inner circle passed through three points and the outer circle passed through only one point, 3-1 model, and (3) the inner circle passed through only one point and the outer circle passed through three points, 1-3 model. Initially, an exhaustive ad hoc algorithm using the mentioned necessary conditions for the establishment of a pair of concentric circles was introduced. However, the computational complexity was $O(n^4)$ which was too high.

To overcome this drawback, an improved algorithm was suggested. The more efficient procedure was as follows: (1) construct the convex hull from the simple polygon by using the Graham scan method in $O(n)$ time, (2) generate the Voronoi diagrams; the farthest Voronoi diagram from the convex hull and the nearest Voronoi diagram from the point set in $O(n \log n)$, (3) establish the pair of concentric circles with minimum radial separation for each of the following three cases, 2-2 model, 3-1 model, and 1-3 model, and (4) compare the results from the above three cases and

select the roundness error from the minimum among all cases. The computational complexity for the last two steps was $O(n^2)$. Hence, the overall complexity was $O(n^2)$. A comparison between this method and the method of least squares was also illustrated to show its superior performance to the least squares method.

Huang et al. (1993a) proposed a new minimum zone method for straightness analysis of any planar line or spatial line. This method rotated the enclosing lines in "half-filed" only during the data exchange process. The advantage of the half-filed data exchange process was that it screened out unwanted data points, which would make the mathematical model simpler and the computational time shorter. Using the least squares result as the initial condition, the data exchange scheme started with a 1-1 model where one control point was on one control line and another control point was on the other control line with both lines being parallel to the least squares line. Next the strict control line rotation scheme (CLRS) was executed to establish a 2-1 model. Two conditions for the minimum zone solution were: (1) at least three points must be in contact with the two enclosing parallel lines in the form of a 1-2 (or 2-1) model and (2) these three points must lie on the lines in an upper-lower-upper sequence or a lower-upper-lower sequence. Each control line would rotate according to its control point in the direction that would most likely yield one of the two sequences. Hence, only the points within a specified quarter-field for each of the two directions, equivalent to half-field search, would be considered. During the rotation of each control line, any point within the corresponding quarter-fields might become the first contact point depending on its position. Since each point would correspond

to a rotation angle, the very first contact point would be the one having the smallest angle with respect to the control line. However, there were four possible conditions of the 2-1 model that did not meet the required sequences. As a result, one of the control points must be discarded by being pushed inside the enclosing field. Clearly, the discarded point was the outside one on the two-point side. The remaining two points formed a 1-1 model again and the CLRS would start over. The whole procedure would be repeated until the minimum zone criteria were met. The results obtained from considered examples showed that this method was more efficient than the LSQ.

Huang et al. (1993b) extended Huang et al. (1993a)'s work to cover flatness analysis by using the similar scheme called the control plane rotation scheme (CPRS). The criteria for the minimum zone solution were: (1) at least four points must be in contact with the two parallel planes in the form of a 3-1 model or a 2-2 model, (2) in case of a 3-1 model, when projected onto the upper or lower plane, the single contact point must be inside of the triangle formed by the other three points, and (3) in case of a 2-2 model, when projected onto the upper or lower plane, the line linking two contact points on the same plane must intersect with the other line connecting the other two contact points. The procedure was similar to Huang et al. (1993a) as follows: (1) construct the fitted plane by using the method of least squares, (2) establish a 1-1 model with two control points and generate the planes parallel to the least squares plane from these two points, (3) establish a 2-1 (or 1-2) model by using the CPRS to obtain an alternate sequence when projected onto 2D space, (4)

determine a 3-1 or 2-2 model by turning to the side view of the 2-1 model until the three-point view became the two-point view and using the CPRS to obtain an alternate sequence again, (5) check the optimality conditions, then stop the procedure if the minimum zone solution was reached or discard the outside projected point on the two-point projected plane if the criteria were not met and repeat step 4. According to the attached results, this method clearly outperformed the least squares method. An application of this method was performed by Huang et al. (1993c) for on-line measurement of gage blocks using phase-shifting interferometry. The experimental results were quite consistent with the specified grade of the inspected gage blocks with only an uncertainty of up to 0.005 μm.

Roy and Zhang (1994) discussed a robust, computational geometry based technique similar to the one presented by Roy and Zhang (1992) to establish the roundness error of a measured workpiece in an industrial environment. The procedures consisted of the following steps: (1) establishment of a sorted set by using the quicksort method, (2) development of an outer convex hull and an inner convex hull, (3) development of a nearest Voronoi diagram and a farthest Voronoi diagram, and (4) calculation of the minimum radial separation for all three possible cases of establishment of a pair of concentric circles and selection of roundness error from the minimum among those three minimum separations. This algorithm yielded better results for a given set of measured points in comparison to other methods such as minimum inscribed circle, minimum circumscribed circle, and the least squares circle.

Roy (1995) discussed the criteria for assessing geometric characteristics of manufactured parts and the development of systematic procedures and algorithms for comparing measured geometric data from the parts with the specified drawing tolerances. The author recommended the methods proposed by Traband et al. (1989) for straightness tolerance and flatness tolerance and the method proposed by Roy and Zhang (1992) for roundness tolerance. A cylindricity tolerance was computed as follows: (1) divide the cylindrical surface into several cross sections and collect data points for each cross section, (2) calculate a pair of concentric circles with minimum radial separation and determine the center point of the circles for each cross section, (3) fit the least squares axis from the evaluated center points, (4) project all the cross-sectional data sets on a plane perpendicular to the least squares axis, (5) repeat step 2 to step 4 with the mapped data sets until the least squares axis remains the same between two consecutive iterations, (6) construct the outer and inner circles by using their center on the least squares axis for each section, (7) for external cylindrical features, pick the circle with the largest diameter from the set of outer circles, then establish the second cylinder making it smaller by the cylindricity tolerance value. The external feature was acceptable if the diameter of the second cylinder were smaller than the diameter of any of the inner circles. The internal cylindrical feature could be evaluated by the similar steps but opposite logic. Location tolerance and its verification were discussed by Roy (1995). Since a profile is used in this work, this method may be impractical in certain cases, particularly where accuracy of the entire profile is critical (ASME, 1995).

Roy and Xu (1995) also presented the development of computational algorithms for tolerance analysis for cylindrical surfaces in a computer-aided automatic inspection environment. 2D convex hulls and Voronoi diagrams were used to generate pairs of concentric circles and their center points. These pairs were then used to simulate the inspected surface and to determine the cylindricity. There were six steps involved as follows: (1) divide the cylindrical surface into several cross-sections and collect a set of measured points for each of its cross-sections, (2) calculate pairs of concentric circles with minimum radial separation from the collected points using 2D convex hulls and Voronoi diagrams and determine their center points, (3) select a pair with minimum radial separation as the profile on each cross-section, (4) find the axis for the cylindrical feature with a least squares method or geometric analysis method, (5) establish the inner and outer circles and collect all inner circles in a set (IC) and all outer circles in another set (OC), and (6) calculate a pair of concentric cylinders for the tolerance zone by identifying the inner cylinder with the smallest diameter in the set IC and the outer cylinder with the largest diameter in the set OC. An example data set for a cylindrical surface was tabulated along with the cylindricity outcome.

A transformation strategy for minimum zone evaluation of circles and cylinders was proposed by Lai and Chen (1996). This strategy employed a nonlinear transformation of coordinate systems to convert a circle into a line and a cylinder into a plane by using polar coordinates and cylindrical coordinates relationships, respectively. This nonlinear mapping could hold the distance relationship between

each measurement point. As a result, finding two concentric circles enclosing all the measurement points was equivalent to finding two parallel lines enclosing the same measurement points in converted coordinates. Then, the straightness algorithm described by Huang et al. (1993a) was applied. Similarly, this procedure could be extended to cylinders by obtaining two parallel planes enclosing the transformed measurement points and applying the flatness algorithm described by Huang et al. (1993b). Care must be taken in selecting the starting position of the mapping if the control points that were adjacent on the original surface were separated on each side of the line (for circles) or plane (for cylinders). A simple adjustment must be done by rotating all the points so that the control points would be on the same side. A series of inverse transformation procedures was then carried out to attain desired feature parameters. The simulated data were used to test the proposed methods. The results obtained indicated that the proposed techniques were more precise than the LSQ method while maintaining the same level of sensitivity in terms of number of data points used and the abrupt peak or valley in the measurement data.

Another convex hull based approach was proposed by Lee (1997) to evaluate flatness tolerance. This method, called the convex hull edge method, was a refined version of the convex hull method suggested by Traband et al. (1989). The author claimed that the original convex hull method could not successfully find all 2-2 models. The reason was that the minimum of maximum distances between pair of edges was not necessarily the minimum zone value. All the data points should be checked if they are contained within the two planes made by the pair. Then, the

minimum, instead of the maximum, of distances between feasible pair of edges is selected as the tolerance zone. With such potential problems, a new search technique was introduced. The minimum zone problem was decomposed into sub-problems each of which was associated with an edge of 3D convex hull. For each edge, the transformation of coordinate system and projection of the transformed points were applied to help tackle the problem easier. The corresponding tolerance in the form of either a 2-2 or a 3-1 model was computed from a 2-1 model of the 2D convex hull and the minimum of these tolerances for all edges became the minimum tolerance zone. The comparisons attached depicted that the method was comparable to other minimum zone methods. It always generated the minimum zone solution and was also computationally efficient.

Samuel and Shunmugam (1999) developed new algorithms based on computational geometric techniques for minimum zone and function-oriented evaluation of straightness and flatness. Even though the function-oriented form evaluation of surfaces had been paid very little attention to by researchers, it had practical significance as the contact between the parts in assembly occurred at their functional boundaries. The enveloping features actually determined the virtual sizes and the resulting assembly conditions. The deviations decide the functional properties such as contact and lubrication. The convex hull concept was the main principle in the development of these algorithms. The techniques used in constructing two- and three-dimensional convex hulls were based on the divide and conquer and merge techniques. The presented algorithms for minimum zone

evaluation were very similar to the ones reported by Traband et al. (1989). In addition, the algorithms for function-oriented evaluation were based on the aforementioned techniques and the minimum and maximum enveloping features. The results obtained from the simulated data and the data used in the literature demonstrated the success of these algorithms.

2.5.2 Numerical Based Algorithms

Chetwynd (1979) examined some of the implications of the limacon method by making comparisons with circular references such as least squares circle, minimum radial zone circle, minimum radial circumscribing circle, and maximum radius inscribing circle. A limacon figure was used as an approximation to a circle. The mathematical model obtained of a reference figure was advantageous due to its linear parameters. These linear functions could be utilized very well with optimization methods in finding those circular references. The graphical comparisons demonstrated the distribution of out-of-roundness values and center separations obtained with the least squares, minimum circumscribing, and maximum inscribing limacons relative to the minimum zone limacons. The least squares and minimum zone limacons tended to have separate identities but were rarely much different. However, there was a quite high probability of the minimum circumscribing limacon being very close to minimum zone even though more widely different values occurred than with the least squares. The maximum inscribing seemed less tied to minimum zone. It was concluded that the limacon provided various advantages over

the circle, especially its linearity, but maintained compatibility in roundness measurement.

Murthy and Abdin (1980) proposed various methods such as Monte Carlo technique, normal least squares fit, simplex search techniques, and spiral search techniques to determine the minimum zone solutions for straightness, flatness, circularity, and sphericity. The straightness deviation was originally derived by using the least squares method. Then it was adjusted to be normal to the mean line. This method was called the normal least squares. The flatness deviation was also obtained in a similar fashion. However, the equations obtained were complex and could not be solved easily. They were then simplified by shifting the coordinate system to the center of the plate. Murthy and Abdin (1980) suggested the use of the normal least squares where the deviations were of a larger degree. When the deviations were small, the difference in results obtained from the least squares and the normal least squares methods was not appreciable. Moreover, the deviations very often obtained by adopting either method might not be the minimum zone solutions.

The normal least squares fit was also used to find the circularity and sphericity. In order to solve the derived equations, the very tedious mathematical calculations and trial and error procedure were required. Monte Carlo search, simplex search, and spiral search were introduced to find the minimum zone solutions for straightness, flatness, circularity, and sphericity since the methods of least squares and normal least squares might not always produce the minimum zone deviations. In

addition, the starting solutions for these search techniques were the results from either the least squares or the normal least squares methods.

According to Murthy and Abdin (1980), the Monte Carlo search could be used when the variables were few. The simplex search was more suitable for any surface studied involving a number of variables. The spiral search could be easily applied when the number of variables was only 2 or 3. This search actually gave a better value since all possible solutions were searched. The authors suggested that the individual techniques or a combination of these techniques could be applied to evaluate the minimum zone solutions depending on the requirement and the problem.

Chetwynd (1985) presented applications of linear programming to engineering forms such as circularity, straightness, and flatness. The so-called exchange algorithms were used to compute the best-fit geometries. The reference figure to a set of data points was found by first fitting a trial figure to a subset of the data. Then a series of iterations were performed by exchanging one datum point which violated the criteria of fit with one of the defining set to create a new trial solution. The concept of minimum zone was suggested in profiling the reference fitting. The straightness and flatness reference were assumed linearly fit and the limacon approximation was used to linearize the circle parameters about the origin. The primal-dual technique was used in determining such a zone. The main purpose of this work was to show that the mathematical theory such as mathematical programming could have a dramatic effect on form metrology.

Shunmugam (1986) introduced a new simple approach called median technique for assessing the errors on the dimensions of geometric features. The considered features included straightness, circularity, flatness, cylindricity, and sphericity. The principles of the assessment process were as follows: (1) deriving the linear deviations from the assessment features, (2) establishing the trial features passing through the end points by substituting the values corresponding to the end points equations and equating those deviations to zero, (3) computing the crest and valley points by selecting the points corresponding to the maximum positive deviations and the maximum negative deviations, respectively, (4) determining the median features by selecting points from the crest and valley points so that the errors were minimum. The trial was repeated for all possible combinations of the points. The approximation processes from the nonlinear to linear forms of errors were accomplished by assuming that the features were well-aligned with the X axis for straightness, well-centered trace for circularity, aligned parallel to the XY plane for flatness, well-aligned with the Z axis for cylindricity, and well-centered for sphericity. Note that these assumptions can be mathematically written by using linear deviations for straightness and flatness, and limacon approximation for circularity, cylindricity, and sphericity. Shunmugam (1986) demonstrated and concluded that the median approach was more efficient (faster and more accurate) than the least squares method.

Shunmugam (1987a) compared the linear and normal deviations of forms tolerances using the least squares and minimum deviation methods. A simplex search

method was used in a search procedure for both approaches. The obtained results showed that the minimum deviation technique was more accurate than the least squares method and the difference was quite appreciable. In both techniques, the normal deviation resulted differently from the linear deviation but the difference was quite insignificant for practical measurement. In addition, the computational time required of the normal deviation approach was longer that of the linear deviation approach, which was not justifiable in view of the marginal difference in the values.

The so-called minimum average deviation technique was proposed by Shunmugam (1987b). The major drawback of the minimum deviation technique above was that a few points on the features control the position of the assessment features. Hence, a different criterion for minimizing the sum of absolute deviation values was used instead. Then a simplex search was applied with a reasonable number of trials to find form errors based on the minimum deviation principles. This method attempted to find the assessment features in such a way that the areas above and below them were equal and the sums of the areas were minimum. Its advantage over the minimum deviation was that it was statistically more consistent since the deviations above and below the ideal features were equal. The results showed that this technique was superior to the least squares method.

Elmaraghy et al. (1990) presented a procedure for determining the geometric tolerances from the measured 3D coordinates on the surface of a cylindrical feature. The data analyzed were the 3D measured coordinates of uniformly spaced points on the circumference of many cross sections along the cylinder length. Unconstrained

nonlinear optimization and the Hooke-Jeeve direct search were used to fit the data to the minimum tolerance zone. The goal was to adjust the position and orientation of the center of a circle or axis of a cylinder to obtain the minimum deviation zone. Since no constraint was formulated and the number of variables was not big, the convergence should be reliable and fast. The starting point (0,0) was used for the nominal position of the center of a circle. Six cross sections and eight longitudinal sections of a cylinder and its circles were used. A set of coordinates of the surface points was created by simulation using random number generation. The following steps were the proposed procedure: (1) determining the size deviation among all cross sections of the cylinder, (2) finding the roundness deviation of each cross section and selecting the maximum roundness deviations among all cross sections as the cylinder roundness deviation, (3) evaluating the runout deviation based on the nominal center position of the cross sections, (4) identifying the cylindricity deviation, (5) examining the straightness deviation of the longitudinal surface element within each longitudinal section and choosing the maximum straightness among all longitudinal sections as the longitudinal straightness deviation of the cylinder, (6) finding the profile deviation in longitudinal sections, (7) determining the straightness deviation of the cylinder axis as defined by a cylindrical deviation zone, (8) calculating the perpendicularity deviation of the cylinder axis, and (9) evaluating the position deviation. Note that this work samples data uniformly, which is not quite efficient compared to other sampling strategies like the Hammersley sampling and the Halton-Zaremba sampling methods.

Shunmugam (1991) presented a generalized algorithm to establish the reference figures on form errors such as straightness, flatness, circularity, and cylindricity. The algorithm was based on the theory of discrete and linear Chebyshev approximation. It was guaranteed to give optimal results. In so doing, the algorithm attempted to minimize the maximum value of the absolute error by calculating error for the specific feature and optimizing the enveloping figure using the Stiefel exchange algorithm. To establish the enveloping surfaces, a certain geometrical condition known as the 180° rule was used as recommended by Chetwynd (1985). Some modifications were required for different geometrical features to avoid the cyclical exchanges which might occur leading to the selection of the same reference set again and again. The author also expressed a concern about the sampling strategy used in collecting data. Otherwise, relevant information might be missed and result in a certain degree of disagreement among the measurement results. Another similar work on the basis of the theory of discrete and linear Chebyshev approximation was discussed by Dhanish and Shunmugam (1991) as well. The linear deviations were again used. In addition to Shunmugam (1991), the sphericity computation was taken into consideration. An advantage of algorithms from both papers was the reduction of their mathematical complexity, hence the fast convergence.

Wang (1992) presented a nonlinear optimization method for determining the form tolerances by using sample measurement points obtained with a CMM. An ideal feature must be established from the actual measurements such that all of the deviations of the feature from the ideal were within the tolerance zone. The ideal

form feature lied in the middle between the boundaries of the minimum zone. The form error was determined by minimizing the maximum value of the deviations of the sample points with respect to the position and orientation of the ideal form. This minimax problem was reformulated into a nonlinearly constrained optimization problem by introducing an additional variable. The introduced variable specified the half width of the zone and was minimized resulting in the minimum zone. The error models used were the same as the normal deviation models suggested by Shunmugam (1987a). The obtained results showed that this algorithm was superior to the most widely used method in industry, the method of least squares. Refinements were also recommended by using a simple mechanism of tilting and bending to improve the effectiveness and efficiency of the algorithm.

Kanada and Suzuki (1993a) studied an application of some nonlinear optimization techniques for minimum zone flatness. A noncontact sensor was used to collect 3D data uniformly. The convergence criteria such as the downhill simplex method and the repetitive bracketing method were considered. In the downhill simplex method, a condition for approximation was used in formulation of the objective function. In the repetitive bracketing method, the optimization parameters were alternately searched since this method was a 1D search. The reduction process of data volume was also applied. The results from those two criteria were compared with one another and also with those of the LSQ. Clearly, the downhill simplex method was advantageous over the repetitive bracketing method and the two optimization techniques were superior to the LSQ. Note that the uniform sampling

used in this work is not as efficient as other sampling methods, as mentioned elsewhere.

Kanada and Suzuki (1993b) also applied several algorithms to calculate the minimum zone straightness. The algorithms used were the Nelder-Mead simplex method, the linear search method with quadratic interpolation, the linear search method with golden section, the linearized objective function method which was newly developed by considering the characteristics of the measured profile, and the mixed method between the linearized objective function method and the linear search method with quadratic interpolation. The comparisons of the five methods were then studied from the viewpoints of the minimum zone straightness value, computing time, number of iterations, and computing accuracy. The results implied illustrated that the linearized objective function method overestimated the zone straightness by about 5 % as compared with the other methods. However, it was the best in terms of computing time while the Nelder-Mead simplex method was the worst.

Kanada (1995) proposed a sphericity algorithm based on the downhill simplex method as opposed to the least squares method. The data used were simulated by applying surface harmonics (Laplace's spherical function) with a computer. Even though the initial simplex could start at an arbitrary size and position, the computation efficiency may decrease due to this setting. Hence the origin (0, 0, 0) was used. The comparison between this method and the LSQ method demonstrated that the difference was markedly small. In addition, the comparison between the sphericity and the roundness values showed that the roundness values on longitudinal lines were

almost one third of the sphericity values, and the roundness values on the equatorial plane was very similar to the sphericity values. Interestingly, two or three measurements on equatorial planes at 90° to each other might not represent the sphericity. As a result, using circular profiles to represent a sphere may not produce the accurate sphericity through profile circularity.

Carr and Ferreira (1995a) developed algorithms to verify minimum zone straightness and flatness. Even though computing the minimum zone was inherently a nonlinear optimization problem, the proposed algorithms solved a sequence of linear programs that converge to the solution of the nonlinear problem. Initially, the nonlinear minimax problem (a nonlinear objective function and a nonlinear constraint) was formulated. Since a direct implementation of this formulation was very difficult, a transformed model was investigated. Instead of searching for a reference plane (or straight line), a transformed model searched for two parallel supporting planes so that all measured points were below one plane and above the other while both planes were as close together as possible. In other words, this model placed a reference plane through the origin and searched for a direction vector so that the difference between the distance of the farthest point and the distance of the nearest point from the reference plane is less than the specified tolerance. The new model was still a constrained nonlinear programming problem but the objective function and all but one constraint were linear. This main idea was applied to obtain both flatness and straightness solutions. Whenever a nominal zone direction vector was not known, the LSQ solution direction vector was used as the initial solution.

The results tabulated demonstrated that the proposed algorithms were as efficient as other minimum zone methods while they were relatively easy to implement.

Carr and Ferreira (1995b) also discussed another approach for verifying cylindricity and straightness of a median line. The main idea was similar to the above approach of Carr and Ferreira (1995a). In addition, this model could be applied to minimum circumscribed and maximum inscribed cylinders. The formulation outcome was a constrained nonlinear programming problem with a continuous linear objective function. The final formulation solved a sequence of linear programs that converged to a local optimal solution. The straightness of a median line was computed by modifying the cylindricity formulation to find only one cylinder, the one that enclosed all of the measured points. Again the LSQ solution was used as the initial condition for this algorithm. The obtained outcomes showed that this algorithm was robust and efficient. Since most of the works in determining minimum zone algorithms in literature were conducted under the assumption that the sampled points accurately represented the part surface, the authors recommended future research in sampling techniques to accurately sample (represent) the part surface.

A comparative analysis of CMM form fitting algorithms was conducted by Lin et al. (1995). This work described three minimum tolerance zone algorithms: the minimum max-deviation method (minimax) (Wang, 1992), minimize average deviation method (minavg) (Shunmugam, 1987b), and the convex hull method (Traband et al., 1989). The LSQ technique was also used to compare with those algorithms in terms of tolerance zone, solution uniqueness, and computational

efficiency. The mathematical formulations of straightness, flatness, circularity, and cylindricity were illustrated for the LSQ method, the minimax method, and the minavg method. Only the formulations of straightness and flatness were discussed for the convex hull method because this computational geometry based approach could not lend itself to other geometrical forms. These algorithms were implemented first and then validated with the data taken from the published literature. Moreover, the mentioned algorithms were tested by using the same measurement data with various sizes generated by a template-based simulator. The tabulated outcomes for straightness and flatness generally showed that the LSQ method produced the widest zone among all four algorithms. The LSQ and the convex hull methods produced unique solutions whereas the other two methods could not guarantee unique solutions. In computational efficiency, the LSQ algorithm was the fastest and the convex hull method utilizing the geometrical structure of the part surfaces came in second. The minimax and minavg methods required the most computational time for high sample sizes, especially for the evaluation of cylindricity. In most cases, the minavg algorithm produced smaller zone sizes (by a small amount) than the minimax algorithm due to the limacon approximation used in its formulation. This might lead to a smaller tolerance zone than the actual one.

Dowling et al. (1995) conducted a comparison of the orthogonal least squares and minimum zone methods for straightness and flatness. The major drawback of the least squares method in most literature was that it tended to overestimate the true deviation range. It was also possible that the estimated deviation range by any

method might underestimate the true deviation range. The authors statistically pointed out that the minimum zone method might underestimate the deviation range. This implied that some unmeasured points of a feature could lie outside of the estimated deviation range. Clearly, the estimation accuracy depended on sample size and estimation method. It was assumed that the sample points measured were a good representative of the entire feature surface, including all extreme points. This assumption might hold true if the sample size is dense enough. However, this was not the case in practice, especially for relatively few measurements. Thus the estimation methods were always applied to the sample. The LSQ method treated the data as a sample rather than as the entire population of measurements. This was a superior property of the LSQ method over the minimum zone method.

The orthogonal or normal deviations of both form tolerances were used for both methods. The minimum zone algorithm tested was the convex hull algorithm proposed by Traband et al. (1989). The data used in this work was a set of actual data collected with a CMM as well as simulated data. The actual data provided by the National Institute of Standards and Technology was only used to illustrate the differences between both methods. Then the simulated data that included several variations from process, surface, measurement, and fixturing were generated and analyzed. The sampling was done using the stratified sampling method. It was chosen over the uniform sampling to avoid the periodic variation. The empirical results showed that the orthogonal LSQ method had less mean squared error than the minimum zone method, particularly for small sample sizes. This implied that the

LSQ method for straightness and flatness had better statistical properties than the minimum zone method.

Orady et al. (1996) developed a nonlinear optimization method with data filtering and rebuilding for the evaluation of straightness error. The improvements were incorporated to improve accuracy, efficiency and robustness of nonlinear optimization especially when the number of data points was quite large. When the measured data points were contaminated with the outlier points, both the LSQ method and the nonlinear optimization method were often misguided by the outlier points to produce the wrong results. Hence, the outlier points should be identified and deleted before applying the nonlinear optimization method. A data filter using an outlier identification method based on Grubbs concept was introduced in the proposed procedure. A simple method called control zone method was applied to rebuild a new data set. Only the data points outside the control zone were reserved while the data points inside the control zone were deleted. The straightness verification steps were as follows: (1) apply the LSQ to the measured data set, (2) identify and delete the outlier points in the measured data set using the data filter, (3) define the control zone and delete the data points inside it, and (4) use the LSQ results as initial condition for the nonlinear optimization method. The developed algorithm was verified using the same examples as those in Traband (1989). The results obtained were as good as those reported in Traband (1989). It is important to note that when the presence of one or more outliers is located, careful investigation is called for. Immediately deleting outliers using the proposed algorithm is not a good solution. The

experimental circumstances surrounding data measurement must be carefully studied first. The outlying response may be more informative about some factors or errors. Care must be taken not to reject or discard an outlying observation unless reasonable nonstatistical grounds are known before doing so. The worst case is that two analyses must be conducted, one with the outlier and one without (Montgomery, 1997).

Another optimization approach for straightness and flatness tolerance evaluation was presented by Cheraghi et al. (1996). Initially, the straightness and flatness evaluation problems were formulated as nonlinear optimization problems with linear objective function and nonlinear constraints. They were then transformed into linear programming problems as functions, of an angle for straightness and angles for flatness. A search procedure was developed for straightness evaluation to find an optimal value. The flatness search procedure was similar to that of the straightness procedure. In addition, it consisted of two loops. The outer loop searched for optimal value of the first angle while the inner loop found optimal value of the other angle for a given value of the first one. Both search procedures continued until no improvement in the objective function values could be achieved. Note that the constraints involved sine and cosine functions and had nonconvex sinusoidal forms. As a result, the feasible region might be nonconvex as well. To ensure that the solution obtained was optimal, several runs with different starting solutions and fixed step size were executed. The comparisons between the proposed methods and other existing techniques demonstrated that they were superior to the LSQ method and comparable to other minimum zone methods with fast computational time.

Suen and Chang (1997) developed a neural network interval regression method for minimum zone roundness. An interval bias adaptive linear neural network structure with a least mean squares learning algorithm and a cost function were used to carry out the interval regression analysis. The mathematical model of the minimum zone roundness was first transformed into a linear interval form which could be solved by the interval regression method. Next, the regression method was implemented by using a two-layer neural network with a specified output function to adjust the coefficients of the linear function of the interval model. The training pair should be transformed into a specific range through the normalization process before input into the network; otherwise the network might not be able to converge. Also, the penalty coefficient must decay appropriately. Its equation was given with specified constants. Then the supervised least mean squares learning algorithm was used to train the connection weights. The error between the actual output of neural network and the given target output was then used to iteratively adjust the network until the energy converged. The provided results clearly illustrated that this algorithm was more efficient than the LSQ method.

The LSQ (L_2-norm) method is normally selected to determine the best-fit feature under the assumption that the errors are normally distributed. However, this may or may not hold in practice. Namboothiri and Shunmugam (1998a) proposed a form error evaluation using L_1-approximation and singular value decomposition (SVD) technique to tackle this issue. Two possible cases, non-degenerate dead point case and degeneracy case, were discussed with some examples. The comparisons

between the presented algorithm and the LSQ method were also tabulated. In addition, the "wild points" could be identified. This suggested the location where the part should be compensated or reworked by further machine operations. This algorithm was also extended to obtain the function-oriented form evaluation (Namboothiri and Shunmugam, 1998b).

Sharma et al. (2000) solved nonlinear optimization problems for form tolerance evaluation by applying genetic algorithm based minimum zone approach. The basic form tolerances such as straightness, flatness, circularity, and cylindricity were tackled. Genetic algorithms are search algorithms based on the mechanics of natural selection and genetics. The reasons reported as to why they were more attractive than the gradient-based methods were the existence of several local minima and the existence of discontinuous functional relationships in the evaluation of the objective function in some cases. The genetic algorithm adopts a probabilistic approach to overcome those obstacles. The form tolerance problems were modeled similarly to the ones proposed by Carr and Ferreira (1995a; 1995b). The important parameters such as the initial population, crossover ratio, mutation rate, and maximum number of generations were suggested based on the trial runs for this application. In addition, a comparison between this method and other methods reported in the literature such as the LSQ, convex hull, Voronoi diagram, minimum circumscribing, and maximum inscribing methods were tabulated. Clearly, the results obtained were comparable to those of other minimum zone methods and better than those of the LSQ method.

Another genetic algorithm based approach for cylindricity evaluation was proposed by Lai et al. (2000). Similar to the findings of Sharma et al. (2000), this method performed better than the LSQ method for a numerical example provided. A set of initial values used was estimated by (1) finding the directional cosines of the initial cylindrical axis and (2) finding the initial values of the intersecting parameters. Various sets of genetic parameters like population size and mutation probability were investigated before they were carefully chosen. This approach shows that the genetic algorithm is a good alternative for solving complicated form evaluation problems.

Very few researches have concentrated on the conicity tolerance. Tsukada et al. (1988) used the least squares method to nonlinearly model the differences between the measured surface profile and the least squares surface. A nonlinear programming technique, the modified Newton-Raphson method, was then applied to find an ideal conical surface. To improve the computation efficiency, the initial conditions for this optimization model were obtained by fitting a least squares cone to the measured data first. A set of simulation data was processed to examine the effectiveness of the proposed algorithm. The form errors of the conical surface were then visualized by a perspective projection and a contour map for clear understanding.

As the least squares method may result in some overestimations of the conicity, Kim and Lee (1997) suggested the minimum zone based conicity algorithm. The algorithm consisted of two phases. The first phase was to find initial values for a cone using a least squares embedded approach. Regardless of the angular components of the measured data points, the 3D points were mapped into 2D points

and a least squares line was fitted to them. The tolerance zone of the fitted line was then calculated and the cone axis with the smallest zone was selected. The second phase was to search for the minimum conical tolerance zone with the initial values from the first phase. This was done by formulating the problem as a nonlinear constrained optimization problem. The sequential quadratic programming (SQP) was used to solve the formulated problem.

Chatterjee and Roth (1998) addressed the conicity evaluation for the right circular cone by using the Chebychev approximation method. This approach was based on the geometrical characteristics of the data points' locations with respect to the substitute cone. The determination of the conicity for a finite set of data points when the vertex of the cone was specified was studied. Also, the problem of determining the substitute cone when the axis was specified was explained. The substitute cones for both cases were estimated by minimizing the maximum normal deviation of the data points from the substitute surface. In addition, the discussed algorithm was combined with a simplex search algorithm to determine the general Chebychev cone for a set of data points without a specified vertex point. The simplex in this case was a tetrahedron as there were three unknowns for the vertex position. At each step of the simplex search, the envelope width corresponding to the Chebychev cone for a chosen vertex location was minimized. An experiment was conducted by measuring sixty points of the outside taper of a lathe collet holder. The results included showed the superiority of this method in comparison to the least squares method.

Choi and Kurfess (1999a) proposed a general zone fitting method that can be applied to characterize various geometric features. This work addressed the tolerance zone representation that is widely practiced with computer-aided design (CAD) models but not completely compatible with the current ANSI Standard (ASME, 1995). While other verification methods focused on the data fitting of the measured points to a substitute surface, the presented algorithm directly placed a set of points into the specified tolerance zone in the same reference frame as the design model by using rigid body transformation and optimization algorithms. If the proposed procedure is successful, a measured part conforms to the given specification. Otherwise, it fails. The advantage of the proposed approach is the potential applicability to non-uniform tolerance zones. A few examples for cube, cylinder, and taper models were demonstrated. The shortcoming is that this approach does not provide information towards the quality of the inspected part. Hence, the zone fitting was extended to a minimum zone evaluation algorithm (Choi and Kurfess, 1999b). This method was applied to evaluate the flatness and conicity. There were some differences in flatness results compared to other published literature. These were conjectured to be due to the differences on the numerical tolerances.

CHAPTER 3

OVERVIEW OF RESEARCH

The design, manufacturing, inspection and service of components are all significantly impacted by tolerances. Hence, tolerance verification usually undertaken during measurement and inspection affects tolerance specification as well as process selection to achieve it. Form tolerance (for individual features) verification using CMMs has been studied extensively in the last two decades. Two problems have been studied in the literature: sampling point selection and data fitting (minimum tolerance zone estimation). The form tolerances for complex shapes like cones is typically left to be dealt-with by the use of profile tolerance definition. Such a procedure may be impractical in cases where accuracy of the whole profile is a requirement. Sufficient number of industrial parts such as nozzles, tapered cylinders, frustum holes and tapered rollers in bearings possess conical features that must be efficiently inspected for form. Considering these many applications of cone-shaped objects, it is logical that cone tolerances be studied more exclusively and extensively.

Hence, the primary objective of this research was to develop comprehensive guidelines for cone and/or conical frustum verification using CMMs. Specifically, four major research issues were addressed: sampling point selection, path determination, zone estimation, and experimental analysis.

This research derived the sampling strategies for cone verification based on Hammersley sequence, Halton-Zaremba sequence, and Aligned Systematic sampling. Methodology and a set of MATLAB programs were developed to implement and simulate these strategies. Methodology for simple probe path planning for cone inspection was also developed and implemented using MATLAB. It must be noted that the probe path was nonlinear and must be developed so as to avoid collisions of the probe with the part while sampling points. The trajectory path was simulated and visually examined before being transformed into a CMM part program to collect data automatically. The linear and nonlinear minimum zone formulations of the conicity were undertaken next. The conical tolerance zone determination techniques using the method of least squares and the optimization approaches, for both linear and nonlinear cases were modeled. This preliminary methodology was implemented through a set of MATLAB programs and LINGO, a software package for linear and nonlinear optimization, for zone estimation.

The effect and appropriateness of the sampling strategy, sample size, the description and fitting of the conicity tolerance were experimentally studied for minimum conical zone evaluations. A factorial experiment with nested blocking factor was designed for data collection. The data collection was specifically designed to empirically determine the role of individual and interactive variables in sampling and zone estimation. A program in SAS, a statistical analysis tool, was implemented for the design to analyze the results of those factors.

The guideline development of the effectiveness of the data collection and data fitting techniques in terms of the accuracy of the minimum conical zone evaluation while minimizing the sample size (or cost) was an important goal of this dissertation. It was estimated that the results of this experimental analysis would provide a knowledge base for the inspection of conical features in manufactured parts. This would result in better solutions and standards for part verification in industry using coordinate metrology. The integrative study conducted is outlined in Figure 8.

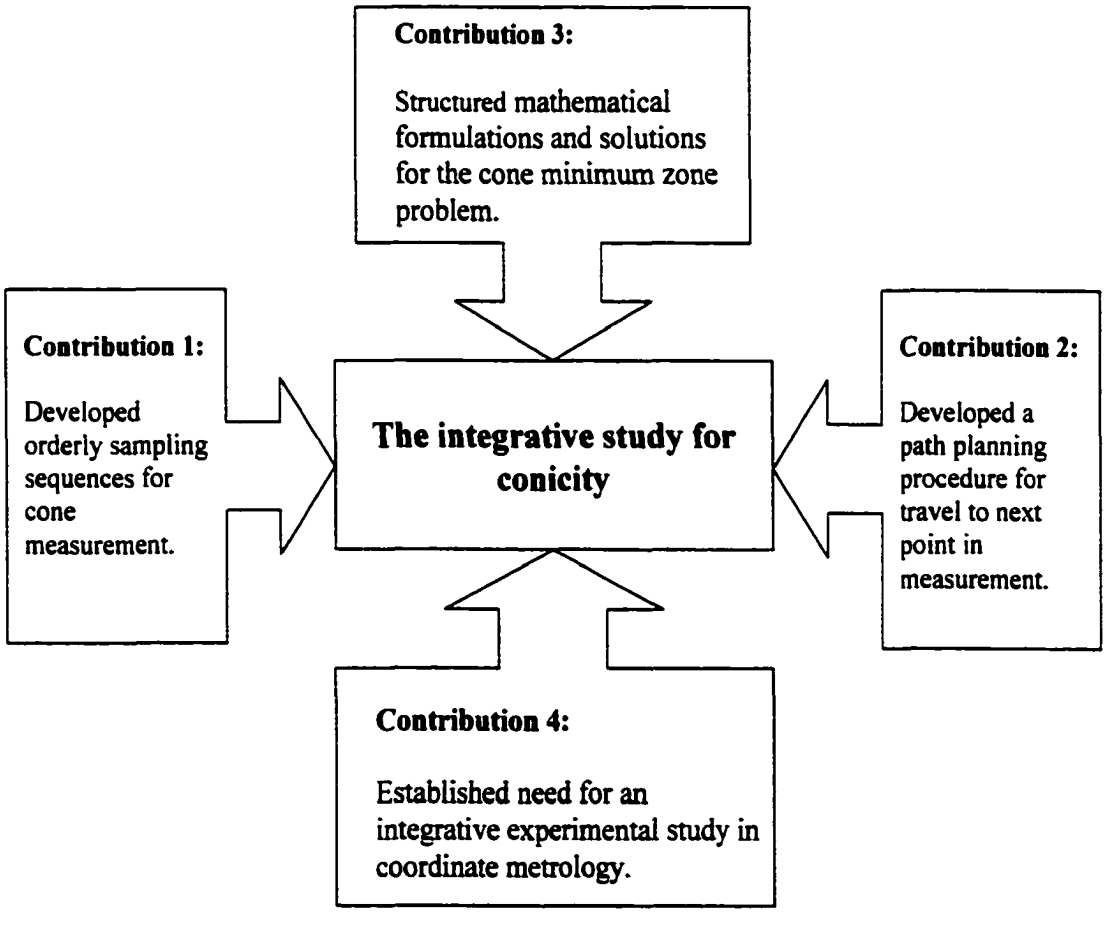


Figure 8. Integrative Investigation of Cone Tolerances Using Coordinate Metrology.

CHAPTER 4

SAMPLING STRATEGIES FOR CONICAL OBJECT

Inspection research using coordinate measuring machine (CMM) can be largely categorized into two main areas: sampling point selection or data collection and data fitting. The former is discussed in this chapter and the latter is addressed in Chapter 7. The advantages of the sampling methods compared to the complete (non-parametric) enumeration are reduced cost, faster speed, greater scope, and greater accuracy (Cochran, 1977). The purpose of sampling theory is to make sampling more efficient or to maximize the amount of information collected. Attempts have been made in the literature to develop sampling methods that provide, at the lowest possible cost, estimates that are precise enough to achieve the quantity of information pertinent to a population parameter. Sampling strategies and their designs are the keys to permitting valid inference about the dimensions and forms of a workpiece (Lee et al., 1997). The sampling strategy deals with the selection of points for inspection such that representative data to verify flatness, straightness, cylindricity or roundness is obtained. The selection of the location of the measurement points is achieved intuitively using uniform or random sampling. Sample size (the number of points measured) is typically proportional to time and cost and for a given sampling strategy, savings in time may be achieved through a reduction of the sample size. It has been suggested that an alternate strategy may be selected at a lower sample size

while maintaining the same level of accuracy. Different sampling strategies used with the same sample size may impact the level of sampling accuracy. In other words, with the same sample size, some strategies may provide better information than do others. With the same level of accuracy, some strategies may require less number of sample points than do others. Menq et al. (1990) introduced an approach to determine a suitable sample size for inspection based on manufacturing accuracy, tolerance specification, and the uniform sampling scheme. In dimensional surface measurements, it is generally accepted that the larger the sample size, the smaller the error associated with the measurement. Dowling et al. (1995) emphasized the importance of the sample size in the selection of the estimation algorithms. Even though the sample location was not taken into much consideration, the graphical results clearly showed the improving zone evaluation with denser sample sizes. The methods of sampling can simply be categorized into two groups, random sampling and systematic sampling. In random sampling, the probability of each available unit to be randomly selected is equal. However, in systematic sampling, only the first point is drawn at random, and the coordinates of the subsequent sample points are taken from a sequence defined mathematically. The advantages of using a mathematical sequence for samples selection are the ease of execution and the determinism. In other words, the experiment is repeatable and the sampling error can be controlled. Taking an arbitrary sequence of sample coordinates can yield in arbitrarily large error. According to Woo and Liang (1993), a two dimensional (2D) sampling strategy based on the Hammersley sequence shows a remarkable

improvement of nearly quadratic reduction in the number of samples to the uniform sampling while maintaining the same level of accuracy. The Halton-Zaremba based strategy in 2D space was also suggested by Woo et al. (1995) without discernible difference in the performance to the Hammersley strategy. The only differences are that the total number of sample points in the Halton-Zaremba sequence must be a power of two and the binary representations of the odd bits are inverted. Also, Liang et al. (1998a and 1998b) compared the 2D Halton-Zaremba sampling scheme to the uniform and the random sampling theoretically and experimentally for roughness surface measurement with the similar results. Lee et al. (1997) demonstrated a methodology in extending the Hammersley sequence for advance geometries such as circle, cone, and sphere. The sampling strategies proposed in this dissertation for conical feature inspection are along the lines of Lee et al.'s (1997) work on Hammersley sequence. In addition, the Halton-Zaremba and the aligned systematic sampling sequences are derived for cone inspection in this work.

The development processes of all sampling schemes derived for the conical feature are explained in detail in the following sections. Section 4.1 discusses the Hammersley sequence and the Hammersley based sampling strategy. Section 4.2 presents the Halton-Zaremba sequence and its sampling scheme. To avoid capturing the systematic errors of the measurements, randomizing the initial point of the foregoing sequences was also introduced. The aligned systematic sampling strategy is demonstrated in Section 4.3. Since a pseudo random number generator was used in this study, an argument can be made that the numbers generated might not be truly

random. Therefore, the final section, Section 4.4, describes the properties of random numbers and tests for a random number generator to check whether that generator is providing numbers that possess the desired properties, uniformity and independence. A Windows-based MATLAB program was written to implement and simulate the sampling strategies derived.

4.1 The Hammersley Sampling Strategy

Van der Corput's work in 1935 has led to the conjecture which expresses the fact that no sequence can be too evenly distributed (Roth, 1954). Roth (1954) extended the one dimensional Van der Corput sequence to two dimensions. Such sequence is later on generalized to d dimensions by Hammersley (1960). It has been proved that the Hammersley sequence yields nearly the lowest discrepancy among the available sampling strategies (Woo et al., 1995). Since discrepancy is related to the root mean square errors (RMS errors), it is reasonable to apply the Hammersley sequence to the sampling point selection. In two dimensions, the coordinates (x'_i, y'_i) of the Hammersley sequence can be determined as

$$x'_i = i/N \tag{4.1}$$

$$y'_i = \sum_{j=0}^{k-1} b_{ij} 2^{-j-1} \tag{4.2}$$

where N is the total number of sample points,

$i \in [0, N\text{-}1]$,

b_i denotes the binary representation of the index i,

b_{ij} denotes the jth bit in b_i,

$k = \lceil \log_2 N \rceil$, and

$j = 0, \ldots, k\text{-}1$.

For example, N = 10, so $i \in [0, 9]$ and $k = 4$. Hence, $b_i = (b_{i3}, b_{i2}, b_{i1}, b_{i0}) =$ (0, 0, 0, 0), (0, 0, 0, 1), ..., (1, 0, 0, 1). The coordinates of these points are presented in Table 1. All 10 Hammersley points are shown in Figure 9.

Considering the fact that in the Hammersley sampling method no points are drawn randomly, it is prone to periodic variation. To decrease the probability of capturing the systematic errors of the measurements, Lee et al. (1997) suggested to randomize the sampling point of the Hammersley sequence as

$$x_i = x'_i + x_{rand} \quad ; \text{if } (x'_i + x_{rand}) < 1$$
$$= (x'_i + x_{rand}) - 1 \quad ; \text{otherwise} \qquad (4.3)$$

$$y_i = y'_i + y_{rand} \quad ; \text{if } (y'_i + y_{rand}) < 1$$
$$= (y'_i + y_{rand}) - 1 \quad ; \text{otherwise} \qquad (4.4)$$

where (x_{rand}, y_{rand}) is the coordinate of the initial point drawn at random. For example, if $x_{rand} = 0.2$ and $y_{rand} = 0.4$, Figure 9 can be redrawn as Figure 10. A built-in function, RAND, in MATLAB is used to generate x_{rand} and y_{rand}. It produces uniformly distributed pseudo random numbers on the interval (0.0, 1.0). Since it is a pseudo random number generator, the set of random numbers can be replicated. However, the goal of a generation scheme is to produce a sequence of numbers between zero and one that simulates the ideal properties of uniform distribution and

independence as closely as possible. The properties of random numbers and tests for a random number generator are discussed in Section 4.5.

Table 1. Coordinates of 10 Hammersley Sampling Points.

i	b_i	$b_{i3}2^{-3-1}$	$b_{i2}2^{-2-1}$	$b_{i1}2^{-1-1}$	$b_{i0}2^{-0-1}$	x_i	y_i
0	(0, 0, 0, 0)	0	0	0	0	0	0
1	(0, 0, 0, 1)	0	0	0	0.5	0.1	0.5
2	(0, 0, 1, 0)	0	0	0.25	0	0.2	0.25
3	(0, 0, 1, 1)	0	0	0.25	0.5	0.3	0.75
4	(0, 1, 0, 0)	0	0.125	0	0	0.4	0.125
5	(0, 1, 0, 1)	0	0.125	0	0.5	0.5	0.625
6	(0, 1, 1, 0)	0	0.125	0.25	0	0.6	0.375
7	(0, 1, 1, 1)	0	0.125	0.25	0.5	0.7	0.875
8	(1, 0, 0, 0)	0.0625	0	0	0	0.8	0.0625
9	(1, 0, 0, 1)	0.0625	0	0	0.5	0.9	0.5625

According to Lee et al. (1997), the Hammersley sequence can be embedded into a 3D sampling scheme for a specific feature like cone or sphere. There are two ways to select specified measuring points, central point specified sampling and edge point specified sampling, as suggested by Lee et al. (1997). In the central point specified sampling, all sampled points are drawn based on a given central point. On the other hand, the edge point specified sampling conducts the sampled points from a given edge point. Therefore, the central point specified sampling is suitable for a non-uniform surface form, especially for a rough edge (burrs) and the edge point specified sampling is preferred for a uniform surface form. If the surface errors of a workpiece are uniform, which is the case in this study, either way can be applied. For

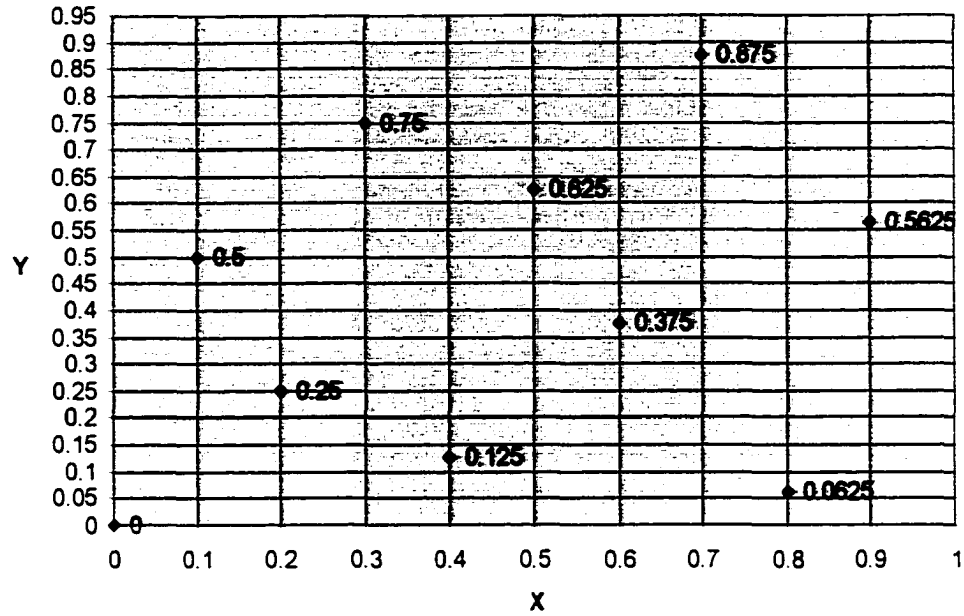


Figure 9. Distribution of 10 Hammersley Sampling Points.

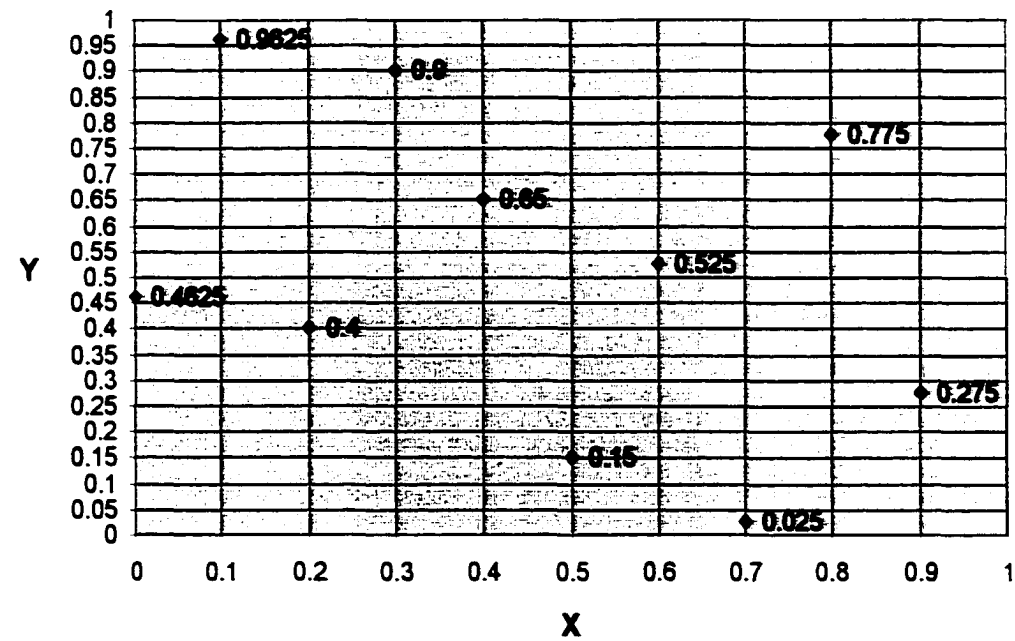


Figure 10. Distribution of 10 Randomized Hammersley Sampling Points.

convenience in controlling the CMM and its path planning, merely the central point specified sampling was implemented and used in this dissertation. If the edge point specified sampling is desired, some simple adjustment needs to be made by replacing y_i with $(1-y_i)$ in Equation (4.5).

To cover a conical feature, the 2D Hammersley sampling strategy must be extended to 3D space. Since cone's profile (2D) has a circular feature when looked from its top view, it is simpler to work with the 2D Polar coordinates (r_i, θ_i) than the 2D Cartesian coordinates (x_i, y_i). The rationale behind the following equations are that the area (A) of a circular surface is proportioned to the square of its radius (R), $A = \pi R^2$ implies that $A \propto R^2$, and a circle can be easily divided into N sections equally (Lee et al., 1997). Thus, the Polar coordinates of a Hammersley point on a circular surface are determined as follows:

$$r_i = y_i^{1/2} R \tag{4.5}$$

$$\theta_i = 360° x_i \tag{4.6}$$

where R is the radius of the circle. Equation (4.5) generates the concentric circles whose radii are varied according to y_i's.

For example, the 100 uniform samples, $m \times m = 10 \times 10$ and $x_i = i/m$, $y_i = i/m$, are to be illustrated. Hence, there are 10 points in each direction along the X and Y axes. Next, 10 concentric circles with radii as $\sqrt{1/10}R, \sqrt{2/10}R, \ldots, \sqrt{10/10}R$ are generated by Equation (4.5) and θ_i for each section can be computed as 360°×1/10, 360°×2/10, ..., 360°×10/10. The 10×10 grid is the locations of the 100 uniform samples. Therefore, the N Hammersley points for a circular surface can be similarly

obtained. Table 2 depicts the Polar Coordinates obtained with R = 1 and Figure 11 plots the 10 Hammersley points on a circular surface.

Table 2. Polar Coordinates of 10 Hammersley Sampling Points.

x_i	y_i	r_i	θ_i
0	0	0	0
0.1	0.5	0.707107	36
0.2	0.25	0.5	72
0.3	0.75	0.866025	108
0.4	0.125	0.353553	144
0.5	0.625	0.790569	180
0.6	0.375	0.612372	216
0.7	0.875	0.935414	252
0.8	0.0625	0.25	288
0.9	0.5625	0.75	324

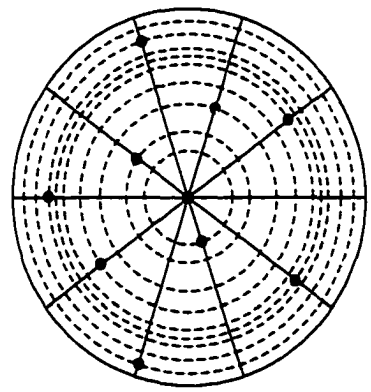


Figure 11. Distribution of 10 Hammersley Points on a Circular Surface.

The method of calculating the polar coordinates of a Hammersley point on a conical surface is very similar to that on a circular surface with an additional axis (Z axis). The area of a conical surface is proportional to the square of its radius of base,

$A = \pi R\sqrt{R^2 + h^2}$, where R is the radius of the cone's base and h is the height of the cone. Let $h = cR$ and c is a constant, then $A = \pi R^2\sqrt{1 + c^2}$ (Lee et al., 1997). This implies that $A \propto R^2$. The projection of a cone from its apex to its base is the circle with the apex in its center point. Therefore, the actual coordinates of the Hammerley points are just the projection of those points on the circular surface to the real cone surface. Since a cone is a 3D feature, thus the sampling points are defined as (radius, degree, height) or (r_i, θ_i, h_i), where $0 \le r_i \le R$, $0 \le \theta_i \le 360°$, and $-h \le h_i \le 0$. The origin (0, 0, 0) is set at the apex of a cone. The following relationship, $r_i/R = h_i/(-h)$, between height and radius of a cone is extracted as depicted in Figure 12. Thus, the Polar coordinates of a Hammersley point on a conical surface are determined as follows:

$$r_i = y_i^{1/2} R \tag{4.7}$$

$$\theta_i = 360° x_i \tag{4.8}$$

$$h_i = r_i(-h)/R \tag{4.9}.$$

Since most the conical manufactured parts are cone-shaped objects without apex in general, this issue should be taken into consideration as well. A conical frustum is a cone with the top sliced off and the cut is parallel to the base. Figure 13 shows the top view of a conical frustum that looks like two concentric circles. Obviously, the range of r_i for a conical frustum is from (R_0 - R_1) to R_0, starting from R_1. The range of θ_i remains unchanged. Figure 14 illustrates the side view section of a conical frustum. The similar relationship to Equation (4.9), $h_i/h = (r_i - R_1)/(R_0 - R_1)$, can be

extracted. Hence, the Polar coordinates of a Hammersley point on a conical frustum surface are determined as follows:

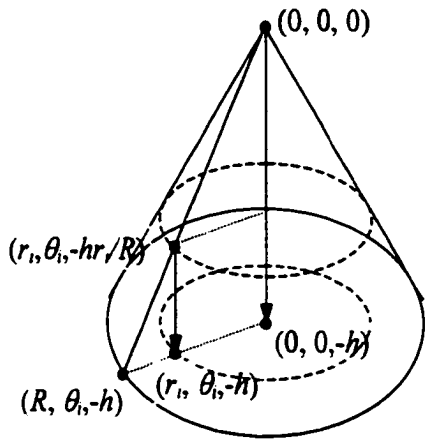


Figure 12. The Projection between a Cone and Its Base Circle.

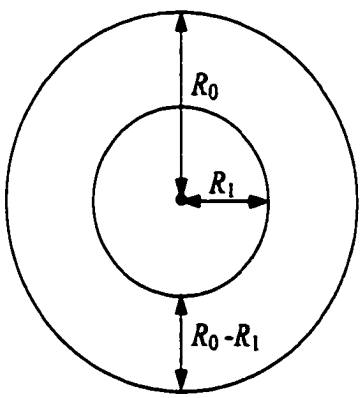


Figure 13. Top View of a Conical Frustum.

$$r_i = y_i^{1/2}(R_0 - R_1) + R_1 \tag{4.10}$$

$$\theta_i = 360°x_i \tag{4.11}$$

$$h_i = (-h)(r_i - R_1)/(R_0 - R_1) \tag{4.12}$$

where h is the height of a conical frustum and

R_0 and R_1 are the bottom and top radii of a conical frustum.

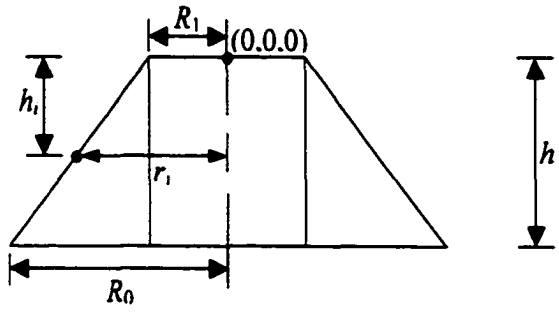


Figure 14. Side View Section of a Conical Frustum.

As the CMM uses the Cartesian coordinates, (r_i, θ_i, z_i) must be transformed to (x_i, y_i, z_i) and the origin (0, 0, 0) is relocated to the center point of the cone's base. A conical frustum can be described by the parametric equations as:

$$x_i = A_i \cos(\theta_i) \tag{4.13}$$

$$y_i = A_i \sin(\theta_i) \tag{4.14}$$

$$z_i = h + h_i \tag{4.15}$$

where A_i is a distance on XY plane between a Hammersley point and the origin. Such relationships are shown in Figure 15 (top view) and Figure 16 (auxiliary view). The

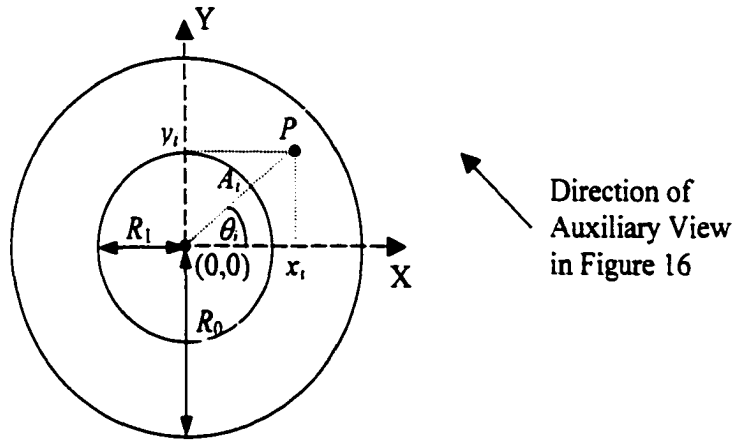


Figure 15. Top View of a Frustum Used to Find The Parametric Equations.

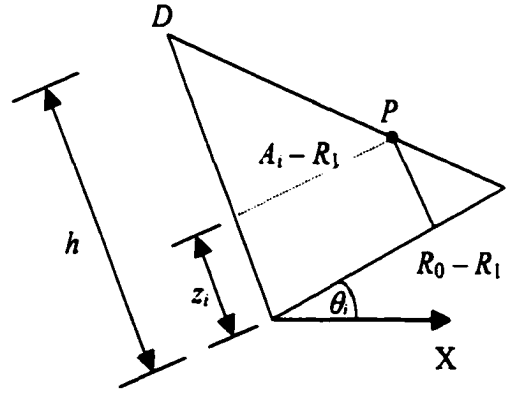


Figure 16. Auxiliary View Normal to the Plane Passing the Origin and Point *P*.

view direction of Figure 16 is depicted in Figure 15. As a result, the following relationship could be obtained, $(h - z_i)/h = (A_i - R_1)/(R_0 - R_1)$. Hence,

$$A_i = (\frac{h - z_i}{h})(R_0 - R_1) + R_1 \qquad (4.16).$$

Consequently,

$$x_i = [(\frac{h - z_i}{h})(R_0 - R_1) + R_1]\cos(\theta_i) \qquad (4.17)$$

$$y_i = [(\frac{h - z_i}{h})(R_0 - R_1) + R_1]\sin(\theta_i) \qquad (4.18)$$

$$z_i = h + h_i \qquad (4.19).$$

The simulation results of this strategy are shown in Figures 19 and 20.

4.2 The Halton-Zaremba Sampling Strategy

The Halton-Zaremba is another mathematical sequence proven to provide low discrepancy (high accuracy). It is concluded by Woo et al. (1995) that no distinguishable difference exists in the performance between the Hammersley and the Halton-Zaremba sequences in 2D space. The obvious limitation of the Halton-Zaremba sequence is that the number of points must be a power of two. On the contrary, its advantage is the ease of implementation in digital hardware (Woo et al., 1995). In two dimensions, the coordinates (x'_i, y'_i) of the Halton-Zaremba sequence can be determined as

$$x'_i = i/N \qquad (4.20)$$

$$y'_i = \sum_{j=0}^{k-1} b'_{ij} 2^{-j-1} \tag{4.21}$$

where N is the total number of sample points,

$i \in [0, N\text{-}1]$,

b_i denotes the binary representation of the index i,

b_{ij} denotes the jth bit in b_i,

$b'_{ij} = 1 - b_{ij}$ for j odd

$= b_{ij}$ otherwise,

$k = \lceil \log_2 N \rceil$, and

$j = 0, \ldots, k\text{-}1$.

For example, N = 16 = 2^4 and $k = 4$ bits. The coordinates of these points are presented in Table 3. All 16 Halton-Zaremba points are shown in Figure 17.

Similar to the Hammersley sampling method, the Halton-Zaremba strategy is a systematic sampling and very sensitive to periodic variation. To decrease the probability of capturing the systematic errors of the measurements, the similar idea in randomizing the initial point was applied as follows:

$$x_i = x'_i + x_{rand} \quad ; \text{if } (x'_i + x_{rand}) < 1$$

$$= (x'_i + x_{rand}) - 1 \quad ; \text{otherwise} \tag{4.22}$$

$$y_i = y'_i + y_{rand} \quad ; \text{if } (y'_i + y_{rand}) < 1$$

$$= (y'_i + y_{rand}) - 1 \quad ; \text{otherwise} \tag{4.23}$$

where (x_{rand}, y_{rand}) is the coordinate of the initial point drawn at random.

The only differences between the Hammersley sequence and the Halton-Zaremba sequence are the limitation of the total number of sample points and the inverted odd bit of the binary representation. These differences do not at all affect the development process derived in extending the 2D sampling strategy to 3D space in Section 4.1. Hence, Equations (4.5) to (4.19) are also valid for the Halton-Zaremba sampling strategy. The simulation results of this strategy are shown in Figures 21 and 22.

Table 3. Coordinates of 16 Halton-Zaremba Sampling Points.

i	B_i	$b'_{i3}2^{-3-1}$	$b'_{i2}2^{-2-1}$	$b'_{i1}2^{-1-1}$	$b'_{i0}2^{-0-1}$	x_i	y_i
0	(0, 0, 0, 0)	0.0625	0	0.25	0	0	0.3125
1	(0, 0, 0, 1)	0.0625	0	0.25	0.5	0.0625	0.8125
2	(0, 0, 1, 0)	0.0625	0	0	0	0.125	0.0625
3	(0, 0, 1, 1)	0.0625	0	0	0.5	0.1875	0.5625
4	(0, 1, 0, 0)	0.0625	0.125	0.25	0	0.25	0.4375
5	(0, 1, 0, 1)	0.0625	0.125	0.25	0.5	0.3125	0.9375
6	(0, 1, 1, 0)	0.0625	0.125	0	0	0.375	0.1875
7	(0, 1, 1, 1)	0.0625	0.125	0	0.5	0.4375	0.6875
8	(1, 0, 0, 0)	0	0	0.25	0	0.5	0.25
9	(1, 0, 0, 1)	0	0	0.25	0.5	0.5625	0.75
10	(1, 0, 1, 0)	0	0	0	0	0.625	0
11	(1, 0, 1, 1)	0	0	0	0.5	0.6875	0.5
12	(1, 1, 0, 0)	0	0.125	0.25	0	0.75	0.375
13	(1, 1, 0, 1)	0	0.125	0.25	0.5	0.8125	0.875
14	(1, 1, 1, 0)	0	0.125	0	0	0.875	0.125
15	(1, 1, 1, 1)	0	0.125	0	0.5	0.9375	0.625

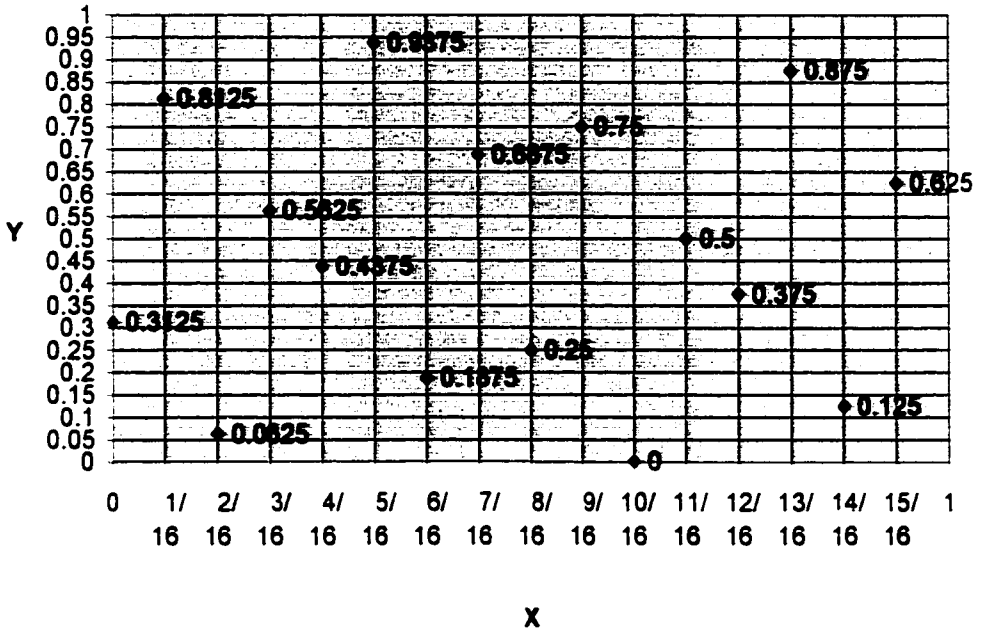


Figure 17. Distribution of 16 Halton-Zaremba Sampling Points.

4.3 The Aligned Systematic Sampling Strategy

As mentioned before, in systematic sampling, only the first point is drawn at random and the subsequent points are taken according to a predetermined mathematical pattern. There exist two versions of systematic sampling; one is aligned and the other is unaligned sampling. The aligned sampling is commonly adapted as systematic sampling.

Suppose that a population is arranged in the form of *am* columns and each column consists of *bn* units (P. Sukhatme and B. Sukhatme, 1970). When a systematic sample of *ab* units is to be selected, the location of the first unit is determined as a pair of random numbers (p, q) such that p is less than or equal to m

and q is less than or equal to n. Then the coordinates (x_i, y_i) of the subsequent sampling points are expressed as $(p + im, q + jn)$ where i and j are integer numbers varying from 0 to a-1 and from 0 to b-1, respectively. Hence, the total number of sample points is equal to ab. Figure 18 shows an example set of aligned systematic sampling in 2D where $N = 9$, $a = 3$, $m = 3$, $b = 3$, $n = 4$, and a pair of random numbers $(p, q) = (1, 2)$.

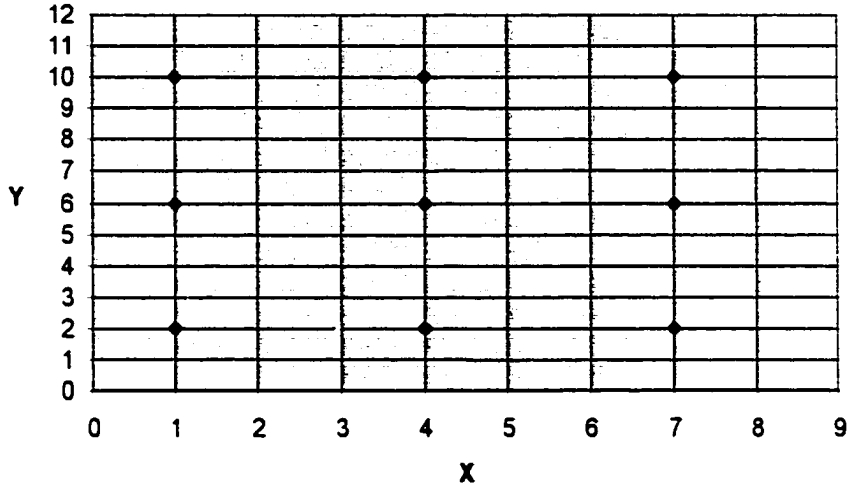


Figure 18. An Example of 9 Aligned Systematic Sampling Points.

Using the similar approach in extending the 2D sampling strategy to 3D space to that in Section 4.1, the 3D equations in the Polar coordinates can be obtained as follows:

$$r_i = R\sqrt{\frac{y_i}{bn}} \tag{4.24}$$

$$\theta_i = 360°x_i/(am) \tag{4.25}$$

$$h_i = r_i(-h)/R \qquad (4.26).$$

Equations (4.24), (4.25), and (4.26) can be generalized for a conical frustum as:

$$r_i = (y_i/(bn))^{1/2}(R_0 - R_1) + R_1 \qquad (4.27)$$

$$\theta_i = 360°x_i/(am) \qquad (4.28)$$

$$h_i = (-h)(r_i - R_1)/(R_0 - R_1) \qquad (4.29).$$

Clearly, the transformation process from the Polar coordinates to the Cartesian coordinates is not dependent on the sampling strategies. Thus, Equations (4.13) to (4.19) are still valid for the aligned systematic sampling strategy. The simulation results of this strategy are shown in Figures 23 and 24.

4.4 The Random Numbers Generation

The random numbers used in this dissertation must have two important properties, uniformity and independence. Each random number is an independent sample drawn from a continuous uniform distribution between zero and one (Banks and Carson II, 1984). Any method for generating such numbers on a computer is a recursive algorithm or a pseudo-random number generator that can replicate the same sequence of random numbers. An argument can be made that the generated numbers are not truly random. However, modern and carefully constructed random number generators generally succeed at producing a sequence of numbers that are truly random (Kelton et al., 1998). To be sure, some tests were conducted. If there are any departures detected in the results, the generation scheme must be modified.

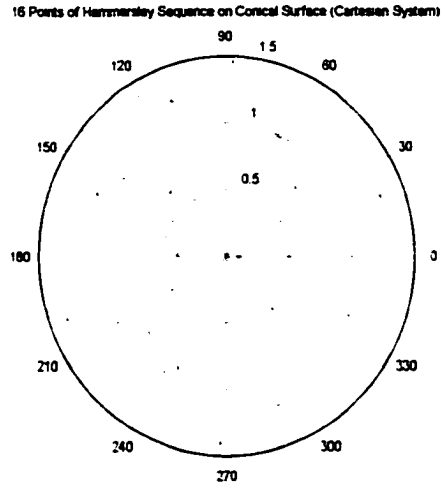


Figure 19. A Top View of 16 Randomized Hammersley Points on a Cone.

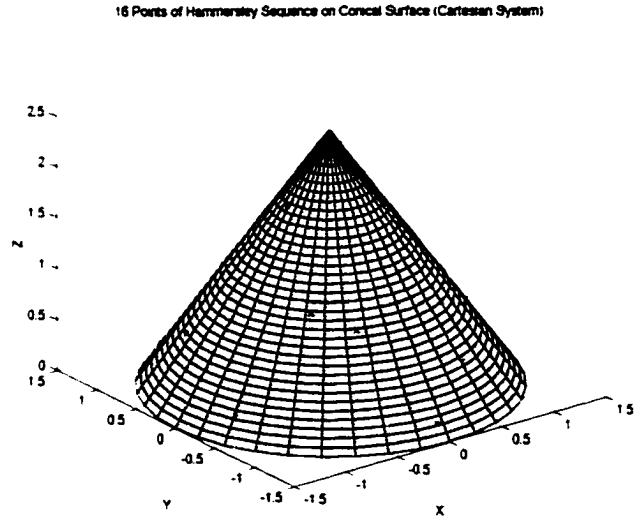


Figure 20. A 3-D View of 16 Randomized Hammersley Points on a Cone.

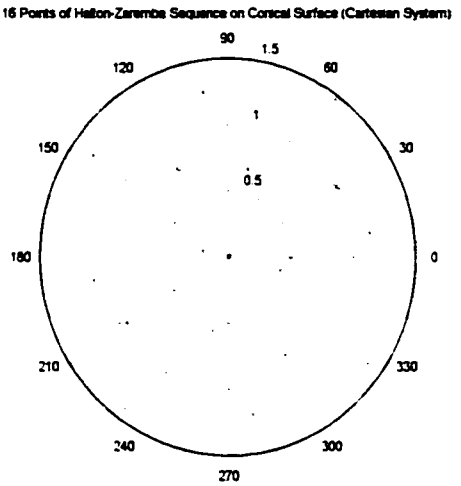


Figure 21. A Top View of 16 Randomized Halton-Zaremba Points on a Cone.

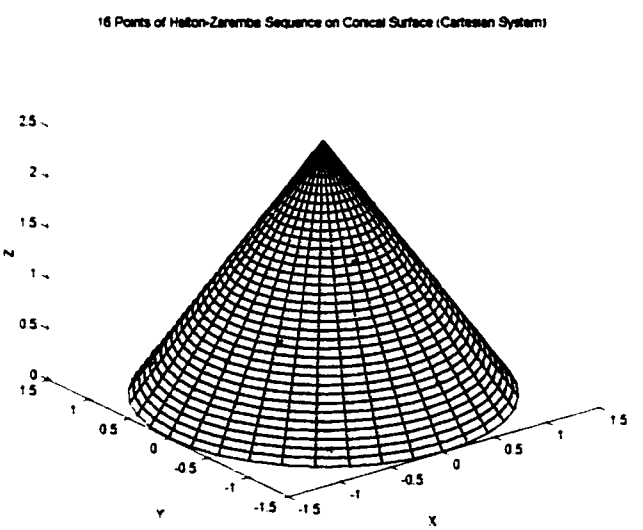


Figure 22. A 3-D View of 16 Randomized Halton-Zaremba Points on a Cone.

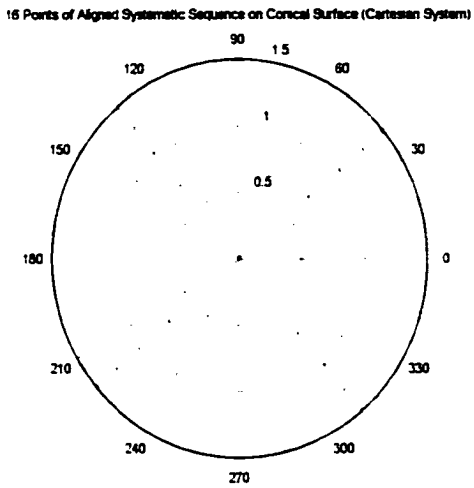


Figure 23. A Top View of 16 Aligned Systematic Sampling Points on a Cone.

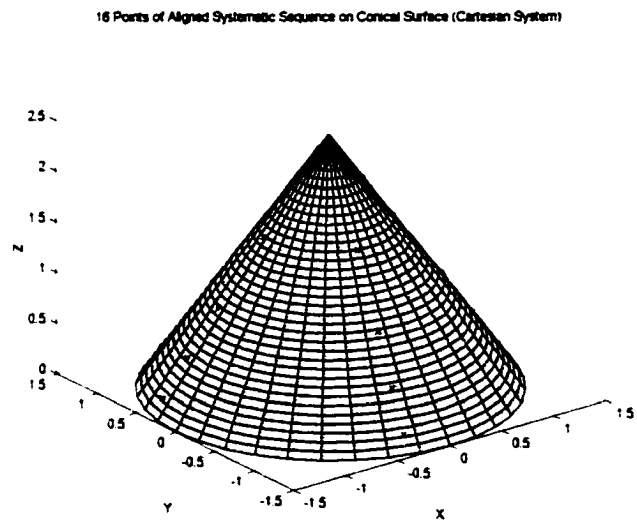


Figure 24. A 3-D View of 16 Aligned Systematic Sampling Points on a Cone.

MATLAB has a built-in function, RAND, that produces uniformly distributed pseudo-random numbers on the interval (0.0, 1.0). Even though MATLAB is widely accepted, certain tests should be performed to confirm the properties of random numbers generated by MATLAB's RAND. Three tests, frequency test, runs test, and autocorrelation test, were used to determine if RAND possesses the desired properties. The first test regards testing for uniformity. The second and third tests concern testing for independence. Subsection 4.4.1 briefly describes the frequency test. The runs test is presented in Subsection 4.4.2. The final subsection, 4.4.3, discusses the autocorrelation test.

4.4.1 Frequency Test

The frequency test uses the Kolmogorov-Smirnov test to validate the uniformity. This test compares the theoretical uniform distribution to the distribution of a sample of generated random numbers based on the largest absolute deviation between the continuous cumulative distribution function (cdf) and the empirical cdf over the range of the random variable (Banks and Carson, 1984). The test procedure follows these steps (Banks and Carson, 1984):

1. Rank the data from the smallest to the largest. Let $R_{(i)}$ denotes the ith smallest observation and

$$R_{(1)} \le R_{(2)} \le \ldots \le R_{(N)}.$$

2. Compute

$$D^+ = \max_{1 \le i \le N} \{\frac{i}{N} - R_{(i)}\} \text{ and } D^- = \max_{1 \le i \le N} \{R_{(i)} - \frac{i-1}{N}\}.$$

3. Compute the statistic $D = \max(D^+, D^-)$.
4. Determine the critical value, D_α, from Kolmogorov-Smirnov critical values table.
5. If D is greater than D_α, the null hypothesis that the data are a sample from a uniform distribution is rejected. Otherwise, there are no differences between the empirical distribution and the uniform distribution.

A MATLAB program for Kolmogorov-Smirnov test was implemented to test its RAND function. Using $N = 2048$, $\alpha = 0.05$, and 1000 replications, the test results show that RAND generates a sample of a uniform distribution 955 times. In other words, RAND was acceptable with 95% confidence level. Thus, the uniformity of the generated random numbers was verified.

4.4.2 Runs Tests

The run test examines the hypothesis of independence of the generated random numbers. In other words, if there is a pattern in the random numbers, run test should be able to detect it. The run tests contain runs up and runs down test, runs above and below the mean test, the length of runs test for runs up and down and for runs above and below the mean.

4.4.2.1 Runs Up and Runs Down

An up run is a sequence of numbers in which each number is succeeded by a larger number. Similarly, a down run is a sequence of numbers in which each number is succeeded by a smaller number. The numbers are given a "+" or a "–"

depending on what they are followed by, a larger number or a smaller number, respectively. Each succession of +'s and -'s form a run. Let a denote the total number of runs in a sequence, the mean and variance of a are given by

$$\mu_a = (2N - 1)/3$$

$$\sigma_a^2 = (16N - 29)/90.$$

For $N > 20$, the distribution of a is reasonably approximated by a normal distribution, $N(\mu_a, \sigma_a^2)$. Therefore, this distribution could be used to test the independence of generated random numbers. The test statistic is $Z_0 = (a - \mu_a)/\sigma_a$ where $Z_0 \sim N(0,1)$. If $-z_{\alpha/2} \leq Z_0 \leq z_{\alpha/2}$, failure to reject the hypothesis of independence occurs (Banks and Carson, 1984).

4.4.2.2 Runs Above and Below The Mean

The test for runs up and runs down is not completely adequate in some situations for the independence test of a group of numbers. For example, there could be 20 consecutive numbers above the mean and the next 20 consecutive numbers below the mean. Even though this incidence is highly unlikely, there is a possibility. A similar test, runs above and below the mean, is more appropriate to test this example (Banks and Carson, 1984). The definition of Runs is changed to describe where each number is located comparing to the mean. A "+" or "-" implies that a number is above the mean or below the mean, respectively. Let n_1 and n_2 be the number of observations above and below the mean and let b denote the total number of runs, the mean and variance of b are described by

$$\mu_b = (2n_1n_2/N) + (1/2)$$

$$\sigma_b^2 = (2n_1n_2(2n_1n_2 - N))/(N^2(N - 1)).$$

For either n_1 or n_2 greater than 20, the distribution of b is reasonably approximated by a normal distribution, $N(\mu_b, \sigma_b^2)$. The test statistic is $Z_0 = (b - \mu_b)/\sigma_b$ where $Z_0 \sim N(0,1)$. If $-z_{\alpha/2} \leq Z_0 \leq z_{\alpha/2}$, failure to reject the hypothesis of independence occurs.

Two MATLAB programs for runs up and runs down test and for runs above and below the mean test were implemented to test its RAND function. Using N = 2048, α = 0.05, and 1000 replications, the test results show that RAND generates a sample of an independent distribution 957 and 954 times, respectively for each test. In other words, RAND was acceptable with 95% confidence level for both tests.

4.4.2.3 Length of Runs

If a sequence of numbers continues in a like fashion: three numbers above the mean followed by three numbers below the mean, the foregoing runs tests couldn't detect this pattern. This is where the length of runs comes in (Banks and Carson, 1984). Let Y_i be the number of runs of length i in random numbers N. If the random numbers N are independent, the expected value of Y_i for runs up and down is given by

$$E(Y_i) = \frac{2}{(i+3)!}[N(i^2+3i+1) - (i^3+3i^2-i-4)], \qquad i \leq N-2$$

$$E(Y_i) = \frac{2}{N!}, \qquad i = N-1.$$

The expected value of Y_i for runs above and below the mean is given by

$$E(Y_i) = \frac{Nw_i}{E(I)}, \qquad N > 20$$

where w_i is the approximate probability that a run has length i and is given by

$$w_i = (\frac{n_1}{N})^i (\frac{n_2}{N}) + (\frac{n_1}{N})(\frac{n_2}{N})^i, \qquad N > 20, \text{ and}$$

$E(I)$ is the approximate expected length of a run and is given by

$$E(I) = \frac{n_1}{n_2} + \frac{n_2}{n_1}, \qquad N > 20.$$

The approximate expected total number of runs of all lengths is given by

$$E(A) = \frac{N}{E(I)}, \qquad N > 20.$$

Let O_i be the observed number of runs of length i. The test statistic is

$$\chi_0^2 = \sum_{i=1}^{L} \frac{[o_i - E(Y_i)]^2}{E(Y_i)}$$

where $L = N - 1$ for runs up and down and $L = N$ for runs above and below the mean. Let the minimum value of expected frequencies be equal to five. If an expected frequency is too small, it can be combined with the expected frequency in an adjacent class interval. If the random numbers are independent, then χ_0^2 is chi-square distributed with $L - 1$ degrees of freedom.

Two MATLAB programs for length of runs for runs up and down test and for runs above and below the mean test were implemented to test its RAND function. Using $N = 2048$ and $\alpha = 0.05$, $\chi_0 = 7.5306$, $\nu = 3$ for run length for runs up and down, and $\chi_0 = 12.7755$, $\nu = 7$ for run length for runs above and below the mean, the test statistic for each test was less than its corresponding critical values, 7.81 and 14.07, respectively. Hence, failure to reject the hypothesis of independence occurred and RAND was adequate.

4.4.3 Tests for Autocorrelation

These tests deal with the dependence between numbers in a sequence. The numbers in the sequence might be related, for example, every number at 8^{th}, 16^{th}, 24^{th}, and so on position might be a very large or very low number. This implies the correlation between these numbers. Therefore, autocorrelation (or serial correlation) tests attempt to determine correlations of a series with lagged values of itself. Since this test was done by using autocorrelation function implemented in the Statistical Product and Service Solutions (SPSS) program, the detailed test procedures that can be found in Banks and Carson (1984) are omitted. A MATLAB program was implemented to generate 2048 random numbers and they were imported to SPSS. Autocorrelations are calculated for lags of 1, 2, ..., and 32. The desired property of independence implies zero autocorrelation. As illustrated in Figure 25, the subsequent test results show very small autocorrelations meaning that there are no distinguishable relationship between successive random numbers at lags of 1, ..., 32. Hence, RAND was validated.

After all these tests, the desired properties, uniformity and independence, of generated random numbers were confirmed. Hence, RAND function was found to be adequate for generating uniformly distributed random numbers in this work.

In summary, this chapter outlines formal procedures for using different sampling strategies at different samples sizes for the inspection of conical features.

Extension to other forms is possible, thus providing a structured environment for data sampling in coordinate metrology.

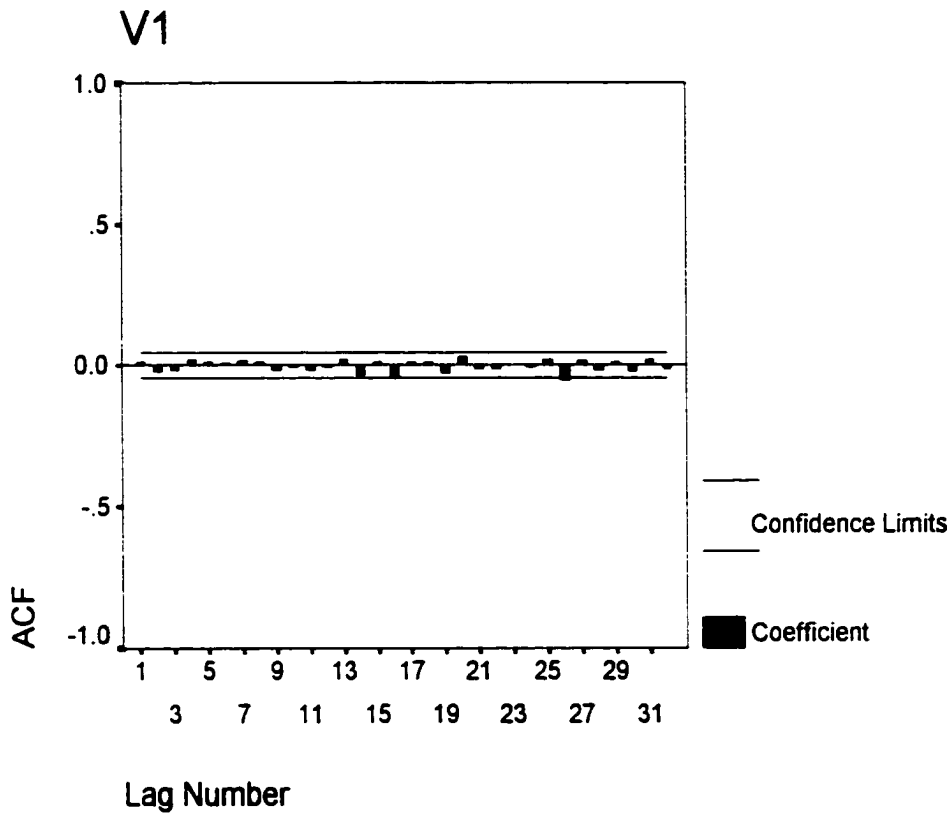


Figure 25. An Example Result of Autocorrelation Tests.

CHAPTER 5

CMM PATH PLANNING FOR EXTERNAL CONICAL SURFACE INSPECTION

A Coordinate Measuring Machine (CMM) is an electromechanical system designed to perform coordinate metrology (Groover, 2001). Positioning CMM's probe relative to the inspected part can be accomplished in several ways, ranging from manual control to direct computer control (DCC). Since the coordinates of the sample points obtained from sampling strategies were very critical in this study, it was very difficult or nearly impossible to use the manual drive in precisely positioning the probe to the desired coordinates. The DCC via part programming was the only way to accomplish this task. The programming statements consist of motion commands, measurement commands, and report formatting commands. The motion commands are used to direct the probe to a desired location. The measurement commands call the various corresponding data processing and calculation routines for particular features of the inspected part. As its name suggests, the report formatting commands permit the specification of the output reports. A set of specific CMM commands which consists of two files, a source file and a path file, was used to write a part program. Consequently, the automatic design of a geometric route must be determined before the actual operation. To generate collision-free trajectories of probe motions, a geometrical model of the inspected part whose dimensions were

given according to the engineering drawing and the obtained coordinates were both taken into consideration together. The problem of moving in space while avoiding collisions with the environment is known as obstacle avoidance or path planning (Jacak, 1999). The path planning module should be able to determine the collision-free route from the initial to the final points. It is important to note that the probe can move along a straight line only. The sampling points, however, are located on the curves of cone or frustum. Thus, a simple path planning is developed for conical object inspection. The main objective of this simple path planning procedure is to generate a collision-free path for all necessary positioning and measuring points so that the probe could automatically visit them without interference. The issue of minimizing the path distance is not taken into consideration. The implemented procedure is an example of off-line programming meaning that it is prepared off-line based on the part drawing and then downloaded to the CMM controller for execution (Groover, 2001).

The development processes of such procedure derived for external conical feature are explained in detail in the following sections. Section 5.1 presents the overview of the procedure and its flow chart. Section 5.2 describes the installation of the procedure for actual inspection.

5.1 The Path Planning Procedure for Conical Feature

A limitation of the CMM probe is that it can travel only along straight lines. The sampling points, however, are located on the curves of cone or frustum. As a

result, the generated paths for each curve would be a group of several straight lines. The probe movements can be functionally divided into two groups, measuring and positioning. When the probe moves from a position to touch the actual surface of the object and moves back out to the same spot, this movement is called measuring and the obtained coordinates are kept for fitting calculation. When the probe travels with some allowance around the inspected object to adjust its positions closer to the measuring coordinates, this movement is called positioning. No coordinate is collected for fitting calculation while positioning. Since the probe movement must avoid the actual surface by using allowance while positioning, the positioning surface, actual surface coupled with allowance, is named the imaginary surface in the following procedure. For convenience, only the positioning in vertical, in horizontal (XY plane), and the hypotenuse directions of the imaginary conical object (triangular side when projected from side view) were adopted in this procedure. The procedure follows these steps:

1. All coordinates of the sampling points, the number of sampling points, and cone parameters (radii and height) are given by the selected sampling strategy.
2. The probe is automatically moved from a safe position to an initial point slightly above the cone. This allowance value can be set to any number. The default is set at 0.2 inch.
3. The inspected object is scanned or measured from top to bottom. Therefore, the coordinates of the sampling points are sorted in descending order of Z's values

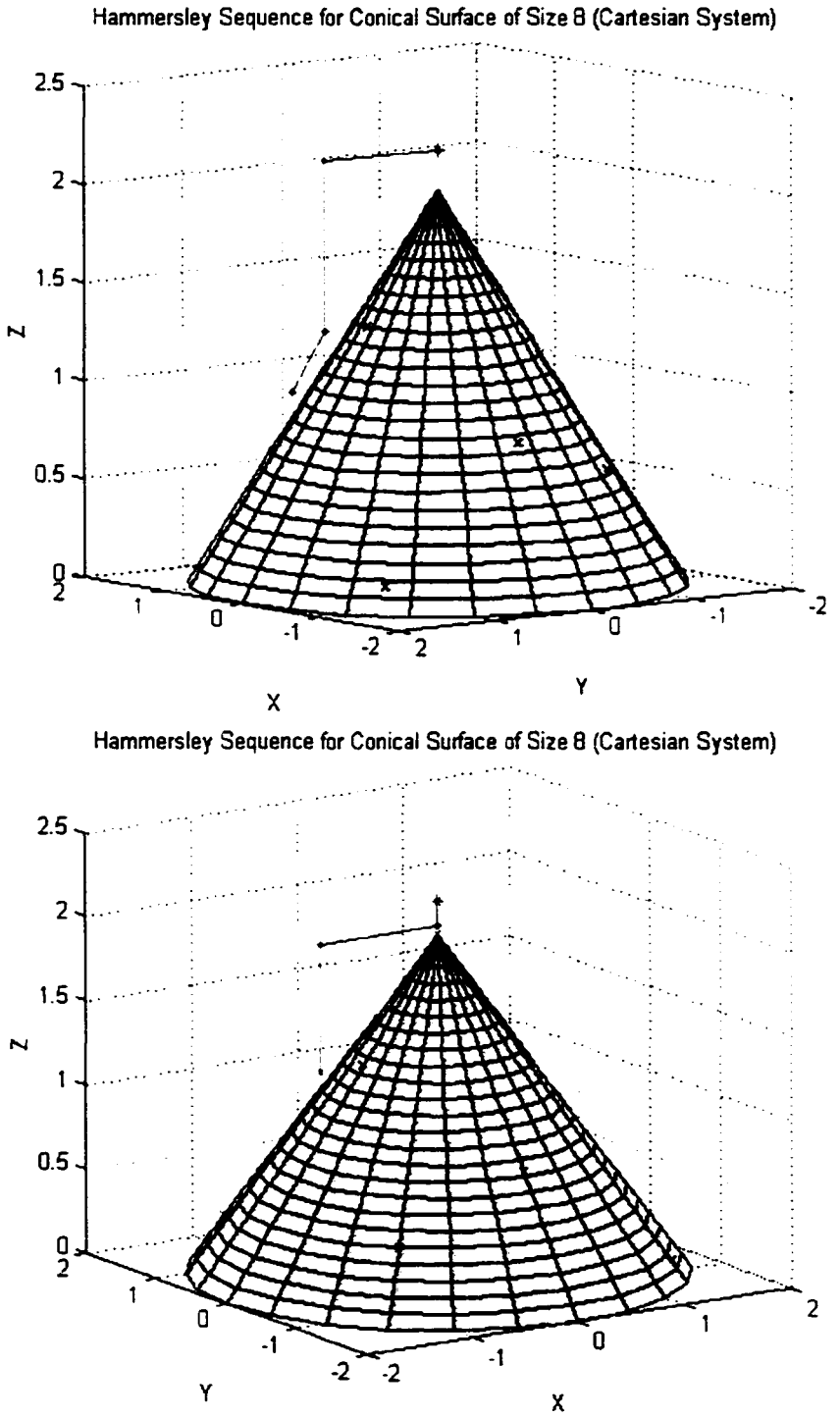


Figure 26. Vertical Positioning Movements.

and the sorted coordinates are visited according to their order. Ties are broken arbitrarily.

4. A vertical path positioning which is just a simple movement along Z axis is required to move from the initial point to the first sorted sampling point. The x's and y's are kept constant. Figure 26 shows all vertical movements used in this procedure. The probe is then moved down and up to take a measurement if the first sorted sampling point is at the apex of cone. If the sampling point is on the hypotenuse side, a horizontal positioning is done first and followed by the vertical positioning. Finally, the probe is moved in and out to take a measurement.
5. If there are several points located at the same level (same z's), a set of horizontal path positioning is required from travelling from one point to the next. If none at the same level, Step 5 is stopped and Step 6 is executed. A horizontal positioning is a movement on the plane parallel to the XY plane by fixing the z's and travelling with the following obstacle avoidance procedure around the inspected conical object. In such procedure, the property of the tangent line was utilized. Mathematically, a circle $(x - x_0)^2 + (y - y_0)^2 = r^2$ and a line $Ax + By + C = 0$ are tangent if and only if *delta* $= r^2(A^2 + B^2) - (Ax_0 + By_0 + C)^2 = 0$. In other words, there is only one point on the line that touches the circle. The line and circle do not intersect if *delta* < 0, and they intersect in two points if *delta* > 0. Note that care must be taken for the line equation when the tangent line is parallel to Y axis. In addition, if a negative *delta* is very close to zero, a small allowance threshold must be used to avoid accidentally hitting the inspected object due to the size of

the ruby and the deviation of the inspected part. A small example utilizing the tangent line property is used to explain the horizontal positioning. Let (x_1, y_1) and (x_2, y_2) be the first and second sampling point (the starting and destination point, respectively) with the same height (z) on the actual surface (circle I). After taking a measurement at (x_1, y_1), the trajectory from (x_1, y_1) to (x_2, y_2) is to be determined. The horizontal movements used in this procedure are depicted in Figure 27. The horizontal positioning follows these steps:

1. Both points are perpendicularly mapped onto the imaginary surface (circle II), the mapped points are (m_1, n_1) and (m_2, n_2), respectively. Therefore, the consideration of the travelling path is shifted to a pair of mapped points on the imaginary surface. Note that circle II is circle I with some given allowance.
2. If an imaginary line segment between (m_1, n_1) (or a mapped point (P_1, P_3, P_5, ...) on the imaginary surface) and (m_2, n_2) does not intersect with the circle I, the probe is simply moved to (m_2, n_2). This can be accomplished by checking the *delta* values, as mentioned above. In this case, the horizontal positioning is stopped right then. Finally, the probe is moved in and out to take a measurement at (x_2, y_2). Otherwise, the positioning is proceeded to the next step.
3. An imaginary line which is tangent to the circle I at (x_1, y_1) (or a mapped point (P_2, P_4, P_6, ...) on the actual surface) is created and two intersection points between the imaginary line and the circle II are determined. The

intersection point P_1 (or P_3, P_5, P_7, ...) contributing to the shorter distance between itself and the destination point (m_2, n_2) is selected.

4. The probe is moved to P_1 (or P_3, P_5, P_7, ...) without collisions with the inspected object.
5. P_1 (or P_3, P_5, P_7, ...) is perpendicularly mapped onto the actual surface (circle I) and the mapped point P_2 (or P_4, P_6, P_8, ...) is obtained.
6. Step 2 to Step 5 are repeated using the mapped point obtained in Step 5 and (m_2, n_2). Note that the intersection points obtained in Step 2 are P_1, P_3, P_5, and so on. The mapped points obtained in Step 4 are P_2, P_4, P_6, and so on.

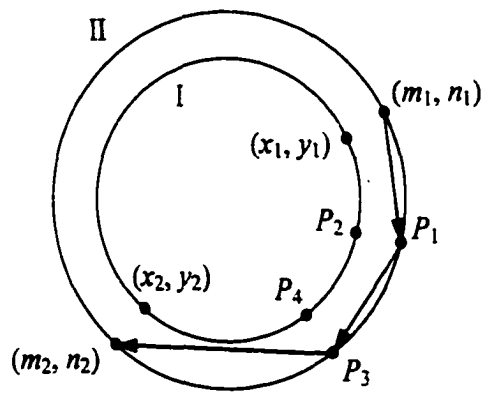


Figure 27. Horizontal Positioning Movements.

6. An hypotenuse positioning is the movement from the higher z to a lower one along the triangular side of the imaginary cone or conical frustum according to the sorted sampling points after all of the measurements at the higher z's are accomplished. Since the radius of cone or conical frustum is not constant, this

factor is taken into consideration in determining the next location on the imaginary cone. Such positioning is illustrated in rectangle boxes in Figure 28. The computed location may or may not precisely reside at the same location as the mapped point of the next sorted sampling point. If it is, then a measurement is taken. Otherwise, a set of horizontal positioning is required.

7. Step 5 and Step 6 are repeated until every sampling point is measured. Then the probe is moved to a safe position, far and away from the object.

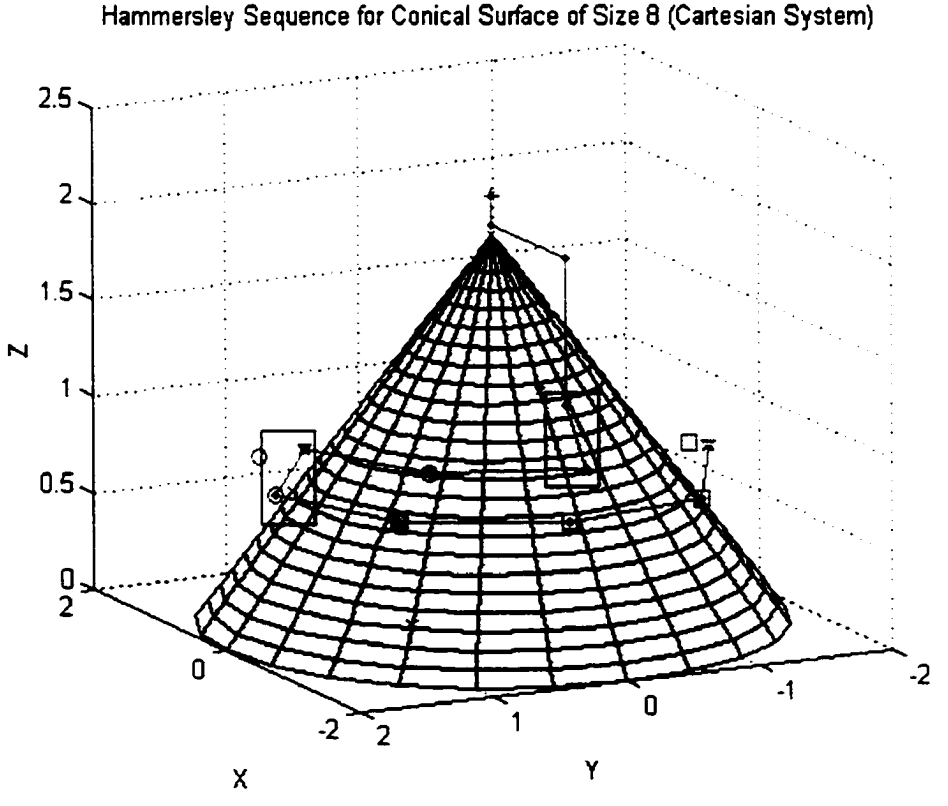


Figure 28. Hypotenuse Positioning Movements.

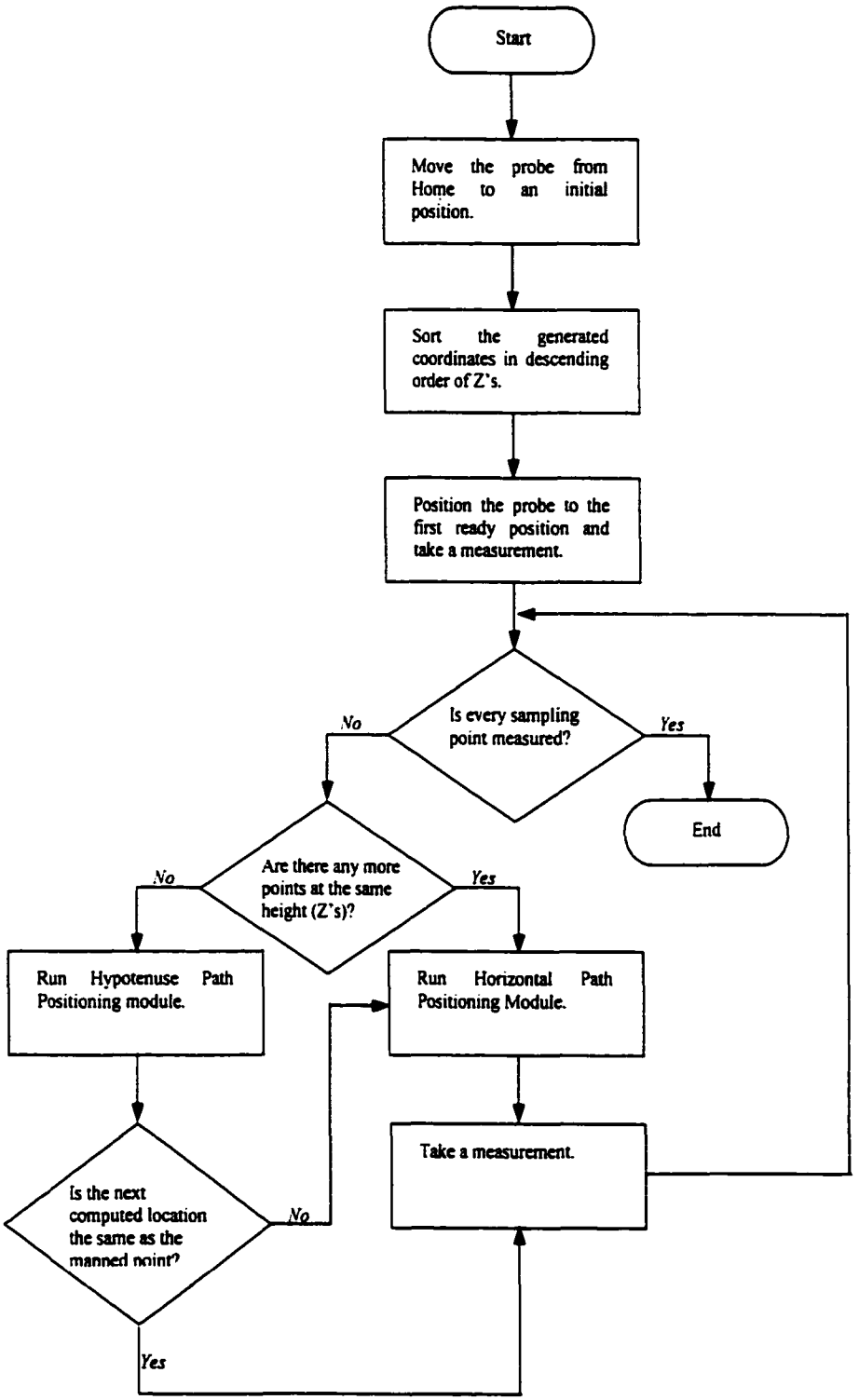


Figure 29. Flow Chart of Path Planning Procedure.

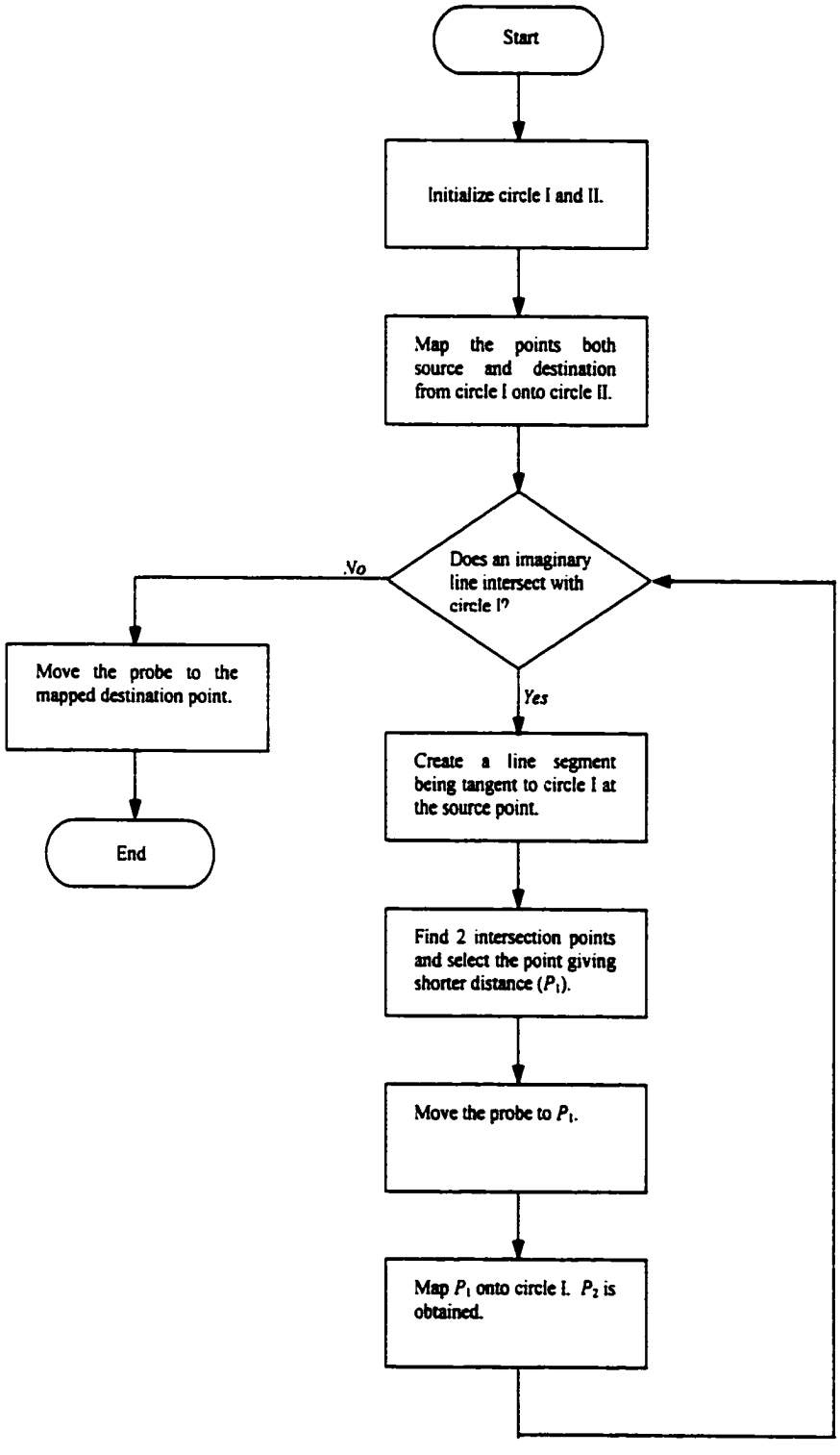


Figure 30. Flow Chart of Horizontal Path Positioning.

5.1.1 Equations for Conical Horizontal Positioning

As mentioned earlier, the horizontal positioning utilizes the property of the tangent line to guide the probe movement. The implicit equation of the tangent to the circle (of the actual cone) at the point $P(x_1, y_1)$ is given by (Faux and Pratt, 1979)

$$2x_1(x - x_1) + 2y_1(y - y_1) = 0$$

or
$$x = \frac{-2y_1 y + 2x_1^2 + 2y_1^2}{2x_1} \qquad (5.1).$$

Given that the circle, a section parallel to XY plane, of the imaginary cone is $x^2 + y^2 = r^2$ and the tangent intersects the circle at two points, substitute Equation (5.1) in the circle:

$$\left(\frac{-2y_1 y + 2x_1^2 + 2y_1^2}{2x_1}\right)^2 + y^2 = r^2$$

$$(-2y_1 y)^2 + 2(-2y_1 y)(2x_1^2 + 2y_1^2) + (2x_1^2 + 2y_1^2)^2 + 4x_1^2 y^2 = 4x_1^2 r^2$$

$$(4y_1^2 + 4x_1^2)y^2 - 4y_1(2x_1^2 + 2y_1^2)y + (2x_1^2 + 2y_1^2)^2 - 4x_1^2 r^2 = 0 \qquad (5.2).$$

Equation (5.2) is a quadratic equation and can be easily solved to obtain y's values. y's are then substituted in Equation (5.1) to calculate x's. As there are two intersection points, the one producing the shorter distance to the destination point (m_2, n_2) is selected. Note that if P lies on Y axis, Equation (5.1) is undefined. The following are used instead of Equations (5.1) and (5.2),

$$y = y_1$$

and
$$x = (r^2 - y_1^2)^{1/2} \qquad (5.3).$$

5.1.2 Equations for Conical Hypotenuse Positioning

A point P_1 on the imaginary surface is located at (m_1, n_1, z_1). The probe is to be moved to P_2 (m_2, n_2, z_2) also on the imaginary surface. z_2 is known by extracting the next point from the sorted sampling points. However, m_2 and n_2 are still unknown. Figure 31 shows the side view snap shot of the inspected conical frustum. Clearly,

$$\Delta h = z_1 - z_2 \tag{5.4}$$

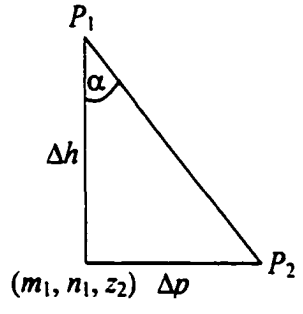


Figure 31. Side View Snap Shot of the Inspected Conical Frustum.

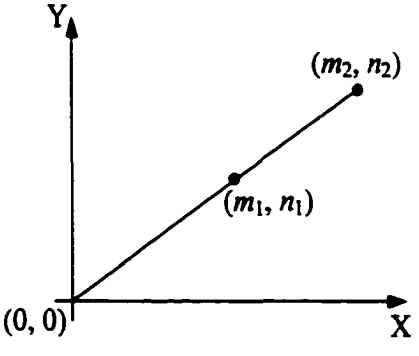


Figure 32. Top View for the Projected Hypotenuse Movement.

and $(R_0 - R_1)/h = \Delta p/\Delta h$, hence $$\Delta p = \frac{(R_0 - R_1)\Delta h}{h} \qquad (5.5).$$

Note that allowances are already included in Equation (5.5). Since z_1's and z_2's are known, Z axis is not needed in determining coordinates in 2D XY space. Z axis is disregarded in Figure 32 and X and Y axes are sufficient. An equation of a straight line is $y = mx + c$. Obviously from Figure 32, $c = 0$ and $m = n_1/m_1$. Hence,

$$n_2 = (n_1/m_1)m_2 \qquad (5.6)$$

The distance $$\Delta p = ((m_1 - m_2)^2 + (n_1 - n_2)^2)^{1/2}$$

$$(\Delta p)^2 = m_1^2 - 2m_1m_2 + m_2^2 + n_1^2 - 2n_1n_2 + n_2^2 \qquad (5.7)$$

Substitute Equation (5.6) in Equation (5.7),

$$(\Delta p)^2 = m_1^2 - 2m_1m_2 + m_2^2 + n_1^2 - \frac{2n_1n_1m_2}{m_1} + (\frac{n_1m_2}{m_1})^2$$

$$[m_1^2 + n_1^2 - (\Delta p)^2] + (-2m_1 - \frac{2n_1^2}{m_1})m_2 + (1 + \frac{n_1^2}{m_1^2})m_2^2 = 0 \qquad (5.8).$$

The above quation is a quadratic equation and can be solved to obtain m_2's values easily. Then m_2's are substituted in Equation (5.6) to determine n_2's. As two coordinates are resulted, the quadrant of P_1 implies which coordinate should be selected. The selected one is always farther from the origin than P_1. Note that if P_1 lies on Y axis, Equation (5.6) is undefined. The following equations are used instead of Equations (5.6) to (5.8),

$$m_1 = m_2 \text{ and}$$

$$\Delta p = n_2 - n_1 \text{ where } P_1 \text{ is on +Y or}$$

$$= n_1 - n_2 \text{ where } P_1 \text{ is on -Y} \qquad (5.9).$$

5.1.3 Mapping Equations between Actual Surface and Imaginary Surface

The mapping points between the actual surface and the imaginary surface can be simply calculated by using the following relationship shown in Figure 33. Clearly, $\tan(\theta) = \frac{n}{m} = \frac{y}{x}$ or $\theta = \tan^{-1}(\frac{n}{m}) = \tan^{-1}(\frac{y}{x})$. One of these two points is known and used to find its counterpart. Hence, the allowances along X (a_x) and Y (a_y) axes can be described by

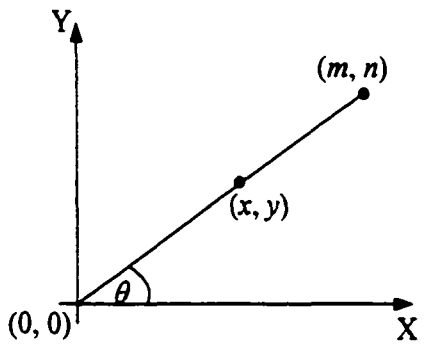


Figure 33. Top View of the Mapped Points.

$$a_x = (\text{given allowance})\cos(\theta)$$

$$a_y = (\text{given allowance})\sin(\theta).$$

The allowance is set to a default at 0.4. The quadrant of (x, y) and (m, n) implies if a_x and a_y should be added or subtracted by the known point. If (x, y) is known but (m, n) is not,

$(m, n) = (x, y) + (a_x, a_y)$, when (x, y) is in quadrant 1 or 4;

$(m, n) = (x, y) - (a_x, a_y)$, when (x, y) is in quadrant 2 or 3.

If (m, n) is known but (x, y) is not,

$$(x, y) = (m, n) - (a_x, a_y), \text{ when } (m, n) \text{ is in quadrant 1 or 4;}$$

$$(x, y) = (m, n) + (a_x, a_y), \text{ when } (m, n) \text{ is in quadrant 2 or 3.}$$

A trajectory set of vertical, horizontal, and hypotenuse movements for given sampling strategy, size, and conical object dimensions was determined by the path planning procedure with the above equations. A set of MATLAB programs for path planning was implemented to generate and simulate such path so that all the sampling points were definitely visited and visually checked without a collision between the inspected conical object and the CMM probe.

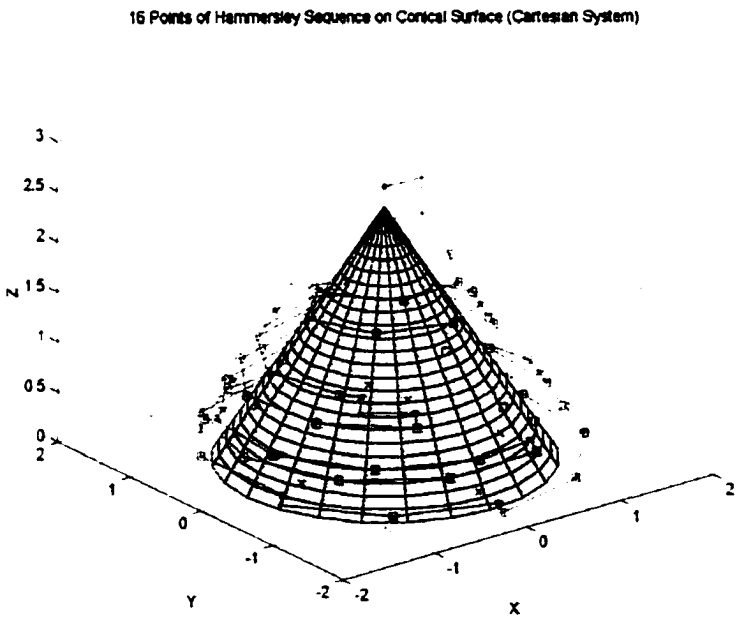


Figure 34. An Example of Path Planning for Hammersley Sequence.

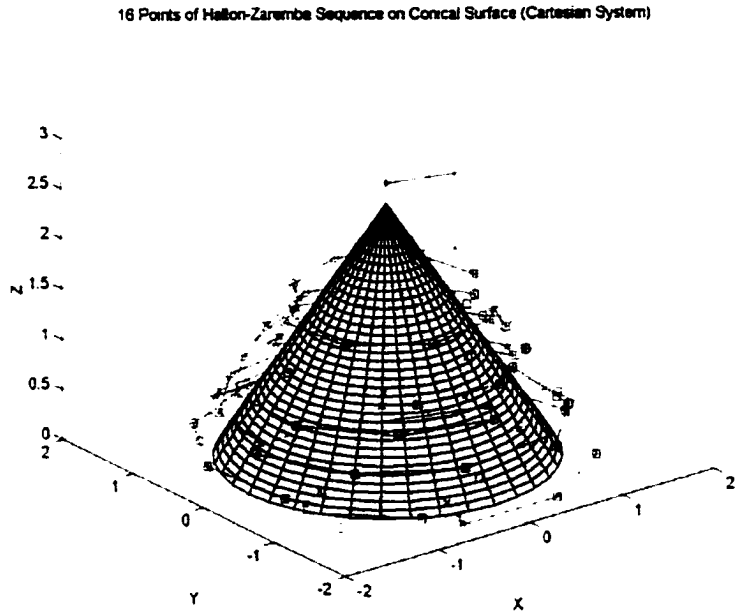


Figure 35. An Example of Path Planning for Halton-Zaremba Sequence.

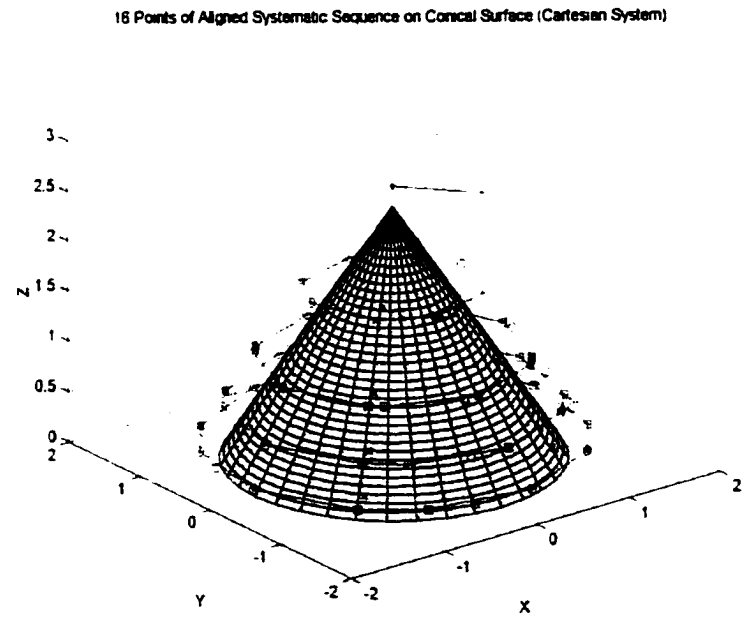


Figure 36. An Example of Path Planning for Aligned Systematic Sampling.

5.2 The Installation of The Off-line Path Planning Procedure

For simplicity, the CMM probe is realigned so that its zero point is located at the center point of the cone base. Instead of aligning the part to the CMM axes, the CMM measurement axes are mathematically aligned relative to the inspected part. This step simply eases the computational effort required and the time consumed in calculating and controlling the coordinates of the CMM probe. After alignment, the probe is moved to a safe (home) position.

As mentioned earlier, a set of part programs consisting of two files, a source file and a path file, was prepared off-line. The source file or program file is generally the same for almost every feature. The only difference is the calculation routine which is called corresponding to the inspected feature. Hence, the source file for different sizes of conical feature is virtually the same. However, the path file which is used to control the movements, measuring and positioning, of the probe is dependent upon the sampling strategy and the sample size. Therefore, this path file achieves only one-way communication between a set of MATLAB programs, generating an obstacle avoidance path, and the CMM controller. After the preparation of the part program set, both files then were loaded and executed on the CMM controller. The obtained results were stored on a temporary space before they were analyzed by fitting algorithms.

5.3 Limitations of the Conical Feature Path Planning Procedure

This section presents some limitations relevant to the CMM and the derived path planning procedure. The limitations that should be pointed out are probe compensation, overtravel of the measuring probe, the measurement angles, and shanking of the probe stylus.

As mentioned in Section 2.2, the probe compensation was automatically taken into account by the CMM measurement software during the qualification process. Next, an overtravel of the probe might occur if the measuring speed is too fast. Not only that but damages might also occur if the probe cannot stop before it hits the inspected object or worktable with too much momentum. Hence, a relatively slow speed should be employed for the probe while measuring. The measurement velocity can be configured from the machine parameters settings module in the CMM measurement software (TUTOR^{TM}). In this research, the maximum value of measuring speed used was 15 % of the default value and the maximum value of positioning speed used was 80 % of the default value.

Moreover, there was a concern about the angle of the probe hits. Since the probe hits were taken neither perpendicular nor parallel to the probe body for the conical surfaces, this gave results that were less repeatable than those taken either perpendicular or parallel. According to Brown & Sharpe Mfg. Co. (1996), if the probe hits are taken within 80 degrees of perpendicular, skidding errors will be much less than one micron (0.000040 inch). All surfaces of the conical objects used in this work were about 30 degrees to the probe body. Assuming that the skidding errors

have the linear relationship to the deviated angles of the inspected surfaces, the skidding errors for the conical objects were much less than three micron (0.00012 inch). To avoid such problems or to access a complex surface without a collision, probe orientation can be adjusted to better suit the part surfaces (Lim and Menq, 1994; Yau and Menq, 1995). However, this can only be done manually with the CMM used in this research. The angular position available for adjustment is from 15 to 90 degrees vertically and horizontally with 15-degree step. Moreover, several sets of high numbers of data points are to be collected, which is extremely inconvenient to adjust the probe angle manually to suit various sizes of conical part surfaces. Therefore, the probe orientation is not taken into account for path planning. The default orientation is used throughout.

Lastly, another possible cause of error is shanking, when the probe contacts the part with the shank of the stylus, not the tip. The measuring system will assume that the hit was taken and record that point. Increasing the diameter of the ruby ball increases the ball/stem clearance and lessens the chance of shanking. Also increasing the depth of the stylus (effective working length or EWL) should ease the problem and cover many sizes of conical part surfaces inspection. However, using the larger ruby ball reduces the effect of surface finish on the inspected part. The probe is already designed to avoid the shanking and/or accessing the complex surfaces by using probe orientations (15 degree-step on both the vertical and horizontal planes). Nevertheless, the probe orientations of MicroVal PFx model can merely be adjusted manually, which would create a lot of inconveniences as mentioned above. To avoid

the shanking problem in this study, the angle to be used between the inspected conical surfaces and the probe stylus of MicroVal PFx model must be greater than or equal to 25 degrees.

The limitations of the proposed path planning procedure and the CMM used should be taken into consideration. Probe compensation, overtravel of the measuring probe, the measurement angles, and shanking of the probe stylus can affect the accuracy of the measurement. Their corrections must be realized before the CMM MicroVal PFx and the path planning procedure can be used together successfully.

In summary, a formal procedure for path planning was developed for traveling between points selected through a given sampling strategy, while avoiding obstacles and reducing travel path. This structure could be extended to the inspection of other forms to formalize inspection procedures in coordinate metrology.

CHAPTER 6

EXPERIMENTAL DESIGN

This chapter describes the experimental design that was followed to develop some understanding of the sampling and zone fitting procedures. A factorial design with nested blocking factor was developed to investigate overall mean performance patterns of the relevant factors.

6.1 Experimental Samples

Five pieces of aluminum cones and five pieces of aluminum conical frustums were tested in this study. Each piece had a small pin at the center of its base. Two different sizes of square plates were used to position the conical objects at a small height from the CMM worktable, such that the probe could access the sampling points near the bottom of the conical objects. The pins on the parts were designed to mate with the small holes at the center of the plates to guide the zero point alignment of the CMM and to stably fix the objects by inserting the pins into these holes. The dimensional drawings of these objects are shown in Figures 37 to 40. The specified size tolerances of the sample objects were maintained within 0.005 inch.

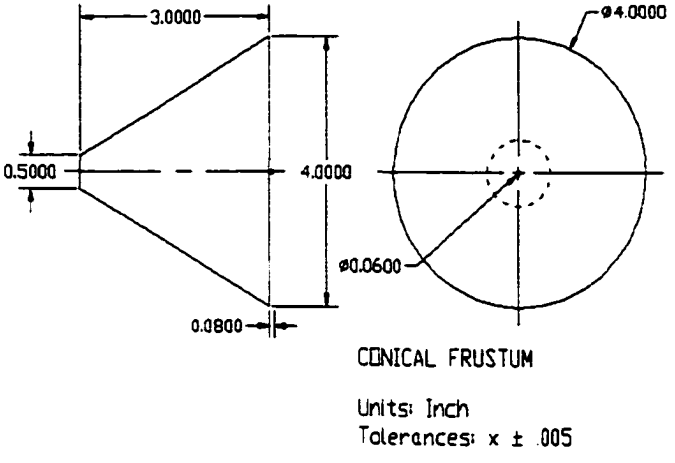


Figure 37. A Dimensional Drawing of the Conical Frustum Specimen.

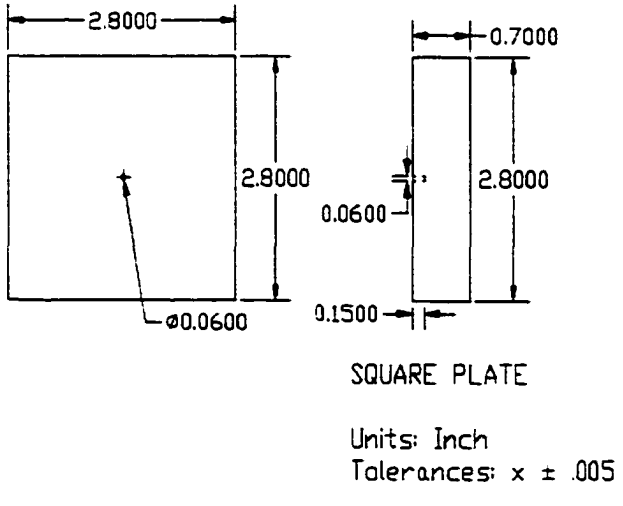


Figure 38. A Dimensional Drawing of the Big Square Plate.

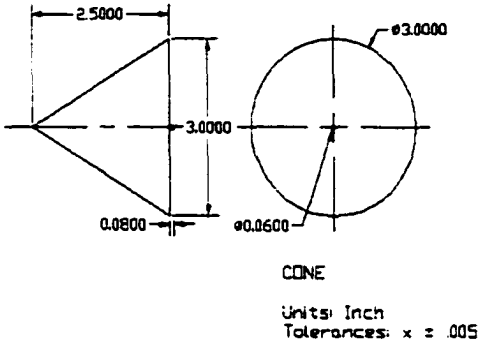


Figure 39. A Dimensional Drawing of the Conical Specimen.

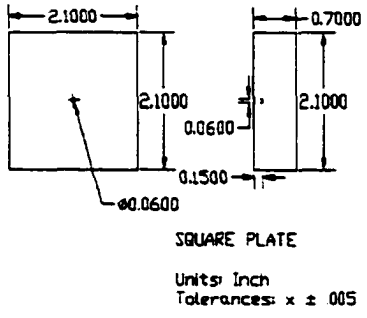


Figure 40. A Dimensional Drawing of the Small Square Plate.

6.2 Equipment and Tools

The Brown & Sharpe MicroVal PFx™ 454 Coordinate Measuring Machine (CMM) was used to take measurements on the sample conical objects. The repeatability of the machine is within 0.00015 inch or 0.003 mm and the linear displacement accuracy is 0.0002 inch or 0.005 mm for each of the X, Y, and Z axes. A personal computer (PC) was used as the CMM controller (furnished and retrofitted to the CMM by Brown & Sharpe). The measurement software, TUTOR™, for Windows 3.1 was used for data acquisition. The square plates were tightly fixed on the worktable by the clamping tools and the inspected objects were fixed on the plates by the aforementioned pins during the measurement. The tip of the probe was a single ruby ball tip (PH9/PH10). Before accurate measurements could be made, the probe was qualified with the reference sphere with diameter of 0.70004 inch. In addition, the reference offset for the probe was verified as well.

6.3 Designing of the Experiment

A series of experiments was planned in this research to test the suggested guidelines for data collection, data fitting, and path planning. Since this study involved data that were subject to experimental errors, statistical methodology was a very objective approach to the design of the experiment and the analysis of the data (Montgomery, 1997). The results of the study should provide a coherent science base for the effective selection of sample size, sampling strategy, and fitting algorithm. The following factors and their levels were selected:

- 3 sampling strategies; HM, HZ, AS,
- 4 inspection sample sizes; 8, 16, 64, 256,
- 2 areas of conical surface; 13.738857 $inch^2$, 22.710816 $inch^2$,
- 4 specimens for each surface area,
- 4 conicity algorithms; the linear LSQ, the linear optimization, the normalized linear LSQ, and the nonlinear optimization.

Sampling strategies, inspection sample sizes, and conicity algorithms were the main factors of interest.

For each surface area, five specimens were made but only four were randomly selected for the experiment. Using multiple specimens was to account for process variability. Moreover, different operators and/or different machines used may cause some variability. Even the same machinist who operates the operation repeatedly may not be perfectly consistent in setting up the same machine for every manufactured part. Consequently, the specimen factor would be treated as a random factor in this experiment. The levels of the other factors were specifically selected. Hence, they would be treated as fixed factors. The major advantage of using the random factor is that inferences can be made about the entire population of factor levels (other specimens not considered in the analysis).

The conicity was selected as the response variable. The effects of sample sizes, sampling methods, and conicity algorithms were investigated on this response. In real machining shops, the environmental conditions such as temperature, lights, relative humidity, and floor vibration often affect machine geometry (Hocken et al.,

1993). In this research, the experiment was performed in the Precision Measurement Laboratory with controlled conditions, to minimize the effects of these noise sources.

Choice of experimental design basically involves the consideration of number of factors, sample size (number of replicates), run order for the experimental trials, randomization restrictions, and treatment arrangement. If there are two or more factors of interest, the most efficient type of experiment is factorial design. In each complete trial of such a design, all possible combinations of the treatments of the factors are investigated. There were four factors in this experiment, surface areas, sampling strategies, inspection sample sizes, and conicity algorithms. Hence, the factorial design was appropriately selected.

On the contrary, each surface area consisted of four specimens that were unique for that particular surface. That is, specimen 1 from surface area 1 had no connection with specimen 1 from the other surface area, specimen 2 from surface area 1 had no connection with specimen 2 from the other area, and so forth. Therefore, the specimens were nested within the levels of surface areas.

In any experiment, variability arising from a noise factor can impact the results. There are three techniques used to increase the precision of an experiment, randomization, analysis of covariance, and blocking. Usually, a randomization of the order of the individual trials of the experiment is the technique used to guard against an unknown and uncontrolled noise factor. Also, the analysis of covariance is normally used to compensate for a known but uncontrollable nuisance source of variability. In addition, the blocking principle is generally used to systematically

eliminate the effect of known and controllable nuisance factors. If the specimens differ slightly in their tolerances, as might happen if they are produced in different machines, then they will contribute to the variability observed in the tolerance data. A design that would accomplish this requires each foregoing factors to be tested once on each of four specimens, which is a randomized complete block design. Therefore, the blocks or the specimens form a more homogeneous unit. Within a block, the order in which the three sampling strategies were tested was randomly determined.

As a result, from the foregoing discussions, the factorial design with nested blocking factor was chosen for this experiment. It is important to note that interaction between blocks and treatments is assumingly negligible. If these interactions exist, they cannot be separated from the error component. Also, there is no interaction between nested factors since every level of the lower hierarchical factor does not appear with every level of the higher hierarchical factor. Thus, the linear statistical model for this design is

$$y_{ijklm} = \mu + A_i + B_{j(i)} + C_k + D_l + E_m + (AC)_{ik} + (AD)_{il} + (AE)_{im} + (CD)_{kl} + (CE)_{km} + (DE)_{lm} + (ACD)_{ikl} + (ACE)_{ikm} + (ADE)_{ilm} + (CDE)_{klm} + (ACDE)_{iklm} + \varepsilon_{ijklm} \quad (6.1)$$

where $i = 1, a = 2,$

$j = 1, 2, \ldots, b = 4,$

$k = 1, 2, \ldots, c = 3,$

$l = 1, 2, \ldots, d = 4,$

$m = 1, 2, \ldots, e = 4,$

A_i is the effect of the ith surface area,

$B_{j(i)}$ is the effect of the jth specimen within the ith level of surface area,

C_k is the effect of the kth sampling method,

D_l is the effect of the lth sample size,

E_m is the effect of the mth conicity algorithm,

$(AC)_{ik}$ is the surface area × sampling method interaction,

$(AD)_{il}$ is the surface area × sample size interaction,

$(AE)_{im}$ is the surface area × conicity algorithm interaction,

$(CD)_{kl}$ is the sampling method × sample size interaction,

$(CE)_{km}$ is the sampling method × conicity algorithm interaction,

$(DE)_{lm}$ is the sample size × conicity algorithm interaction,

$(ACD)_{ikl}$ is the surface area × sampling method × sample size interaction,

$(ACE)_{ikm}$ is the surface area × sampling method × conicity algorithm interaction,

$(ADE)_{ilm}$ is the surface area × sample size × conicity algorithm interaction,

$(CDE)_{klm}$ is the sampling method × sample size × conicity algorithm interaction,

$(ACDE)_{iklm}$ is the surface area × sampling method × sample size × conicity algorithm interaction,

ε_{ijklm} is the error term.

Table 4. Overview of Data Sheet Table.

Area of Surface (A)				1												2											
Specimen (B)				1			2			3			4			1			2			3			4		
Sampling Method (C)				HM	HZ	AS	HM	HZ	AS	HM	HZ	AS	HM	HZ	AS	HM	HZ	AS	HM	HZ	AS	HM	HZ	AS	HM	HZ	AS
Sample Size (D)	8	DATA FITTING (E)	NLLSQ																								
			LLSQ																								
			LOPT																								
			NLOPT																								
	16	DATA FITTING (E)	NLLSQ																								
			LLSQ																								
			LOPT																								
			NLOPT																								
	64	DATA FITTING (E)	NLLSQ																								
			LLSQ																								
			LOPT																								
			NLOPT																								
	256	DATA FITTING (E)	NLLSQ																								
			LLSQ																								
			LOPT																								
			NLOPT																								

Data fitting algorithms used for calculating the form error

NLLSQ: The normalized linear LSQ.
LLSQ: The linear LSQ.
LOPT: The linear model with minimum zone method.
NLOPT: The nonlinear model with minimum zone method.

Sampling strategies used for data collection

HM: Hammersley Sampling.
HZ: Halton-Zaremba Sampling.
AS: Aligned Systematic Sampling.

Table 4 shows the overview data sheet developed for this design. As mentioned earlier, if all levels of every factor were specifically chosen in the experiment, inferences are applied only to the factor levels considered in the analysis. The conclusions cannot be extended to similar treatments that were not explicitly considered. Since the mixed model was used, the determinations of the hypotheses, the expected mean squares, and the appropriate test statistics of all factors were not straightforward. The hypotheses tested are as follows:

H_0: $A_1 = A_2 = 0$

H_1: at least one $A_i \neq 0$

H_0: $\sigma^2_{B(A)} = 0$

H_1: $\sigma^2_{B(A)} > 0$

H_0: $C_1 = C_2 = \cdots = C_k = 0$

H_1: at least one $C_k \neq 0$

H_0: $D_1 = D_2 = \cdots = D_l = 0$

H_1: at least one $D_l \neq 0$

H_0: $E_1 = E_2 = \cdots = E_m = 0$

H_1: at least one $E_m \neq 0$

H_0: $(AC)_{ik} = 0$ for all i, k

H_1: at least one $(AC)_{ik} \neq 0$

H_0: $(AD)_{il} = 0$ for all i, l

H_1: at least one $(AD)_{il} \neq 0$

H_0: $(AE)_{im} = 0$ for all i, m

H_1: at least one $(AE)_{im} \neq 0$

H_0: $(CD)_{kl} = 0$ for all k, l (6.2)

H_1: at least one $(CD)_{kl} \neq 0$

H_0: $(CE)_{km} = 0$ for all k, m

H_1: at least one $(CE)_{km} \neq 0$

H_0: $(DE)_{lm} = 0$ for all l, m

H_1: at least one $(DE)_{lm} \neq 0$

H_0: $(ACD)_{ikl} = 0$ for all i, k, l

H_1: at least one $(ACD)_{ikl} \neq 0$

H_0: $(ACE)_{ikm} = 0$ for all i, k, m

H_1: at least one $(ACE)_{ikm} \neq 0$

H_0: $(ADE)_{ilm} = 0$ for all i, l, m

H_1: at least one $(ADE)_{ilm} \neq 0$

H_0: $(CDE)_{klm} = 0$ for all k, l, m

H_1: at least one $(CDE)_{klm} \neq 0$

H_0: $(ACDE)_{iklm} = 0$ for all i, k, l, m

H_1: at least one $(ACDE)_{iklm} \neq 0$.

The expected mean squares (EMS) can be derived by identifying all sources of variability and their degrees of freedom as shown in Table 5 and by using the rules for expected mean squares. Table 6 depicts the EMS table. Then the proper test

statistics for all effects are determined such that the expected value of the numerator mean square differs from the expected value of the denominator mean square only by the variance component of the treatment.

Table 5. Degree of Freedom.

Sources of Variability	Degrees of Freedom
A	a-1 = 2-1 = 1
B(A)	$a(b$-1) = 2(4-1) = 6
C	c-1 = 3-1 = 2
D	d-1 = 4-1 = 3
E	e-1 = 4-1 = 3
AC	$(a$-1)(c-1) = 1×2 = 2
AD	$(a$-1)(d-1) = 1×3 = 3
AE	$(a$-1)(e-1) = 1×3 = 3
CD	$(c$-1)(d-1) = 2×3 = 6
CE	$(c$-1)(e-1) = 2×3 = 6
DE	$(d$-1)(e-1) = 3×3 = 9
ACD	$(a$-1)(c-1)(d-1) = 1×2×3 = 6
ACE	$(a$-1)(c-1)(e-1) = 1×2×3 = 6
ADE	$(a$-1)(d-1)(e-1) = 1×3×3 = 9
CDE	$(c$-1)(d-1)(e-1) = 2×3×3 = 18
ACDE	$(a$-1)(c-1)(d-1)(e-1) = 1×2×3×3 = 18
Error	383 - 101 = 282
Total	($abcde$-1) = 2×4×3×4×4 - 1 = 383

Thus, the expected mean squares for all effects are:

Table 6. Expected Mean Square Derivation.

	σ^2	$bcde\sigma^2_A$	$cde\sigma^2_{B(A)}$	$abde\sigma^2_C$	$abce\sigma^2_D$	$abcd\sigma^2_E$	$bde\sigma^2_{AC}$	$bce\sigma^2_{AD}$	$bcd\sigma^2_{AE}$	$dbe\sigma^2_{CD}$	$abd\sigma^2_{CE}$	$abc\sigma^2_{DE}$	$be\sigma^2_{ACD}$	$bd\sigma^2_{ACE}$	$bc\sigma^2_{ADE}$	$ab\sigma^2_{CDE}$	$b\sigma^2_{ACDE}$
A	×	×	×														
B(A)	×		×														
C	×			×													
D	×				×												
E	×					×											
AC	×						×										
AD	×							×									
AE	×								×								
CD	×									×							
CE	×										×						
DE	×											×					
ACD	×												×				
ACE	×													×			
ADE	×														×		
CDE	×															×	
ACDE	×																×

$$E(MS_A) = \sigma^2 + bcde\sigma^2_A + cde\sigma^2_{B(A)}$$

$$E(MS_{B(A)}) = \sigma^2 + cde\sigma^2_{B(A)}$$

$$E(MS_C) = \sigma^2 + abde\sigma^2_C$$

$$E(MS_D) = \sigma^2 + abce\sigma^2_D$$

$$E(MS_E) = \sigma^2 + abcd\sigma^2_E$$

$$E(MS_{AC}) = \sigma^2 + bde\sigma^2_{AC}$$

$$E(MS_{AD}) = \sigma^2 + bce\sigma^2_{AD}$$

$$E(MS_{AE}) = \sigma^2 + bcd\sigma^2_{AE}$$

$$E(MS_{CD}) = \sigma^2 + dbe\sigma^2_{CD} \qquad (6.3)$$

$$E(MS_{CE}) = \sigma^2 + abd\sigma^2_{CE}$$

$$E(MS_{DE}) = \sigma^2 + abc\sigma^2_{DE}$$

$$E(MS_{ACD}) = \sigma^2 + be\sigma^2_{ACD}$$

$$E(MS_{ACE}) = \sigma^2 + bd\sigma^2_{ACE}$$

$$E(MS_{ADE}) = \sigma^2 + bc\sigma^2_{ADE}$$

$$E(MS_{CDE}) = \sigma^2 + ab\sigma^2_{CDE}$$

$$E(MS_{ACDE}) = \sigma^2 + b\sigma^2_{ACDE}$$

and

$$E(MS_{Error}) = \sigma^2.$$

Consequently, the appropriate test statistics for this model are easily determined as follows:

$$F_A = \frac{\sigma^2 + bcde\sigma_A^2 + cde\sigma_{B(A)}^2}{\sigma^2 + cde\sigma_{B(A)}^2} = \frac{MS_A}{MS_{B(A)}}$$

$$F_{B(A)} = \frac{\sigma^2 + cde\sigma_{B(A)}^2}{\sigma^2} = \frac{MS_{B(A)}}{MS_{Error}}$$

$$F_C = \frac{\sigma^2 + abde\sigma_C^2}{\sigma^2} = \frac{MS_C}{MS_{Error}}$$

$$F_D = \frac{\sigma^2 + abce\sigma_D^2}{\sigma^2} = \frac{MS_D}{MS_{Error}}$$

$$F_E = \frac{\sigma^2 + abcd\sigma_E^2}{\sigma^2} = \frac{MS_E}{MS_{Error}}$$

$$F_{AC} = \frac{\sigma^2 + bde\sigma_{AC}^2}{\sigma^2} = \frac{MS_{AC}}{MS_{Error}}$$

$$F_{AD} = \frac{\sigma^2 + bce\sigma_{AD}^2}{\sigma^2} = \frac{MS_{AD}}{MS_{Error}}$$

$$F_{AE} = \frac{\sigma^2 + bcd\sigma_{AE}^2}{\sigma^2} = \frac{MS_{AE}}{MS_{Error}}$$

$$F_{CD} = \frac{\sigma^2 + abe\sigma_{CD}^2}{\sigma^2} = \frac{MS_{CD}}{MS_{Error}} \qquad (6.4)$$

$$F_{CE} = \frac{\sigma^2 + abd\sigma_{CE}^2}{\sigma^2} = \frac{MS_{CE}}{MS_{Error}}$$

$$F_{DE} = \frac{\sigma^2 + abc\sigma_{DE}^2}{\sigma^2} = \frac{MS_{DE}}{MS_{Error}}$$

$$F_{ACD} = \frac{\sigma^2 + be\sigma_{ACD}^2}{\sigma^2} = \frac{MS_{ACD}}{MS_{Error}}$$

$$F_{ACE} = \frac{\sigma^2 + bd\sigma^2_{ACE}}{\sigma^2} = \frac{MS_{ACE}}{MS_{Error}}$$

$$F_{ADE} = \frac{\sigma^2 + bc\sigma^2_{ADE}}{\sigma^2} = \frac{MS_{ADE}}{MS_{Error}}$$

$$F_{CDE} = \frac{\sigma^2 + ab\sigma^2_{CDE}}{\sigma^2} = \frac{MS_{CDE}}{MS_{Error}}$$

$$F_{ACDE} = \frac{\sigma^2 + b\sigma^2_{ACDE}}{\sigma^2} = \frac{MS_{ACDE}}{MS_{Error}}.$$

As mentioned previously, the order in which the three sampling strategies were tested was randomly determined. This was accomplished by using a random permutation function, RANDPERM, in MATLAB from 1 to 12. The randomized sequence is {8, 7, 1, 10, 4, 3, 11, 12, 6, 5, 9, 2}. This sequence was then expanded to cover all combinations within a block by blowing up each number with 4. For example, index number 1 would be converted to a new set of indices 1, 2, 3, and 4 for its corresponding fitting algorithms. Index number 2 would be converted to a new set of indices 5, 6, 7, and 8. Therefore, every index in the permuted sequence was converted to a new index set from 1 to 48. This new sequence was then used to apply randomization to each blocking factor in the experiment.

It is important to note that the following assumption was made and must be checked before the data analysis can be relied on. This assumption is that the errors are normally and independently distributed with mean zero and constant but unknown variance σ^2. Also, the installation of the conical objects was done arbitrarily to avoid

the repetition of a same pattern of machined surface. In addition, the coordinates of sampling points generated by each sampling method for each surface area remained the same throughout the entire set of specimens for each sample size.

Note that all the sampling strategies and their simulations were implemented in MATLAB. The coordinates generated were then fed to a set of part programs that were executed on a CMM's controller (PC) for data collection. The actual coordinates of the obtained sampling points for each and every considered factor were stored in text files. They were then formatted into Excel spreadsheets via Visual Basic for Applications programs. Visual Basic for Applications was also used to implement both of the LSQ based conicity algorithms (LLSQ and NLLSQ) and to formulate both of the optimization based conicity algorithms (LOPT and NLOPT) before calling the optimization engine in LINGO6. The underlying optimization technique performed by LINGO6 in this work is generalized reduced gradient algorithm (GRG). Every numerical computation was performed on a PC with Pentium III 500 MHz running Microsoft Windows 98. All equations of these four conicity fitting algorithms are presented in Chapter 7. The statistical data analyses by SAS programs are discussed in detail in Chapter 8.

CHAPTER 7

MINIMUM CONICAL TOLERANCE ZONE EVALUATION

Tolerance zone evaluation involves a fitting of the sampled discrete points. Conicity verification has received very little attention in the current literature. Although there are quite a number of conical industrial parts such as nozzles, tapered cylinders, frustum holes, and tapered rollers, requiring cone feature verification, often profile tolerancing is used to determine their conicity. Traditional inspection of cones is done through the measurement of diameter (or roundness) and the angularity separately rather than through an evaluation of the conicity. For example, tapered rollers used in bearings are inspected in this manner currently (Cogdel, 1999) using hard gauges. This really is the solution of two 2D problems rather than the 3D solution of a cone. This procedure results in significant inconsistencies. In some sense, lack of universal standards or ambiguity created by some existing standards (Cogdel, 1999) is partially responsible for lack of 3D treatment.

As described in Section 2.1, the ANSI Y14.5M-1994 (ASME, 1995) defines dimensioning and tolerancing to standardize and harmonize the United States practices and methodology with the universal standards. This should improve coordinating and integrating these techniques into electronic data systems. However, it gives very little direction regarding the evaluation of these zones. The achievement of formal guidelines for conicity evaluation is the primary goal of this chapter.

Conicity is a condition of a surface generated by rotating the hypotenuse of a right triangle about one of its leg (axis) with its vertex above the center of its base. Note that this definition is relaxed to cover conical frustum as well.

The analysis of typical form features by Shunmugam (1986; 1987a; 1987b) is the basis of the cone development discussed here. The proposed estimation algorithm always results in smaller zones than the LSQ method (Lin et al., 1995). Since it is modeled as an optimization problem, it cannot guarantee unique solutions. It is important to note that Shunmugam's algorithm uses linear deviation and the limacon approximation in linear problem formulation, which might lead to a slightly smaller tolerance zone than the actual one (Lin et al., 1995).

The most commonly used method to find such zone estimation in practice is the method of least squares (LSQ) due to its uniqueness, efficiency, robustness, and simplicity for linear systems. Even though the LSQ zone evaluation is based on sound mathematical principles, it does not follow the intent of the ANSI Y14.5M-1994 (ASME, 1995) well. It might overestimate the tolerance zone since it attempts to minimize the sum of the squares of the errors. In other words, it does not attempt to minimize the zone of the errors directly. Not only does it reject bad parts, but it might also reject some good parts. In addition, if the LSQ is applied perpendicularly to the imaginary mean features, the resulting normal equations are very complex. In case of three-dimensional features, the solutions of the normal equations become even more complicated (Murthy and Abdin, 1980; Traband et al., 1989). On the other hand, the optimization based zone evaluation attempts to find the minimum zone of

the errors that are consistent with ANSI Y14.5M-1994 (ASME, 1995) definition. The essence of this method lies in the construction and use of models. The conical model formulation for both linear form and nonlinear form proposed in this dissertation is similar to the cylinder formulation suggested by Wang (1992).

For simplicity of the development process of the models of the errors, a coordinates conversion between the Cartesian coordinates to Polar coordinates is used. The conversion equations between the two coordinate systems are as follows:

$$r_i = \sqrt{x_i^2 + y_i^2},$$

$$\theta_i = \tan^{-1}\frac{y_i}{x_i},$$

and $$z_i = z_i .$$

The development of conicity is shown sequentially through a discussion of zone estimation of other common features. Section 7.1 discusses the use of a linear deviation and the limacon approximation to formulate the linear forms for standard features (straightness, flatness, circularity or roundness, and cylindricity). Then a linear form for conicity is developed using the insights gained. Section 7.2 presents details for nonlinear development procedures. The least square method and its model for conical zone evaluation are addressed in Section 7.3. The final section, Section 7.4, demonstrates the linear and nonlinear optimization models for minimum tolerance zone evaluation of standard features leading to minimum conical tolerance zone evaluation.

7.1 Linear Formulation

7.1.1 Straightness

Let the measurement values be represented by (x_i, y_i) and $y = mx + c$ be the ideal straight line; where c is the intercept on the y-axis. The assessment of straightness error is illustrated in Figure 41. Since,

$$y_i' = mx_i + c.$$

Hence, $$d_i = y_i - y_i' = y_i - mx_i - c \qquad (7.1)$$

where d_i is the linear distance or linear deviation between a measured point and a point on the ideal line.

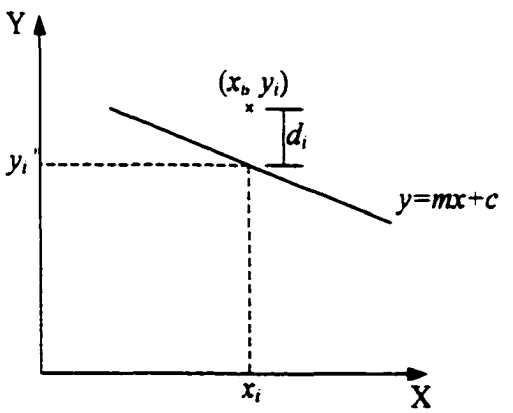


Figure 41. Assessment of Linear Straightness Error.

7.1.2 Flatness

Let (x_i, y_i, z_i) be the measurements of flatness as shown in Figure 42. The assessment plane is $z = mx + ny + c$ where c is the intercept on z-axis. P is a point (x_i, y_i, z_i') on the ideal plane. Thus,

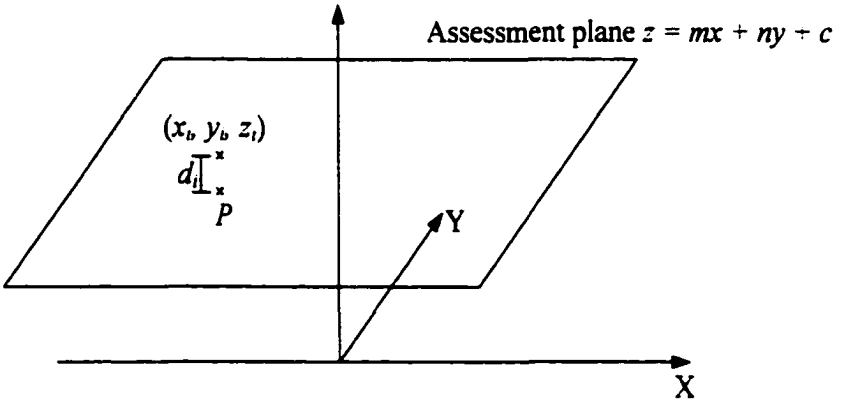


Figure 42. Assessment of Linear Flatness Error.

$$z_i' = mx_i + ny_i + c$$

and
$$d_i = z_i - z_i' = z_i - mx_i - ny_i - c \qquad (7.2)$$

where d_i is the linear deviation between a measured point and a point on the ideal plane.

7.1.3 The Limacon Approximation

The limacon approximation is used to linearize the parameters about the origin of a circle. Its illustration is shown in Figure 43. With this approximation, the

linear functions of circularity and cylindricity can be obtained as provided in the following subsections. Even though an attempt is made to place the

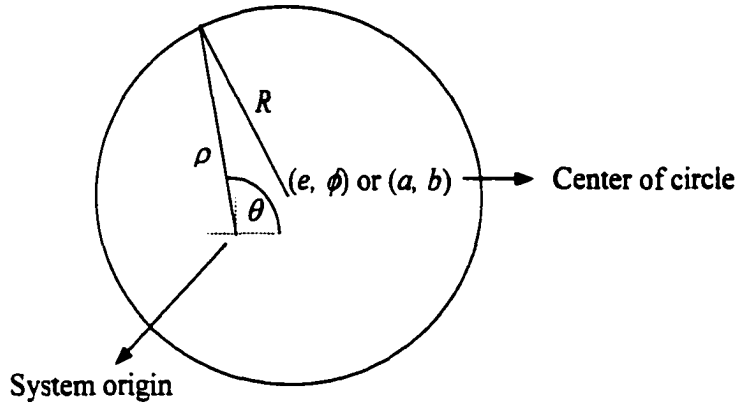


Figure 43. Definition of Circle.

center of the circle at the system origin, this is hardly accomplished. As a result, there is always a small margin of difference between these two points. Let (a, b) and (e, ϕ) be coordinates of the circle center in the Cartesian Coordinates and the Polar Coordinates, respectively. In other words, the distance between the center and the origin is equal to e and the angle between the ray of the two and x-system axis is ϕ. Hence, the angle between the ray and the line with length ρ is equal to $\theta - \phi$. Using Pythagorus theorem,

$$\rho = e\cos(\theta - \phi) + (R^2 - e^2 \sin^2(\theta - \phi))^{1/2}.$$

Assume that e is much less than R. Hence,

$$\rho \cong e\cos(\theta - \phi) + R \qquad (7.3).$$

Using Trigonometric Identities and the definition of the Polar Coordinates,

$$\cos(\theta - \phi) = \cos(\theta)\cos(\phi) + \sin(\theta)\sin(\phi)$$

and $$a = e\cos(\phi),\ b = e\sin(\phi).$$

Hence, $$\cos(\theta - \phi) = (a/e)\cos(\theta) + (b/e)\sin(\theta) \qquad (7.4).$$

Substitute Equation (7.4) in Equation (7.3), $\rho \cong a\cos(\theta) + b\sin(\theta) + R$ (7.5).

Equation (7.5) (Chetwynd, 1985) is extended to linearize the parameters in determining circularity, cylindricity, and conicity in subsections 7.1.4, 7.1.5, and 7.1.6.

7.1.4 Circularity (Roundness)

Let $(r_i,\ \theta_i)$ be the circularity measurements, where r_i is the distance from the measured point to the system origin with an angle θ_i. The center of the circle is located at $(x_0,\ y_0)$ and R_0 is the radius of the circle. The assessment of circularity error is shown in Figure 44. As mentioned before, the Limacon approximation can be applied to linearize the parameters about the origin of a circle. Therefore,

$$\rho \cong x_0\cos(\theta_i) + y_0\sin(\theta_i) + R_0$$

$$d_i = r_i - \rho = r_i - (R_0 + x_0\cos(\theta_i) + y_0\sin(\theta_i)) \qquad (7.6)$$

where d_i is the distance between a measured point and a corresponding point on the ideal circle.

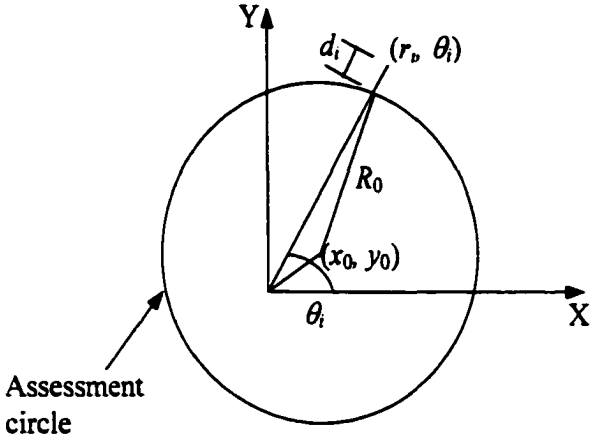


Figure 44. Assessment of Linear Circularity Error.

7.1.5 Cylindricity

Let (r_i, θ_i, z_i) be the cylindricity measurements, where r_i is the distance from the z-axis with a height z_i and angle θ_i. Also, let O_i (x_i, y_i, z_i) be points on the axis of

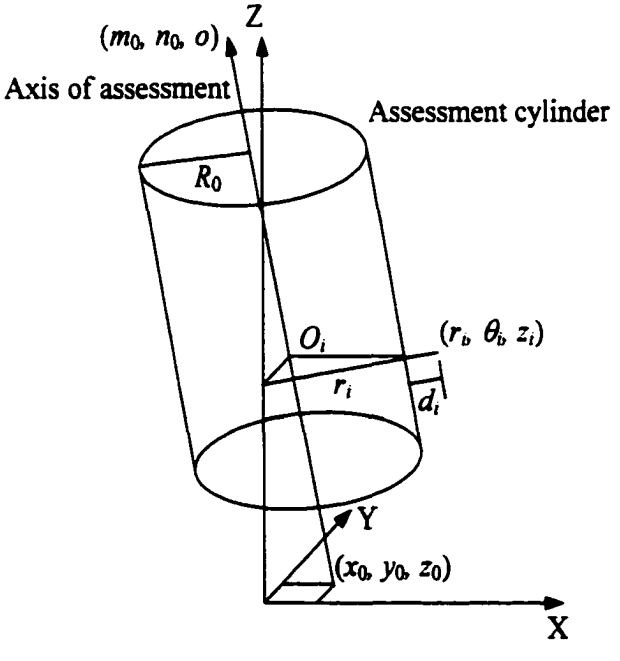


Figure 45. Assessment of Linear Cylindricity Error.

the ideal cylinder and $[m_0\ n_0\ o]$ be the normalized direction vector of the cylinder and its axis. The radius of the cylinder is denoted by R_0. All details are shown in Figure 45. To have a clear picture, cylinder base is drawn higher than its real position, which is on the plane XY. Thus, the center axis passing a point (x_0, y_0, z_0) is described by

$$(x - x_0)/m_0 = (y - y_0)/n_0 = (z - z_0)/o \qquad (7.7).$$

For simplicity, let z_0 be equal to 0. Hence, the center axis can be described simultaneously by

$$x = mz + x_0 \qquad (7.8)$$

and

$$y = nz + y_0 \qquad (7.9)$$

where $m_0 = mo$ and $n_0 = no$. Hence, $[m_0, n_0, o]$ can be rewritten as $o[m, n, 1]$. Similar to the use of the Limacon approximation in circularity,

$$d_i = r_i - \rho = r_i - (R_0 + x_i \cos(\theta_i) + y_i \sin(\theta_i)).$$

By Equations (7.8) and (7.9),

$$d_i = r_i - (R_0 + (mz_i + x_0) \cos(\theta_i) + (nz_i + y_0) \sin(\theta_i)) \qquad (7.10)$$

where d_i is the distance between a measured point and a corresponding point on the surface of the ideal cylinder.

7.1.6 Conicity

The characteristics of the cone is partially similar to the cylinder. The main idea here is to utilize the similarity between cylindricity and conicity by using the embedded circle structure, then derive the rest of cone's characteristics by using analytical geometry. As a result, Equation (7.10) can be extended further since it

already exploits the circle structure. The main difference between the two features is their radii. The radius of the cone is not constant while that of the cylinder is. The cone's radius changes proportionally to its height. This relationship is depicted in Figure 46. The following equation is obtained:

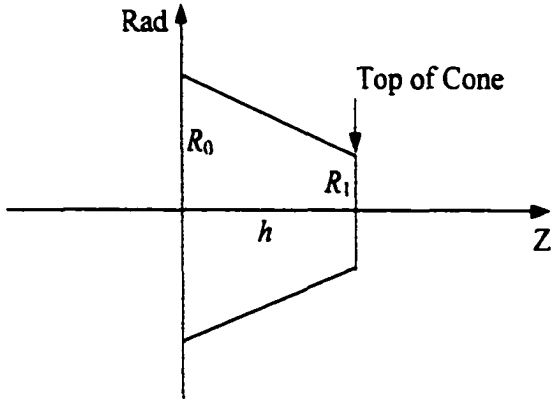


Figure 46. The Relationship of Cone's Radius and Cone's Height.

$$Rad_i = R_0 + Sz_i \qquad (7.11),$$

where Rad_i is the radius of cone at the height z_i , R_0 is the radius of cone's base, and $S = (\Delta Rad_i)/(\Delta z_i)$ is the rate of change of Rad's according to z's. S is also a constant. The dimensions of cone such as radii and height (h) are provided in Figures 37 and 39,

$$Rad_i = R_0 + ((R_1 - R_0)(z_i - z_0)/h) \qquad (7.12),$$

where R_1 is the radius of the cone's top and z_0 is the starting point of the cone base (usually $z_0 = 0$). The assessment of conicity error is shown in Figure 47. Note that cone base is actually located on plane XY but it is intentionally drawn higher for having a clear picture, for illustration purpose. Therefore, R_0 in Equation (7.10) must be replaced by Rad_i in Equation (7.12) as follows:

$$d_i = r_i - (Rad_i + (mz_i + x_0)\cos(\theta_i) + (nz_i + y_0)\sin(\theta_i))$$

$$d_i = r_i - (R_0 + (((R_1 - R_0)\, z_i)/h) + (mz_i + x_0)\cos(\theta_i) + (nz_i + y_0)\sin(\theta_i)) \quad (7.13)$$

where d_i is the distance between a measured point and a corresponding point on the surface of the ideal cone.

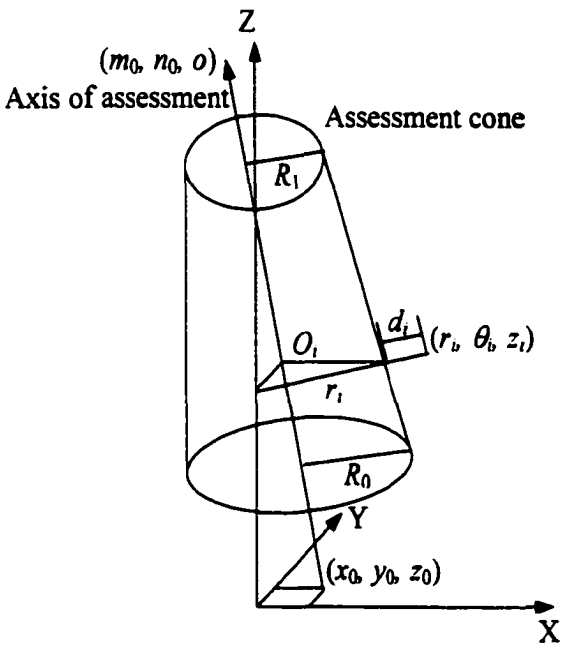


Figure 47. Assessment of Linear Conicity Error.

7.2 Nonlinear Formulation

7.2.1 Straightness

The nonlinear formulation for straightness can be obtained by using a similar approach to the linear formulation. The major difference between both approaches is

that instead of considering the linear deviation between the measured points and the assessment points, the normal deviation between them is applied. In other words, the normal deviation helps to generalize the straightness formulation and

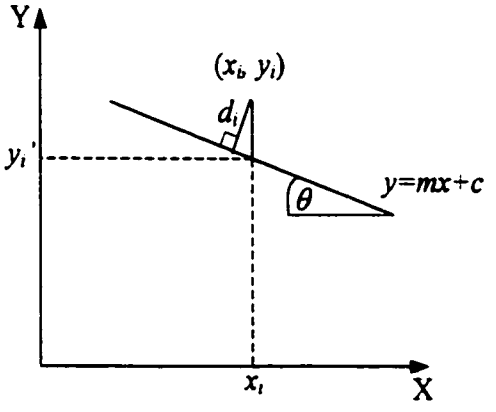


Figure 48. Assessment of Nonlinear Straightness Error.

to probably find more reliable zone solutions. The key idea is depicted in Figure 48. Thus,

$$d_i = (y_i - y_i') \cos(\theta) = (y_i - mx_i - c) \cos(\theta)$$ and

$$\tan(\theta) = m.$$

Consequently, $$\cos(\theta) = \frac{1}{\sqrt{1+m^2}}$$

and $$d_i = \frac{(y_i - mx_i - c)}{\sqrt{1+m^2}} \qquad (7.14)$$

where d_i is the normal distance between a measured point and a corresponding point on the surface of the ideal line.

7.2.2 Flatness

Again, the main idea of nonlinear flatness formulation is the use of normal deviation to calculate the error as shown in Figure 49. The normal vector of the assessment plane $z = mx + ny + c$ is $\begin{bmatrix} m \\ n \\ -1 \end{bmatrix}$. Also, plane XY ($z = c$) has $\begin{bmatrix} 0 \\ 0 \\ -1 \end{bmatrix}$ as its normal vector. Let θ be the angle between z-axis and the line segment from (x_i, y_i, z_i) to P (or be the angle between the assessment plane and plane XY). Given that $\mathbf{a}$ and $\mathbf{b}$ are vectors with the same size, the angle θ between any two vectors can be measured by $\cos(\theta) = \mathbf{ab}/\|\mathbf{a}\|\|\mathbf{b}\|$ and $\|\mathbf{a}\| = \sqrt{\sum_{j=1}^{n} a_j^2}$. Therefore,

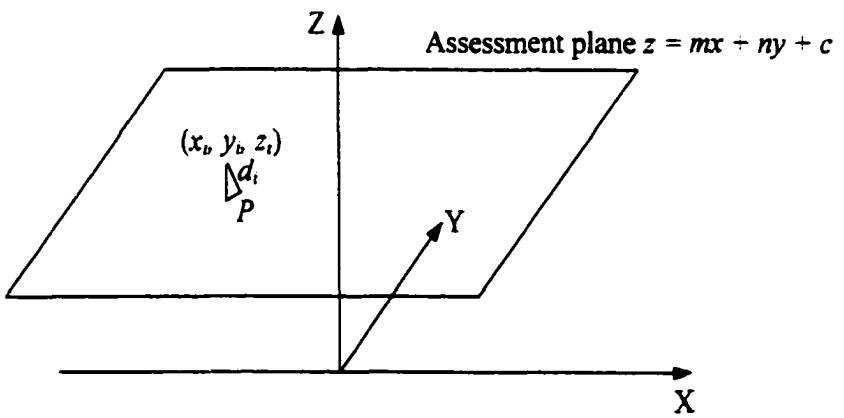


Figure 49. Assessment of Nonlinear Flatness Error.

$$\cos(\theta) = \frac{\begin{bmatrix}0 & 0 & -1\end{bmatrix}\begin{bmatrix}m\\ n\\ -1\end{bmatrix}}{\sqrt{0^2+0^2+(-1)^2}\sqrt{m^2+n^2+(-1)^2}} = \frac{1}{\sqrt{m^2+n^2+1}},$$

$z_i' = mx_i + ny_i + c,$ and

$$d_i = (z_i - z_i')\cos(\theta) = \frac{[z_i - (mx_i + ny_i + c)]}{\sqrt{m^2+n^2+1}} \qquad (7.15)$$

where d_i is the normal distance between a measured point and a corresponding point on the surface of the assessment plane.

7.2.3 Circularity (Roundness)

An ideal circle is described by $(x-x_0)^2+(y-y_0)^2 = R_0^2$ where (x_0, y_0) is its center point and R_0 is its radius as depicted in Figure 50. The normal deviation is also used in determining error from a measurement point to a corresponding point on an ideal surface. Hence, d_i can be simply found as:

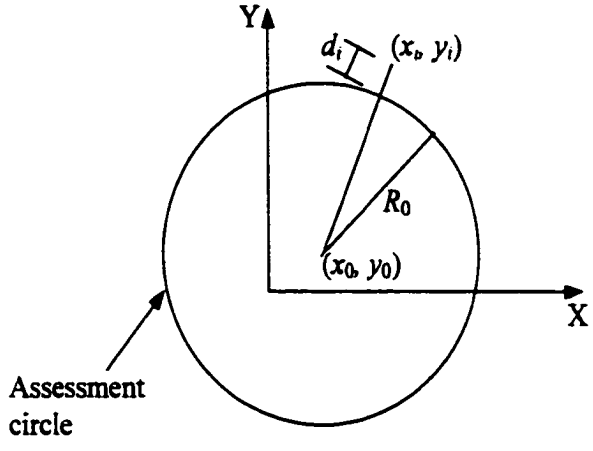


Figure 50. Assessment of Nonlinear Circularity Error.

$$d_i = \sqrt{(x_i - x_0)^2 + (y_i - y_0)^2} - R_0 \tag{7.16}$$

where d_i is the normal distance between a measured point and a corresponding point on the surface of the assessment circle.

7.2.4 Cylindricity

The assessment of nonlinear cylindricity error is shown in Figure 51. By Equations (7.8) and (7.9), the direction vector of the assessment cylinder is [m n 1] and P_I is ($mz_i + x_0$, $nz_i + y_0$, z_i). The distance (D) between P and P_1 is equal to $\sqrt{(x_i - x_0 - mz_i)^2 + (y_i - y_0 - nz_i)^2}$. The line segment PP_1 is on the plane that is

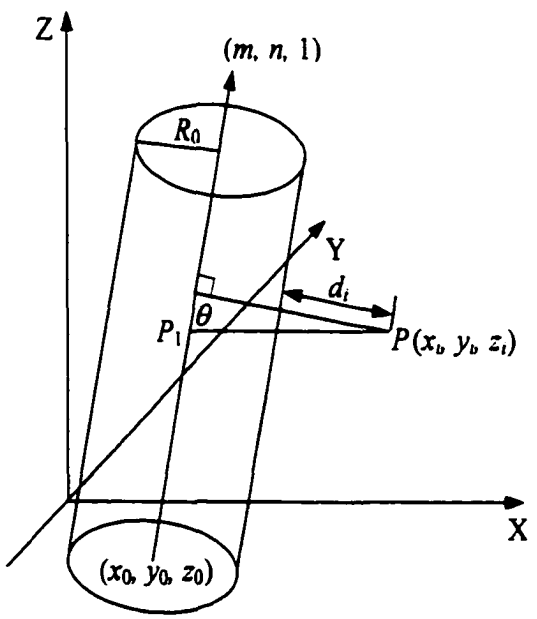


Figure 51. Assessment of Nonlinear Cylindricity Error.

parallel to plane XY. Hence, it can be described by

$$y = \frac{(y_t - y_0 - nz_t)}{(x_t - x_0 - mz_t)}x + c$$

where c is the intercept on the y-axis. A vector parallel to the line segment is $\begin{bmatrix} (x_t - x_0 - mz_t) \\ (y_t - y_0 - nz_t) \\ 0 \end{bmatrix}$. Since θ is an angle between the two vectors, thus

$$\cos(\theta) = \frac{\begin{bmatrix} m & n & 1 \end{bmatrix} \begin{bmatrix} (x_t - x_0 - mz_t) \\ (y_t - y_0 - nz_t) \\ 0 \end{bmatrix}}{\sqrt{m^2 + n^2 + 1}\sqrt{(y_t - y_0 - nz_t)^2 + (x_t - x_0 - mz_t)^2}}$$

$$= \frac{m(x_t - x_0 - mz_t) + n(y_t - y_0 - nz_t)}{(\sqrt{m^2 + n^2 + 1})D} \qquad (7.17).$$

It is seen from Figure 51 that $d_t = D\sin(\theta) - R_0$. Hence,

$$d_t = \frac{\sqrt{(m^2 + n^2 + 1)\left[(x_t - x_0 - mz_t)^2 + (y_t - y_0 - nz_t)^2\right] - \left[m(x_t - x_0 - mz_t) + n(y_t - y_0 - nz_t)\right]^2}}{\sqrt{m^2 + n^2 + 1}}$$

$$- R_0 \qquad (7.18)$$

where d_t is the normal distance between a measured point and a corresponding point on the surface of the assessment cylinder. Note that o (from Figure 45 to Figure 51) can be determined as follows:

$$\sqrt{m_0^2 + n_0^2 + o^2} = 1,$$

$$m^2o^2 + n^2o^2 + o^2 = 1.$$

m and n are known after solving the minimax problem. Consequently,

$$(m^2 + n^2 + 1)o^2 = 1 \qquad \text{and}$$

$$o = \sqrt{\frac{1}{m^2 + n^2 + 1}}.$$

7.2.5 Conicity

As mentioned in Section 7.1.6, the main difference between cylindricity and conicity is their radii variation over the Z axis. The cylinder's radius remains constant while the cone's does not. The assessment of nonlinear conicity error is illustrated in Figure 52. Notice that P is not normal to the surface of the assessment cone but still is normal to the cone's axis, which is how the cone is measured in practice. Hence, the procedure used with the linear conicity formulation can be extended here. By Equations (7.12), (7.17), and (7.18),

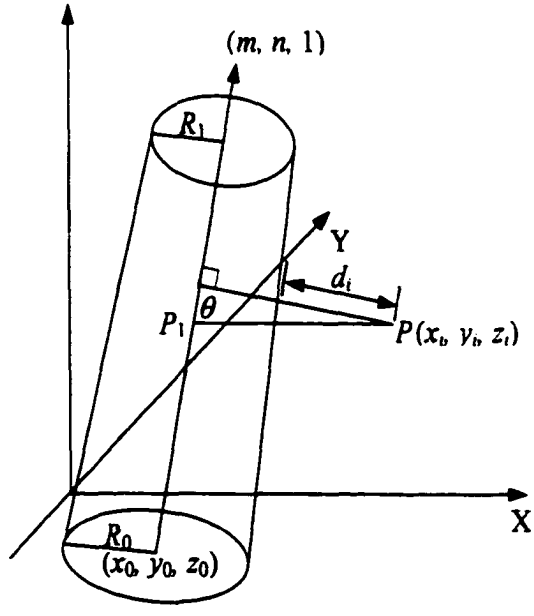


Figure 52. Assessment of Nonlinear Conicity Error.

$$d_i' = \frac{\sqrt{(m^2+n^2+1)\left[(x_i - x_0 - mz_i)^2 + (y_i - y_0 - nz_i)^2\right] - \left[n(x_i - x_0) - m(y_i - y_0)\right]^2}}{\sqrt{m^2+n^2+1}} - Rad_i$$

(7.19).

Notice that z_i's used in Equations (7.11) and (7.12) is for a right circular cone without tilting which is nearly impossible to achieve in practice. The actual manufactured cone is illustrated in Figure 53. The cone's axis is slightly tilted with an angle of α between itself and z-axis.

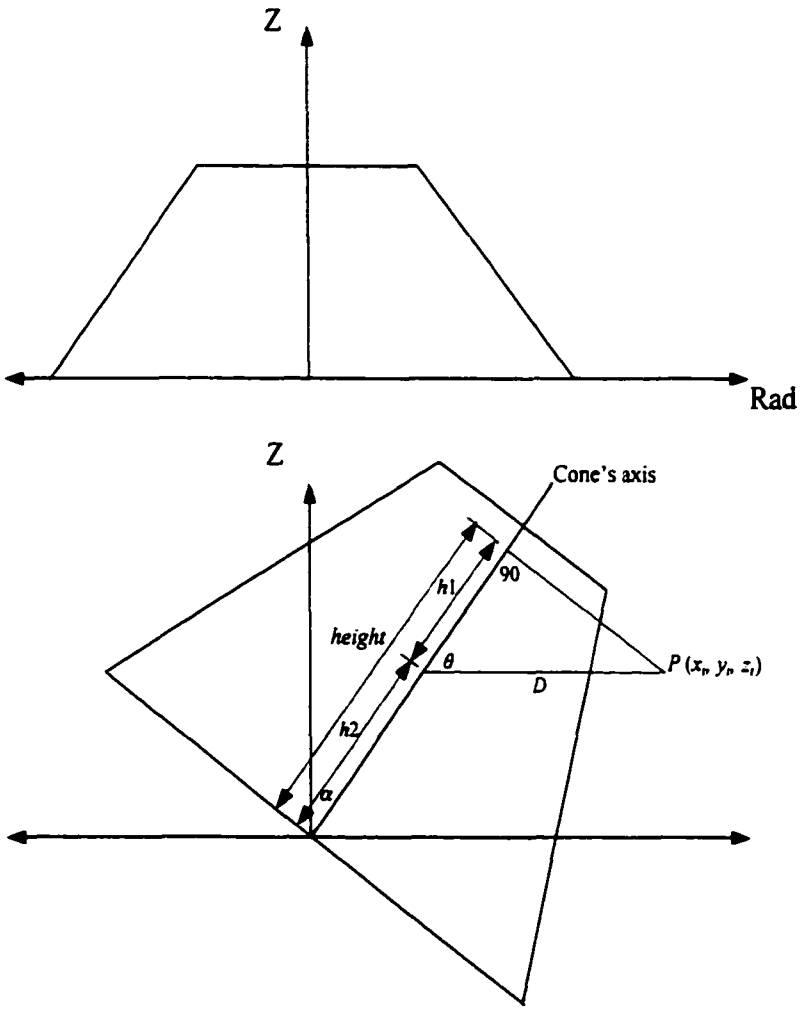


Figure 53. A Slightly Tilted Cone.

Therefore, there must be a minor adjustment in Equations (7.11) and (7.12) to make the measured point normal to the cone's axis as shown in Figure 53. Hence, Equation (7.12) becomes

$$Rad_i = R_0 + ((R_1 - R_0)height/h).$$

Clearly, $height = h1 + h2$, $h2\cos(\alpha) = z_i$, and $h1 = D\cos(\theta)$. Therefore,

$$Rad_i = R_0 + ((R_1 - R_0)/h)(z_i/\cos(\alpha) + D\cos(\theta)) \qquad (7.20) \text{ and}$$

$$d_i' = \frac{\sqrt{(m^2+n^2+1)\left[(x_i - x_0 - mz_i)^2 + (y_i - y_0 - nz_i)^2\right] - \left[n(x_i - x_0) - m(y_i - y_0)\right]^2}}{\sqrt{m^2+n^2+1}} - R_0$$

$$-\left(\frac{R_1 - R_0}{h}\right)\left(\frac{z_i}{\cos(\alpha)} + D\cos(\theta)\right)$$

(7.21).

From Figure 53, $\cos(\alpha) = \sin(\theta)$ and this relationship can be calculated by using Equations (7.17) and (7.18). d_i' is normal to the cone's axis but not to the cone surface. Let γ be the angle between the hypotenuse of cone and the z-axis and $\gamma = \tan^{-1}\left(\frac{R_1 - R_0}{h}\right)$. To make the deviation normal to the cone surface,

$$d_i = d_i'\cos(\gamma) = d_i'\left(\frac{h}{\sqrt{h^2 + (R_1 - R_0)^2}}\right) \qquad (7.22).$$

7.3 The Least Squares Based Zone Evaluation

The least squares based zone evaluation (LSQ) is the most commonly used method for form tolerance evaluation due to the lack of better algorithms and due to its simplicity. The method of least squares is typically used to estimate the regression

coefficients in a multiple linear regression model. This is often called model fitting. To illustrate, suppose that there is a single dependent variable or response r that depends on k independent or regressor variables, x_1, x_2, ..., x_k. This relationship can be described as

$$y = \beta_0 + \beta_1 x_1 + \beta_2 x_2 + \cdots + \beta_k x_k + \varepsilon .$$

Notice that it is called linear regression model because the above equation is a linear function of the unknown parameters β_j, $j = 0, 1, \ldots, k$, which are also called the partial regression coefficients. Let n be the number of observations. The above model can be rewritten as

$$y_i = \beta_0 + \beta_1 x_{i1} + \beta_2 x_{i2} + \cdots + \beta_k x_{ik} + \varepsilon_i$$

$$= \beta_0 + \sum_{j=1}^{k} \beta_j x_{ij} + \varepsilon_i ; i = 1,2,\ldots,n .$$

The method of least squares chooses the β's in the above equation so that the sum of the squares of the errors, ε_i, is minimized. The least squares function is

$$L = \sum_{i=1}^{l} \varepsilon_i^2$$

$$= \sum_{i=1}^{l} (y_i - \beta_0 - \sum_{j=1}^{k} \beta_j x_{ij})^2 .$$

The function L is partially differentiated with respect to β_0, β_1, ..., β_k and the results are equated to zero. Hence, the least sqaures estimators, $\hat{\beta}_0, \hat{\beta}_1, \ldots, \hat{\beta}_k$, must satisfy

$$\left.\frac{\partial L}{\partial \beta_0}\right|_{\hat{\beta}_0, \hat{\beta}_1, \ldots, \hat{\beta}_k} = 0 \text{ and } \left.\frac{\partial L}{\partial \beta_j}\right|_{\hat{\beta}_0, \hat{\beta}_1, \ldots, \hat{\beta}_k} = 0; j = 1,2,\ldots,k .$$

Simplifying the above conditions, the least squares normal equations are obtained as follows:

$$\begin{aligned}
&t\hat{\beta}_0 + \hat{\beta}_1 \sum_{i=1}^{t} x_{i1} + \hat{\beta}_2 \sum_{i=1}^{t} x_{i2} + \cdots + \hat{\beta}_k \sum_{i=1}^{t} x_{ik} = \sum_{i=1}^{t} y_i \\
&\hat{\beta}_0 \sum_{i=1}^{t} x_{i1} + \hat{\beta}_1 \sum_{i=1}^{t} x_{i1}^2 + \hat{\beta}_2 \sum_{i=1}^{t} x_{i1}x_{i2} + \cdots + \hat{\beta}_k \sum_{i=1}^{t} x_{i1}x_{ik} = \sum_{i=1}^{t} x_{i1}y_i \\
&\vdots \\
&\hat{\beta}_0 \sum_{i=1}^{t} x_{ik} + \hat{\beta}_1 \sum_{i=1}^{t} x_{ik}x_{i1} + \hat{\beta}_2 \sum_{i=1}^{t} x_{ik}x_{i2} + \ldots + \hat{\beta}_k \sum_{i=1}^{t} x_{ik}^2 = \sum_{i=1}^{t} x_{ik}y_i
\end{aligned} \tag{7.23}$$

It is simpler to solve the normal equations in matrix form. Thus, Equation (7.23) can be rewritten as:

$$\begin{bmatrix}
t & \sum x_{i1} & \sum x_{i2} & \cdots & \sum x_{ik} \\
\sum x_{i1} & \sum x_{i1}^2 & \sum x_{i1}x_{i2} & \cdots & \sum x_{i1}x_{ik} \\
\vdots & \vdots & \vdots & & \vdots \\
\sum x_{ik} & \sum x_{ik}x_{i1} & \sum x_{ik}x_{i2} & \cdots & \sum x_{ik}^2
\end{bmatrix}
\begin{bmatrix} \hat{\beta}_0 \\ \hat{\beta}_1 \\ \vdots \\ \hat{\beta}_k \end{bmatrix}
=
\begin{bmatrix} \sum y_i \\ \sum x_{i1}y_i \\ \vdots \\ \sum x_{ik}y_i \end{bmatrix}
\text{ or}$$

$$\mathbf{X'X}\hat{\boldsymbol{\beta}} = \mathbf{X'y}.$$

Thus, the least squares estimator of $\hat{\boldsymbol{\beta}}$ is

$$\hat{\boldsymbol{\beta}} = (\mathbf{X'X})^{-1}\mathbf{X'y} \tag{7.24}$$

where

$$\hat{\beta} = \begin{bmatrix} \beta_0 \\ \beta_1 \\ . \\ . \\ . \\ \beta_k \end{bmatrix}, \mathbf{X} = \begin{bmatrix} 1 & x_{11} & x_{12} & . & . & . & x_{1k} \\ 1 & x_{21} & x_{22} & . & . & . & x_{2k} \\ . & . & . & & & & . \\ . & . & . & & & & . \\ . & . & . & & & & . \\ 1 & x_{t1} & x_{t2} & . & . & . & x_{tk} \end{bmatrix}, \text{and } \mathbf{y} = \begin{bmatrix} y_1 \\ y_2 \\ . \\ . \\ . \\ y_t \end{bmatrix}.$$

Next, the linear form tolerance models are illustrated as multiple linear regression models. A program written in Visual Basic for Application in Microsoft Excel is developed to solve regression model fitting by computing $\hat{\beta}$'s.

7.3.1 Straightness Tolerance Zone

$$\varepsilon_i = d_i = y_i - c - mx_i \tag{7.25}$$

where $$\hat{\beta} = \begin{bmatrix} c \\ m \end{bmatrix}, \mathbf{X} = \begin{bmatrix} 1 & x_1 \\ 1 & x_2 \\ . & . \\ . & . \\ . & . \\ 1 & x_t \end{bmatrix}, \mathbf{y} = \begin{bmatrix} y_1 \\ y_2 \\ . \\ . \\ . \\ y_t \end{bmatrix}.$$

The residuals are the distances between the sample points and the least squares line and can be determined as follows:

$$res_i = d_i \tag{7.26}.$$

Note that the residuals are computed perpendicularly to the least squares line. Whereas Equation (7.25) is derived linearly from the measured points to the ideal line. Therefore, it cannot be used to determine the normal residuals as shown in Equation (7.26). The straightness tolerance zone is obtained as follows:

$$Z_{str} = max(res_i) - min(res_i) \tag{7.27}$$

7.3.2 Flatness Tolerance Zone

$$\varepsilon_i = d_i = z_i - c - mx_i - ny_i \tag{7.28}$$

where $$\hat{\beta} = \begin{bmatrix} c \\ m \\ n \end{bmatrix}, \mathbf{X} = \begin{bmatrix} 1 & x_1 & y_1 \\ 1 & x_2 & y_2 \\ . & . & . \\ . & . & . \\ . & . & . \\ 1 & x_t & y_t \end{bmatrix}, \mathbf{y} = \begin{bmatrix} z_1 \\ z_2 \\ . \\ . \\ . \\ z_t \end{bmatrix}.$$

The normal residuals are determined as follows:

$$res_i = d_i \tag{7.29}$$

The flatness tolerance zone is then obtained as follows:

$$Z_{fla} = max(res_i) - min(res_i) \tag{7.30}$$

7.3.3 Circularity Tolerance Zone

$$\varepsilon_i = d_i = r_i - R_0 - x_0 \cos(\theta_i) - y_0 \sin(\theta_i) \tag{7.31}$$

where $$\hat{\beta} = \begin{bmatrix} R_0 \\ x_0 \\ y_0 \end{bmatrix}, \mathbf{X} = \begin{bmatrix} 1 & \cos(\theta)_1 & \sin(\theta)_1 \\ 1 & \cos(\theta)_2 & \sin(\theta)_2 \\ . & . & . \\ . & . & . \\ . & . & . \\ 1 & \cos(\theta)_t & \sin(\theta)_t \end{bmatrix}, \mathbf{y} = \begin{bmatrix} r_1 \\ r_2 \\ . \\ . \\ . \\ r_t \end{bmatrix}.$$

The normal residuals are determined as follows:

$$res_i = d_i \tag{7.32}$$

The circularity tolerance zone is then obtained as follows:

$$Z_{cir} = max(res_i) - min(res_i) \quad (7.33).$$

7.3.4 Cylindricity Tolerance Zone

$$\varepsilon_i = d_i = r_i - R_0 - mz_i \cos(\theta_i) - x_0 \cos(\theta_i) - nz_i \sin(\theta_i) - y_0 \sin(\theta_i) \quad (7.34)$$

$$\text{where } \hat{\beta} = \begin{bmatrix} R_0 \\ m \\ x_0 \\ n \\ y_0 \end{bmatrix}, \mathbf{X} = \begin{bmatrix} 1 & z_1\cos(\theta_1) & \cos(\theta_1) & z_1\sin(\theta_1) & \sin(\theta_1) \\ 1 & z_2\cos(\theta_2) & \cos(\theta_2) & z_2\sin(\theta_2) & \sin(\theta_2) \\ . & . & . & . & . \\ . & . & . & . & . \\ . & . & . & . & . \\ 1 & z_t\cos(\theta_t) & \cos(\theta_t) & z_t\sin(\theta_t) & \sin(\theta_t) \end{bmatrix}, \mathbf{y} = \begin{bmatrix} r_1 \\ r_2 \\ . \\ . \\ . \\ r_t \end{bmatrix}.$$

The normal residuals are determined as follows:

$$res_t = d_t \quad (7.35).$$

The cylindricity tolerance zone is then obtained as follows:

$$Z_{cyl} = max(res_t) - min(res_t) \quad (7.36).$$

7.3.5 Conicity Tolerance Zone

$$\varepsilon_i = d_i = r_i - R_0 - ((R_l - R_0)/h)z_i - mz_i \cos(\theta_i) - x_0 \cos(\theta_i) - nz_i \sin(\theta_i) - y_0 \sin(\theta_i) \quad (7.37)$$

where

$$\hat{\beta} = \begin{bmatrix} R_0 \\ S = \dfrac{(R_1 - R_0)}{h} \\ m \\ x_0 \\ n \\ y_0 \end{bmatrix}, \mathbf{X} = \begin{bmatrix} 1 & z_1 & z_1\cos(\theta_1) & \cos(\theta_1) & z_1\sin(\theta_1) & \sin(\theta_1) \\ 1 & z_2 & z_2\cos(\theta_2) & \cos(\theta_2) & z_2\sin(\theta_2) & \sin(\theta_2) \\ . & . & . & . & . & . \\ . & . & . & . & . & . \\ . & . & . & . & . & . \\ 1 & z_t & z_t\cos(\theta_t) & \cos(\theta_t) & z_t\sin(\theta_t) & \sin(\theta_t) \end{bmatrix}, \mathbf{y} = \begin{bmatrix} r_1 \\ r_2 \\ . \\ . \\ . \\ r_t \end{bmatrix}.$$

The residuals are determined as follows:

$$res_i = d_i \qquad (7.38).$$

Recall that the cone is inspected under the assumption that it is properly aligned with the system axes. Hence, the residuals are already normal to the cone axis but not to the cone surface. The normal conicity tolerance zone can then be obtained as follows:

$$Z_{con} = max(res_i)\cos(\gamma) - min(res_i)\cos(\gamma) \qquad (7.39)$$

where γ is the angle between the hypotenuse of cone and the z-axis and $\gamma = \tan^{-1} S$.

During the process of the least squares method, the normal deviation measurements can also be used. The form tolerance models obtained are in nonlinear forms leading to more complicated procedure in determining the solutions of the least squares normal equations (Rawlings et al., 1998; Murthy and Abdin, 1980; Traband et al., 1989). Since explicit solutions cannot be easily obtained, iterative numerical methods are used instead. According to Murthy and Abdin (1980), when the deviations are small, the difference in results obtained from the least squares and the normal least squares methods are not appreciable. Shunmugam (1987) also stated similar findings. In addition, the larger computation time for the normal least squares is not justifiable in view of the marginal difference in values. Moreover, the solutions found by using the least squares or the normal least squares methods may not actually be the minimum tolerance zones (Murthy and Abdin, 1980). The purpose of this research is not to compare the least squares and the normal least squares methods, but rather present integrative models for conicity evaluation. Therefore, only the traditional least squares method is presented here.

7.4 The Optimization Based Minimum Zone Evaluation

Even though the optimization based zone evaluation attempts to determine the minimum zone are consistent with the ANSI Y14.5M-1994 (ASME, 1995), the lack of proper models for complex features has prevented extensive study. Once the optimization models are obtained, the optimization techniques can be simply applied to iteratively solve such models. This method is based on mathematical programming techniques, linear and nonlinear programming. Linear programming merely defines a specific class of programming problems that meet the following conditions (Ravindran et al., 1987):

1. The variables involved are nonnegative.
2. The objective function can be described by a linear function of the related variables.
3. The operating rules governing the process can be expressed as a constraint set of linear equations or linear inequalities.

As will be seen subsequently, the linear programming problems can be manipulated into the following form (Bazaraa et al., 1990):

Minimize $c_1x_1 + c_2x_2 + ... + c_nx_n$

$$
\begin{aligned}
&a_{11}x_1 + a_{12}x_2 + \cdots + a_{1n}x_n \geq b_1 \\
&a_{12}x_1 + a_{22}x_2 + \cdots + a_{2n}x_n \geq b_2 \\
&\vdots \\
&a_{m1}x_1 + a_{m2}x_2 + \cdots + a_{mn}x_n \geq b_m \\
&x_1, x_2, \ldots, x_n \geq 0
\end{aligned}
$$

Subject to

$c_1x_1 + c_2x_2 + ... + c_nx_n$ is the objective function to be minimized. The coefficients c_1, c_2, ..., c_n are the known cost coefficients and x_1, x_2, ..., x_n are the decision variables to be determined. The inequalities $\sum_{j=1}^{n} a_{ij}x_j \geq b_i$ denote the ith constraints and its coefficients are called the technological coefficients. b_i represents the minimal requirements to be satisfied. The last constraints on x_1, x_2, ..., x_n are the nonnegativity constraints. By simple manipulations, the problem can be transformed from one form to another equivalent form as shown below.

An equality constraint can be transformed into an equation constraint by subtracting the nonnegative surplus or slack variable $x_{n+i} \geq 0$ from $\sum_{j=1}^{n} a_{ij}x_j \geq b_i$. This leads to $\sum_{j=1}^{n} a_{ij}x_j - x_{n+i} = b_i$. Similarly, $\sum_{j=1}^{n} a_{ij}x_j \leq b_i$ is equivalent to $\sum_{j=1}^{n} a_{ij}x_j + x_{n+i} = b_i$. Also an equation $\sum_{j=1}^{n} a_{ij}x_j = b_i$ is equivalent to two inequalities $\sum_{j=1}^{n} a_{ij}x_j \leq b_i$ and $\sum_{j=1}^{n} a_{ij}x_j \geq b_i$.

If a decision variable is unrestricted in sign, it can be replaced by $x_j' - x_j''$ where $x_j' \geq 0$ and $x_j'' \geq 0$. Hence, the suitable equivalent form can be obtained easily.

To convert a maximization problem into a minimization problem and conversely, the following manipulation is used:

$$\text{Maximum} \sum_{j=1}^{n} c_j x_j = \text{- minimum} \sum_{j=1}^{n} -c_j x_j \, .$$

Similarly, the nonlinear programming is characterized by groups of terms involving intrinsically nonlinear functions in either objective function or a constraint set.

To evaluate the form feature, an ideal feature must be established from the actual measurements such that the maximum deviation between the ideal feature and the sampled points is the least possible value. The form error, ε, of the feature is then determined by minimizing the maximum deviation of the measured points with respect to the position and orientation of the ideal form. This implies that

$$\varepsilon = \underset{s}{\text{Min}}(\underset{i}{\text{Max}}\, d_i) \quad (i = 1, 2, \ldots, t)$$

where t is the number of the sampled points and s is a vector which defines the rigid translation and the rotation of the ideal form. This problem is referred to as a min-max problem and it can be easily transformed to a constrained optimization problem by introducing an additional variable, h. The equivalent problem is obtained as follows:

$$\underset{s,h}{\text{Minimize}} : \varepsilon = h$$

$$\text{Subject to: } |d_i| \le h; i = 1,2,\ldots,t \qquad \text{and}$$

$$h \ge 0.$$

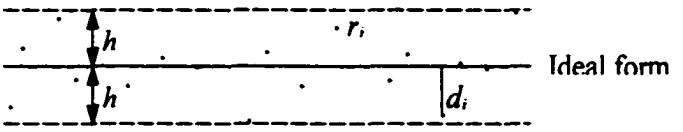


Figure 54. Sampled Points of An Ideal Form and Its Tolerance Zone

d_i is the model of the errors discussed in Section 7.1 for linear form and Section 7.2 for nonlinear form. As shown in Figure 54, the group of the constraints d_i ensures that all of the deviations are contained within the minimum zone. The solution of the above problem minimizes h resulting in a minimum zone, $Z = 2h$. For most practical problems the variables represent physical quantities and must be nonnegative (Bazaraa et al., 1990). In addition, most mathematical programming techniques are designed to solve problems where the variables are nonnegative. Therefore, the unrestricted variables are transformed into nonnegative forms. The additional constraints for each specific feature are introduced for both linear and nonlinear forms as follows.

7.4.1 The Additional Constraints for Straightness

m and c are unrestricted in sign and hence the suitable equivalent constraints are:

$$\begin{aligned} m &= m' - m'' \\ c &= c' - c'' \\ m', m'', c', c'' &\geq 0 \end{aligned}$$

7.4.2 The Additional Constraints for Flatness

m, n and c are unrestricted in sign and hence the suitable equivalent constraints are:

$$
\begin{aligned}
&m = m' - m'' \\
&n = n' - n'' \\
&c = c' - c'' \\
&m', m'', n', n'', c', c'' \geq 0
\end{aligned}
$$

7.4.3 The Additional Constraints for Circularity

x_0 and y_0 are unrestricted in sign and R_0 is nonnegative. Hence the suitable equivalent constraints are:

$$
\begin{aligned}
&x_0 = x_0' - x_0'' \\
&y_0 = y_0' - y_0'' \\
&R_0, x_0', x_0'', y_0', y_0'' \geq 0
\end{aligned}
$$

7.4.4 The Additional Constraints for Cylindricity

m, n, x_0, and y_0 are unrestricted in sign and R_0 is nonnegative. Hence the suitable equivalent constraints are:

$$
\begin{aligned}
&m = m' - m'' \\
&n = n' - n'' \\
&x_0 = x_0' - x_0'' \\
&y_0 = y_0' - y_0'' \\
&R_0, m', m'', n', n'' x_0', x_0'', y_0', y_0'' \geq 0
\end{aligned}
$$

7.4.5 The Additional Constraints for Conicity

m, n, x_0, and y_0 are unrestricted in sign and h, R_0, R_1 are nonnegative. Hence the suitable equivalent constraints are:

$$
\begin{aligned}
& m = m' - m'' \\
& n = n' - n'' \\
& x_0 = x_0' - x_0'' \\
& y_0 = y_0' - y_0'' \\
& h, R_0, R_1, m', m'', n', n'' x_0', x_0'', y_0', y_0'' \geq 0
\end{aligned}
$$

$m', m'', c', c'', n', n'', x_0', x_0'', y_0'$, and y_0'' are additional variables used in transforming the unrestricted $m, c, n, x_0,$ and y_0 into nonnegative forms for the corresponding optimization models of the mentioned features. The nonnegative forms may then be used in the deviation models.

In summary, this chapter provides a formal structure for fitting data points and thereby determining the enclosing form tolerance zone for the inspection of cones. This is a first step towards the inclusion of conical features in form metrology along with flatness, straightness, circularity, and cylindricity. Such methodologies could be extended for more complex forms such as sphere and torus.

CHAPTER 8

RESULTS AND ANALYSES

Since the developed cylindricity model is the basis for the cone development in the proposed conicity model, and since there is little literature on conicity verification, the cylindricity model is verified by comparing its results to those obtained from the published cylindricity methods. This section begins with the comparisons of the cylindricity results against the published data from Shunmugam (1987), Carr and Ferreira (1995b), and Roy and Xu (1995). The cylindricity model tested is Equation 7.18 from Chapter 7.

The main intent of this chapter is to provide details on the results of the integrative analysis conducted. A SAS program was developed to analyze the results, in order that these may be used for developing guidelines for inspection. It is expected that analysis presented in this chapter can be improved and extended, whereby comprehensive standards and solutions can be developed for problems faced by industry.

8.1 Cylindricity Comparisons

To check the validity and accuracy of the developed cylindricity evaluation model, several numerical examples were tested by using the published data from

Shunmugam (1987b), Carr and Ferreira (1995b), and Roy and Xu (1995). To limit the search range and obtain the logical results, the range of the cylinder's radius should be given or estimated before applying the optimization algorithms. The converted data, degree to radian, in Table 7 were calculated from Shunmugam (1987b). The linear deviation for cylindricity was applied with the linear LSQ method to evaluate form errors. Wang (1992) developed nonlinear minimax model to evaluate the cylindricity with the same data set. Their results and the results from this work are compared in Tables 8 and 9. Other feature parameters are also illustrated.

The results published in Wang (1992) are as follows: Zone = 1.774, R_0 = 2.461, $m = 0.687$, $x_0 = 0.364$, $n = 0.006$, $y_0 = 0.763$.

It is important to note that the differences between these and those of Shunmugam (1987b)'s were quite large. Furthermore, the direction vector, [m n 1] or [m_0 n_0 o], should be closer to [0 0 1] due to the assumption of the Limacon approximation. In addition, Wang (1992)'s results could not exactly be regenerated here and were close to those in Table 8. Probably, the transformed data were used in Wang (1992). The variations might have resulted by the different optimization algorithms used. If the transformed data is used, the results cannot be accepted when compared to those of Shunmugam (1987b) since the optimization algorithms are more numerically sensitive than the LSQ based approach. The LSQ method computes the cylindricity zone from the linear residuals (maximum residual – minimum residual). These residuals were equal to the differences between the measured points and the points on the substitute feature (cylinder). The linear

differences could remain the same even though different data sets were used. Figure 55 illustrates these examples. Hence, using the transformed or actual data would produce the same results for cylindricity zone and R_0 but different results for other

Table 7. The Coordinates Data Set of Cylinder (Shunmugam, 1987b).

θ_i (radian)	r_i	Actual z_i	Transformed z_i
0	5	50	1
0	4	25	0
0	3	0	-1
0.785398163	3	50	1
0.785398163	4	25	0
0.785398163	2	0	-1
1.570796327	4	50	1
1.570796327	3	25	0
1.570796327	4	0	-1
2.35619449	3	50	1
2.35619449	3	25	0
2.35619449	3	0	-1
3.141592654	1	50	1
3.141592654	3	25	0
3.141592654	2	0	-1
3.926990817	2	50	1
3.926990817	2	25	0
3.926990817	3	0	-1
4.71238898	2	50	1
4.71238898	2	25	0
4.71238898	1	0	-1
5.497787144	3	50	1
5.497787144	3	25	0
5.497787144	2	0	-1

Table 8. Comparison of Results for Cylindricity Using Transformed z_i.

Method	Cylindricity Zone	R_0	m	x_0	n	y_0
Linear + LLSQ method	2.247906145	2.791666667	0.640165043	0.558925565	-0.036611652	0.676776695
NL + SQP method	1.738922724	2.433166223	0.713647125	0.354066488	0	0.813776464
NL + GRG method	1.738923089	2.433166346	0.713646751	0.354067366	0	0.813776318

Note: The linear deviation applied with the linear LSQ is presented by Shunmugam (1987b).
The nonlinear deviation applied with sequential quadratic programming (SQP) is presented by (Wang, 1992).
The nonlinear deviation applied with generalized reduced gradient algorithm (GRG) is presented in Chapter 7.

Table 9. Comparison of Results for Cylindricity Using Actual z_i.

Method	Cylindricity Zone	R_0	m	x_0	n	y_0
Linear + LLSQ method	2.247906145	2.791666667	0.025606602	-0.081239478	-0.001464466	0.713388348
NL + SQP method	2.111642355	2.67682546	0.026663811	0	0.001672177	0.621006558
NL + GRG method	2.111642355	2.676825395	0.026663812	0	0.001672181	0.621006482

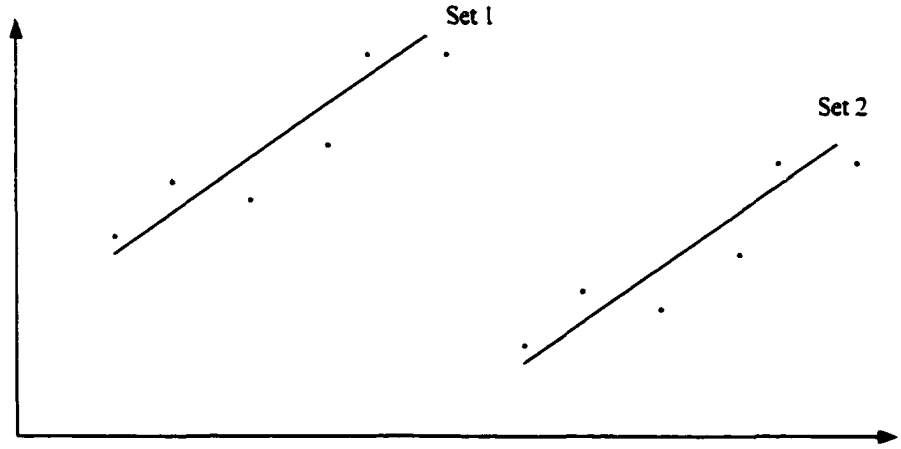


Figure 55. The Corresponding Residuals of Each Set are Identical.

parameters. The reason for using the transformed data z_i was stated in Shunmugam (1987a). That was to facilitate the computation while using linear deviation with the LSQ method. Conversely, using different data sets for nonlinear optimization problem likely produces different results due to the nature of nonlinear functions such as power, division, etc., in objective function and constraints. Therefore, the reliable comparisons should be drawn only from the actual data set. As seen from Table 9, the results of the proposed model were almost identical to those of Wang (1992)'s and were superior to those of Shunmugam (1987b)'s.

Carr and Ferreira (1995b) also provided some example data sets as shown in Tables 10, 12, and 14. They were used to test the validity and accuracy of the proposed cylindricity model by comparing it against the published results from Carr and Ferreira (1995b) and the results from the model taken from Wang (1992). These results are illustrated in Table 11, 13, and 15.

Table 10. The Coordinates Data Set 1 of Cylinder (Carr and Ferriera, 1995b).

x_i	y_i	z_i
30	0.001475	7.892267
1.05636	-29.981396	27.519008
-29.366428	-6.132937	13.137551
28.698913	8.739131	40.731883
-12.893256	-27.088078	56.081574
-22.315616	20.050269	31.164982
14.611799	-26.201056	2.074327
28.323328	9.888835	31.782012
-14.26238	-26.39288	0.461891
-22.304724	20.062385	4.010534
-26.057635	14.866056	41.206363
-25.432673	-15.911603	55.82619
17.043966	-24.688119	31.615727

x_i	y_i	z_i
25.129457	16.386287	39.235138
-25.917641	15.108801	42.071436
25.36219	-16.03271	45.731882
-2.34494	29.908214	2.847871
-2.62016	-29.88536	19.694054
-20.170149	-22.206503	45.384629
29.952444	-1.68852	21.92032
30.001	0.001475	7.892267
1.056395	-29.982395	27.519008
-29.367407	-6.133141	13.137551
28.699869	8.739422	40.731883
-12.893685	-27.088981	56.081574
-22.316359	20.050938	31.164982
14.612286	-26.201929	2.074327
28.324273	9.889165	31.782012
-14.262855	-26.393767	0.461891
-22.305468	20.063053	4.010534
-26.058504	14.866552	41.206363
-25.433521	-15.912134	55.82619
17.044534	-24.688942	31.615727
25.130294	16.386834	39.235138
-25.918505	15.109304	42.071436
25.363036	-16.024245	45.731882
-2.345018	29.909211	2.847871
-2.620248	-29.886356	19.694054
-20.171721	-22.207243	45.384629
29.953442	-1.688577	21.92032

Table 11. Comparison of Results for Cylindricity Using Data in Table 10.

Method	Cylindricity Zone	R_0	m	x_0	n	y_0
Carr and Ferreira (1995b)	0.001	NA	NA	NA	NA	NA
NL + SQP method	0.004809865	30.00206564	8.71539E-06	0	0	0
NL + GRG method	0.004809871	30.00206564	8.71526E-06	0	0	0

Note that the cylindricity zone from Carr and Ferreira (1995b) in Table 11 was not close to the rest. There were some conflicts that should be pointed out as follows:

1. As stated in Carr and Ferreira (1995b), data set 1 was generated as two cylinders with axes equal to the Z-axis and radii equal to 30.000 and 30.001, respectively. Hence, these two cylinders were not tilted in any direction. However, the radii of the 16^{th} and 19^{th} data points calculated from the given coordinates were equal to 30.00480747 and 29.99939476, respectively. They were the maximum and minimum among all data points and likely contributed to the cylindricity zone. As a result, the zone should be roughly estimated around 30.00480747 – 29.99939476 = 0.00541271. Using the appropriate model and fitting algorithm should produce cylindricity close to 0.00541271 with a small orientation for the minimum zone evaluation.
2. The radius of data set 1 of Carr and Ferreira (1995b) was also included in its Appendix and equal to 30.005, not 30.001 as stated in its Implementation and results section.

The model presented by Carr and Ferreira (1995b) was similar to that of Wang (1992) and the proposed model. One of the main differences was the use of the additional linearization that was not used in Wang (1992) and the presented model. Another difference was the optimization algorithms used. The respective models used were successive linear programming (SLP), sequential quadratic programming (SQP), and generalized reduced gradient algorithm (GRG).

Table 12. The Coordinates Data Set 2 of Cylinder (Carr and Ferriera, 1995b).

x_i	y_i	z_i
60.051121	0.002953	3.946134
-57.932024	15.399312	15.983017
57.43213	17.488707	20.365942
55.022756	-23.936632	11.505062
29.1801	-52.423113	1.037163
-58.861558	-11.113569	20.134482
-44.597179	40.113733	2.005267
-23.247383	-55.406652	17.669299
34.041568	-49.309081	15.807863
-34.084135	-49.427745	12.479981
50.684216	-32.022045	22.865941
57.318676	17.619539	22.082457
-40.40813	-44.485701	22.692315
-39.83837	44.994386	7.411167
-10.261352	-59.146784	22.600675
53.919844	26.493193	18.949042
-8.540012	59.442972	13.092342
-59.369089	8.361285	7.133233
-38.029817	46.404843	4.995216
47.946099	-35.92538	27.276243

Table 13. Comparison of Results for Cylindricity Using Data in Table 12.

Method	Cylindricity Zone	R_0	m	x_0	n	y_0
Carr and Ferreira (1995b)	0.18396	NA	-0.00062	NA	-0.00292	NA
NL + SQP method	0.194828343	60.00478139	0	0.005930704	0	0
NL + GRG method	0.194828184	60.00478136	0	0.00593079	0	0
LSQ (Carr and Ferreira, 1995b)	0.21197	NA	-0.004900147	NA	-0.005460164	NA

$[m_0\ n_0\ o]$ is equal to [-0.00062 –0.00292 1] for data set 2 in Carr and Ferreira (1995b). Recall that $m_0 = mo$ and $n_0 = no$. Hence, m and n could be calculated with the results shown in Table 13.

Table 14. The Coordinates Data Set 3 of Cylinder (Carr and Ferriera, 1995b).

x_i	y_i	z_i
-11.820859	50.421254	-15.817382
42.403448	-6.693162	56.567707
10.366902	80.249947	26.965969
18.527457	61.577469	-13.680418
23.930322	23.878386	-41.820643
66.363729	0.636729	49.246025
-3.608026	-24.493246	39.678687
75.507564	20.208045	6.298139
48.919097	55.614254	-13.266609
65.713317	2.841028	3.498858
46.632786	80.517454	4.866333
13.598993	83.519129	30.375
84.570573	18.219363	28.224203
2.322453	-10.802862	51.268799
82.820384	38.516367	9.148307
3.553158	75.111087	30.738097
-5.898713	21.39033	60.097056
30.009532	-24.696147	35.870356
-3.793621	-14.263808	46.897322
58.357492	87.161327	11.960644
33.207329	64.844079	-10.665479
34.46129	41.806234	94.623903
-26.871029	3.103967	39.48246
-4.153639	67.427229	23.451422
22.371	47.845956	88.060867
67.398986	16.520701	79.062822
79.257377	49.418921	4.727043
-37.543275	31.718373	8.573268
49.576671	65.965076	-6.501629
96.781947	53.421231	22.908004
-18.623157	23.988046	47.691608
58.416292	-4.557784	48.525368

x_i	y_i	z_i
48.408528	15.833662	81.511728
31.694971	-2.169579	63.538387
-18.366214	2.837799	46.415679
81.087477	11.573666	46.319607
57.311572	-9.09605	38.123767
68.59397	33.580936	-6.118165
89.036231	21.72231	35.086999
3.141412	52.730721	67.919265

Table 15. Comparison of Results for Cylindricity Using Data in Table 14.

Method	Cylindricity Zone	R_0	m	x_0	n	y_0
Carr and Ferreira (1995b)	0.00941	NA	1.000052	NA	1.000052	NA
NL + SQP method	0.009410136	49.99953289	1.000058463	3.998826419	1.000046417	4.998637542
NL + GRG method	0.009410193	49.99953288	1.000058461	3.998826401	1.000046416	4.998637497
LSQ (Carr and Ferreira, 1995b)	0.01037	NA	1.0000866	NA	1.000052	NA

[m_0 n_0 o] was equal to [0.57736 0.57736 0.57733] for data set 3 in Carr and Ferreira (1995b). Recall that $m_0 = mo$ and $n_0 = no$. Hence, m and n could be calculated as shown in Table 15.

Table 16. The Coordinates Data Set of Cylinder (Roy and Xu, 1995).

x_i	y_i	z_i
-5.011	0.019	0
-4.701	1.715	0
-3.625	3.449	0
-2.376	4.401	0

x_i	y_i	z_i
0.035	4.999	0
2.018	4.572	0
3.901	3.115	0
4.718	1.626	0
4.992	0.059	0
4.726	-1.589	0
3.815	-3.22	0
2.356	-4.405	0
-0.792	-4.928	0
-2.014	-4.569	0
-3.912	-3.117	0
-4.802	-1.384	0
-5.001	0.019	5
-4.638	1.885	5
-3.984	3.019	5
-2.226	4.472	5
-0.007	4.988	5
2.219	4.472	5
3.802	3.238	5
4.745	1.566	5
4.97	0.52	5
4.64	-1.875	5
3.768	-3.288	5
2.321	-4.434	5
0.001	-5.015	5
-1.712	-4.705	5
-3.278	-3.788	5
-4.415	-2.365	5
-4.99	0	10
-4.644	1.823	10
-3.531	3.527	10
-1.704	4.703	10
0.387	4.99	10
1.496	4.78	10
3.782	3.29	10
4.778	1.502	10
4.999	0.085	10
4.803	-1.404	10
3.596	-3.484	10
1.913	-4.625	10
0.19	-4.989	10
-1.868	-4.641	10

x_i	y_i	z_i
-3.493	-3.58	10
-4.641	-1.834	10
-4.989	0.001	15
-4.636	1.852	15
-3.51	3.56	15
-1.688	4.706	15
0.413	5	15
1.473	4.799	15
3.798	3.291	15
4.796	1.487	15
5.022	0.066	15
4.816	-1.399	15
3.6	-3.472	15
1.923	-4.605	15
0.23	-4.987	15
-1.798	-4.643	15
-3.46	-3.588	15
-4.614	-1.878	15

Roy and Xu (1995) also provided an example data set as shown in Table 16. They were used to test the validity and accuracy of the proposed cylindricity model by comparing to the published results from the Voronoi based method in Roy and Xu (1995), to the results from the model taken from Wang (1992), and to the results from the linear deviation model with the linear LSQ. These results are illustrated in Table 17. In Roy and Xu (1995), o = 0.9999987 was also included and the maximum and minimum radius were 5.0159080 and 4.987094, respectively.

It can be seen from the foregoing comparisons that the results obtained by the proposed method were close to those of the published methods and smaller than those of the LSQ. Hence, Equation (7.18) should be acceptable.

Table 17. Comparison of Results for Cylindricity Using Data in Table 16.

Method	Cylindricity Zone	R_0	m	x_0	n	y_0
Roy and Xu (1995)	0.02881336	NA	0.001567376	-0.00911603	0.00054574	-0.001820852
NL + SQP method	0.029548125	5.000751946	0.001017511	0	0.000104874	0
NL + GRG method	0.029548126	5.000751947	0.001017512	0	0.000104875	0
Linear + LLSQ method	0.047010885	5.000549929	0.000383747	-0.003347658	0.00050644	-0.00234218

8.2 Results from Experimental Analyses

This section presents the experimental analyses conducted in this research. The step-by-step procedure for data collection is given in Appendix A and the analysis procedure is discussed here.

The response measure or conicity was obtained by applying the mentioned 4 fitting algorithms to the coordinates collected. A statistical method, the factorial design with nested blocking factor, implemented in SAS was used to analyze the resulting data.

8.2.1 Model Adequacy Checking

The validity of the experimental design model was checked to detect any violations of normality, independence, and constant variance assumptions by constructing a plot of residuals in time sequence, a plot of residuals versus fitted values, 5 plots of residuals versus all 5 main effects, a box plot of residuals, and a normal probability plot of residuals. These plots are presented in Appendix B.

Obviously, there were two residuals that were very much larger than any of the others. Moreover, there was a residual that was very much smaller than others. They were outliers that might seriously distort the results of statistical analysis. Hence, further investigation was called for.

Observations of the conicity were made at different levels of sample size, sampling strategy, fitting procedure, and specimen type. Even though the conicity values looked acceptable, the parameters obtained by applying the LSQ based fitting to the coordinates collected via the aligned systematic sampling with small sample sizes of 8 and 16 were invalid as shown in Appendix C. The conjecture for these invalidities might be the interaction between those three factors (sampling method, sample size, and fitting algorithm). It was highly likely that the aligned systematic sampling did not provide much information of the inspected parts with the same sample sizes as Hammersley and Halton-Zaremba sampling methods did. Similar results were also reported by Lee et al. (1997). The uniform sampling, a systematic sampling, was investigated by Lee et al. (1997). With a much smaller sample size, the RMSE of the Hammersley sampling was always several times lower than that of the uniform sampling on cone for both Wiener and isotropic surfaces. At the sample size of 16 for the Hammersley sampling, its RMSE was about 13 times lower than that of the uniform sampling with the sample size of 100. When the sample size increased, the RMSE of the uniform sampling decreased drastically.

Moreover, the way the LSQ approach was modeled should play a role in resulting invalid parameters since there were no constraints or boundaries for these

parameters explicitly taken into formulation. Combined with high RMSE sampling like the aligned systematic sampling and small sample sizes of 8 and 16, the invalid results were consequently obtained.

The aligned systematic sampling and the uniform sampling methods with high sample sizes like 64 and 256 probably provided valid results as confirmed in this work and in Lee et al. (1997). Higher sample sizes probably provided a lot of information of the inspected part. This, in turn, induced the implicit constraints for the LSQ based fitting. Consequently, the parameters obtained by applying such fitting algorithm to the coordinates collected via the aligned systematic sampling with the sample sizes of 64 and 256 were valid and illustrated in Appendix D.

Due to the invalid parameters, their corresponding conicity values should not be included in the analysis. Therefore, they were treated as missing data in statistical analysis by replacing them with "." for all 32 of them. The statistical results are shown in Appendix E.

The model adequacy was then checked by constructing a plot of residuals in time sequence, 5 plots of residuals versus all 5 main effects, a plot of residuals versus fitted values, a box plot of residuals, and a normal probability plot of residuals to find any violations of normality, independence, and constant variance assumptions.

The normal probability plot of residuals resembled a straight line. This implied that the underlying error distribution was normal. There was, however, a presence of two outliers. These two were the results of both of the LSQ based fitting algorithms applied to the coordinates collected via the Halton-Zaremba method with

the sample size of 8. The inspection of relevant parameters did not reveal any invalidation. As mentioned before, the normalized LSQ was calculated from the LLSQ. Thus, the unusually low conicity of the normalized LSQ was the outcome of the unusually low conicity of the LLSQ. The calculations, experimental circumstances surrounding this run, and data coding and coping were examined. Nothing was found to be the cause of the outliers. The conjecture of the cause might be the low sample size and the location of the Halton-Zaremba scheme on the specimen number 1. After careful consideration, these two outliers were not discarded from the analysis and it was believed that the normality assumption was not violated.

The independence assumption was also validated by checking a plot of residuals in time order of data collection. They appeared to be structureless. There was no reason to suspect any violation of the independence or constant variance assumptions. In addition, they should be unrelated to any other variables including the predicted values and all 5 main effects. These plots of residuals versus predicted values and versus each of all 5 main effects did not reveal any obvious pattern. However, there might be some nonconstant variance in the residuals plot against sampling strategies. This plot looked like a small inward-opening megaphone but it was not extreme. This probably leaded to the slight drift of the residuals versus the predicted values plot. Nevertheless, nonconstant variance appeared vaguely. Thus, the assumption of homogeneity of variances should hold.

In conclusion, the usual diagnostics analyses of residuals did not graphically indicate any major concerns. Hence, the experimental design model used was adequate.

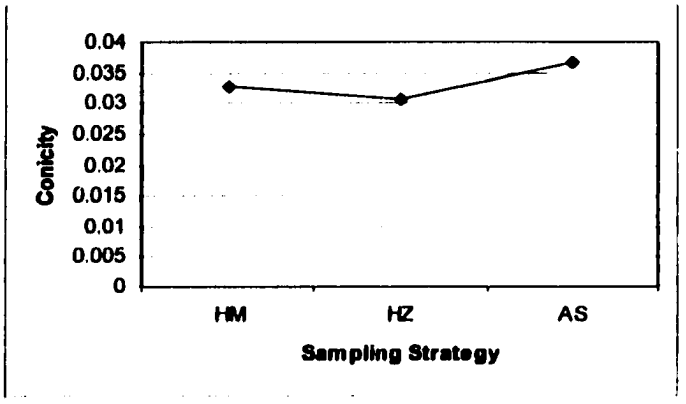
8.2.2 Analysis of Variance for the Conicity Testing Experiment

Computer output for the conicity testing obtained from the GLM procedure in SAS is provided in Appendix E. Using a 0.05 level of significance (α), the surface area was not statistically significant. In other words, it did not affect the determination of conicity. The same could be said for the interaction between sampling strategy and fitting algorithm. Nor was the interaction between surface area, sampling strategy, sample size, and fitting algorithm. The other main effects and their interactions were statistically significant or affected the determination of conicity.

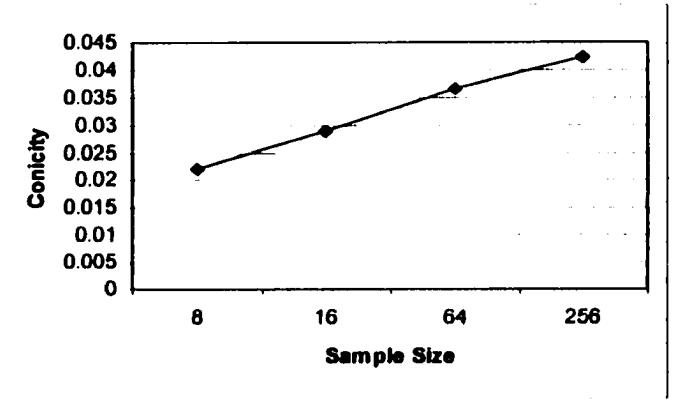
As expected, the analysis of variance showed that specimen was significant since conicity depended on each specimen and how it was machined. There were several uncontrollable factors such as skills of machinists, different machines used, etc. in manufacturing these specimens. Moreover, it was of no interest in determining which specimen would perform better in terms of conicity. In addition, the specimen was treated as a blocking factor. This meant that randomization had been applied only to treatment within this block (restriction on randomization). Thus, its normality assumption was quite questionable and F test was then not reliable. Hence, this factor and its treatments were not taken into consideration for finding the influential factors on the response variable, conicity. However, to investigate the effect of the blocking

factor, examining this F ratio was reasonable. The ratio was rather large meaning that decreasing experimental errors through blocking outweighed the assumingly negligible interactions between block and treatments that might exist in the error component. In other words, the blocking factor had a large effect and the noise reduction obtained by blocking was helpful in improving the precision of the experiment.

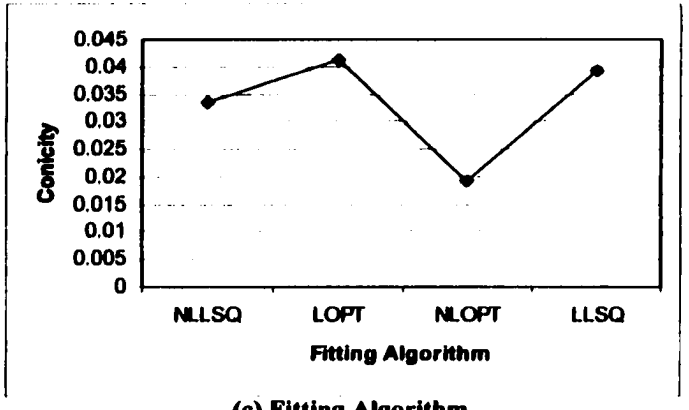
The analysis of variance also showed that the sampling scheme, sample size, and conicity algorithm appeared to be significant. The 2-variable interactions between surface area and sampling strategy, surface area and sample size, surface area and fitting algorithm, sampling method and sample size, and sample size and fitting algorithm were significant as well. The 3-variable interactions between surface area, sampling strategy, and sample size; surface area, sampling strategy, and fitting algorithm; surface area, sample size, and fitting algorithm; and sampling strategy, sample size, and fitting algorithm were also significant. The comparisons between the means of each main effect might be obscured by their interactions. Therefore, the levels of each factor must be examined with levels of the other factors fixed to draw valid conclusions about the main effects. To assist in the practical interpretation of this experiment, it was helpful to construct graphs of the average response for the relevant significant combinations. Figures 56 to 60 present plots of the relevant significant main effects, 2-way, and 3-way interactions. The main effects are just graphs of the averages of conicity at the levels of these main factors. The interaction is indicated by the lack of parallelism of the lines.



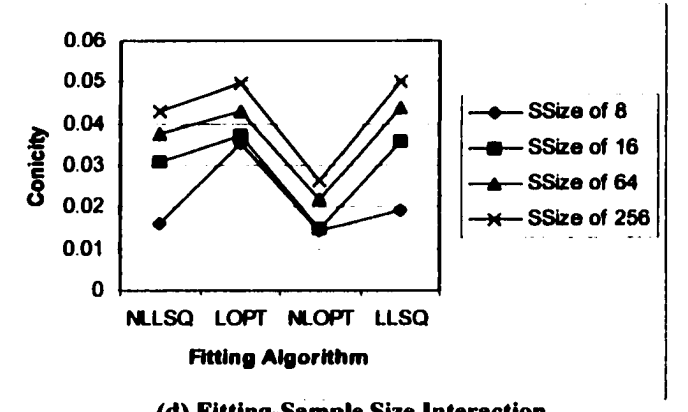
(a) Sampling Strategy



(b) Sample Size

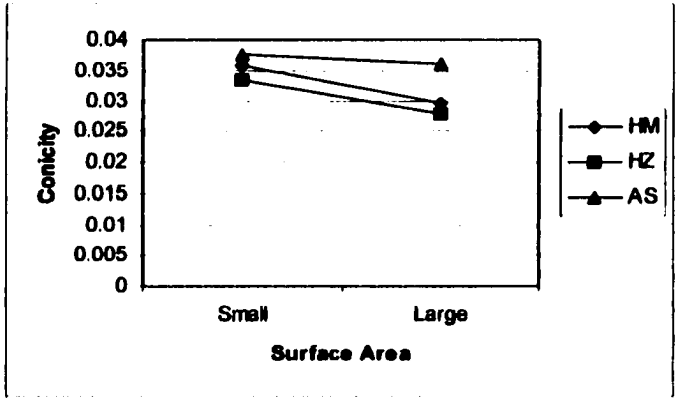


(c) Fitting Algorithm

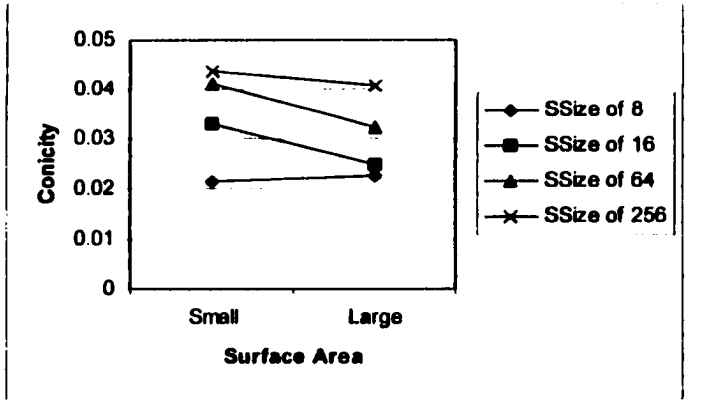


(d) Fitting-Sample Size Interaction

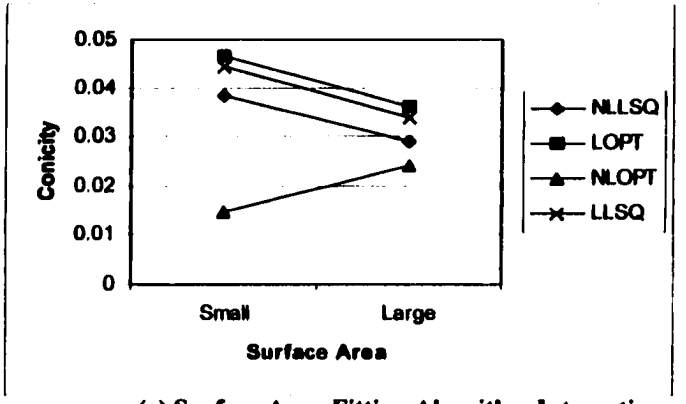
Figure 56. Main Effects Plots and A 2-way Interaction Plot.



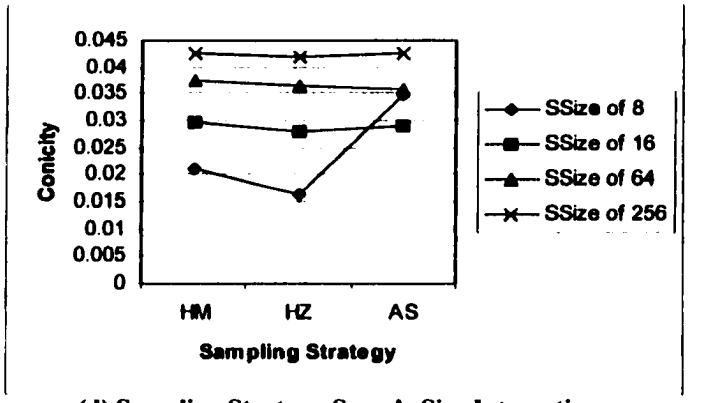
(a) Surface Area-Sampling Strategy Interaction



(b) Surface Area-Sample Size Interaction

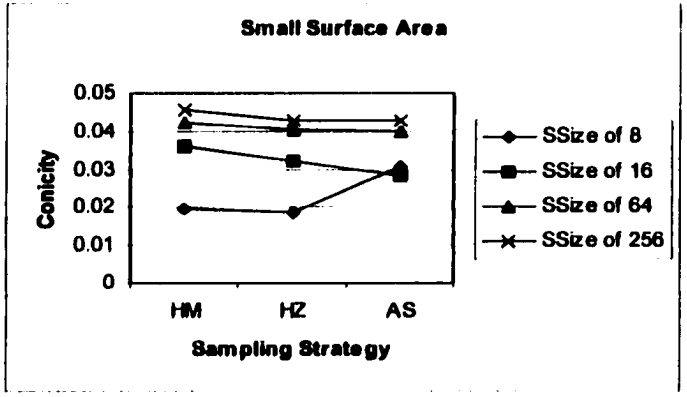


(c) Surface Area-Fitting Algorithm Interaction

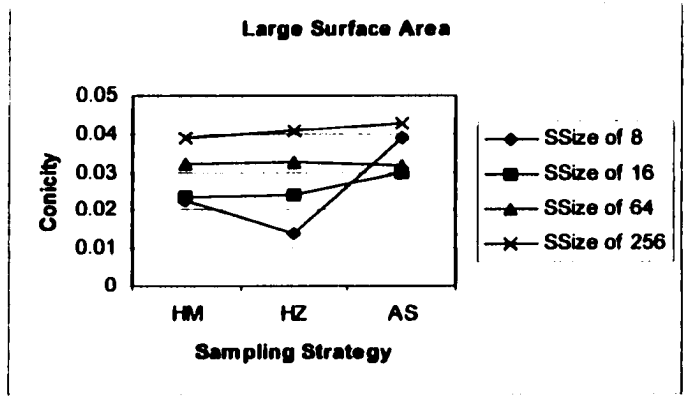


(d) Sampling Strategy-Sample Size Interaction

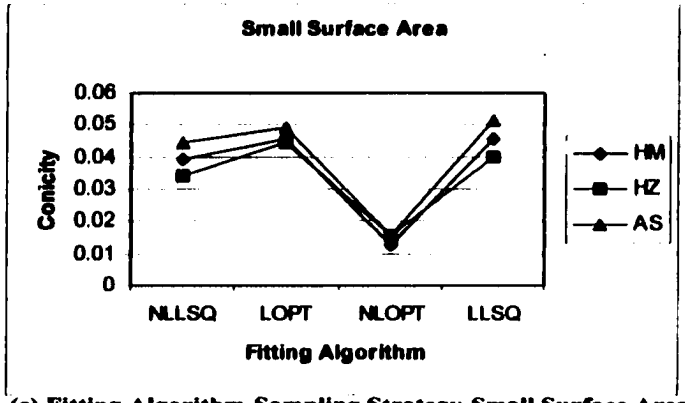
Figure 57. 2-way Interaction Plots.



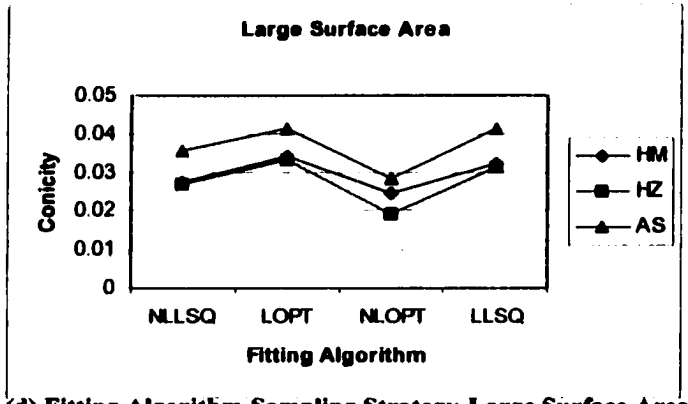
(a) Sampling Strategy-Sample Size-SmallSurface Area



(b) Sampling Strategy-Sample Size-Large Surface Area



(c) Fitting Algorithm-Sampling Strategy-Small Surface Area



(d) Fitting Algorithm-Sampling Strategy-Large Surface Area

Figure 58. 3-way Interaction Plots.

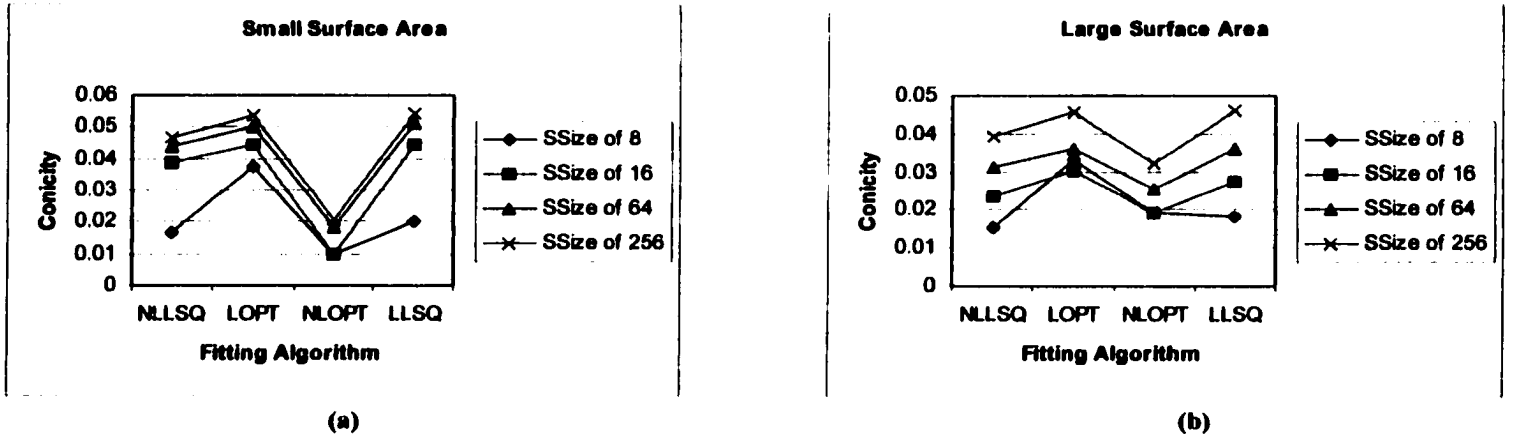
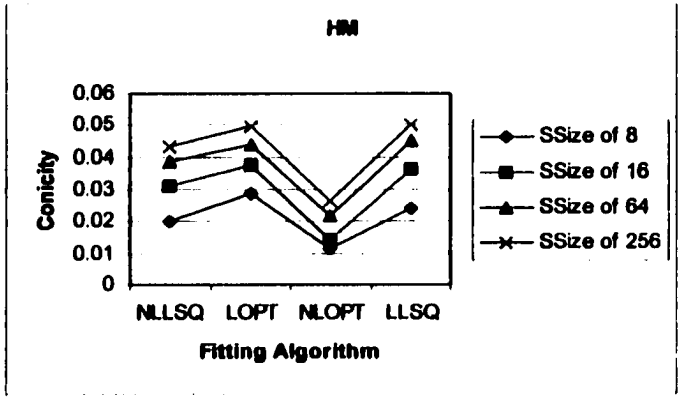
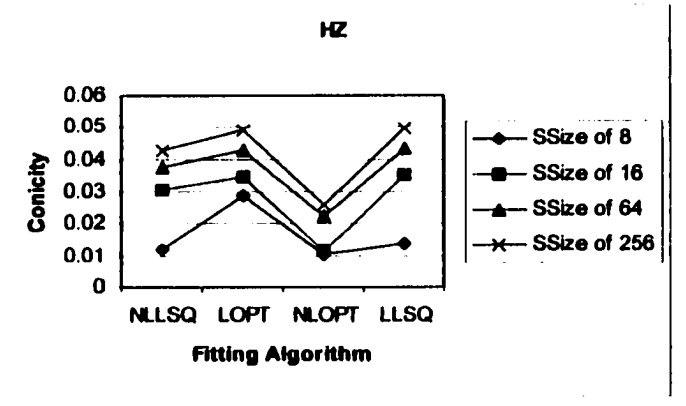


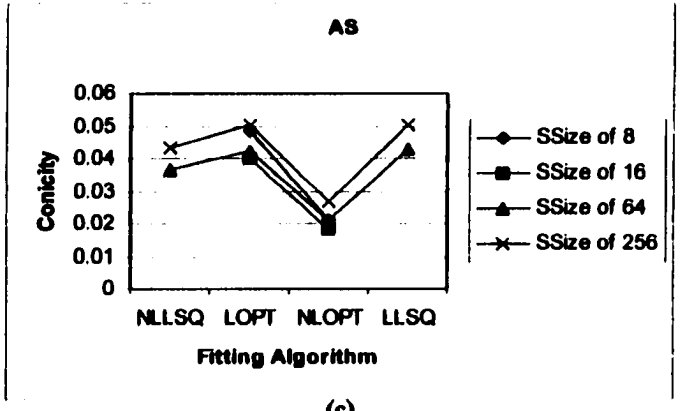
Figure 59. 3-way Interaction Plots between Fitting Algorithm, Sample Size, and Surface Area.



(a)



(b)



(c)

Figure 60. 3-way Interaction Plots between Fitting Algorithm, Sample Size, and Sampling Strategy.

In general, higher sample size intuitively leads to more accurate result since more information can be obtained by using higher sample size. This could be clearly seen in Figures 56 (b) and (d), 57 (b) and (d), 58 (a) and (b), 59, and 60. The higher conicity could be calculated by using higher sample size. This interpretation held for every level of sample size across the levels of other factors. Note that the sample size of 256 did not produce much better result than that of 64 for the small surface area tested. However, the gap was much appreciable for the larger surface area. The sample size evidently depended on the surface area inspected. Apparently, the sample sizes of 8 and 16 did not represent the inspected object very well. In addition, they might cause the invalid parameters as mentioned in Subsection 8.2.1. Hence, the samples size that was acceptable for discrete inspection of conical features in this experiment was either 64 or 256. Which size should be selected depends on cost permitted. Note that for interchangeability, sample size reduction can result in many benefits. However, process variation detection and other diagnostics will actually benefit from large data sets. Since the present research is more concerned with interchangeability issues dealing with form features, the experimental analysis seeks to identify smaller sample sizes.

Obviously, the sampling method that gives the most information should be selected. However, examining only the sampling strategy plot may lead to the invalid conclusion due to the interactions involved and the missing data technique used. Therefore, the plots in Figures 56 (a), 57 (a) and (d), 58, and 60 were taken into consideration. All three levels of sampling method seemed to provide similar results.

The AS seemed acceptable or even better than the other two. Recall that 32 data points were removed from the analysis due to the invalidities of their parameters. These data points were corresponding to AS, sample sizes of 8 and 16, and the LSQ based fitting algorithms as illustrated in Figure 60 (c). The remaining data resulted in interaction between main effects as shown in Figures 57 (d), 58 (a) and (b). Nonetheless, the HM results appeared slightly better than the other two sampling methods' results for sample size of 64. The analysis showed equivalent results, for sample size of 256, across all levels of sampling strategy. This implied that the number of sample points was very high (256) or the information gained (conicity) was quite sufficient. Therefore, the advantage of sampling method was not fully utilized. Note that the number of sample size used in the HZ must be a power of 2, which might prove cumbersome in computations. Thus, the sampling method recommended for sample size of 64 was HM.

On the contrary, compared to the above two factors, a fitting algorithm is more suitable than others if its conicity is lower. Plots in Figures 56 (c) and (d), 57 (c), 58 (c) and (d), 59, and 60 were taken into consideration. The NLOPT clearly produced the lowest conicity among others except the plot in Figure 59 (b) which was probably caused by the missing data. Therefore, the fitting algorithm selected should be the NLOPT.

Basically, the interpretation of the experiment was to select the factors contributing to the high and low response simultaneously. The factors, such as sample size and sampling strategy, were used to gain as much information as possible

from the inspected objects. Hence, the higher the response, the more attractive that level would be. On the other hand, the fitting algorithm was applied to calculate the minimum enclosing zone. This implied that the lower response was desired to avoid the overestimation of such zone or the rejection of some good parts. Simply put the maximum response of the levels of sampling strategy and sample size and the minimum response of the level of conicity algorithm should be chosen. Since the objective of this experiment was to find the effect and appropriateness of the sampling strategy, sample size, the description and fitting of the conicity tolerance and their interactions, the following levels of each controllable significant factor could be recommended based on analysis conducted at the levels tested: (1) the high level of sample size (64 or 256) which would represent the conical object experimented very well, (2) the Hammersley sampling method which would help reduce the sample size and cover the inspected conical object thoroughly, and (3) the NLOPT fitting algorithm which would produce the minimum enclosing zone. More experiments and analysis along these lines must be conducted to develop a comprehensive knowledge-base for cone inspection guidelines. This will serve as a first step towards the development of a comprehensive and integrative standard for the measurement of conical form features. Such a study will also help in the development of solutions for form inspection in industry.

In summary, this chapter suggests a formal procedure for conducting experiments and analysis to investigate the combined effect of multiple variables

(sample size, sampling strategy, zone fitting, and part size) in making form measurements through coordinate metrology.

CHAPTER 9

CONTRIBUTIONS, CONCLUSIONS AND RECOMMENDATIONS

Very little, if any, literature exists in cone feature verification using CMMs. No standards for measuring conical features exist in ANSI form feature descriptions. Further, sampling and path planning are seldom discussed with respect to complex forms. The primary objective of this research was to develop a comprehensive knowledge base for conical feature verification using CMMs. To accomplish this goal, three sampling models for conical feature inspection, a CMM probe path planning procedure, four minimum enclosing zone algorithms, and a factorial design with nested blocking factor were developed, implemented, and statistically experimented. The results of this study provided guidelines for establishing levels of the relevant factors during conical tolerance verification. Conclusions and recommendations for future research are made in this chapter, thus setting the stage for a comprehensive standard for cone measurement in industry.

9.1 Contributions

Conicity verification has received very little attention in the current literature, although there are quite a number of conical industrial parts, such as nozzles, tapered cylinders, frustum holes, and tapered rollers, requiring cone feature verification. To

investigate conical tolerance verification, four major research issues were studied: (1) sampling point selection, (2) path determination, (3) zone estimation, and (4) experimental analysis.

Based on the objectives of this dissertation, the contributions of this work are summarized below:

1. Three separate sampling methods were developed and implemented for sampling points in a repetitive and yet time-conserving manner. Note that no literature exists in the development and hence the comparison of alternate sampling methods for cones.

2. A simple path planning procedure for conical surface was developed to automatically guide the probe movement, consistent with each sampling strategy and sample size. Current literature shows no evidence of path planning in cone inspection. The goals for path planning were to avoid hitting the obstacles and to maintain the precision of sampling location without human intervention. Thus, a fast and accurate data collection could be achieved using the guidelines developed here.

3. Four separate minimum zone algorithms were mathematically formulated: linear LSQ, linear optimization, normalized linear LSQ, and nonlinear optimization. Note that the details with which these are developed and corresponding comparative analysis presented for cones are not matched in literature even for simpler shapes such as cylinders, circles or spheres.

4. To reliably study the performance of the sampling point selections and the zone estimations, and how they must be combined during measurement, and to

develop a comprehensive method for the inspection of cones, a factorial design with nested blocking factor was modeled and tested. Experimental results were then statistically analyzed. Consequently, valid and objective conclusions were obtained. It must be understood that previous reporting in coordinate metrology has not established the need for a comprehensive study of this kind. Moreover, how experimental design and analysis can be used in coordinate metrology to make comprehensive reports of testing and conclusions has been demonstrated.

9.2 Conclusions

1. There are two factors in sampling point selection: sampling location and size. The purpose of sampling theory is to maximize the amount of information collected. The sampling strategies are then developed to achieve the quantity of information pertinent to a population parameter at the lowest possible cost. Hence, sampling strategies are the keys to permitting valid inference about the dimensions and forms of a workpiece (Lee et al., 1997). The sampling strategies dealt with the location of points on the inspected conical form. The main advantages of using the mathematical sequence based methods are the ease of execution and the determinism. In other words, the experiment is repeatable and the sampling error can be controlled. To avoid capturing some systematic error of the measurement, randomizing the initial point was introduced. This hybrid avoidance might not be as good as randomizing every point (random sampling) but it was used to take advantage of both the randomization and the mathematical sequence. In dimensional discrete

measurements, sample size (the number of points measured) was very critical since it contributed directly to the information collected from the inspected parts. It is generally accepted that the larger the sample size, the smaller the error associated with the measurement. The graphical results published by Dowling et al. (1995) clearly showed the improving zone evaluation with denser sample sizes. Sample size is typically proportional to time and cost and for a given sampling strategy, savings in time may be achieved through a reduction of the sample size. It has been suggested that an alternate sampling strategy may be selected at a lower sample size while maintaining the same level of accuracy. Therefore, sample size was included as a factor of interest in statistical analysis. Three sampling models, Hammersley sequence based method, Halton-Zaremba sequence based method, and Uniform sampling method (Aligned Systematic), were derived based on the procedure presented by Lee et al. (1997). They were statistically compared to find the best method of various sample sizes. It is important to note that the aligned systematic sampling with small sample sizes like 8 or 16 coupled with the linear LSQ could result in invalid parameters for conical surface. Therefore, the sample size of 64 was recommended due to the high information provided and low cost compared to that at higher sample sizes. The sampling method recommended was Hammersley based scheme due to the high information collected and ease of computation over the other two.

2. Tolerance conical zone evaluation involves a fitting of the sampled discrete points. The linear error model using the Limacon approximation was derived. In

addition, the nonlinear form of the errors was also developed. Then, they were fitted to find the substitute (ideal) conical feature and its minimum enclosing zone. The most commonly used method to find such zone estimation in practice is the method of least squares (LSQ) due to its uniqueness, efficiency, robustness, and simplicity for linear systems. Even though the LSQ zone evaluation is based on sound mathematical principles, it does not follow the intent of the ANSI Y14.5M-1994 (ASME, 1995) well. It might overestimate the tolerance zone since it attempts to minimize the sum of the squares of the errors. In other words, it does not attempt to minimize the zone of the errors directly. Not only does it reject bad parts, but it might also reject some good parts. This, in turn, leads to higher production cost. With this disadvantage, another approach is called for. The optimization approach which is a better match for the definition of the minimum zone than the LSQ has shown its potential for basic features inspection in literature. The LSQ and optimization approaches (linear LSQ, normalized linear LSQ, linear and nonlinear optimizations) were formulated by using the error models derived to find such zones. As concluded from experimental analysis, the differences of the linear and nonlinear deviations were quite appreciable. Coupled with the nonlinear deviation, the optimization algorithm (NLOPT) was the most effective and recommended for adoption in practice by the experimental analysis conducted in this research.

With the implementation of these guidelines, the conical feature inspection is more accurate, reliable, and efficient. The possibility of rejecting some good parts is also reduced, resulting in a cost savings.

3. No explicit experimental analysis of path planning in relation with sample point determination and zone estimation was conducted in this research.

9.3 Recommendations for Future Research

1. The path planning procedure can be easily extended to cover internal conical features (nozzles, for example). The CMM probe path study shows that further work in optimizing the inspection path (time) must allow better utilization of sampling theories with a range of sampling points, not only for the conical features but also other features. Shortest path algorithm may be derived and employed. Refer to Kim and Raman (2000) for how TSP was employed for path minimization in flatness. Thus, further improvements to inspection results can result.

2. Sampling strategies and sizes should be taken into consideration for other form features. Torus and other complex shapes should be studied comprehensively for both sampling and fitting issues, using an approach suggested for cones in this dissertation.

3. With regards to zone fitting, the gradient-based algorithms are most suitable if a smooth objective function (continuous first and second derivatives) can be formulated. Hence, using a gradient-based method with global strategy (making several runs from several initial solutions to avoid local optima traps) may be formulated. However, this kind of optimization model is not easily formulated. Many minimax fit models do not have smooth objective functions. They may suffer from numerical instabilities with respect to convergence because the first or second

derivatives of the objective functions are not continuous. The comparisons between different optimization algorithms may suggest the use of more robust and efficient algorithms for specific features. Alternatively, heuristic search algorithms like genetic algorithm, simulated annealing, and tabu search may be able to avoid the local optima traps and find the best minimum conical zone. Literature using genetic algorithm on simpler forms show that good results could be obtained.

4. The support vector machine regression also shows some potential in finding minimum enclosing zone such as straightness and flatness. Other features may too benefit from this technique together with the use of kernel functions.

5. Adaptive sampling (Badar et al., 2000; 2001) utilizing search methods may again be used, combined with knowledge regarding the errors caused by manufacturing processes.

6. Software developed based on the findings of this research could allow for the development of better standards and solutions for industry.

REFERENCES

ASME Y14.5M-1994. (1995). *Dimensioning and Tolerancing*. New York, NY: The American Society of Mechanical Engineers.

Badar, M.A., Raman, S., and Pulat, P.S. (2000). Search-based selection of sample points for form error estimation. In *Proceedings of the ASME Manufacturing Engineering Division 2000* (pp.73-80). Orlando, Florida.: American Society of Mechanical Engineers.

Badar, M.A., Raman, S., and Pulat, P.S. (2001). Intelligent search-based selection of sample points for form error estimation. Internal Publication, University of Oklahoma, Norman, OK.

Banks, J., and Carson, II, J.S. (1984). *Discrete-event system simulation*. Englewood Cliffs, New Jersey: Prentice-Hall, Inc.

Bazaraa, M.S., Jarvis, J.J., and Sherali, H.D. (1990). *Linear programming and network flows* (2nd Ed.). New York: John Wiley & Sons, Inc.

Bazaraa, M.S., Sherali, H.D., and Shetty, C.M. (1993). *Nonlinear Programming: Theory and Algorithms* (2nd Ed.). New York: John Wiley & Sons, Inc.

Brown & Sharpe Manufacturing Company. (1996). *MicroVal PFx User's Manual, 82-90033-3*. North Kingstown, RI: author.

Carpinetti, L.C.R., and Chetwynd, D.G. (1995). Genetic search methods for assessing geometric tolerances. *Computer Methods in Applied Mechanics and Engineering*, 122, 193-204.

Carr, K., and Ferreira, P. (1995a). Verification of form tolerances Part I: Basic issues, flatness, and straightness. *Precision Engineering*, 17(2), 131-143.

Carr, K., and Ferreira, P. (1995b). Verification of form tolerances Part II: Cylindricity and straightness of a median line. *Precision Engineering*, 17(2), 144-156.

Caskey, G., Hari, Y., Hocken, R., Machireddy, R., Raja, J., Wilson, R., Zhang, G., Chen, K., and Yang, J. (1992). Sampling Techniques for Coordinate Measuring Machines. In *Proceedings of the 1992 NSF Design and Manufacturing Systems Conference* (pp. 983-988). Atlanta, Georgia.: Society of Manufacturing Engineers.

Chang, T.C., Wysk, R.A., and Wang, H.P. (1998). *Computer-aided manufacturing* (2nd Ed.). Upper Saddle River, NJ: Prentice-Hall, Inc.

Chatterjee, G., and Roth, B. (1998). Chebychev approximation methods for evaluating conicity. *Journal of the International Measurement Confederation*, 23(2), 63-76.

Cheraghi, S.H., Lim, H.S., and Motavalli, S. (1996). Straightness and flatness tolerance evaluation: an optimization approach. *Precision Engineering*, 18(1), 30-37.

Chetwynd, D.G. (1979). Roundness measurement using limacons. *Precision Engineering*, 1(3), 137-141.

Chetwynd, D.G. (1985). Applications of linear programming to engineering metrology. *Proceedings of the Institute of Mechanical Engineers*, 199(B2), 93-100.

Choi, W., and Kurfess, T.R. (1999). Dimensional Measurement Data Analysis, Part 1: A Zone Fitting Algorithm. *Journal of Manufacturing Science and Engineering*, 121(2), 238-245.

Choi, W., and Kurfess, T.R. (1999). Dimensional Measurement Data Analysis, Part 2: Minimum Zone Evaluation. *Journal of Manufacturing Science and Engineering*, 121(2), 246-250.

Chung, S.H. (1997). *Methods for determination of the conicity tolerance.* Unpublished M.S. Thesis, University of Oklahoma, Norman, OK.

Cochran, W.G. (1977). *Sampling Techniques* (3rd Ed.). New York: John Wiley & Sons, Inc.

Cogdel, D. (1999), Timken Company, Personal Communication with Dr. Raman, March 17, 1999

Daniel, C., and Wood, F.S. (1980). *Fitting equations to data: Computer analysis of multifactor data* (2nd Ed.). New York: John Wiley & Sons, Inc.

DEA spa. (1995). *TUTOR for WINDOWS: Application Guide, Code: M1U041EB.* Moncalieri, Italy: author.

DEA spa. (1995). *TUTOR for WINDOWS: Programming Manual, Code: M1U040EB.* Moncalieri, Italy: author.

DEA spa. (1995). *TUTOR for WINDOWS: Installation Guide, Code: M1U039EB.* Moncalieri, Italy: author.

DEA spa. (1995). *TUTOR for WINDOWS: User's Guide, Code: M1U038EB.* Moncalieri, Italy: author.

Dhanish, P.B., and Shunmugam, M.S. (1991). An algorithm for form error evaluation – using the theory of discrete and linear Chebyshev approximation. *Computer Methods in Applied Mechanics and Engineering*, 92(3), 309-324.

Dowling, M.M., Griffin, P.M., Tsui, K.L., and Zhou, C. (1995). A Comparison of the Orthogonal Least Squares and Minimum Enclosing Zone Methods for Form Error Estimation. *Manufacturing Review*, 8(2), 120-138.

Elmaraghy, W.H., Elmaraghy, H.A., and Wu, Z. (1990). Determination of Actual Geometric Deviations Using Coordinate Measuring Machine Data. *Manufacturing Review*, 3(1), 32-39.

Faux, I.D., and Pratt, M.J. (1979). *Computational Geometry for Design and Manufacture*. Chichester, England: Ellis Horwood Ltd.

Fishman, G.S. (1996). *Monte Carlo: Concepts, Algorithms, and Applications*. New York: Springer-Verlag.

Fujii, R. (1998). *Sampling point strategies for various types of surface measurements.* Unpublished Project Report, University of Oklahoma, Norman, OK.

Gasson, P.C. (1983). *Geometry of spatial forms*. Chichester, England: Ellis Horwood Limited.

Gen, M., and Cheng, R. (1997). *Genetic Algorithms and Engineering Design*. New York: John Wiley & Sons Ltd.

Grant, E.L., and Leavenworth, R.S. (1996). *Statistical quality control* (7th Ed.). Boston, Massachusetts: The McGraw-Hill Companies, Inc.

Groover, M.P. (2001). *Automation, Production Systems, and Computer-Integrated Manufacturing* (2nd Ed.). Upper Saddle River, NJ: Prentice-Hall, Inc.

Haataja, J. (1999). Using Genetic Algorithms for Optimization: Technology Transfer in Action. In K. Miettinen, P. Neittaanmaki, M.M. Makela, and J. Periaux (Eds.), *Evolutionary Algorithms in Engineering and Computer Science* (pp. 3-22). Chichester, England: John Wiley & Sons Ltd.

Hammersley, J.M. (1960). Monte Carlo methods for solving multivariable problems. *Annals of the New York Academy of Sciences*, 86, 844-874.

Halton, J.H., and Zaremba, S.K. (1969). The Extreme and L^2 Discrepancies of Some Plane Sets. *Monatshefte fur Mathematik*, 73, 316-328.

Hazelrigg, G.A. (1996). *Systems engineering: An approach to information-based design.* Upper Saddle River, NJ: Prentice-Hall, Inc.

Henzold, G. (1995). *Handbook of Geometrical Tolerancing.* Chichester, England: John Wiley & Sons Ltd.

Hocken, R.J., Raja, J., and Babu, U. (1993). Sampling Issues In Coordinate Metrology. *Manufacturing Review*, 6(4), 282-294.

Hong, J.T., Liao, Y.S., and Fan, K.C. (1991). A computational geometry approach to minimum zone evaluation of straightness. *Journal of the Chinese Institute of Engineers*, 14(5), 463-470.

Huang, S.T., Fan, K.C., and Wu, J.H. (1993a). A new minimum zone method for evaluating straightness errors. *Precision Engineering*, 15(3), 158-165.

Huang, S.T., Fan, K.C., and Wu, J.H. (1993b). A new minimum zone method for evaluating flatness errors. *Precision Engineering*, 15(1), 25-32.

Huang, S.T., Wu, J.H., and Fan, K.C. (1993c). A minimum zone method for evaluating flatness error of gage blocks measured by phase-shifting interferometry. *Journal of the Chinese Institute of Engineers*, 16(5), 641-650.

Jacak, W. (1999). *Intelligent robotic systems: Design, Planning, and Control.* New York: Kluwer Academic/ Plenum Publishers.

Kalpakjian, S., and Schmid, S.R. (2001). *Manfucturing Engineering and Technology* (4th Ed.). Upper Saddle River, NJ: Prentice-Hall, Inc.

Kanada, T. (1995). Evaluation of spherical form errors: Computation of sphericity by means of minimum zone method and some examinations with using simulated data. *Precision Engineering*, 17(4), 281-289.

Kanada, T., and Suzuki, S. (1993a). Evaluation of minimum zone flatness by means of nonlinear optimization techniques and its verification. *Precision Engineering*, 15(2), 93-99.

Kanada, T., and Suzuki, S. (1993b). Application of several computing techniques for minimum zone straightness. *Precision Engineering*, 15(4), 274-280.

Kelton, W.D., Sadowski, R.P., and Sadowski, D.A. (1998). *Simulation with Arena.* Boston, Massachusetts: The McGraw-Hill Companies, Inc.

Kim, H.M., and Lee, B.C. (1997). Geometric form evaluation of cone based on the minimum zone criteria. In *Proceedings of the Twelfth Annual Meeting of the American Society of Precision Engineering* (pp. 86-89). Norfolk, Virginia.: American Society for Precision Engineering.

Kim, W.S. (1998). *An Investigation of sampling strategies in flatness inspection.* Unpublished M.S. Thesis, University of Oklahoma, Norman, OK.

Kim, W.S., and Raman, S. (2000). On the selection of flatness measurement points in coordinate measuring machine inspection. *International Journal of Machine Tools and Manufacture*, 40(3), 427-443.

Lai, J.Y., and Chen, I.H. (1996). Minimum zone evaluation of circles and cylinders. *International Journal of Machine Tools and Manufacture*, 36(4), 435-451.

Lai, H.Y., Jywe, W.Y., Chen, C.K., and Liu, C.H. (2000). Precision modeling of form errors for cylindricity evaluation using genetic algorithms. *Precision Engineering*, 24(4), 310-319.

Le, V.B., and Lee D.T. (1991). Out-of-Roundness Problem Revisited. *IEEE Transactions on Pattern Analysis and Machine Intelligence*, 13(3), 217-223.

Lee, G., Mou, J., and Shen, Y. (1997). Sampling strategy design for dimensional measurement of geometric features using coordinate measuring machine. *International Journal of Machine Tools and Manufacture*, 37(7), 917-934.

Lee, M.K. (1997). A new convex-hull based approach to evaluating flatness tolerance. *Computer-Aided Design*, 29(12), 861-868.

Liang, R., Woo, T.C., and Hsieh, C.C. (1998a). Accuracy and Time in Surface Measurement, Part 1: Mathematical Foundations. *Journal of Manufacturing Science and Engineering*, 120(1), 141-149.

Liang, R., Woo, T.C., and Hsieh, C.C. (1998b). Accuracy and Time in Surface Measurement, Part 2: Optimal Sampling Sequence. *Journal of Manufacturing Science and Engineering*, 120(1), 150-155.

Lim, C.P., and Menq, C.H. (1994). CMM feature accessibility and path generation. *International Journal of Production Research*, 32(3), 597-618.

Lin, S.S., Varghese, P., Zhang, C., and Wang, H.P.B. (1995). A Comparative Analysis of CMM Form-Fitting Algorithms. Manufacturing Review, 8(1), 47-58.

Lu, E., Ni, J., and Wu, S.M. (1994). An Algorithm for the Generation of an Optimum CMM Inspection Path. *Journal of Dynamic Systems, Measurement and Control*, 116(3), 396-404.

Mavridou, T.D., and Pardalos, P.M. (1997). Simulated Annealing and Genetic Algorithms for the Facility Layout Problem: A Survey. *Computational Optimization and Applications*, 7(1), 111-126.

Menq, C.H., Yau, H.T., Lai, G.Y., and Miller, R.A. (1990). Statistical evaluation of form tolerances using discrete measurement data. *American Society of Mechanical Engineers, Production Engineering Division (Publication) PED*, 47, 135-149.

Montgomery, D.C. (1997). *Design and Analysis of experiments* (4^{th} Ed.). New York: John Wiley & Sons, Inc.

Montgomery, D.C., and Runger, G.C. (1994). *Applied Statistics and Probability for Engineers*. New York: John Wiley & Sons, Inc.

Murthy, T.S.R., and Abdin, S.Z. (1980). Minimum zone evaluation of surfaces. *International Journal of Machine Tool Design and Research*, 20, 123-136.

Namboothiri, V.N.N., and Shunmugam, M.S. (1998a). Form error evaluation using L_1-approximation. *Computer Methods in Applied Mechanics and Engineering*, 162(1-4), 133-149.

Namboothiri, V.N.N., and Shunmugam, M.S. (1998b). Function-oriented form evaluation of engineering surfaces. *Precision Engineering*, 22(2), 98-109.

Namboothiri, V.N.N., and Shunmugam, M.S. (1999). On determination of sample size in form error evaluation using coordinate metrology. *International Journal of Production Research*, 37(4), 793-804.

Nash, S.G., and Sofer, A. (1996). *Linear and Nonlinear Programming*. New York: The McGraw-Hill Companies, Inc.

Orady, E.A., Li, S., and Chen, Y. (1996). Evaluation of minimum zone straightness by nonlinear optimization method. *Manufacturing Science and Engineering*, 4, 413-423.

Pham, D.T., and Karaboga, D. (2000). *Intelligent Optimisation Techniques: Genetic Algorithms, Tabu Search, Simulated Annealing and Neural Networks.* London: Springer-Verlag.

Preparata, F.P., and Shamos, M.I. (1985). *Computational Geometry: An introduction.* New York: Springer-Verlag.

Raj, D. (1968). *Sampling theory.* New York: McGraw-Hill, Inc.

Rardin, R.L. (1998). *Optimization in operations research.* Upper Saddle River, NJ: Prentice-Hall, Inc.

Ravindran, A., Phillips, D.T., and Solberg, J.J. (1987). *Operations research: Principles and practice* (2nd Ed.). New York: John Wiley & Sons, Inc.

Rawlings, J.O., Pantula, S.G., and Dickey, D.A. (1998). *Applied regression analysis: A research tool* (2nd Ed.). New York: Springer-Verlag.

Reklaitis, G.V., Ravindran, A., and Ragsdell, K.M. (1983). *Engineering optimization: Methods and applications.* New York: John Wiley & Sons, Inc.

Roos, C., Terlaky, T., and Vial, J.Ph. (1997). *Theory and Algorithms for Linear Optimization.* Chichester, England: John-Wiley & Sons Ltd.

Roth, K.F. (1954). On irregularities of distribution. *Mathematika*, 1(2), 73-79.

Roy, U. (1995). Computational Methodologies for Evaluating Form and Positional Tolerances in a Computer Integrated Manufacturing System. *International Journal of Advanced Manufacturing Technology*, 10(2), 110-117.

Roy, U., and Xu, Y. (1995). Form and orientation tolerance analysis for cylindrical surfaces in computer-aided inspection. *Computers in Industry*, 26(2), 127-134.

Roy, U., and Zhang, X. (1992). Establishment of a pair of concentric circles with the minimum radial separation for assessing roundness error. *Computer-Aided Design*, 24(3), 161-168.

Roy, U., and Zhang, X. (1994). Development and application of Voronoi diagrams in the assessment of roundness error in an industrial environment. *Computers and Industrial Engineering*, 26(1), 11-26.

Samuel, G.L., and Shunmugam, M.S. (1999). Evaluation of straightness and flatness error using computational geometric techniques. *Computer Aided Design*, 31(13), 829-843.

Segre, A.M. (1988). *Machine Learning of Robot Assembly Plans*. Boston: Kluwer Academic Publishers.

Sharma, R., Rajagopal, K., and Anand, S. (2000). A Genetic Algorithm Based Approach for Robust Evaluation of Form Tolerances. *Journal of Manufacturing Systems*, 19(1), 46-57.

Shashidhar, P.N. (1992). *Automated Precision Inspection*. Unpublished Project Report, University of Oklahoma, Norman, OK.

Shunmugam, M.S. (1986). On assessment of geometric errors. *International Journal of Production Research*, 24(2), 413-425.

Shunmugam, M.S. (1987a). Comparison of linear and normal deviations of forms of engineering surfaces. *Precision Engineering*, 9(2), 96-102.

Shunmugam, M.S. (1987b). New approach for evaluating form errors of engineering surfaces. *Computer-Aided Design*, 19(7), 368-374.

Shunmugam, M.S. (1991). Establishing Reference Figures for Form Evaluation of Engineering Surfaces. *Journal of Manufacturing Systems*, 10(4), 314-321.

Snyder, M.A. (1966). *Chebyshev Methods in Numerical Approximation*. Englewood Cliffs, NJ: Prentice-Hall, Inc.

Staff of Research and Education Association. (1984). *The Vector Analysis Problem Solver*. New York: Research and Education Association.

Staff of LINDO Systems Inc. (2001). *Powerful LINGO Solvers*. http://www.lindo.com/lgosolvef.html.

Stuart, A. (1976). *Basic ideas of scientific sampling* (2nd Ed.). London: Charles Griffin and Company.

Suen, D.S., and Chang, C.N. (1997). Application of neural network interval regression method for minimum zone circle roundness. *Measurement science & technology*, 8(3), 245-252.

Traband, M.T., Joshi, S., Wysk, R.A., and Cavalier, T.M. (1989). Evaluation of Straightness and Flatness Tolerances Using the Minimum Zone. *Manufacturing Review*, 2(3), 189-195.

Tsukada, T., Kanada, T., and Liu, S. (1988). Method for the evaluation of form errors of conical tapered parts. *Precision Engineering*, 10(1), 8-12.

Trucks, H.E. (1974). *Designing for economical production*. Dearborn, Michigan: Society of Manufacturing Engineers.

Wang, Y. (1992). Minimum Zone Evaluation of Form Tolerances. *Manufacturing Review*, 5(3), 213-220.

Woo, T.C., and Liang, R. (1993). Dimensional measurement of surfaces and their sampling. *Computer Aided Design*, 25(4), 233-239.

Woo, T.C., Liang, R., and Pollock, S.M. (1993). Hammersley Sampling for Efficient Surface Coordinate Measurements. In *Proceedings of the 1993 NSF Design and Manufacturing Systems Conference* (pp. 1489-1496). Charlotte, North Carolina.: Society of Manufacturing Engineers.

Woo, T.C., Liang, R., Hsieh, C.C., and Lee, N.K. (1995). Efficient Sampling for Surface Measurements. *Journal of Manfuacturing Systems*, 14(5), 345-354.

Yau, H.T., and Menq, C.H. (1995). Automated CMM path planning for dimensional inspection of dies and molds having complex surfaces. *International Journal of Machine Tools and Manufacture*, 35(6), 861-876.

Zurada, J.M. (1992). *Introduction to Artificial Neural Systems*. St. Paul, MN: West Publishing Company.

APPENDIX A

PERFORMING GUIDES FOR THE EXPERIMENT

To avoid any confusion in carrying out the entire experiment, this section presents an experiment procedure of this research starting from generating the sampling points according to the studied sampling strategies to executing the SAS program:

1. In MATLAB, change the working directory to where the program or "m" files are stored or include it in the searched path. Run "conesampling.m" and save the generated master path file as "...a.pat". File naming should be consistent for ease of recognition as follows:
    a. The first two letters are named after the sampling strategies such as "hm", "hz", and "as".
    b. The third letter is a number. 8, 1, 6, and 2 represent 8, 16, 64, and 256 collected points.
    c. The fourth letter represents the size of the cone. "s" is for the smaller ones (right cones) and "l" is for the bigger ones (conical frustums).
    d. The last letter represents the way the CMM execute the measuring or constructing the inspected parts: "a" or "o". "a" is the suffix used in the master path file and "o" is used in the duplicated path files.

2. Run "editpathfile.m" in MATLAB and load the above master path file. This program generates the duplicate path files in the format suitable for the CMM.

3. Copy those duplicate files to the CMM controller (PC).

4. Prepare the CMM programs for both sizes of all specimens.

5. Execute the CMM programs for each selected specimen.

6. Backup the result files *.mea and delete them from the controller.

7. Merge and format *.mea files into a text file to be loaded in Excel for each specimen by running "FolderList.exe". This program is written by using Visual Basic. If the directory structure causes some errors, edit the source code accordingly.

8. Execute "DataAnalysis6.xls" with Macros enabled in Excel. This macro program automatically loads and arranges the above text file into Excel cells. This macro is written by using Visual Basic for Application. The source code can be edited rather easily if needed. There are 384 combinations for every factor considered in this experiment. Hence, the macro should be executed 384 times to obtain all the results.

9. Run "SAS Conicity.xls" to format the files to be imported into SAS for all 384 data.

10. Run "Conicity Analysis.sas" in SAS.

11. If invalid parameters are encountered, the data removal process is called for by rerunning Steps 9 and 10 but with "SAS Conicity for Missing Data.xls" and "Conicity Analysis for Missing Data.sas".

APPENDIX B

MODEL ADEQUACY CHECKING PLOTS FOR THE EXPERIMENTAL DESIGN USED BEFORE REMOVING THE INVALID DATA

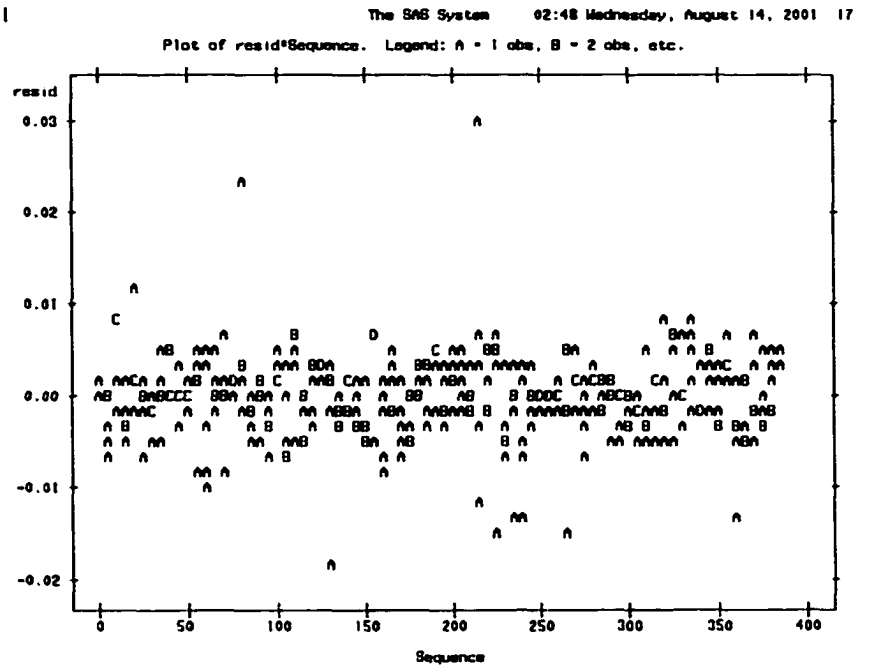


Figure A1. Plot of Residuals in Time Sequence.

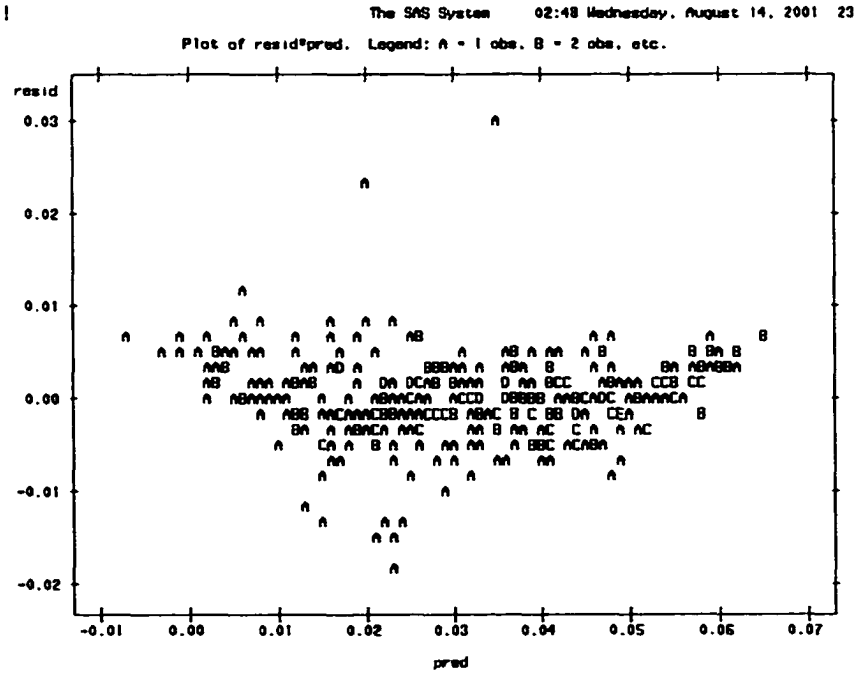


Figure A2. Plot of Residuals Versus Fitted Values.

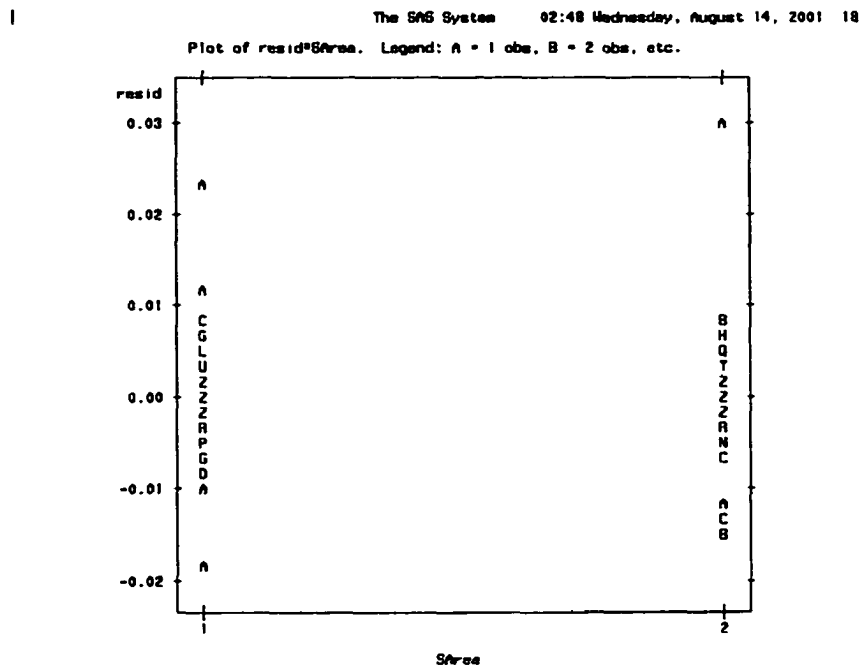


Figure A3. Plot of Residuals Versus SArea.

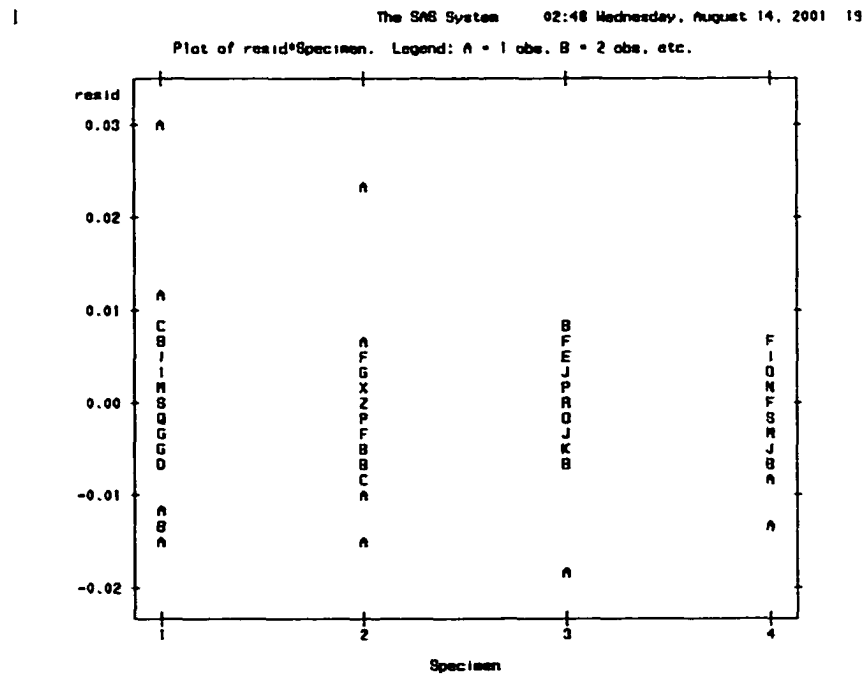


Figure A4. Plot of Residuals Versus Specimen.

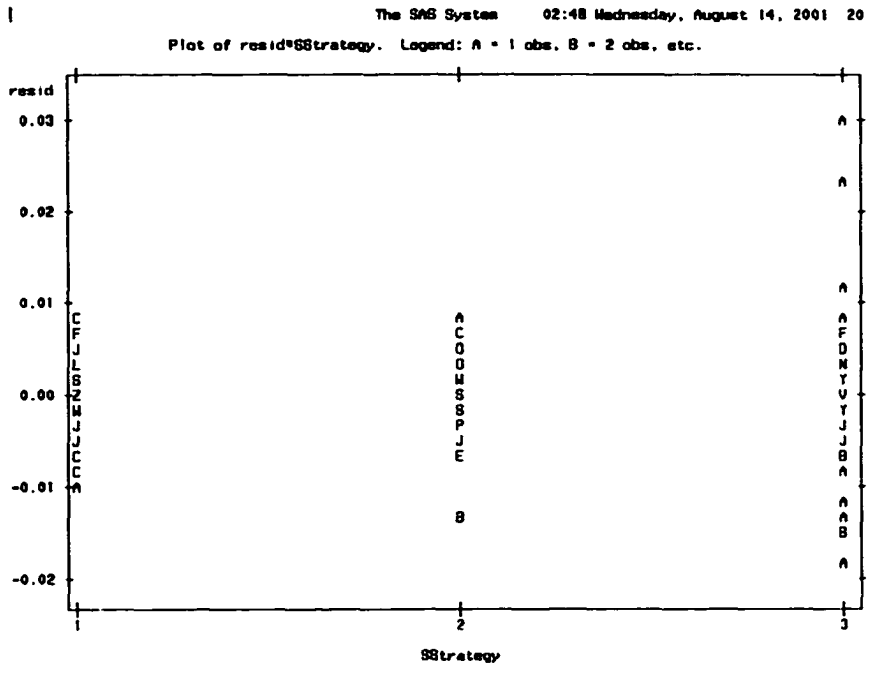


Figure A5. Plot of Residuals Versus SStrategy.

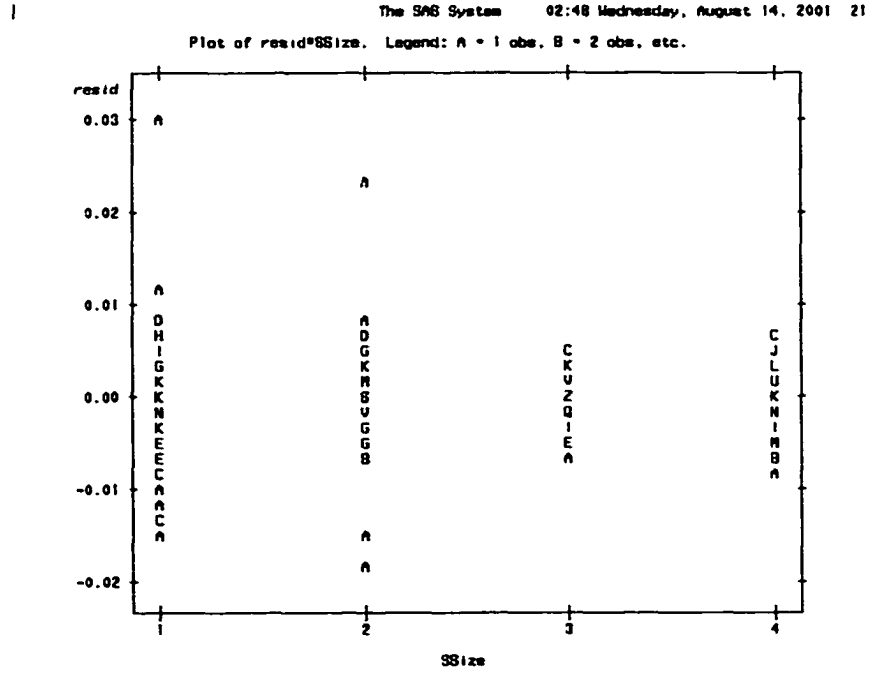


Figure A6. Plot of Residuals Versus SSize.

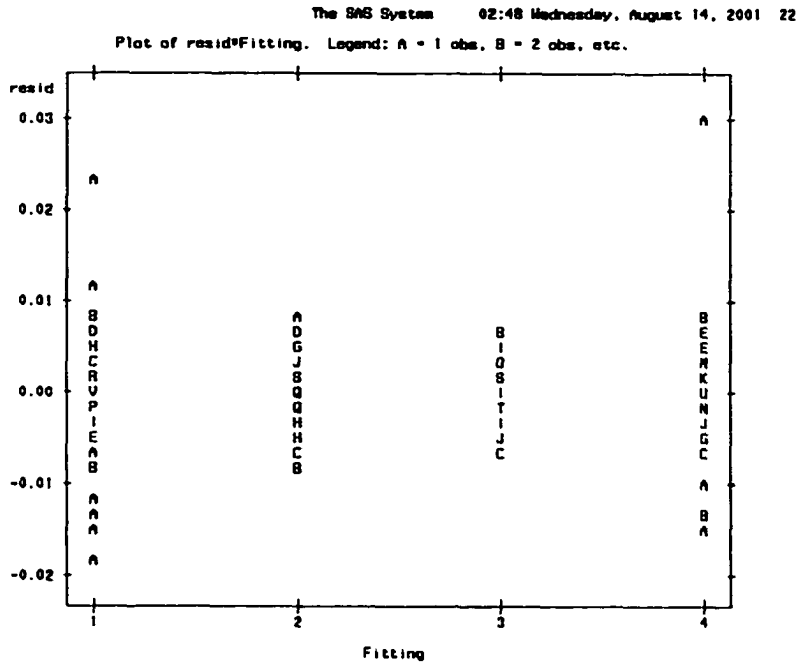


Figure A7. Plot of Residuals Versus Fitting.

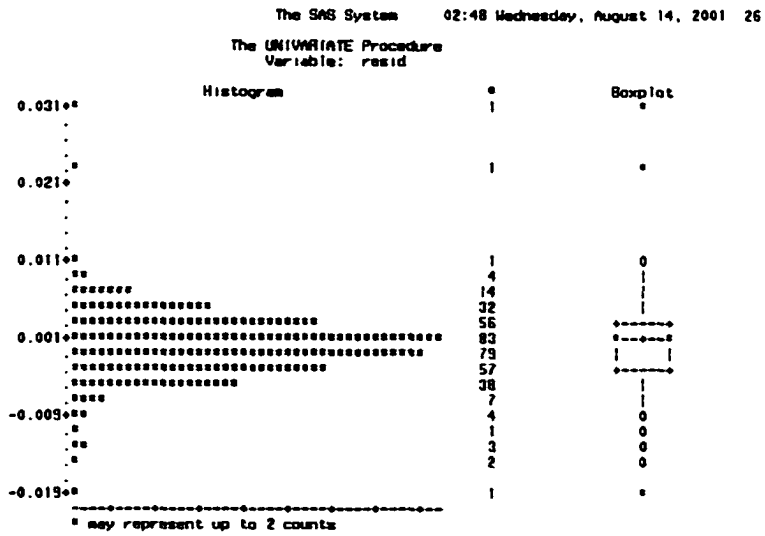


Figure A8. Box Plot of Residuals.

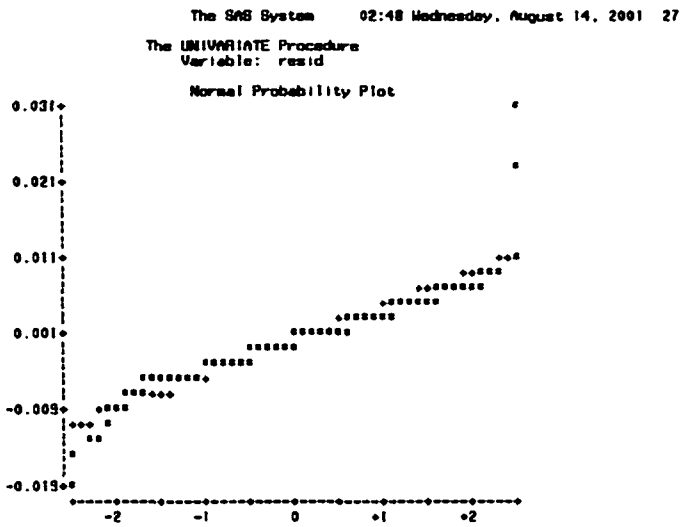


Figure A9. Normal Probability Plot of Residuals.

APPENDIX C

INVALID PARAMETERS OBTAINED BY USING ALIGNED SYSTEMATIC SAMPLING

Parameters	Fitting			
	Normalized LLSQ	LLSQ	LOPT	NLOPT
R0	83.16086698	83.16086698	1.9705	2.0495
S	-32.03736576	-32.03736576	-0.58273018	-0.594327757
m	39.23446713	39.23446713	0.008544415	0
X0	-101.1983594	-101.1983594	0.04260321	0
n	20.94183939	20.94183939	0	0.004956086
Y0	-54.0536615	-54.0536615	0.059567483	0.011145313
R1	NA	NA	0.2395	0.2395
CHeight	NA	NA	2.9705	3.045457625

(a) Sample Size of 8 for the Large Specimen #1

Parameters	Fitting			
	Normalized LLSQ	LLSQ	LOPT	NLOPT
R0	5.234977933	5.234977933	2.013642771	2.0495
S	7.035893769	7.035893769	-0.577105738	-0.589677117
m	-9.52817328	-9.52817328	0	0
X0	-3.96495583	-3.96495583	0	0
n	-5.031698669	-5.031698669	0	0.003796806
Y0	-2.170242151	-2.170242151	0	0.017108497
R1	NA	NA	0.253758823	0.2605
CHeight	NA	NA	3.0495	3.033863701

(b) Sample Size of 8 for the Large Specimen #2

Parameters	Fitting			
	Normalized LLSQ	LLSQ	LOPT	NLOPT
R0	45.33640167	45.33640167	2.017755631	2.0495
S	-9.912263893	-9.912263893	-0.583404739	-0.594560196
m	11.61189141	11.61189141	0	0
X0	-53.99900583	-53.99900583	0	0
n	6.246442075	6.246442075	0	0.004908753
Y0	-28.88613059	-28.88613059	0	0.011051484
R1	NA	NA	0.2605	0.2395
Cheight	NA	NA	3.012069517	3.044267024

(c) Sample Size of 8 for the Large Specimen #3

Parameters	Fitting			
	Normalized LLSQ	LLSQ	LOPT	NLOPT
R0	4.712829232	4.712829232	2.012827894	2.0495
S	4.788900268	4.788900268	-0.580739877	-0.593798225
m	-6.721031172	-6.721031172	0	0
X0	-3.326265477	-3.326265477	0	0
n	-3.5466361	-3.5466361	0	0.003238668
Y0	-1.815608399	-1.815608399	0	0.006808342
R1	NA	NA	0.241861639	0.2395
CHeight	NA	NA	3.0495	3.048173479

(d) Sample Size of 8 for the Large Specimen #4

Parameters	Fitting			
	Normalized LLSQ	LLSQ	LOPT	NLOPT
R0	-31.46954881	-31.46954881	2.0495	2.0495
S	6.951054449	6.951054449	-0.603193656	-0.596209971
m	-8.985711238	-8.985711238	0.004252101	0
X0	39.9777627	39.9777627	0.00675615	0
n	5.735548848	5.735548848	0	0
Y0	-25.41449945	-25.41449945	0	0
R1	NA	NA	0.257713244	0.2605
CHeight	NA	NA	2.9705	3.000620733

(e) Sample Size of 16 for the Large Specimen #1

Parameters	Fitting			
	Normalized LLSQ	LLSQ	LOPT	NLOPT
R0	-20.15993649	-20.15993649	2.027368228	2.0495
S	2.262743315	2.262743315	-0.581960462	-0.590931691
m	-3.391453267	-3.391453267	0.0006328	0
X0	26.49744902	26.49744902	0.004619202	0
n	2.178647197	2.178647197	0	0
Y0	-16.84914927	-16.84914927	0	0.003976694
R1	NA	NA	0.2526798	0.2605
CHeight	NA	NA	3.0495	3.027422673

(f) Sample Size of 16 for the Large Specimen #2

Parameters	Fitting			
	Normalized LLSQ	LLSQ	LOPT	NLOPT
R0	0.129589325	0.129589325	2.026100182	2.044553144
S	-2.072642725	-2.072642725	-0.585211485	-0.593985443
m	1.772522918	1.772522918	0	0
X0	2.275744542	2.275744542	0	0
n	-1.118022488	-1.118022488	0	1.72064E-06
Y0	-1.450949	-1.450949	0.001956996	0.006181431
R1	NA	NA	0.2605	0.2395
CHeight	NA	NA	3.017029276	3.038884479

(g) Sample Size of 16 for the Large Specimen #3

Parameters	Fitting			
	Normalized LLSQ	LLSQ	LOPT	NLOPT
R0	-10.9666344	-10.9666344	2.049296958	2.049297837
S	2.125774101	2.125774101	-0.596722008	-0.59461495
m	-3.236085199	-3.236085199	0.002160093	0
X0	15.51872447	15.51872447	0	0
n	2.068068078	2.068068078	0	0
Y0	-9.867749674	-9.867749674	0	0
R1	NA	NA	0.2605	0.2605
CHeight	NA	NA	2.997705689	3.008329737

(h) Sample Size of 16 for the Large Specimen #4

Parameters	Fitting			
	Normalized LLSQ	LLSQ	LOPT	NLOPT
R0	35.4880281	35.4880281	1.532524931	1.5444925
S	-2.145126348	-2.145126348	-0.583837873	-0.588596372
m	2.096032553	2.096032553	0.004424754	0
X0	-45.77407666	-45.77407666	0	0
n	-0.714818333	-0.714818333	0	0.001450883
Y0	14.48751274	14.48751274	0	0.018325889
R1	NA	NA	0.009	0.008550268
CHeight	NA	NA	2.6095	2.6095

(i) Sample Size of 8 for the Small Specimen #1

Parameters	Fitting			
	Normalized LLSQ	LLSQ	LOPT	NLOPT
R0	17.45151683	17.45151683	1.513102184	1.544793826
S	-8.849468053	-8.849468053	-0.580433693	-0.599078673
m	11.13252415	11.13252415	0	0
X0	-21.46276153	-21.46276153	0	0
n	-3.518314851	-3.518314851	0	0.004666867
Y0	6.778307253	6.778307253	0	0.013545825
R1	NA	NA	0	0
CHeight	NA	NA	2.606847605	2.578615958

(j) Sample Size of 8 for the Small Specimen #2

Parameters	Fitting			
	Normalized LLSQ	LLSQ	LOPT	NLOPT
R0	22.46610082	22.46610082	1.517437042	1.547848876
S	-3.468475364	-3.468475364	-0.580146008	-0.598202583
m	3.873516899	3.873516899	0	0
X0	-28.21768192	-28.21768192	0	0
n	-1.249063584	-1.249063584	0	0.002144287
Y0	8.924073037	8.924073037	0	0.018867469
R1	NA	NA	0.003546033	8.99987E-06
CHeight	NA	NA	2.6095	2.587484443

(k) Sample Size of 8 for the Small Specimen #3

Parameters	Fitting			
	Normalized LLSQ	LLSQ	LOPT	NLOPT
R0	15.6703173	15.6703173	1.532068452	1.54701833
S	6.733503868	6.733503868	-0.587411654	-0.596364673
m	-9.892398553	-9.892398553	0	0
X0	-19.04332445	-19.04332445	0	0
n	3.08229038	3.08229038	0	0.000657264
Y0	6.038005888	6.038005888	0	0.016175612
R1	NA	NA	0	0.009
CHeight	NA	NA	2.608168293	2.578989666

(l) Sample Size of 8 for the Small Specimen #4

Parameters	Fitting			
	Normalized LLSQ	LLSQ	LOPT	NLOPT
R0	27.11297396	27.11297396	1.533863713	1.542099723
S	-8.866348999	-8.866348999	-0.584350915	-0.587507079
m	10.38034986	10.38034986	0.009141599	0
X0	-32.0740468	-32.0740468	0	0
n	-5.428631464	-5.428631464	0	0.000753706
Y0	16.71357725	16.71357725	0	0.018017838
R1	NA	NA	0.009	0.009
CHeight	NA	NA	2.6095	2.6095

(m) Sample Size of 16 for the Small Specimen #1

Parameters	Fitting			
	Normalized LLSQ	LLSQ	LOPT	NLOPT
R0	-0.361500213	-0.361500213	1.517692779	1.542429285
S	0.521880815	0.521880815	-0.581622902	-0.598651881
m	-1.397156593	-1.397156593	0	0
X0	2.37612964	2.37612964	0	0
n	0.728336927	0.728336927	0	0.0029746
Y0	-1.238123803	-1.238123803	0	0.01291377
R1	NA	NA	0.009	0
CHeight	NA	NA	2.593936336	2.576504532

(n) Sample Size of 16 for the Small Specimen #2

Parameters	Fitting			
	Normalized LLSQ	LLSQ	LOPT	NLOPT
R0	11.75134712	11.75134712	1.522199729	1.54414302
S	-11.79404579	-11.79404579	-0.588666073	-0.596979188
m	14.05258178	14.05258178	0.022999867	0
X0	-12.81366316	-12.81366316	0	0
n	-7.313439118	-7.313439118	0	0.000297841
Y0	6.673434599	6.673434599	0	0.01816585
R1	NA	NA	0.009	0
CHeight	NA	NA	2.570557059	2.586594391

(o) Sample Size of 16 for the Small Specimen #3

Parameters	Fitting			
	Normalized LLSQ	LLSQ	LOPT	NLOPT
R0	15.24583458	15.24583458	1.533848037	1.540550938
S	-5.02816995	-5.02816995	-0.587447416	-0.592160391
m	5.558945565	5.558945565	0	0
X0	-17.18695523	-17.18695523	0	0
n	-2.909983331	-2.909983331	0	0
Y0	8.959272391	8.959272391	0	0.015674227
R1	NA	NA	0.009	0
CHeight	NA	NA	2.595718352	2.601577143

(p) Sample Size of 16 for the Small Specimen #4

APPENDIX D

EXAMPLES OF VALID PARAMETERS OBTAINED BY USING ALIGNED SYSTEMATIC SAMPLING

Parameters	Fitting			
	Normalized LLSQ	LLSQ	LOPT	NLOPT
R0	1.539578361	1.539578361	1.535398586	1.543165855
S	-0.585570454	-0.585570454	-0.584939102	-0.587915637
m	-0.000209097	-0.000209097	0.005473048	0
X0	9.10566E-05	9.10566E-05	0	0
n	2.76861E-05	2.76861E-05	0	0.001669468
Y0	-3.34042E-05	-3.34042E-05	0	0.018542943
R1	NA	NA	0.009	0.009
CHeight	NA	NA	2.6095	2.6095

(a) Sample Size of 64 for the Small Specimen #1

Parameters	Fitting			
	Normalized LLSQ	LLSQ	LOPT	NLOPT
R0	1.539668486	1.539668486	1.542546578	1.543257919
S	-0.591562113	-0.591562113	-0.59460321	-0.594302499
m	-0.000485332	-0.000485332	0.003263665	0
X0	0.000255125	0.000255125	0	0
n	5.62453E-05	5.62453E-05	0	0.001680285
Y0	-8.12073E-05	-8.12073E-05	0	0.016955321
R1	NA	NA	0.009	0.009
CHeight	NA	NA	2.579109146	2.581611086

(b) Sample Size of 64 for the Small Specimen #4

Parameters	Fitting			
	Normalized LLSQ	LLSQ	LOPT	NLOPT
R0	1.533193445	1.533193445	1.512131673	1.547746765
S	-0.592254834	-0.592254834	-0.581439022	-0.599573205
m	-0.000272284	-0.000272284	0	0
X0	0.000150143	0.000150143	0	0
n	-0.00015454	-0.00015454	0	0.005664825
Y0	-2.94028E-05	-2.94028E-05	2.61056E-05	0.014954934
R1	NA	NA	0.009	0
CHeight	NA	NA	2.585192281	2.581414167

(c) Sample Size of 256 for the Small Specimen #2

Parameters	Fitting			
	Normalized LLSQ	LLSQ	LOPT	NLOPT
R0	1.534248938	1.534248938	1.518401608	1.5495
S	-0.58993831	-0.58993831	-0.581714885	-0.597674631
m	-0.000241566	-0.000241566	0	0
X0	-0.00012315	-0.00012315	0	0
n	-0.000287056	-0.000287056	0	0.00416287
Y0	8.76916E-05	8.76916E-05	0	0.019490935
R1	NA	NA	0.009	0
CHeight	NA	NA	2.59474469	2.592547715

(d) Sample Size of 256 for the Small Specimen #3

Parameters	Fitting			
	Normalized LLSQ	LLSQ	LOPT	NLOPT
R0	2.045792044	2.045792044	2.033868924	2.0495
S	-0.589641088	-0.589641088	-0.583922798	-0.591259013
m	-3.44319E-05	-3.44319E-05	0	0
X0	0.000102692	0.000102692	0	0
n	-2.17751E-05	-2.17751E-05	0	0.002009778
Y0	-5.89836E-05	-5.89836E-05	0.000192318	0.00625921
R1	NA	NA	0.2605	0.2605
CHeight	NA	NA	3.0369921	3.02574669

(e) Sample Size of 64 for the Large Specimen #2

Parameters	Fitting			
	Normalized LLSQ	LLSQ	LOPT	NLOPT
R0	2.038883454	2.038883454	2.030468722	2.043476978
S	-0.591661667	-0.591661667	-0.587453563	-0.593436578
m	0.000148748	0.000148748	0	0
X0	-2.03122E-05	-2.03122E-05	0	0
n	-0.00016169	-0.00016169	0	0.002444509
Y0	5.63763E-05	5.63763E-05	0	0.006050247
R1	NA	NA	0.2605	0.2395
CHeight	NA	NA	3.012950868	3.039881676

(f) Sample Size of 64 for the Large Specimen #3

Parameters	Fitting			
	Normalized LLSQ	LLSQ	LOPT	NLOPT
R0	2.031650286	2.031650286	2.003714574	2.0495
S	-0.588893587	-0.588893587	-0.57787766	-0.595033014
m	0.000319584	0.000319584	0	0
X0	-0.000171312	-0.000171312	0	0
n	-7.93956E-05	-7.93956E-05	0	0
Y0	3.79135E-05	3.79135E-05	0	0.005899964
R1	NA	NA	0.2605	0.2395
CHeight	NA	NA	3.016580662	3.041848028

(g) Sample Size of 256 for the Large Specimen #1

APPENDIX E

STATISTICAL RESULTS AFTER INVALID DATA REMOVAL

The GLM Procedure

Class Level Information

Class	Levels	Values
SArea	2	1 2
Specimen	4	1 2 3 4
SStrategy	3	1 2 3
SSize	4	1 2 3 4
Fitting	4	1 2 3 4

Number of observations 384

NOTE: Due to missing values, only 352 observations can be used in this analysis.

The GLM Procedure

Dependent Variable: Conicity Conicity

Source	DF	Sum of Squares	Mean Square	F Value	Pr > F
Model	93	0.08362052	0.00089915	54.03	<.0001
Error	258	0.00429387	0.00001664		
Corrected Total	351	0.08791439			

R-Square	Coeff Var	Root MSE	Conicity Mean
0.951159	12.32680	0.004080	0.033095

Source	DF	Type I SS	Mean Square	F Value	Pr > F
SArea	1	0.00200283	0.00200283	120.34	<.0001
Specimen(SArea)	6	0.01765927	0.00294321	176.84	<.0001
SStrategy	2	0.00209783	0.00104891	63.02	<.0001
SSize	3	0.01928198	0.00642733	386.19	<.0001
Fitting	3	0.02665436	0.00888479	533.85	<.0001
SArea*SStrategy	2	0.00039629	0.00019814	11.91	<.0001
SArea*SSize	3	0.00136358	0.00045453	27.31	<.0001
SArea*Fitting	3	0.00634926	0.00211642	127.17	<.0001
SStrategy*SSize	6	0.00394041	0.00065673	39.46	<.0001
SStrategy*Fitting	6	0.00017553	0.00002925	1.76	0.1082
SSize*Fitting	9	0.00153676	0.00017075	10.26	<.0001
SArea*SStrateg*SSize	6	0.00050323	0.00008387	5.04	<.0001
SArea*SStrat*Fitting	6	0.00044395	0.00007399	4.45	0.0003
SArea*SSize*Fitting	9	0.00046352	0.00005150	3.09	0.0015
SStrat*SSize*Fitting	14	0.00047067	0.00003362	2.02	0.0168
SAre*SStr*SSiz*Fitti	14	0.00028105	0.00002008	1.21	0.2706

Source	DF	Type III SS	Mean Square	F Value	Pr > F
SArea	1	0.00173352	0.00173352	104.16	<.0001
Specimen(SArea)	6	0.01765927	0.00294321	176.84	<.0001
SStrategy	2	0.00113215	0.00056608	34.01	<.0001
SSize	3	0.01501400	0.00500467	300.71	<.0001
Fitting	3	0.02687719	0.00895906	538.31	<.0001
SArea*SStrategy	2	0.00025886	0.00012943	7.78	0.0005
SArea*SSize	3	0.00133198	0.00044399	26.68	<.0001
SArea*Fitting	3	0.00596522	0.00198841	119.47	<.0001
SStrategy*SSize	6	0.00186130	0.00031022	18.64	<.0001
SStrategy*Fitting	6	0.00011618	0.00001936	1.16	0.3263

The GLM Procedure

Dependent Variable: Conicity Conicity

Source	DF	Type III SS	Mean Square	F Value	Pr > F
SSize*Fitting	9	0.00153676	0.00017075	10.26	<.0001
SArea*SStrateg*SSize	6	0.00051230	0.00008538	5.13	<.0001
SArea*SStrat*Fitting	6	0.00043715	0.00007286	4.38	0.0003
SArea*SSize*Fitting	9	0.00046352	0.00005150	3.09	0.0015
SStrat*SSize*Fitting	14	0.00047067	0.00003362	2.02	0.0168
SAre*SStr*SSiz*Fitti	14	0.00028105	0.00002008	1.21	0.2706

Tests of Hypotheses Using the Type III MS for Specimen(SArea) as an Error Term

Source	DF	Type III SS	Mean Square	F Value	Pr > F
SArea	1	0.00173352	0.00173352	0.59	0.4719

The GLM Procedure

Level of Specimen	Level of SArea	N	Conicity Mean	Conicity Std Dev
1	1	44	0.03062898	0.01680647
2	1	44	0.03992479	0.01820922
3	1	44	0.04416496	0.01854395
4	1	44	0.02720322	0.01304866
1	2	44	0.04213174	0.01324785
2	2	44	0.03166733	0.01128597
3	2	44	0.02626963	0.01007631
4	2	44	0.02277051	0.00739415

The GLM Procedure

Level of SStrategy	N	Conicity Mean	Conicity Std Dev
1	128	0.03271621	0.01604647
2	128	0.03067970	0.01549075
3	96	0.03682097	0.01543751

The GLM Procedure

Level of SSize	N	Conicity Mean	Conicity Std Dev
1	80	0.02199632	0.01309501
2	80	0.02894353	0.01389175
3	96	0.03658882	0.01387817
4	96	0.04231016	0.01460619

The GLM Procedure

Level of Fitting	N	Conicity Mean	Conicity Std Dev
1	80	0.03363594	0.01337544
2	96	0.04133675	0.01283010
3	96	0.01937876	0.01109539
4	80	0.03912408	0.01548150

The GLM Procedure

Level of SArea	Level of SStrategy	N	Conicity Mean	Conicity Std Dev
1	1	64	0.03593904	0.01919333
1	2	64	0.03351087	0.01675589
1	3	48	0.03749523	0.01809950
2	1	64	0.02949339	0.01138326
2	2	64	0.02784854	0.01366348
2	3	48	0.03614671	0.01237672

The GLM Procedure

Level of SArea	Level of SSize	N	Conicity Mean	Conicity Std Dev
1	1	40	0.02158153	0.01343939
1	2	40	0.03230833	0.01653495
1	3	48	0.04094968	0.01617593
1	4	48	0.04373722	0.01728642
2	1	40	0.02241112	0.01289904
2	2	40	0.02497873	0.00923363
2	3	48	0.03222796	0.00942344
2	4	48	0.04088311	0.01132434

The GLM Procedure

Level of SArea	Level of Fitting	N	Conicity Mean	Conicity Std Dev
1	1	40	0.03826196	0.01350139
1	2	48	0.04647912	0.01164448
1	3	48	0.01466424	0.00871981
1	4	40	0.04448015	0.01563914
2	1	40	0.02900993	0.01167078
2	2	48	0.03619438	0.01196319
2	3	48	0.02409328	0.01128718
2	4	40	0.03376801	0.01349335

The GLM Procedure

Level of SStrategy	Level of SSize	N	Conicity Mean	Conicity Std Dev
1	1	32	0.02127191	0.00864113
1	2	32	0.02976393	0.01495395
1	3	32	0.03736493	0.01539084
1	4	32	0.04246408	0.01597245
2	1	32	0.01625625	0.00929386
2	2	32	0.02805866	0.01244177
2	3	32	0.03658305	0.01307515
2	4	32	0.04182087	0.01360151
3	1	16	0.03492530	0.01790490
3	2	16	0.02907247	0.01520450
3	3	32	0.03581849	0.01345976
3	4	32	0.04264554	0.01460404

The GLM Procedure

Level of SSize	Level of Fitting	N	Conicity Mean	Conicity Std Dev
1	1	16	0.01618502	0.00625997
1	2	24	0.03526255	0.01281236
1	3	24	0.01449375	0.00946063
1	4	16	0.01916216	0.00766489
2	1	16	0.03094143	0.00980239
2	2	24	0.03732982	0.01056615
2	3	24	0.01460572	0.00892517
2	4	16	0.03587289	0.01140306
3	1	24	0.03765155	0.01009821
3	2	24	0.04303552	0.01174471
3	3	24	0.02192731	0.00976344
3	4	24	0.04374090	0.01175041
4	1	24	0.04305063	0.00990339
4	2	24	0.04371911	0.01160149
4	3	24	0.02648826	0.01165367
4	4	24	0.04398267	0.01149850

The GLM Procedure

Level of SArea	Level of SStrategy	Level of SSize	N	Conicity Mean	Conicity Std Dev
1	1	1	16	0.01979671	0.00851224
1	1	2	16	0.03588981	0.01811294
1	1	3	16	0.04229287	0.01838598
1	1	4	16	0.04577677	0.01960578
1	2	1	16	0.01866532	0.01149919
1	2	2	16	0.03214563	0.01375553
1	2	3	16	0.04051368	0.01509086
1	2	4	16	0.04271827	0.01581841
1	3	1	8	0.03098240	0.02097526
1	3	2	8	0.02847076	0.01925137
1	3	3	16	0.04004248	0.01584573
1	3	4	16	0.04271663	0.01717671
2	1	1	16	0.02274712	0.00878723
2	1	2	16	0.02363804	0.00734547
2	1	3	16	0.03243699	0.00998483
2	1	4	16	0.03915140	0.01092926
2	2	1	16	0.01384658	0.00582166
2	2	2	16	0.02397168	0.00975022
2	2	3	16	0.03265241	0.00962405
2	2	4	16	0.04092347	0.01141909
2	3	1	8	0.03886820	0.01454208
2	3	2	8	0.02967418	0.01113267
2	3	3	16	0.03159449	0.00923351
2	3	4	16	0.04257445	0.01207164

The GLM Procedure

Level of SArea	Level of SStrategy	Level of Fitting	N	Conicity Mean	Conicity Std Dev
1	1	1	16	0.03926026	0.01411910
1	1	2	16	0.04578532	0.01505185
1	1	3	16	0.01287409	0.00850513
1	1	4	16	0.04583649	0.01618149
1	2	1	16	0.03427229	0.01424202
1	2	2	16	0.04442516	0.00990266
1	2	3	16	0.01566737	0.00974974
1	2	4	16	0.03967867	0.01659396
1	3	1	8	0.04424469	0.00861459
1	3	2	16	0.04922687	0.00933667
1	3	3	16	0.01545128	0.00810532
1	3	4	8	0.05137040	0.01001870
2	1	1	16	0.02756055	0.01040286
2	1	2	16	0.03394859	0.01064193
2	1	3	16	0.02428477	0.01081373
2	1	4	16	0.03217964	0.01200125
2	2	1	16	0.02708651	0.01289822
2	2	2	16	0.03337120	0.01211062
2	2	3	16	0.01945311	0.01120564
2	2	4	16	0.03148332	0.01493572
2	3	1	8	0.03575553	0.01025734
2	3	2	16	0.04126334	0.01213377
2	3	3	16	0.02854195	0.01060987
2	3	4	8	0.04151415	0.01189392

The GLM Procedure

Level of SArea	Level of SSize	Level of Fitting	N	Conicity Mean	Conicity Std Dev
1	1	1	8	0.01696077	0.00554463
1	1	2	12	0.03737776	0.01122752
1	1	3	12	0.00993915	0.00529672
1	1	4	8	0.01997151	0.00677487
1	2	1	8	0.03839116	0.00573793
1	2	2	12	0.04456340	0.00686647
1	2	3	12	0.00986882	0.00498741
1	2	4	8	0.04450214	0.00680672
1	3	1	12	0.04408598	0.00816379
1	3	2	12	0.05020874	0.01013761
1	3	3	12	0.01826864	0.00877925
1	3	4	12	0.05123536	0.00952094
1	4	1	12	0.04655260	0.00985585
1	4	2	12	0.05376658	0.01165766
1	4	3	12	0.02058035	0.00964752
1	4	4	12	0.05404937	0.01145807
2	1	1	8	0.01540926	0.00720098
2	1	2	12	0.03314734	0.01440199
2	1	3	12	0.01904835	0.01066902
2	1	4	8	0.01835281	0.00885991
2	2	1	8	0.02349171	0.00679139
2	2	2	12	0.03009623	0.00849265
2	2	3	12	0.01934263	0.00962958
2	2	4	8	0.02724364	0.00788039
2	3	1	12	0.03121712	0.00749929
2	3	2	12	0.03586231	0.00856620
2	3	3	12	0.02558597	0.00964546
2	3	4	12	0.03624645	0.00868921
2	4	1	12	0.03954866	0.00900974
2	4	2	12	0.04567164	0.01047765
2	4	3	12	0.03239616	0.01071144
2	4	4	12	0.04591597	0.01044415

The GLM Procedure

Level of SStrategy	Level of SSize	Level of Fitting	N	Conicity Mean	Conicity Std Dev
1	1	1	8	0.02029617	0.00499413
1	1	2	8	0.02871200	0.00651454
1	1	3	8	0.01174475	0.00683436
1	1	4	8	0.02433473	0.00614682
1	2	1	8	0.03124578	0.01220271
1	2	2	8	0.03727076	0.01283335
1	2	3	8	0.01421808	0.00895462
1	2	4	8	0.03632110	0.01429282
1	3	1	8	0.03881974	0.01209154
1	3	2	8	0.04365059	0.01412399
1	3	3	8	0.02186016	0.01065147
1	3	4	8	0.04512925	0.01409523
1	4	1	8	0.04327993	0.01219793
1	4	2	8	0.04983449	0.01420735
1	4	3	8	0.02649472	0.01245055
1	4	4	8	0.05024719	0.01416448
2	1	1	8	0.01207386	0.00451652
2	1	2	8	0.02858806	0.00886342
2	1	3	8	0.01037349	0.00417081
2	1	4	8	0.01398958	0.00519183
2	2	1	8	0.03063709	0.00753541
2	2	2	8	0.03487727	0.00897923
2	2	3	8	0.01129558	0.00550869
2	2	4	8	0.03542469	0.00859602
2	3	1	8	0.03740029	0.00939267
2	3	2	8	0.04293134	0.01095497
2	3	3	8	0.02255891	0.01021415
2	3	4	8	0.04344166	0.01091736
2	4	1	8	0.04260637	0.00865630
2	4	2	8	0.04913607	0.01025286
2	4	3	8	0.02601298	0.01108974
2	4	4	8	0.04946806	0.01004814
3	1	2	8	0.04848759	0.01088723
3	1	3	8	0.02136301	0.01216605
3	2	2	8	0.03984143	0.01036435
3	2	3	8	0.01830351	0.01108530
3	3	1	8	0.03673463	0.00990136
3	3	2	8	0.04252464	0.01153188
3	3	3	8	0.02136286	0.00972637
3	3	4	8	0.04265181	0.01149525
3	4	1	8	0.04326559	0.00990930
3	4	2	8	0.05012676	0.01160824
3	4	3	8	0.02695707	0.01295062
3	4	4	8	0.05023275	0.01150524

The GLM Procedure

Duncan's Multiple Range Test for Conicity

NOTE: This test controls the Type I comparisonwise error rate, not the experimentwise error rate.

Alpha	0.05
Error Degrees of Freedom	258
Error Mean Square	0.000017

Number of Means	2
Critical Range	.0008564

Means with the same letter are not significantly different.

Duncan Grouping	Mean	N	SArea
A	0.0354805	176	1
B	0.0307098	176	2

The GLM Procedure

Tukey's Studentized Range (HSD) Test for Conicity

NOTE: This test controls the Type I experimentwise error rate, but it generally has a higher Type II error rate than REGWQ.

Alpha	0.05
Error Degrees of Freedom	258
Error Mean Square	0.000017
Critical Value of Studentized Range	2.78487
Minimum Significant Difference	0.0009

Means with the same letter are not significantly different.

Tukey Grouping	Mean	N	SArea
A	0.0354805	176	1
B	0.0307098	176	2

The GLM Procedure

Level of Specimen	Level of SArea	N	Conicity Mean	Conicity Std Dev
1	1	44	0.03062898	0.01680647
2	1	44	0.03992479	0.01820922
3	1	44	0.04416496	0.01854395
4	1	44	0.02720322	0.01304866
1	2	44	0.04213174	0.01324785
2	2	44	0.03166733	0.01128597
3	2	44	0.02626963	0.01007631
4	2	44	0.02277051	0.00739415

The GLM Procedure

Duncan's Multiple Range Test for Conicity

NOTE: This test controls the Type I comparisonwise error rate, not the experimentwise error rate.

Alpha	0.05
Error Degrees of Freedom	258
Error Mean Square	0.000017
Harmonic Mean of Cell Sizes	115.2

NOTE: Cell sizes are not equal.

Number of Means	2	3
Critical Range	.001059	.001114

Means with the same letter are not significantly different.

Duncan Grouping	Mean	N	SStrategy
A	0.0368210	96	3
B	0.0327162	128	1
C	0.0306797	128	2

The GLM Procedure

Tukey's Studentized Range (HSD) Test for Conicity

NOTE: This test controls the Type I experimentwise error rate, but it generally has a higher Type II error rate than REGWQ.

Alpha	0.05
Error Degrees of Freedom	258
Error Mean Square	0.000017
Critical Value of Studentized Range	3.33385
Minimum Significant Difference	0.0013
Harmonic Mean of Cell Sizes	115.2

NOTE: Cell sizes are not equal.

Means with the same letter are not significantly different.

Tukey Grouping	Mean	N	SStrategy
A	0.0368210	96	3
B	0.0327162	128	1
C	0.0306797	128	2

The GLM Procedure

Duncan's Multiple Range Test for Conicity

NOTE: This test controls the Type I comparisonwise error rate, not the experimentwise error rate.

Alpha	0.05
Error Degrees of Freedom	258
Error Mean Square	0.000017
Harmonic Mean of Cell Sizes	87.27273

NOTE: Cell sizes are not equal.

Number of Means	2	3	4
Critical Range	.001216	.001280	.001323

Means with the same letter are not significantly different.

Duncan Grouping	Mean	N	SSize
A	0.0423102	96	4
B	0.0365888	96	3
C	0.0289435	80	2
D	0.0219963	80	1

The GLM Procedure

Tukey's Studentized Range (HSD) Test for Conicity

NOTE: This test controls the Type I experimentwise error rate, but it generally has a higher Type II error rate than REGWQ.

Alpha	0.05
Error Degrees of Freedom	258
Error Mean Square	0.000017
Critical Value of Studentized Range	3.65698
Minimum Significant Difference	0.0016
Harmonic Mean of Cell Sizes	87.27273

NOTE: Cell sizes are not equal.

Means with the same letter are not significantly different.

Tukey Grouping	Mean	N	SSize
A	0.0423102	96	4
B	0.0365888	96	3
C	0.0289435	80	2
D	0.0219963	80	1

The GLM Procedure

Duncan's Multiple Range Test for Conicity

NOTE: This test controls the Type I comparisonwise error rate, not the experimentwise error rate.

Alpha	0.05
Error Degrees of Freedom	258
Error Mean Square	0.000017
Harmonic Mean of Cell Sizes	87.27273

NOTE: Cell sizes are not equal.

Number of Means	2	3	4
Critical Range	.001216	.001280	.001323

Means with the same letter are not significantly different.

Duncan Grouping	Mean	N	Fitting
A	0.0413367	96	2
B	0.0391241	80	4
C	0.0336359	80	1
D	0.0193788	96	3

The GLM Procedure

Tukey's Studentized Range (HSD) Test for Conicity

NOTE: This test controls the Type I experimentwise error rate, but it generally has a higher Type II error rate than REGWQ.

Alpha	0.05
Error Degrees of Freedom	258
Error Mean Square	0.000017
Critical Value of Studentized Range	3.65698
Minimum Significant Difference	0.0016
Harmonic Mean of Cell Sizes	87.27273

NOTE: Cell sizes are not equal.

Means with the same letter are not significantly different.

Tukey Grouping	Mean	N	Fitting
A	0.0413367	96	2
B	0.0391241	80	4
C	0.0336359	80	1
D	0.0193788	96	3

Obs	SArea	Specimen	SStrategy	SSize	Fitting	Conicity	Sequence	pred	resid
1	1	1	1	1	1	0.023623	9	0.015413	0.008209122
2	1	1	1	1	2	0.031415	10	0.022541	0.008874530
3	1	1	1	1	3	0.004009	11	0.002434	0.001575075
4	1	1	1	1	4	0.028127	12	0.019392	0.008734532
5	1	1	1	2	1	0.038185	17	0.036152	0.002033496
6	1	1	1	2	2	0.043965	18	0.042263	0.001701340
7	1	1	1	2	3	0.004257	19	0.002797	0.001460070
8	1	1	1	2	4	0.044436	20	0.042941	0.001494407
9	1	1	1	3	1	0.041221	5	0.041691	-.000470724
10	1	1	1	3	2	0.043007	6	0.047007	-.003999296
11	1	1	1	3	3	0.008628	7	0.011767	-.003138653
12	1	1	1	3	4	0.047860	8	0.049301	-.001441344
13	1	1	1	4	1	0.042143	13	0.044379	-.002236206
14	1	1	1	4	2	0.048654	14	0.051925	-.003270659
15	1	1	1	4	3	0.009788	15	0.015092	-.005304374
16	1	1	1	4	4	0.048837	16	0.052306	-.003468989
17	1	1	2	1	1	0.008281	45	0.008805	-.000524076
18	1	1	2	1	2	0.034711	46	0.030782	0.003928563
19	1	1	2	1	3	0.004336	47	0.004823	-.000486238
20	1	1	2	1	4	0.009408	48	0.010848	-.001439555
21	1	1	2	2	1	0.035876	37	0.030928	0.004948210
22	1	1	2	2	2	0.040952	38	0.036221	0.004731227
23	1	1	2	2	3	0.005155	39	0.005668	-.000512496
24	1	1	2	2	4	0.041231	40	0.036360	0.004870822
25	1	1	2	3	1	0.039119	1	0.037907	0.001211701
26	1	1	2	3	2	0.045099	2	0.044280	0.000818554
27	1	1	2	3	3	0.008586	3	0.015633	-.007046795
28	1	1	2	3	4	0.045359	4	0.044828	0.000530299
29	1	1	2	4	1	0.040598	25	0.040043	0.000554995
30	1	1	2	4	2	0.047064	26	0.047012	0.000052655
31	1	1	2	4	3	0.010482	27	0.017140	-.006657903
32	1	1	2	4	4	0.047047	28	0.047272	-.000225329
33	1	1	3	1	1	.	21	.	.
34	1	1	3	1	2	0.042649	22	0.044256	-.001606780
35	1	1	3	1	3	0.005793	23	0.008006	-.002213235
36	1	1	3	1	4	.	24	.	.
37	1	1	3	2	1	.	33	.	.
38	1	1	3	2	2	0.042155	34	0.040651	0.001503712
39	1	1	3	2	3	0.006212	35	0.006587	-.000375455
40	1	1	3	2	4	.	36	.	.
41	1	1	3	3	1	0.038923	41	0.038105	0.000818694
42	1	1	3	3	2	0.045103	42	0.044785	0.000318156
43	1	1	3	3	3	0.008964	43	0.012852	-.003887271
44	1	1	3	3	4	0.045106	44	0.045022	0.000083277
45	1	1	3	4	1	0.039535	29	0.040682	-.001146887
46	1	1	3	4	2	0.045821	30	0.047809	-.001988488
47	1	1	3	4	3	0.010142	31	0.014954	-.004812311
48	1	1	3	4	4	0.045815	32	0.048015	-.002200373
49	1	2	1	1	1	0.016261	57	0.024709	-.008448725

Obs	SArea	Specimen	SStrategy	SSize	Fitting	Conicity	Sequence	pred	resid
50	1	2	1	1	2	0.023118	58	0.031837	-.008718385
51	1	2	1	1	3	0.008922	59	0.011730	-.002808579
52	1	2	1	1	4	0.019461	60	0.028688	-.009226525
53	1	2	1	2	1	0.045059	65	0.045447	-.000388550
54	1	2	1	2	2	0.051498	66	0.051559	-.000060581
55	1	2	1	2	3	0.010199	67	0.012093	-.001894421
56	1	2	1	2	4	0.052563	68	0.052237	0.000326082
57	1	2	1	3	1	0.052871	53	0.050987	0.001883471
58	1	2	1	3	2	0.060955	54	0.056302	0.004652256
59	1	2	1	3	3	0.022453	55	0.021063	0.001390242
60	1	2	1	3	4	0.061588	56	0.058597	0.002991395
61	1	2	1	4	1	0.057421	61	0.053675	0.003745997
62	1	2	1	4	2	0.066828	62	0.061220	0.005607728
63	1	2	1	4	3	0.026616	63	0.024388	0.002227751
64	1	2	1	4	4	0.066730	64	0.061601	0.005128555
65	1	2	2	1	1	0.015404	93	0.018101	-.002696905
66	1	2	2	1	2	0.034640	94	0.040078	-.005438110
67	1	2	2	1	3	0.012667	95	0.014118	-.001451568
68	1	2	2	1	4	0.017912	96	0.020144	-.002231412
69	1	2	2	2	1	0.035877	85	0.040224	-.004346935
70	1	2	2	2	2	0.041852	86	0.045517	-.003665237
71	1	2	2	2	3	0.014620	87	0.014963	-.000343841
72	1	2	2	2	4	0.041385	88	0.045656	-.004270554
73	1	2	2	3	1	0.047461	49	0.047203	0.000257900
74	1	2	2	3	2	0.054669	50	0.053576	0.001093113
75	1	2	2	3	3	0.027148	51	0.024929	0.002218735
76	1	2	2	3	4	0.055200	52	0.054124	0.001075571
77	1	2	2	4	1	0.050358	73	0.049339	0.001018817
78	1	2	2	4	2	0.058554	74	0.056307	0.002246798
79	1	2	2	4	3	0.028946	75	0.026436	0.002509795
80	1	2	2	4	4	0.058527	76	0.056568	0.001958223
81	1	2	3	1	1	.	69	.	.
82	1	2	3	1	2	0.054973	70	0.053552	0.001421252
83	1	2	3	1	3	0.017599	71	0.017302	0.000297338
84	1	2	3	1	4	.	72	.	.
85	1	2	3	2	1	.	81	.	.
86	1	2	3	2	2	0.048105	82	0.049947	-.001842236
87	1	2	3	2	3	0.015444	83	0.015883	-.000439263
88	1	2	3	2	4	.	84	.	.
89	1	2	3	3	1	0.047833	89	0.047400	0.000432977
90	1	2	3	3	2	0.055576	90	0.054081	0.001495097
91	1	2	3	3	3	0.023581	91	0.022148	0.001433792
92	1	2	3	3	4	0.055593	92	0.054318	0.001274915
93	1	2	3	4	1	0.052259	77	0.049978	0.002281130
94	1	2	3	4	2	0.060725	78	0.057105	0.003620029
95	1	2	3	4	3	0.026508	79	0.024250	0.002257529
96	1	2	3	4	4	0.060736	80	0.057311	0.003425123
97	1	3	1	1	1	0.022339	105	0.028949	-.006610160
98	1	3	1	1	2	0.029569	106	0.036077	-.006507792

Obs	SArea	Specimen	SStrategy	SSize	Fitting	Conicity	Sequence	pred	resid
99	1	3	1	1	3	0.010386	107	0.015970	-.005583868
100	1	3	1	1	4	0.026926	108	0.032928	-.006002071
101	1	3	1	2	1	0.047898	113	0.049688	-.001789627
102	1	3	1	2	2	0.055477	114	0.055799	-.000322637
103	1	3	1	2	3	0.011205	115	0.016333	-.005128451
104	1	3	1	2	4	0.055844	116	0.056477	-.000633373
105	1	3	1	3	1	0.056564	101	0.055227	0.001336440
106	1	3	1	3	2	0.065414	102	0.060543	0.004871909
107	1	3	1	3	3	0.025163	103	0.025303	-.000139554
108	1	3	1	3	4	0.065831	104	0.062837	0.002993665
109	1	3	1	4	1	0.061814	109	0.057915	0.003898975
110	1	3	1	4	2	0.071127	110	0.065461	0.005666484
111	1	3	1	4	3	0.030805	111	0.028628	0.002176522
112	1	3	1	4	4	0.071763	112	0.065842	0.005920892
113	1	3	2	1	1	0.020747	141	0.022341	-.001594040
114	1	3	2	1	2	0.042546	142	0.044318	-.001771625
115	1	3	2	1	3	0.015143	143	0.018359	-.003215686
116	1	3	2	1	4	0.023828	144	0.024384	-.000555576
117	1	3	2	2	1	0.040029	133	0.044464	-.004434955
118	1	3	2	2	2	0.046967	134	0.049757	-.002790474
119	1	3	2	2	3	0.016409	135	0.019204	-.002794716
120	1	3	2	2	4	0.046076	136	0.049896	-.003819887
121	1	3	2	3	1	0.051575	97	0.051443	0.000131993
122	1	3	2	3	2	0.059460	98	0.057816	0.001644050
123	1	3	2	3	3	0.032281	99	0.029169	0.003112069
124	1	3	2	3	4	0.059936	100	0.058364	0.001571961
125	1	3	2	4	1	0.054369	121	0.053579	0.000789777
126	1	3	2	4	2	0.062976	122	0.060547	0.002428074
127	1	3	2	4	3	0.033892	123	0.030676	0.003215924
128	1	3	2	4	4	0.063121	124	0.060808	0.002312478
129	1	3	3	1	1	.	117	.	.
130	1	3	3	1	2	0.060163	118	0.057792	0.002371441
131	1	3	3	1	3	0.019882	119	0.021542	-.001660522
132	1	3	3	1	4	.	120	.	.
133	1	3	3	2	1	.	129	.	.
134	1	3	3	2	2	0.054612	130	0.054187	0.000424280
135	1	3	3	2	3	0.017460	131	0.020123	-.002662871
136	1	3	3	2	4	.	132	.	.
137	1	3	3	3	1	0.051348	137	0.051641	-.000292738
138	1	3	3	3	2	0.059607	138	0.058321	0.001286091
139	1	3	3	3	3	0.026915	139	0.026388	0.000527406
140	1	3	3	3	4	0.059619	140	0.058558	0.001060145
141	1	3	3	4	1	0.055869	125	0.054218	0.001651006
142	1	3	3	4	2	0.064860	126	0.061345	0.003515227
143	1	3	3	4	3	0.030579	127	0.028490	0.002089058
144	1	3	3	4	4	0.064866	128	0.061551	0.003314711
145	1	4	1	1	1	0.018837	153	0.011988	0.006849763
146	1	4	1	1	2	0.025467	154	0.019115	0.006351647
147	1	4	1	1	3	0.005826	155	-0.000991	0.006817372

Obs	SArea	Specimen	SStrategy	SSize	Fitting	Conicity	Sequence	pred	resid
148	1	4	1	1	4	0.022460	156	0.015966	0.006494064
149	1	4	1	2	1	0.032870	161	0.032726	0.000144682
150	1	4	1	2	2	0.037519	162	0.038837	-.001318122
151	1	4	1	2	3	0.004934	163	-0.000629	0.005562803
152	1	4	1	2	4	0.038328	164	0.039515	-.001187116
153	1	4	1	3	1	0.035516	149	0.038266	-.002749187
154	1	4	1	3	2	0.038056	150	0.043581	-.005524869
155	1	4	1	3	3	0.010229	151	0.008341	0.001887965
156	1	4	1	3	4	0.041331	152	0.045875	-.004543717
157	1	4	1	4	1	0.035544	157	0.040953	-.005408766
158	1	4	1	4	2	0.040495	158	0.048499	-.008003553
159	1	4	1	4	3	0.012566	159	0.011666	0.000900101
160	1	4	1	4	4	0.041299	160	0.048880	-.007580458
161	1	4	2	1	1	0.010194	189	0.005379	0.004815022
162	1	4	2	1	2	0.030637	190	0.027356	0.003281172
163	1	4	2	1	3	0.006550	191	0.001397	0.005153492
164	1	4	2	1	4	0.011649	192	0.007422	0.004226543
165	1	4	2	2	1	0.031336	181	0.027502	0.003833680
166	1	4	2	2	2	0.034520	182	0.032795	0.001724484
167	1	4	2	2	3	0.005893	183	0.002242	0.003651053
168	1	4	2	2	4	0.036154	184	0.032934	0.003219619
169	1	4	2	3	1	0.032880	145	0.034482	-.001601594
170	1	4	2	3	2	0.037299	146	0.040854	-.003555717
171	1	4	2	3	3	0.013923	147	0.012207	0.001715991
172	1	4	2	3	4	0.038225	148	0.041402	-.003177831
173	1	4	2	4	1	0.034253	169	0.036617	-.002363689
174	1	4	2	4	2	0.038858	170	0.043586	-.004727527
175	1	4	2	4	3	0.014647	171	0.013714	0.000932185
176	1	4	2	4	4	0.039801	172	0.043847	-.004045372
177	1	4	3	1	1	.	165	.	.
178	1	4	3	1	2	0.038644	166	0.040830	-.002185912
179	1	4	3	1	3	0.008157	167	0.004580	0.003576359
180	1	4	3	1	4	.	168	.	.
181	1	4	3	2	1	.	177	.	.
182	1	4	3	2	2	0.037140	178	0.037226	-.000085756
183	1	4	3	2	3	0.006639	179	0.003161	0.003477589
184	1	4	3	2	4	.	180	.	.
185	1	4	3	3	1	0.033720	185	0.034679	-.000958933
186	1	4	3	3	2	0.038260	186	0.041359	-.003099344
187	1	4	3	3	3	0.011352	187	0.009426	0.001926073
188	1	4	3	3	4	0.039178	188	0.041597	-.002418337
189	1	4	3	4	1	0.034471	173	0.037256	-.002785310
190	1	4	3	4	2	0.039237	174	0.044383	-.005146769
191	1	4	3	4	3	0.011994	175	0.011528	0.000465684
192	1	4	3	4	4	0.040050	176	0.044590	-.004539462
193	2	1	1	1	1	0.029494	201	0.031749	-.002255637
194	2	1	1	1	2	0.042457	202	0.041453	0.001003199
195	2	1	1	1	3	0.026172	203	0.027626	-.001453764
196	2	1	1	1	4	0.035915	204	0.035848	0.000067006

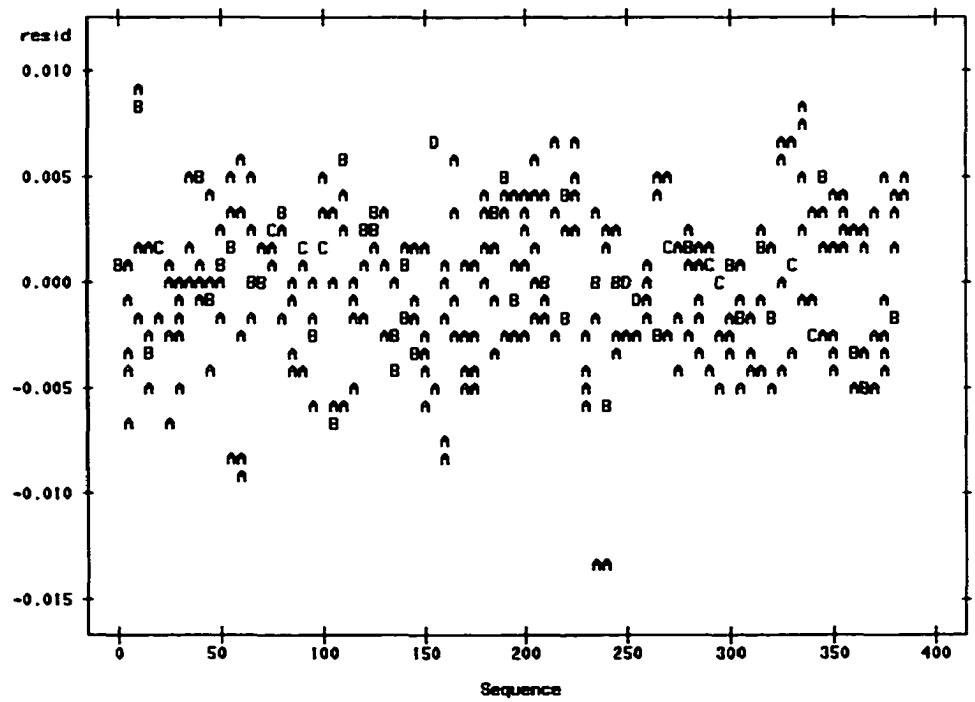
Obs	SArea	Specimen	SStrategy	SSize	Fitting	Conicity	Sequence	pred	resid
197	2	1	1	2	1	0.031098	209	0.032910	-0.001812
198	2	1	1	2	2	0.037877	210	0.038849	-0.000972
199	2	1	1	2	3	0.031814	211	0.032209	-0.000396
200	2	1	1	2	4	0.035907	212	0.036271	-0.000365
201	2	1	1	3	1	0.043651	197	0.042519	0.001133
202	2	1	1	3	2	0.049343	198	0.046865	0.002478
203	2	1	1	3	3	0.042993	199	0.038524	0.004469
204	2	1	1	3	4	0.050655	200	0.047528	0.003127
205	2	1	1	4	1	0.050737	205	0.048752	0.001985
206	2	1	1	4	2	0.058441	206	0.054315	0.004126
207	2	1	1	4	3	0.050125	207	0.044468	0.005657
208	2	1	1	4	4	0.058878	208	0.054759	0.004119
209	2	1	2	1	1	0.008895	237	0.021913	-0.013018
210	2	1	2	1	2	0.027437	238	0.032964	-0.005528
211	2	1	2	1	3	0.016430	239	0.022495	-0.006065
212	2	1	2	1	4	0.010501	240	0.023702	-0.013201
213	2	1	2	2	1	0.031654	229	0.036917	-0.005263
214	2	1	2	2	2	0.034414	230	0.040104	-0.005690
215	2	1	2	2	3	0.020813	231	0.023494	-0.002674
216	2	1	2	2	4	0.036776	232	0.041060	-0.004284
217	2	1	2	3	1	0.040950	193	0.043464	-0.002514
218	2	1	2	3	2	0.047185	194	0.048153	-0.000968
219	2	1	2	3	3	0.039852	195	0.036055	0.003796
220	2	1	2	3	4	0.047497	196	0.048626	-0.001129
221	2	1	2	4	1	0.048910	217	0.051740	-0.002830
222	2	1	2	4	2	0.056694	218	0.057951	-0.001257
223	2	1	2	4	3	0.045796	219	0.041456	0.004340
224	2	1	2	4	4	0.056760	220	0.058234	-0.001474
225	2	1	3	1	1	.	213	.	.
226	2	1	3	1	2	0.065975	214	0.059290	0.006685
227	2	1	3	1	3	0.044613	215	0.041290	0.003323
228	2	1	3	1	4	.	216	.	.
229	2	1	3	2	1	.	225	.	.
230	2	1	3	2	2	0.048517	226	0.045602	0.002915
231	2	1	3	2	3	0.041678	227	0.036590	0.005088
232	2	1	3	2	4	.	228	.	.
233	2	1	3	3	1	0.040286	233	0.041935	-0.001649
234	2	1	3	3	2	0.046694	234	0.046835	-0.000141
235	2	1	3	3	3	0.040035	235	0.036444	0.003591
236	2	1	3	3	4	0.046755	236	0.046852	-0.000096
237	2	1	3	4	1	0.054604	221	0.052420	0.002184
238	2	1	3	4	2	0.063362	222	0.059015	0.004348
239	2	1	3	4	3	0.051784	223	0.045530	0.006253
240	2	1	3	4	4	0.063369	224	0.059021	0.004349
241	2	2	1	1	1	0.021142	249	0.021285	-0.000143
242	2	2	1	1	2	0.030647	250	0.030989	-0.000342
243	2	2	1	1	3	0.014916	251	0.017161	-0.002245
244	2	2	1	1	4	0.025199	252	0.025383	-0.000184
245	2	2	1	2	1	0.021878	257	0.022446	-0.000568

Obs	SArea	Specimen	SStrategy	SSize	Fitting	Conicity	Sequence	pred	resid
246	2	2	1	2	2	0.029164	258	0.028384	0.000780195
247	2	2	1	2	3	0.020102	259	0.021745	-.001643376
248	2	2	1	2	4	0.025292	260	0.025807	-.000515055
249	2	2	1	3	1	0.031700	245	0.032054	-.000353913
250	2	2	1	3	2	0.036458	246	0.036401	0.000057595
251	2	2	1	3	3	0.025148	247	0.028060	-.002911709
252	2	2	1	3	4	0.036805	248	0.037064	-.000258657
253	2	2	1	4	1	0.037564	253	0.038287	-.000722689
254	2	2	1	4	2	0.042750	254	0.043850	-.001100224
255	2	2	1	4	3	0.031697	255	0.034003	-.002306512
256	2	2	1	4	4	0.043599	256	0.044295	-.000695325
257	2	2	2	1	1	0.012309	285	0.011449	0.000860223
258	2	2	2	1	2	0.022025	286	0.022500	-.000475354
259	2	2	2	1	3	0.010382	287	0.012030	-.001648382
260	2	2	2	1	4	0.014388	288	0.013237	0.001150603
261	2	2	2	2	1	0.027887	277	0.026452	0.001434543
262	2	2	2	2	2	0.032305	278	0.029640	0.002665714
263	2	2	2	2	3	0.010406	279	0.013030	-.002623935
264	2	2	2	2	4	0.032422	280	0.030595	0.001826766
265	2	2	2	3	1	0.034984	241	0.032999	0.001984712
266	2	2	2	3	2	0.040000	242	0.037689	0.002310960
267	2	2	2	3	3	0.022495	243	0.025591	-.003096210
268	2	2	2	3	4	0.040625	244	0.038161	0.002464376
269	2	2	2	4	1	0.045303	265	0.041276	0.004027478
270	2	2	2	4	2	0.052301	266	0.047487	0.004814234
271	2	2	2	4	3	0.028488	267	0.030992	-.002503922
272	2	2	2	4	4	0.052589	268	0.047770	0.004819582
273	2	2	3	1	1	.	261	.	.
274	2	2	3	1	2	0.049079	262	0.048825	0.000253291
275	2	2	3	1	3	0.028701	263	0.030826	-.002124771
276	2	2	3	1	4	.	264	.	.
277	2	2	3	2	1	.	273	.	.
278	2	2	3	2	2	0.033349	274	0.035137	-.001787969
279	2	2	3	2	3	0.022145	275	0.026126	-.003980749
280	2	2	3	2	4	.	276	.	.
281	2	2	3	3	1	0.032428	281	0.031471	0.000957345
282	2	2	3	3	2	0.037643	282	0.036370	0.001272955
283	2	2	3	3	3	0.022990	283	0.025980	-.002990102
284	2	2	3	3	4	0.037645	284	0.036387	0.001258197
285	2	2	3	4	1	0.043332	269	0.041956	0.001376661
286	2	2	3	4	2	0.050289	270	0.048550	0.001738577
287	2	2	3	4	3	0.032491	271	0.035066	-.002574442
288	2	2	3	4	4	0.050298	272	0.048556	0.001741923
289	2	3	1	1	1	0.013543	297	0.015887	-.002344541
290	2	3	1	1	2	0.023032	298	0.025591	-.002559296
291	2	3	1	1	3	0.010440	299	0.011764	-.001323075
292	2	3	1	1	4	0.016255	300	0.019986	-.003730186
293	2	3	1	2	1	0.016218	305	0.017048	-.000830352
294	2	3	1	2	2	0.021368	306	0.022987	-.001618540

Obs	SArea	Specimen	SStrategy	SSize	Fitting	Conicity	Sequence	pred	resid
295	2	3	1	2	3	0.014496	307	0.016347	-.001851325
296	2	3	1	2	4	0.018776	308	0.020409	-.001633175
297	2	3	1	3	1	0.026900	293	0.026657	0.000243610
298	2	3	1	3	2	0.030874	294	0.031003	-.000128777
299	2	3	1	3	3	0.017991	295	0.022662	-.004671404
300	2	3	1	3	4	0.031253	296	0.031666	-.000413078
301	2	3	1	4	1	0.033858	301	0.032889	0.000968935
302	2	3	1	4	2	0.038999	302	0.038453	0.000546257
303	2	3	1	4	3	0.023681	303	0.028606	-.004925117
304	2	3	1	4	4	0.039332	304	0.038897	0.000434525
305	2	3	2	1	1	0.013747	333	0.006051	0.007695713
306	2	3	2	1	2	0.021739	334	0.017102	0.004636981
307	2	3	2	1	3	0.009326	335	0.006633	0.002693417
308	2	3	2	1	4	0.016031	336	0.007840	0.008191703
309	2	3	2	2	1	0.027046	325	0.021055	0.005991092
310	2	3	2	2	2	0.030686	326	0.024242	0.006444526
311	2	3	2	2	3	0.007650	327	0.007632	0.000018170
312	2	3	2	2	4	0.031464	328	0.025198	0.006266509
313	2	3	2	3	1	0.029193	289	0.027601	0.001591299
314	2	3	2	3	2	0.033391	290	0.032291	0.001099758
315	2	3	2	3	3	0.016362	291	0.020193	-.003831086
316	2	3	2	3	4	0.033934	292	0.032763	0.001170263
317	2	3	2	4	1	0.038031	313	0.035878	0.002152541
318	2	3	2	4	2	0.043800	314	0.042089	0.001710747
319	2	3	2	4	3	0.021653	315	0.025594	-.003940908
320	2	3	2	4	4	0.044184	316	0.042372	0.001811915
321	2	3	3	1	1	.	309	.	.
322	2	3	3	1	2	0.039417	310	0.043428	-.004011147
323	2	3	3	1	3	0.021948	311	0.025428	-.003480715
324	2	3	3	1	4	.	312	.	.
325	2	3	3	2	1	.	321	.	.
326	2	3	3	2	2	0.031113	322	0.029740	0.001372959
327	2	3	3	2	3	0.016444	323	0.020728	-.004284425
328	2	3	3	2	4	.	324	.	.
329	2	3	3	3	1	0.027252	329	0.026073	0.001178635
330	2	3	3	3	2	0.031662	330	0.030972	0.000689473
331	2	3	3	3	3	0.016918	331	0.020582	-.003664516
332	2	3	3	3	4	0.031664	332	0.030990	0.000674632
333	2	3	3	4	1	0.036042	317	0.036558	-.000515401
334	2	3	3	4	2	0.041867	318	0.043153	-.001285423
335	2	3	3	4	3	0.024414	319	0.029658	-.005254148
336	2	3	3	4	4	0.041871	320	0.043158	-.001287021
337	2	4	1	1	1	0.017131	345	0.012388	0.004743192
338	2	4	1	1	2	0.023391	346	0.022092	0.001298461
339	2	4	1	1	3	0.013287	347	0.008264	0.005022206
340	2	4	1	1	4	0.020334	348	0.016487	0.003847099
341	2	4	1	2	1	0.016760	353	0.013549	0.003210532
342	2	4	1	2	2	0.021298	354	0.019487	0.001810160
343	2	4	1	2	3	0.016739	355	0.012848	0.003890357

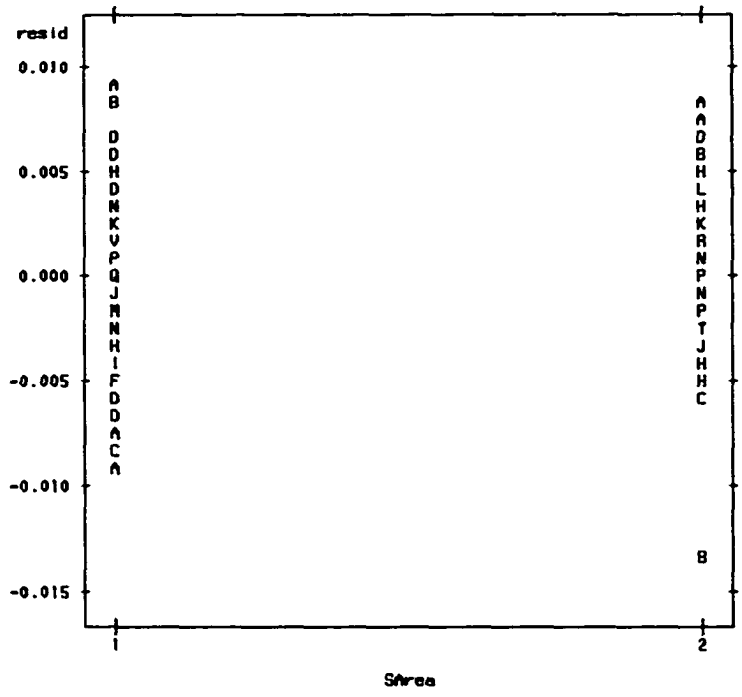
Obs	SAree	Specimen	SStrategy	SSize	Fitting	Conicity	Sequence	pred	resid
344	2	4	1	2	4	0.019423	356	0.016910	0.002513101
345	2	4	1	3	1	0.022135	341	0.023157	-.001022401
346	2	4	1	3	2	0.025097	342	0.027504	-.002406706
347	2	4	1	3	3	0.022277	343	0.019163	0.003114469
348	2	4	1	3	4	0.025712	344	0.028167	-.002454845
349	2	4	1	4	1	0.027159	349	0.029390	-.002231626
350	2	4	1	4	2	0.031382	350	0.034954	-.003572053
351	2	4	1	4	3	0.026881	351	0.025107	0.001574504
352	2	4	1	4	4	0.031540	352	0.035398	-.003857734
353	2	4	2	1	1	0.007014	381	0.002552	0.004462389
354	2	4	2	1	2	0.014969	382	0.013603	0.001366204
355	2	4	2	1	3	0.008154	383	0.003134	0.005020285
356	2	4	2	1	4	0.008199	384	0.004340	0.003858197
357	2	4	2	2	1	0.015393	373	0.017556	-.002162974
358	2	4	2	2	2	0.017323	374	0.020743	-.003420180
359	2	4	2	2	3	0.009413	375	0.004133	0.005280242
360	2	4	2	2	4	0.017889	376	0.021699	-.003809206
361	2	4	2	3	1	0.023040	337	0.024102	-.001062087
362	2	4	2	3	2	0.026349	338	0.028792	-.002442790
363	2	4	2	3	3	0.019825	339	0.016694	0.003130986
364	2	4	2	3	4	0.026758	340	0.029264	-.002505961
365	2	4	2	4	1	0.029029	361	0.032379	-.003349798
366	2	4	2	4	2	0.033322	362	0.038590	-.005268250
367	2	4	2	4	3	0.024200	363	0.022095	0.002104781
368	2	4	2	4	4	0.033715	364	0.038873	-.005157659
369	2	4	3	1	1	.	357	.	.
370	2	4	3	1	2	0.037002	358	0.039929	-.002927027
371	2	4	3	1	3	0.024212	359	0.021929	0.002282402
372	2	4	3	1	4	.	360	.	.
373	2	4	3	2	1	.	369	.	.
374	2	4	3	2	2	0.023741	370	0.026241	-.002500104
375	2	4	3	2	3	0.020406	371	0.017229	0.003177254
376	2	4	3	2	4	.	372	.	.
377	2	4	3	3	1	0.022087	377	0.022574	-.000486595
378	2	4	3	3	2	0.025652	378	0.027473	-.001821572
379	2	4	3	3	3	0.020147	379	0.017083	0.003064115
380	2	4	3	3	4	0.025654	380	0.027490	-.001836353
381	2	4	3	4	1	0.030013	365	0.033059	-.003045654
382	2	4	3	4	2	0.034853	366	0.039654	-.004800732
383	2	4	3	4	3	0.027744	367	0.026169	0.001575375
384	2	4	3	4	4	0.034856	368	0.039659	-.004803522

Plot of resid*Sequence. Legend: A = 1 obs, B = 2 obs, etc.



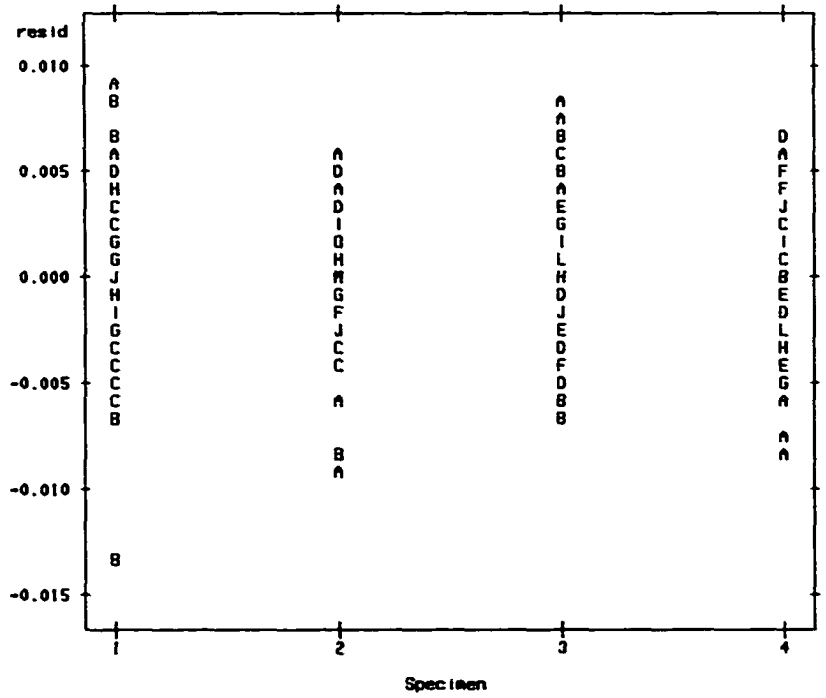
NOTE: 32 obs had missing values.

Plot of resid*SArea. Legend: A = 1 obs, B = 2 obs, etc.



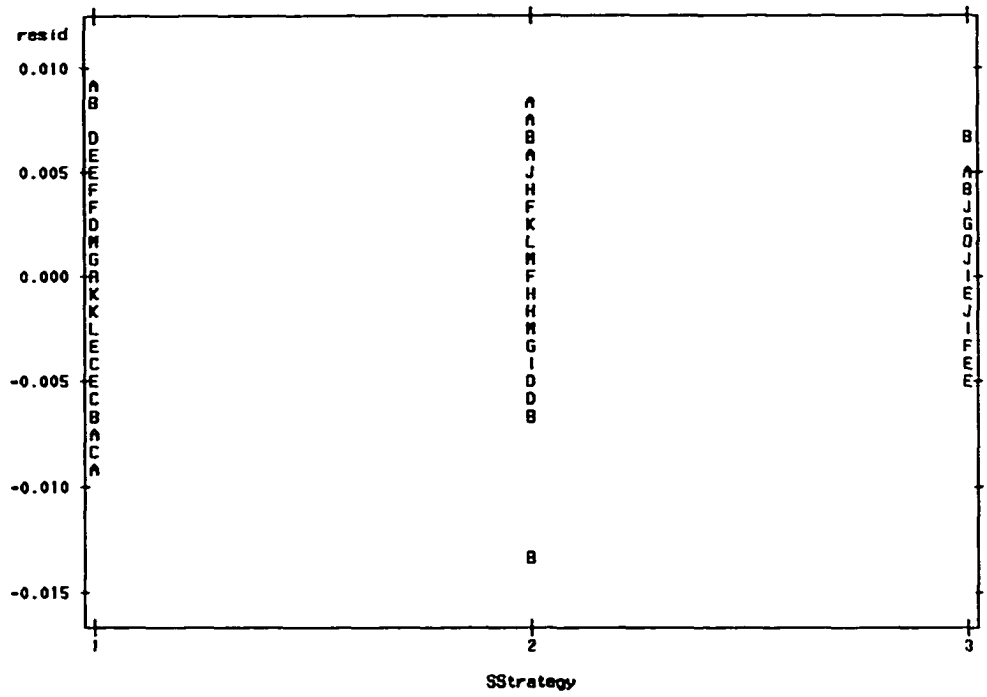
NOTE: 32 obs had missing values.

Plot of resid*Specimen. Legend: A = 1 obs, B = 2 obs, etc.



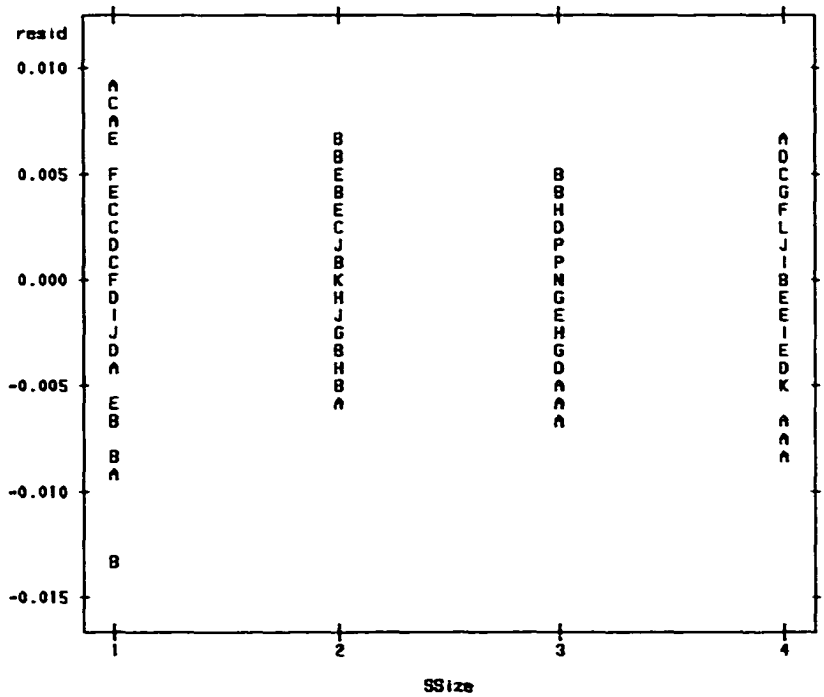
NOTE: 32 obs had missing values.

Plot of resid*SStrategy. Legend: A = 1 obs, B = 2 obs, etc.



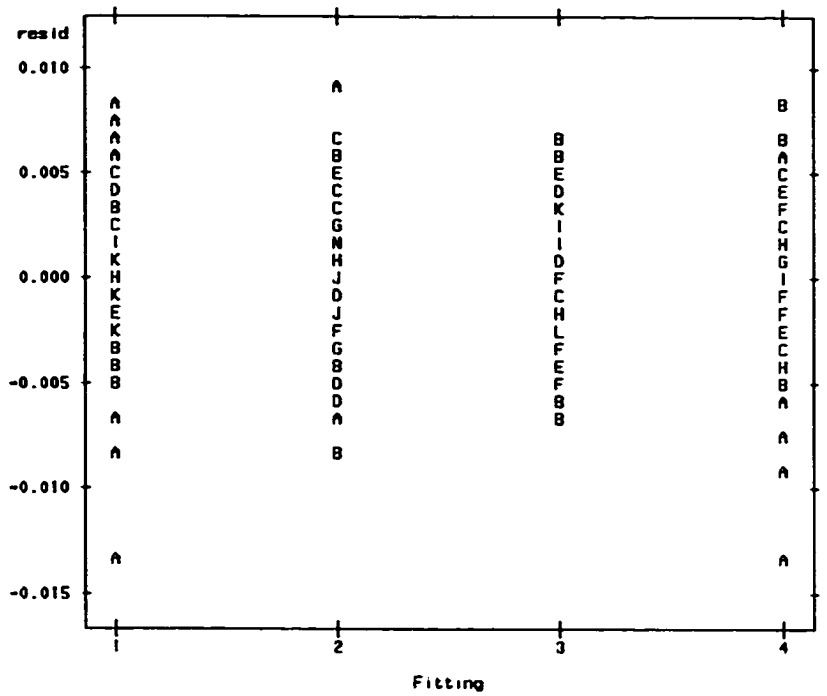
NOTE: 32 obs had missing values.

Plot of resid*SSize. Legend: A = 1 obs, B = 2 obs, etc.



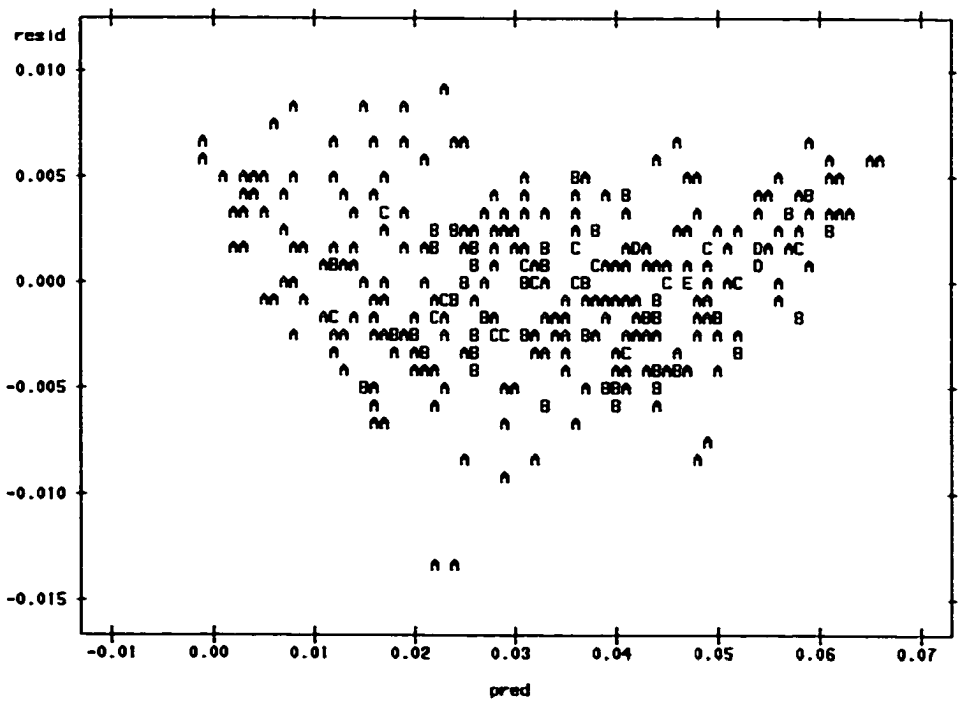
NOTE: 32 obs had missing values.

Plot of resid*Fitting. Legend: A = 1 obs, B = 2 obs, etc.



NOTE: 32 obs had missing values.

Plot of resid*pred. Legend: A = 1 obs, B = 2 obs, etc.



NOTE: 32 obs had missing values.

The UNIVARIATE Procedure
Variable: resid

Moments

N	352	Sum Weights	352
Mean	0	Sum Observations	0
Std Deviation	0.00349761	Variance	0.00001223
Skewness	-0.2518082	Kurtosis	0.49078006
Uncorrected SS	0.00429387	Corrected SS	0.00429387
Coeff Variation	.	Std Error Mean	0.00018642

Basic Statistical Measures

Location		Variability	
Mean	0	Std Deviation	0.00350
Median	0.000055	Variance	0.0000122
Mode	.	Range	0.02208
		Interquartile Range	0.00462

Tests for Location: Mu0=0

Test	-Statistic-		-----p Value------	
Student's t	t	0	Pr > |t|	1.0000
Sign	M	2	Pr >= |M|	0.8730
Signed Rank	S	327	Pr >= |S|	0.8644

Tests for Normality

Test	--Statistic---		-----p Value------	
Shapiro-Wilk	W	0.992428	Pr < W	0.0712
Kolmogorov-Smirnov	D	0.02925	Pr > D	>0.1500
Cramer-von Mises	W-Sq	0.04004	Pr > W-Sq	>0.2500
Anderson-Darling	A-Sq	0.27303	Pr > A-Sq	>0.2500

Quantiles (Definition 5)

Quantile	Estimate
100% Max	8.87453E-03
99%	8.19170E-03
95%	5.60773E-03
90%	4.46864E-03
75% Q3	2.23727E-03

The UNIVARIATE Procedure
Variable: resid

Quantiles (Definition 5)

Quantile	Estimate
50% Median	5.51249E-05
25% Q1	-2.38520E-03
10%	-4.34693E-03
5%	-5.43811E-03
1%	-8.71839E-03
0% Min	-1.32005E-02

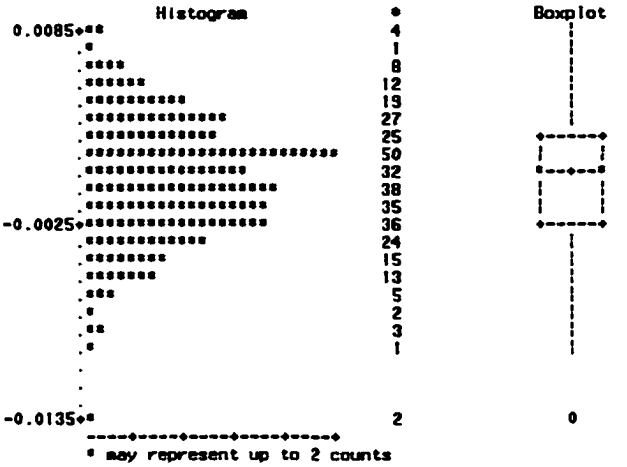
Extreme Observations

-------Lowest-------		-------Highest-------	
Value	Obs	Value	Obs
-0.01320050	212	0.00769571	305
-0.01301824	209	0.00819170	308
-0.00922652	52	0.00820912	1
-0.00871839	50	0.00873453	4
-0.00844873	49	0.00887453	2

Missing Values

Missing Value	Count	-----Percent Of----- All Obs	Missing Obs
.	32	8.33	100.00

The UNIVARIATE Procedure
Variable: resid



The UNIVARIATE Procedure
Variable: resid

